

ผลิตภัณฑ์เชื้อเพลิงจากไฟโรไลซิสของกากสบู่ดำ *Jatropha curcas* L.

นายชिरาวุฒิ เพชรเย็น

วิทยานิพนธ์นี้เป็นส่วนหนึ่งของการศึกษาตามหลักสูตรปริญญาวิทยาศาสตรดุษฎีบัณฑิต

สาขาวิชาวัสดุศาสตร์ ภาควิชาวัสดุศาสตร์

คณะวิทยาศาสตร์ จุฬาลงกรณ์มหาวิทยาลัย

ปีการศึกษา 2552

ลิขสิทธิ์ของจุฬาลงกรณ์มหาวิทยาลัย

FUEL PRODUCTS FROM PYROLYSIS OF PHYSIC NUT *Jatropha curcas* L. WASTE

Mr. Chiravoot Pechyen

A Dissertation Submitted in Partial Fulfillment of the Requirements
for the Degree of Doctor of Philosophy Program in Materials Science

Department of Materials Science

Faculty of Science

Chulalongkorn University

Academic Year 2009

Copyright of Chulalongkorn University

Thesis Title	FUEL PRODUCTS FROM PYROLYSIS OF PHYSIC NUT <i>Jatropha curcas</i> L. WASTE
By	Mr. Chiravoot Pechyen
Field of Study	Materials Science
Thesis Advisor	Associate Professor Duangdao Aht-Ong, Ph.D.
Thesis Co-Advisor	Assistant Professor Viboon Sricharoenchaikul, Ph.D. Duangduen Atong, Ph.D.

Accepted by the Faculty of Science, Chulalongkorn University in Partial Fulfillment of the Requirements for the Doctoral Degree

..... Dean of the Faculty of
Science
(Professor Supot Hannongbua, Dr.rer.nat.)

THESIS COMMITTEE

..... Chairman
(Assistant Professor Sirithan Jiemsirilers, Ph.D.)

..... Thesis Advisor
(Associate Professor Duangdao Aht-Ong, Ph.D.)

..... Thesis Co-Advisor
(Assistant Professor Viboon Sricharoenchaikul, Ph.D.)

..... Thesis Co-Advisor
(Duangduen Atong, Ph.D.)

..... Examiner
(Assistant Professor Sireerat Charuchinda, Ph.D.)

..... Examiner
(Associate Professor Pranut Potiyaraj, Ph.D.)

..... External Examiner
(Pavadee Aungkavattana, Ph.D.)

ชิวาวุฒิ เพชรเย็น : ผลผลิตภัณฑ์เชื้อเพลิงจากไพโรไลซิสของกากสบู่ดำ *Jatropha curcas* L.. (FUEL PRODUCTS FROM PYROLYSIS OF PHYSIC NUT *Jatropha curcas* L. WASTE) อ.ที่ปรึกษาวิทยานิพนธ์หลัก : รศ.ดร.ดวงดาว อาจองค์ , อ.ที่ปรึกษาวิทยานิพนธ์ร่วม : ผศ.ดร.วิบูลย์ ศรีเจริญชัยกุล, ดร.ดวงเดือน อาจองค์, 228 หน้า.

งานวิจัยนี้เป็นการศึกษาผลของภาวะในการทดลองที่ต่างกัน ได้แก่ ขนาดของวัสดุตัวอย่าง อุณหภูมิในการทดลอง และระยะเวลาในการทำการทดลอง ที่มีต่อสมบัติทางกายภาพ และสมบัติทางเคมี ของถ่านชาร์ น้ำมัน และ แก๊ส ที่ได้จากระบวนการไพโรไลซิสของกากสบู่ดำ ด้วยเตาปฏิกรณ์แบบแบนนิ่ง โดยใช้ขนาดของกากสบู่ดำต่างกัน ดังนี้ 0.43-0.50 0.50-0.85 0.85-1.80 และ 1.80-3.60 มิลลิเมตร ของกระบวนการไพโรไลซิสแบบช้า และไพโรไลซิสแบบเร็ว

อุณหภูมิ และเวลาที่เหมาะสมของการไพโรไลซิส คือ ที่อุณหภูมิ 800 องศาเซลเซียส เป็นเวลา 15 นาที ซึ่งจะได้ปริมาณคาร์บอนคงตัวร้อยละ 90.01 ผลผลิตภัณฑ์ร้อยละ 27.51 สารระเหยร้อยละ 4.34 และแก๊สร้อยละ 4.87 จากนั้นนำถ่านชาร์จากกากสบู่ดำมากระตุ้นโดยใช้แก๊สคาร์บอนไดออกไซด์ สารละลายต่างของโปตัสเซียมไฮดรอกไซด์ และโซเดียมไฮดรอกไซด์ ตัวแปรที่ศึกษา คือ อุณหภูมิ ขนาดของถ่านชาร์ของกากสบู่ดำ รวมถึงอัตราส่วนของถ่านชาร์ต่อปริมาณต่างที่ใช้ในการกระตุ้น จากการทดลองพบว่า ภาวะที่เหมาะสมในการกระตุ้นทางกายภาพ คือ กระตุ้นที่อุณหภูมิ 600 องศาเซลเซียส เป็นเวลา 1 ชั่วโมง โดยใช้ถ่านชาร์จากกากสบู่ดำขนาด 0.43-0.50 มิลลิเมตร ส่วนถ่านกัมมันต์ที่ได้จากการกระตุ้นโดยใช้โปตัสเซียมไฮดรอกไซด์ มีคุณภาพดีกว่าถ่านกัมมันต์ที่ได้จากการกระตุ้นโดยใช้โซเดียมไฮดรอกไซด์ เนื่องจากโซเดียมไฮดรอกไซด์เกิดปฏิกิริยากับถ่านอย่างรุนแรงกว่าเมื่อเทียบกับการใช้โซเดียมไฮดรอกไซด์ ผลผลิตภัณฑ์ของเหลวที่เกิดขึ้นมากที่สุดคิดเป็นร้อยละ 21.35 ที่อุณหภูมิ 900 องศาเซลเซียส เป็นเวลา 1 ชั่วโมง ในกรณีกระบวนการไพโรไลซิสแบบช้า ส่วนการไพโรไลซิสแบบเร็วผลผลิตภัณฑ์ของเหลวที่เกิดขึ้นมากที่สุดคิดเป็นร้อยละ 61.54 ที่อุณหภูมิ 500 องศาเซลเซียส ผลผลิตภัณฑ์ของน้ำมันที่เกิดขึ้นมีองค์ประกอบหลักเป็นกรดไขมัน ได้แก่ กรดโอลิกคิดเป็นร้อยละ 15-19 กรดปาล์มมิกคิดเป็นร้อยละ 40-45 และกรดลิกโนลิกคิดเป็นร้อยละ 25-34 น้ำมันที่ได้จากไพโรไลซิสประกอบไปด้วยสารประกอบไฮโดรคาร์บอน ที่มีลักษณะเป็นวงอะโรมาติกตั้งแต่ 1-5 วง ขึ้นไป ซึ่งน้ำมันเหล่านี้สามารถทำให้เกิดตัวได้ด้วยความร้อนหรือด้วยตัวเร่งปฏิกิริยา จึงมีการใช้เทคโนโลยีของตัวเร่งปฏิกิริยามาใช้ร่วมกับกระบวนการแก๊สซิฟิเคชันเพื่อเปลี่ยนน้ำมันให้เป็นแก๊สสังเคราะห์เพิ่มมากขึ้น งานวิจัยนี้จึงเลือกใช้ตัวเร่งปฏิกิริยาชนิด Olivine และ Ni/Olivine มาใช้เพื่อลดปริมาณน้ำมันและเพิ่มปริมาณแก๊สสังเคราะห์ให้สูงขึ้น โดยตัวรองรับ Olivine สังเคราะห์จากการตกตะกอนร่วม ส่วน Ni/Olivine เตรียมจากการนำตัวรองรับ Olivine จุ่มลงในสารละลาย $\text{Ni}(\text{NO}_3)_2$ ซึ่ง Olivine และ 5%Ni/Olivine แสดงประสิทธิภาพในการแตกตัวอะซิโตนที่ 600 องศาเซลเซียสได้ดีที่สุด เนื่องจากเกิดการเปลี่ยนแปลง คาร์บอน และไฮโดรเจนไปเป็นแก๊สสังเคราะห์ปริมาณสูง

ภาควิชา..... วัสดุศาสตร์..... ลายมือชื่อนิติติ
 สาขาวิชา..... วัสดุศาสตร์..... ลายมือชื่ออ.ที่ปรึกษาวิทยานิพนธ์หลัก.....
 ปีการศึกษา..... 2552..... ลายมือชื่ออ.ที่ปรึกษาวิทยานิพนธ์ร่วม.....
 ลายมือชื่ออ.ที่ปรึกษาวิทยานิพนธ์ร่วม.....

4973813923 : MAJOR MATERIALS SCIENCE

KEYWORDS : PYROLYSIS / PHYSIC NUT *Jatropha curcas* L. WASTE / FUEL PRODUCTS / ACTIVATED CARBON / OLIVINE SYNTHESIS AND REFORMING

CHIRAVOOT PECHYEN : FUEL PRODUCTS FROM PYROLYSIS OF PHYSIC NUT *Jatropha curcas* L. WASTE. THESIS ADVISOR : ASSOC.PROF.DUANGDAO AHT-ONG, Ph.D., THESIS CO-ADVISOR : ASSIS.PROF.VIBOON SRICHAROENCHAIKUL, Ph.D., DUANGDUEN ATONG, Ph.D., 228 pp.

This research investigated the effects of different operating conditions, such as sample size, final temperature and hold times, on properties of solid chars, liquid bio-oil and gas prepared by vertical fixed bed pyrolysis of extracted Physic nut (*Jatropha curcas* L.) waste. The size fraction of Physic nut residue was varied from 0.43-0.50, 0.50-0.85, 0.85-1.80 and 1.80-3.60 mm. The variable studied was final temperature (400, 500, 600, 700 and 800°C) and retention time (0.25, 2 and 4 hours) in isothermal and dynamic pyrolysis.

The results showed that suitable pyrolysis condition was 800°C for 15 minutes with 90.01% fixed carbon, 24.23% yield, 4.34% volatile matter and 4.87% ash. Physic nut waste char was activated by physical and chemical means using carbon dioxide gas and by alkaline solution such as KOH and NaOH, respectively. Investigating parameters were activation temperature, activation time particle size of Physic nut residue char, and ratio of char per alkaline solution. The experimental results revealed that the suitable condition for physical activation was at 600°C for 1 hour using char with the size of 0.43-0.50 mm; whereas the appropriate condition for chemical activation using either KOH or NaOH as an activating agents was at 700°C for 1 hour using char with same size. Activated carbon prepared from KOH however gave higher quality than that from NaOH owing to stronger alkaline of KOH solution. The maximum liquid product of 21.35% was observed at the pyrolysis temperature of 900°C for 1 hour under dynamic heating and 61.54% under isothermal heating at 500°C. The bio-oil product mainly consisted of several fatty acids such as oleic acid, palmitic acid, and lignoleic acid in the range of 15-19%, 40-45%, and 25-34%, respectively. Liquid tar from pyrolysis are complex mixture of condensable hydrocarbons which include single ring to five ring aromatic compounds along with other oxygen containing hydrocarbons. Tar can be eliminated by thermal cracking or by the use of catalysts. The catalytic gasification process is an attractive technological alternative to deal with tar and to produce high yield of syn-gas. This research has proved the usefulness and effectiveness of calcined olivine and nickel based steam reforming catalysts on decreasing tar yield and achieve high conversion. Olivine and Ni/Olivine were chosen as a catalyst because of their activity in tar cracking. Phosphor olivine (LiFePO₄) support was synthesized by co-precipitation method. The Ni/Olivine was carried out by wet impregnation of synthesized olivine supports with Ni(NO₃)₂ solution. Olivine and 5%Ni/Olivine displayed excellent reforming capability when applied to in-situ gasification/reforming of glycerol waste. Complete conversion of carbon and hydrogen in materials to product gas as well as superior selectivity of preferred gas species may be achieved with catalyst at 600°C.

Department : Materials Science Student's Signature :

Field of Study : Materials Science Advisor's Signature :

Academic Year : 2009 Co-Advisor's Signature :

Co-Advisor's Signature :

ACKNOWLEDGMENT

I wish to express his deep gratefulness to his advisor, Associate Professor Dr.Duangdao Aht-Ong for providing her encouragement, valuable suggestion, an assistance throughout this study as well as for the discussion and reviewing this thesis during this study, and for everything including her kindness. I would also like to deeply thank to my thesis co-advisors, Assistant Professor Dr.Viboon Sricharoenchaikul and Dr.Duangduen Atong for their knowledge, consistent guidance, and for all that I have learnt from both of them throughout this research.

I also would like to acknowledge Assistant Professor Dr.Sirithan Jiemsirilers, Assistant Professor Dr.Sireerat Charuchinda, Associate Professor Dr.Pranut Potiyaraj and Dr.Pavadee Aungkavattana for their reviewing of thesis, comments and serving on the thesis committee.

I am grateful to The Thailand Graduate Institute of Science and Technology (TGIST, TG-33-09-49-030D) and Excellent Center for Eco Products (XCEP) from National Science and Technology Development Agency (NSTDA), The 90th Anniversary of Chulalongkorn University Fund (Ratchadaphiseksomphot Endowment Fund) and Research Unit of Advanced Ceramic and Polymeric Materials, National Center of Excellent for Petroleum, Petrochemicals, and Advance Materials, Chulalongkorn University for financial support. Thanks also go to all my friends at Department of Materials Science, Department of Environmental Engineering from Chulalongkorn University and Applied Ceramics Laboratory from National Metal and Materials Technology Center, THAILAND for friendship and their help during my studies.

Finally, I would like to extend my deep appreciation to my family for their love attention and support, in particular, to my aunt who has always standing by me regardless of what happens. Many thanks for her understanding and her endless love.

Contents

Chapter	Page
Abstract (Thai).....	iv
Abstract (English).....	v
Acknowledgement.....	vi
Contents.....	vii
List of Tables.....	xii
List of Figures	xiv
Chapter	
I Introduction	1
II Theory and literature review.....	6
2.1 Biomass energy resource.....	6
2.1.1 Virgin biomass	9
2.1.2 Waste biomass	13
2.2 Structure and chemical of biomass	16
2.3 Biomass pyrolysis	22
2.3.1 Operational rperiences	23
2.3.2 Types of pyrolysis	25
2.3.2.1 Conventional pyrolysis.....	25
2.3.2.2 Fast pyrolysis (Ultra Pyrolysis).....	33
2.3.2.3 Flash pyrolysis.....	35
2.3.2.4 Vacuum pyrolysis	39
2.4 Gasification technology	40
2.4.1 Downdraft	40
2.4.2 Updarft	44
2.4.3 Fluid bed	44
2.4.4 Circulating fluid bed	46
2.4.5 Entrained bed	46
Chapter	
2.4.6 Twin fluid bed.....	47
2.4.7 Comparison of pressurized and atmospheric operation.....	47
2.4.8 Summary.....	48
2.5 Products of gasification	50

2.6 Carbon materials.....	53
2.6.1 Preparation of carbons in solid phase activated carbon.....	55
2.6.2 Preparation of carbon in liquid phase.....	58
2.6.3 Preparation of carbons in gas phase.....	62
2.6.4 Activated carbon.....	63
2.6.5 Raw materials for the production of activated carbon.....	63
2.6.6 Production of activated carbon.....	64
2.6.6.1 Carbonization (or pyrolysis).....	64
2.6.6.2 Activation.....	65
2.6.6.2.1 Chemical activation.....	65
2.6.6.2.2 Physical activation.....	67
2.6.6.3 Pyrolysis and steam activation.....	72
2.6.7 Molecular, Crystalline and porous structure of activated carbon.....	72
2.6.8 Chemical nature of the surface of activated carbon.....	75
2.7 Cracking reaction.....	77
2.7.1 Thermal cracking.....	77
2.7.2 Catalytic cracking.....	79
2.7.3 Hydrocracking processing.....	82
2.8 Basic principles of catalysis.....	84
2.8.1 Metal catalyst.....	86
2.8.2 Catalyst support.....	89
2.8.3 Co precipitation method.....	90
2.8.4 Impregnation.....	91
2.9 Literature reviews.....	92

Chapter	Page
III Experiments.....	104
3.1 Biomass raw material.....	104
3.2 Chemicals.....	105
3.3 Pyrolysis reactor and other apparatus.....	106
3.4 Apparatus used in this research included.....	107
3.5 Experimental Part I: Pyrolysis of physic nut waste.....	108
3.5.1 Pyrolysis process: effect of pyrolysis temperature and time and particle size of physic nut waste.....	108
3.5.2 Pyrolysis process: effect of heating method.....	109
3.5.3 Characterization of products from pyrolysis process.....	111

3.5.3.1	Characterization of solid char.....	111
3.5.3.2	Characterization of bio-oil.....	111
3.5.3.3	Characterization of producer gas.....	112
3.6	Experiment Part II: Preparation and characterization of activated carbon	
	from pyrolyzed physic nut waste char	113
3.6.1	Physical Activation by oxidizing gas.....	113
3.6.1.1	The effect of activation temperature	113
3.6.1.1	The effect of activation time.....	114
3.6.2	Chemical activation with alkaline solution	115
3.6.2.1	The effect of concentration of KOH activation	115
3.6.2.2	The effect of temperature for activation.....	115
3.6.2.3	The effect of time of activation.....	116
3.6.2.4	The effect of size of Physic nut residue char.....	116
3.6.2.5	The effect of reagent for alkaline solution.....	117
3.6.3	Characterization of activated carbon.....	117
3.6.3.1	Chemical characterization.....	117
3.6.3.2	Textural characterization.....	119
3.7	Experiment Part III: Synthesis and catalytic activity of catalyst.....	119
3.7.1	Synthesis of olivine support.....	119
Chapter		Page
3.7.2	Synthesis Ni/Olivine catalyst.....	119
3.7.3	Characterization of Olivine and Ni/Olivine.....	120
3.7.4	Catalytic activity of olivine and Ni/olivine catalysts.....	121
IV	Distribution and characterization of products from various pyrolysis	
	Operations.....	123
4.1	Biomass raw materials.....	123
4.2	Results and discussion of the experiments.....	124
4.2.1	Thermal degradation of physic nut waste.....	124
4.2.2	Pyrolysis yields.....	125
4.2.3	Influence of pyrolysis conditions on solid-char.....	131
4.2.4	Influence of pyrolysis conditions on gas.....	137
4.2.5	Influence of pyrolysis conditions on liquid product.....	143
V	Production of activated carbon.....	150
5.1	Raw materials.....	150
5.2	Carbonization processes.....	150

5.3 Activation Processes.....	152
5.3.1 Physical activation by oxidizing gas.....	152
5.3.2 Chemicals activation.....	157
5.3.2.1 The effect of concentration of potassium hydroxide	157
5.3.2.2 The effect of temperature for activation.....	162
5.3.2.3 The effect of time for activation.....	166
5.3.2.4 The effect of size of Physic nut waste char for activation.....	171
5.3.2.5 The effect type of alkaline solution for activation process.....	175
5.4 Comparison of this work with other works.....	180
VI Synthesis and catalytic reforming properties of olivine and Ni/Oilvine catalysts.....	186
6.1 Physical and thermal characteristics of olivine and Ni/olivine catalysts.....	186
6.2 Phase analysis.....	188
Chapter	
6.3 Microstructure analysis.....	189
6.4 Catalytic steam reforming of glycerol using olivine and Ni/olivine catalysts..	193
VII Conclusions.....	201
References.....	205
Biography.....	211

List of Tables

TABLE		PAGE
Table 2.1	Estimated Net Photosynthetic Production of Dry Biomass carbon for World Biosphere.....	10
Table 2.2	Potential Substitute Natural Gas Production in United States from Virgin Biomass Feedstocks at Different Biomass Yields.....	12
Table 2.3	Potential Biomass Energy Available in United States in 2000.....	15
Table 2.4	Energy content of gas, oil, tar from a municipal refuse feedstock based pyrolysis plant.....	24
Table 2.5	Different types of pyrolysis process based on range of temperature.....	25
Table 2.6	Chemical and elemental analysis and heating values of tested materials (wt%)	28
Table 2.7	Yields of conventional pyrolysis product (wt%).....	30
Table 2.8	Elemental analysis (wt%) and heating values (MJ/kg) of charcoal produced by conventional pyrolysis 450°C.....	31
Table 2.9	Elemental analysis (wt%) and heating values (MJ/kg) of bio-oil produced by conventional 450°C.....	32
Table 2.10	Chemical composition of gaseous products of the conventional pyrolysis of hazel nut shells at different operating temperature.....	33
Table 2.11	Biomass feedstock analysis.....	34
Table 2.12	Yields of the products obtained by fast pyrolysis biomass: hazel nut shells..	35
Table 2.13	Gasifier types.....	41
Table 2.14	Gasifier characteristics.....	48
Table 2.15	Typical gasifier characteristics (all air-blown).....	51
Table 2.16	Gasification product gas characteristics.....	52
Table 2.17	Typical product gas compositions from different gasifiers.....	53
Table 2.18	Classification of heterogeneous catalysts.....	85
TABLE		PAGE
Table 4.1	Chemical characteristics of physic nut waste used as raw material for pyrolysis.....	123
Table 4.2	Surface area and porosity characteristics of chars.....	134
Table 4.3	Effect of reaction temperature, hold time, and mode of heating on product distribution and gas characteristics.....	142

Table 4.4	Properties of the bio-oil product.....	145
Table 4.5	Molecular weight distribution of the water-insoluble fraction.....	146
Table 4.6	Results of 1H NMR spectra for bio-oil of different pyrolysis condition at 700 °C	147
Table 5.1	Proximate analysis of physic nut residue.....	150
Table 5.2	Proximate analysis of Physic nut waste char at different temperature and times.....	151
Table 5.3	Characteristics of activated carbon from Physic nut residue at different temperatures and times.....	153
Table 5.4	Effect of KOH concentration (600 °C, 0.25 hour, N ₂ flow rate 100 mL/min)...	158
Table 5.5	Effect of temperature (1:1, 0.25 hour, N ₂ flow rate 100 mL/min).....	162
Table 5.6	Effect of times (1:1, 700°C, N ₂ flow rate 100 mL/min).....	166
Table 5.7	Effect of particle size (1:1, 700°C, N ₂ flow rate 100 mL/min).....	171
Table 5.8	Effect of alkaline solution (1:1, 1 hour, 700°C, N ₂ flow rate 100 mL/min).....	175
Table 5.9	Comparison of physical activation with chemical activation.....	176
Table 5.10	Comparison of this work with R. Zanzi et al. (2001)	181
Table 5.11	Comparison of this work with A.P. Carvaloho et al. (2003)	182
Table 5.12	Comparison of this work with Yun Su Park et al. (2006)	184
Table 6.1	Particle size, BET surface area, and element of olivine and Ni/olivine catalysts.....	192
Table 6.2	Effect of reaction temperature and type of catalysts on product distribution and gas characteristics.....	199

List of Figure

FIGURE		PAGE
Figure 2.1	Main features of biomass energy technology.....	8
Figure 2.2	Structure of starch, cellulose, and hemicelluloses.....	18
Figure 2.3	Structure of plant stalks.....	19
Figure 2.4	Structure of lignin.....	21
Figure 2.5	Flow diagram of the hench scale pyrolysis reactor.....	26
Figure 2.6	Thermogram of pyrolysis of biomass hearting rate = 20 k/min.....	29
Figure 2.7	Fixed-bed gasifiers: updraft and downdraft.....	42
Figure 2.8	Bubbling and circulating fluid-bed gasifiers.....	42
Figure 2.9	Twin fluid-be gasifier.....	43
Figure 2.10	A model of the cubic unit cell of diamond. The internal carbon atoms are bonded to three other carbon atoms, with sp^3 -symmetry, as in methane.....	54
Figure 2.11	The structure of hexagonal graphite, with trigonal planar bonding within the grapheme layers.....	54
Figure 2.12	Scanning electron microscopy (SEM) photograph of carbonized wood (100 x 70 m) showing that the structure of the wood has not.....	56
Figure 2.13	This model shows the ratio of nitrogen molecules to carbon atoms for a carbon of $1000m^{-1}g^{-1}$, filled with adsorbed nitrogen at 77 K.....	57
Figure 2.14	Photograph of the head of a dyke after penetrating through a coal steam.....	58
Figure 2.15	Optical micrograph of spheres of mesophase as developed during the carbonization of anthracene.....	59
Figure 2.16	Drawing of stacking arrangements of mesogens paralle to an equator of the sphere.....	59
Figure 2.17	Models of anisotropic nematic aromatic discotic liquid crystals, growing.....	60
FIGURE		PAGE
Figure 2.18	This diagram comprehensively models the structural changes which occur during the heat treatment of a graphitizable carbon.....	62
Figure 2.19	Chemical reaction of lignin with activated by $ZnCl_2$	66

Figure 2.20	Chemical reaction of char with activated by steam.....	70
Figure 2.21	Ordering of carbon atoms in a crystal of graphite.....	73
Figure 2.22	Comparison of three-dimensional crystal lattice of graphite.....	74
Figure 2.23	Principal types of acidic oxygen surface functional groups.....	76
Figure 2.24	Functional groups of basic character.....	76
Figure 2.25	Model of fragment of an oxidized activated carbon surface.....	77
Figure 2.26	Electron density of the 3 rd band and work function Φ of the transition metals of the fourth period.....	87
Figure 2.27	Acceptor and donor function according to the band model.....	88
Figure 3.1	Physic nut (<i>Jatropha curcas</i> Linn.) residue.....	104
Figure 3.2	Schematic of the pyrolysis reactor setup	106
Figure 3.3	Flow chart of screening test for selected optimum condition.....	108
Figure 3.4	Flow chart of different pyrolysis processes for selected optimum condition.....	110
Figure 3.5	Experiment scheme of the production of activated carbon from physic nut waste by oxidizing gas in a fixed bed reactor.....	114
Figure 3.6	Experiment scheme of the production of activated carbon from physic nut waste by alkaline solution in fixed bed reactor.....	118
Figure 3.7	The experiment procedure of catalyst synthesis.....	120
Figure 3.8	Schematic of the catalytic reforming system setup for linear long chain hydrocarbon.....	122
Figure 4.1	Pyrolytic thermogravimetric analysis of the residue showing weight loss and DTG plots.....	124
Figure 4.2	Product distribution from the pyrolysis of physic nut waste using hold times of 15 and 240 min.	125
Figure 4.3	Char yields from the pyrolysis of physic nut waste.....	126
FIGURE		PAGE
Figure 4.4	Components in char from the pyrolysis of physic nut waste using a hold time of 15 minutes.....	127
Figure 4.5	Product yields from dynamic and isothermal heating of physic nut wastes.....	129
Figure 4.6	Proximate analysis of char from dynamic and isothermal heating of physic nut wastes.....	131
Figure 4.7	Elemental analysis of char from dynamic and isothermal heating of physic nut wastes.....	132

Figure 4.8	SEM of chars: dynamic heating and isothermal heating.....	135
Figure 4.9	FTIR spectra of the char pyrolyzed from physic nut waste.....	136
Figure 4.10	X-ray diffraction pattern of the char pyrolyzed from physic nut waste.....	137
Figure 4.11	Gas produced from isothermal heating of physic nut wastes at 900°C..	138
Figure 4.12	Hydrogen gas produced from isothermal and dynamic heating of physic nut wastes.....	139
Figure 4.13	Methane produced from isothermal and dynamic heating of physic nut wastes.....	139
Figure 4.14	(a) H ₂ /CO and (b) lower heating value (LHV) of product gas.....	140
Figure 4.15	FT-IR spectra of liquid product.....	143
Figure 4.16	Relative distribution of fatty acids in liquid product.....	144
Figure 4.17	¹ H-NMR spectra of Physic nut waste bio-oil of isothermal heating condition at maximum oil yield (700°C).....	148
Figure 4.18	¹ H-NMR spectra of Physic nut waste bio-oil of dynamic heating condition at maximum oil yield (700°C).....	149
Figure 5.1	Effect of activation temperature and time on % yield.....	154
Figure 5.2	Effect of activation temperature and time on bulk density.....	154
Figure 5.3	Effect of activation temperature and time on % ash.....	155
Figure 5.4	Effect of activation temperature and time on iodine number.....	155
Figure 5.5	Effect of activation temperature and time on methylene blue number...	156
FIGURE		PAGE
Figure 5.6	Effect of char : KOH ratio time on % yield at 600°C for 0.25 hour.....	159
Figure 5.7	Effect of char : KOH ratio time on bulk density at 600°C for 0.25 hour.....	159
Figure 5.8	Effect of char : KOH ratio time on % ash at 600°C for 0.25 hour.....	160
Figure 5.9	Effect of char : KOH ratio time on iodine number at 600°C for 0.25 hour.....	160
Figure 5.10	Effect of char : KOH ratio time on methylene blue number at 600°C for 0.25 hour	161
Figure 5.11	Effect of activation temperature on % yield at difference time and char : KOH ratio.....	163
Figure 5.12	Effect of activation temperature on bulk density at difference time and char : KOH ratio.....	163
Figure 5.13	Effect of activation temperature on % ash at difference time and char : KOH ratio.....	164

Figure 5.14	Effect of activation temperature on iodine number at difference time and char : KOH ratio.....	164
Figure 5.15	Effect of activation temperature on methylene blue number at difference time and char : KOH ratio.....	165
Figure 5.16	Effect of activation time on % yield (char : KOH ratio 1 : 1, 700°C, size 0.43-0.50 mm)	168
Figure 5.17	Effect of activation time on bulk density (char : KOH ratio 1 : 1, 700°C, size 0.43-0.50 mm)	168
Figure 5.18	Effect of activation time on % ash (char : KOH ratio 1 : 1, 700°C, size 0.43-0.50 mm)	169
Figure 5.19	Effect of activation time on iodine number (char : KOH ratio 1 : 1, 700°C, size 0.43-0.50 mm).....	169
Figure 5.20	Effect of activation time on methylene blue number (char : KOH ratio 1 : 1, 700°C, size 0.43-0.50 mm).....	170
Figure 5.21	Effect of particle size on % yield (char : KOH ratio 1 : 1, 700°C).....	172
Figure 5.22	Effect of particle size on bulk density (char : KOH ratio 1 : 1, 700°C)....	172
FIGURE		
Figure 5.23	Effect of particle size on % ash (char : KOH ratio 1 : 1, 700°C).....	173
Figure 5.24	Effect of particle size on iodine number (char : KOH ratio 1 : 1, 700°C).173	
Figure 5.25	Effect of particle size on methylene blue number (char : KOH ratio 1 : 1, 700°C)	174
Figure 5.26	The scanning electron micrograph of activated carbon using different activation methods.....	178
Figure 5.27	FTIR spectra of pyrolyzed char and activated carbons.....	179
Figure 5.28	X-ray diffraction analysis of pyrolyzed char and activated carbons.....	180
Figure 6.1	TGA and DTG curves for the LiFePO ₄ olivine.....	187
Figure 6.2	The photograph of the (a) fresh LiFePO ₄ , (b) LiFePO ₄ calcined at 500°C, (c) LiFePO ₄ calcined at 700°C, and (d) LiFePO ₄ calcined at 900°C	187
Figure 6.3	XRD patterns of fresh LiFePO ₄ , LiFePO ₄ calcined at 500, 700, and 900°C, Ni/LiFePO ₄ calcined at 800°C (with LiFePO ₄ calcined at 700°C) and Ni/LiFePO ₄ calcined at 800°C and reduced at 700°C (with LiFePO ₄ support calcined at 700°C).....	189
Figure 6.4	SEM photgraphs of (a) Fresh LiFePO ₄ olivine and LiFePO ₄ calcined at (b) 500°C, (c) 700°C and (d) 900°C	190

Figure 6.5	SEM photographs of Ni/LiFePO ₄ (with LiFePO ₄ support calcined at 700°C).....	191
Figure 6.6	(a) Solid, (b) liquid, (c) gas yield from catalytic reforming of glycerol waste, and (d) gas produced using Ni/Olvine catalyst (LFP-700-Ni-800-700R).....	193
Figure 6.7	Conversion to gas products from catalytic and thermal reforming of glycerol waste.....	195
Figure 6.8	Quality of product gas.....	197
Figure 6.9	Effect of catalyst content of product gas from catalytic reforming of glycerol waste at 600°C.....	198

CHAPTER I

INTRODUCTION

The continuous raises of fossil fuel prices and global concerns on greenhouse gas emissions from utilizations of fossil fuels give biomass a chance of being competed with fossil fuels. Thailand is a biomass rich country, particularly varieties of crops are abundant and largely produced from industrial, commercial, residential sectors and agricultural. Waste streams resulting from these sectors are not efficiently used and considered as environmental problem. In addition, a large portion of the fossil fuel is imported to meet the industrial and domestic needs, thus causing concern for energy security. Therefore, the energy potential of these agricultural residues should be exploited to reduce the dependency on fossil fuel. From the renewable energy plan in Thailand, the utilization of biomass has been projected to increase from 0.5% of the total final energy consumption in 2002 to 8% in 2011 [1].

At present, major agro industries that have been commonly utilized biomass as fuel for cogeneration in Thailand are rice mills, sugar mills and oil palm mills. Some parts of biomass such as paddy husk, fiber and shell, or wood waste are burned directly to produce steam for rotating turbines, exhaust steam to use in process or burned to produce hot water boiler, etc. Apart from combustion, pyrolysis, and gasification are other thermochemical processes that can be used to convert biomass materials into usable products; gas, oil (in the case of pyrolysis), solid char and ash. Typically, combustion process needs air or oxygen, while gasification is a more reactive thermal process that utilizes partially air, oxygen, hydrogen, or steam for conversion. In contrast, pyrolysis is thermal degradation or volatilization of the biomass without the addition of air or oxygen.

So far, various agricultural byproducts and waste materials have been tested for the pyrolysis process, e.g.cassava peel, palm-tree cobs, rice husks, and olive stones; but not on physic nut (*Jatropha curcus* L.). Physic nut is small plant oil which is grown in tropical and subtropical countries as a living fence to protect gardens and fields from

animals. It produces small seeds which contain more than 30% of a non edible oil. Good quality biodiesel may be produced from the oil via transesterification process. Direct used of *Jatropha* oil is also possible with low speed diesel engine. Due to its high oil yield relatively easy to cultivate, it has been designated as one of the strategic plant to be used for supplement of oil from fossil fuel. However, extraction of oil from *Jatropha* seed would also yield residue which needed to be managed. Incineration of the residue would lead to air emission problem. Application of the residue as fertilizer or animal feed can be limited by logistic difficulties.

Therefore, this research first mainly focus on the pyrolysis process of *Jatropha* seed residue (Physic nut waste) in order to evaluate its potential as an alternative source of raw materials for sustainable energy production as well as utilization of this agricultural byproduct. Pyrolysis always produces a gas mainly containing CO₂, CO, H₂ and CH₄, a vapor that can be collected as a liquid and solid char. The thermal energy used to drive the pyrolysis reaction is applied indirectly by thermal conduction through the walls of a containment reactor, which can be characterized as either vertical or horizontal types. A rotary kiln is an example of a horizontal reactor while three main types of vertical reactors are fixed bed (up-draft and down-draft), fluidized, and entrained bed. Pyrolysis typically occurs at temperatures between 400 to 800°C [2]. As the temperature changes, the product distribution can be altered. Lower pyrolysis temperature usually produces more liquid products and higher temperature produces more gases. The speed of the process and rate of heat transfer also influences the product distribution. In this study, the slow (dynamic) and rapid (isothermal) pyrolysis of physic nut waste were investigated in fixed-bed tubular reactor. Slow pyrolysis or carbonization at low temperatures can be used to maximize the yield of solid char. Whereas, fast pyrolysis systems are continuously operated at temperatures generally in the range of 400 to 600°C and residence times of a few seconds to a fraction of a second. Rapid quenching is often used to maximize the production of liquid products, by condensing the gaseous molecules into a liquid.

Solid char from pyrolysis process can be further processed to obtain value-added product, such as activated carbon. Activated carbon is a processed carbon material with a highly developed porous structure and a large internal specific surface

area. It consists, principally of carbon (87 to 97%) but also contains such elements as hydrogen, oxygen, sulfur and nitrogen, as well as various compounds either originating from the raw materials used in its production or generated during its manufacture [3]. Activated carbon, also known as porous carbon, has been widely used as an absorbent in the separation and purification of gas and liquid. The application of this carbon has been considered a major unit operation in the chemical and petro-chemical and petro-chemical industries. In addition to serving as an adsorbent, high porosity carbon have recently been applied in the manufacture of high-performance layer capacitors. Activated carbon is also used as a catalyst or catalyst support and for tar cracking process. Because of the introduction of rigorous environment regulations and the development of new applications, the demand for activated carbon is expected to increase progressively. Therefore, the second objective of this thesis is to obtain these activated carbons from pyrolyzed physic nut waste chars via both chemical (KOH and NaOH) and physical activation (CO_2) process.

Generally, chemical activation process involves carbonizing the material after impregnation with potassium hydroxide (KOH), phosphoric acid (H_3PO_4), zinc chloride (ZnCl_2), carbonates of alkali metals and metal chlorides [4-5]. The temperature range for chemical activation is 400 to 800°C. These temperatures are lower than those needed for activation with gaseous agent (physical activation). During chemical activation the chemistry of pyrolysis changed and the different, macromolecular network system is established with enhanced porosity. In the physical activated process, carbon reacts with the oxidizing agent (steam, carbon dioxide and oxygen) and the resulting carbon oxide diffuse from the carbon surface. Owing to the partial gasification of the granules or grains, a porous structure builds up inside them.

For the pyrolysis liquid product called bio-oil, it actually is immiscible with liquid hydrocarbons, because of its high polarity and hydrophilic nature. Biomass pyrolysis oils contain aldehydes, ketones and other compounds that can react via aldol condensations during storage or handling to form layer molecules. Yields of bio-oil from wood and other biomass were in the range of ~20-70% depending on the feedstock composition. The bio-oil yields from physic nut waste are in the range of 20-30% depending on pyrolysis conditions. Viscosity of the physic nut waste oils was related to

fatty acid chain length and number of unsaturated bonds. Nevertheless, the results indicated that carbon chain length of liquid product from pyrolysis of physic nut waste is greater than that of diesel fuel and with in the range of gas oil. It may be use on slow speed, heavy machinery but further cracking and refining of this product are required in order to utilize it in place of gasoline or diesel. The chemistry of bio-oil can be manipulated by changing the thermal conditions of the process or by conducting pyrolysis in the process of catalysts.

Originally cracking was accomplished thermally but the catalytic process has almost completely replaced thermal cracking because of more gasoline having higher octane and less heavy oil and unsaturated gases products [6]. In addition, catalytic cracking does not reduce the heating value of the gas, as would be the case if the tars (high molecular weight hydrocarbons) were thermally cracked at a high temperature. In catalytic cracking, the catalyst may be used either insitu in the reactor or in a separate reactor downstream. Various catalysts have been used such as dolomite, olivine, alumina, and zeolite. One of the most popular tar catalysts is dolomite, which is effective catalyst when calcined. An alternative to dolomite is olivine, which are a naturally occurring mineral containing magnesium, iron oxide and silica. It has a favorable attrition resistance compared to dolomite and its catalytic activity is comparable. However, there has been no report on either catalytic activity of synthesized olivine or their performance on cracking of linear long chain hydrocarbon, e.g. glycerol. Therefore, the last objective in this research is to synthesize olivine via co-precipitation method followed by retreat those synthesized olivine with nickel metal by wet impregnation method. Steam reforming of waste glycerol from biodiesel production process was conduct to evaluate the performance of synthesized olivine and Ni/olivine catalysts.

This research is organized into several chapters. Chapter 2 provides a literature review related to this work. This includes some background on thermochemical process, a general review of activated carbon, and a review of catalytic cracking. Chapter 3 describes the experimental procedure and the characterization techniques used to evaluate products. The results on the appropriate operating condition (e.g. temperature, particle size and retention time) for pyrolysis of Physic nut waste using fixed bed reactor are presented in Chapter 4. The assessment included slow and fast pyrolysis trials. The

properties of solid char, liquid tar, and fuel gas derived from pyrolysis of physic nut waste were evaluated. In Chapter 5, the preparation and properties of activated carbon from pyrolyzed physic nut waste char via chemical and physical activation were investigated. The synthesis of olivine catalyst by a co-precipitation method and nickel/olivine catalyst via impregnation method were reported in Chapter 6. These two catalysts were later used for *in-situ* gasification/reforming of waste glycerol to investigate their efficiencies on this thermal conversion process for production of quality fuel. Chapter 7 provides the conclusions drawn from this study.

CHAPTER II

THEORY AND LITERATURE REVIEW

2.1 Biomass Energy Resource

As late as the mid 1800s, biomass supplied the vast majority of the world's energy and fuel needs and only started to be phased out in industrialized countries as the fossil fuel era began, slowly at first and then at a rapid rate. But with the onset of the First Oil Shock in the late 1970s, biomass was again realized by many governments and policy makers to be a viable, domestic, energy resource that has the potential of reducing oil consumption and imports and improving the balance of payments and deficit problems caused by dependency on imported oil. Although biomass energy has continued to be utilized in Third World countries as a source of fuels and energy for many years, it has become a renewable and is expected to exhibit substantial growth in the twenty-first century. The terminology "renewable carbon resource" for virgin and waste biomass is actually a misnomer because the earth's carbon is in a perpetual state of flux. Carbon is not consumed in the sense that it is no longer available in any form. Many reversible and irreversible chemical reactions occur in such a manner that the carbon cycle makes all forms of carbon, including fossil carbon resource, renewable. It is simply a matter of time that makes one form of carbon more renewable than another. If society could wait several million years so that natural processes could replenish depleted petroleum or natural gas deposits, presuming that replacement occurs, there would never be a shortage of organic fuels as they are distributed and accepted in the world's energy markets. Unfortunately, this cannot be done, so fixed carbon-containing materials that renew themselves over a time span short enough to make them continuously available in large quantities are needed to maintain and supplement energy supplies. Biomass is a major source of carbon that meets these requirements.

The capture of solar energy as fixed carbon that biomass via photosynthesis, during which carbon dioxide (CO_2) is converted to organic compounds, is the key initial step in the growth of biomass and is depicted by the equation



Carbohydrate, represented by the building block (CH₂O), is the primary organic product. For each gram mole of carbon fixed, about 470 kJ (112 kcal) is absorbed. Oxygen liberated in the process comes exclusively from the water, according to radioactive tracer experiments. Although there are still many unanswered questions regarding the detailed molecular mechanisms of photosynthesis, the prerequisites for virgin biomass growth are well established; CO₂, light in the visible region of the electromagnetic spectrum, the sensitizing capture efficiency of the incident solar radiation in biomass has been variously estimated to range from about 8% to as high as 15%, but in most actual situations, it is generally in the 1% range or less.

The main features of how biomass is used as a source of energy and fuels are schematically illustrated in Figure 2.1. Conventionally, biomass is harvested for feed, food, fiber, and materials of construction or is left in the growth areas where natural decomposition occurs. The decomposing biomass or the waste products from the harvesting and processing of biomass, if disposed of on or in land, can in theory be partially recovered after a long period of time as fossil fuels. This is indicated by the dashed lines in Figure 2.1. Alternatively, biomass and any wastes that result from its processing or consumption could be converted directly into synthetic organic fuels if suitable conversion processes were available. The energy content of biomass could be diverted instead to direct heating applications by combustion. Another route to energy products is to grow certain species of biomass such as the rubber tree (*Hevea brasiliensis*) in which high-energy hydrocarbons are formed within the species by natural biochemical mechanisms. In this case, biomass serves the dual role of a carbon-fixing apparatus and a continuous source of hydrocarbons without being consumed in the process. Other biomass species, such as the guayule bush, produce hydrocarbons also, but must be harvested to recover them. Conceptually, it can be seen from Figure 2.1 that there are several different pathways by which energy products and synthetic fuels might be manufactured.

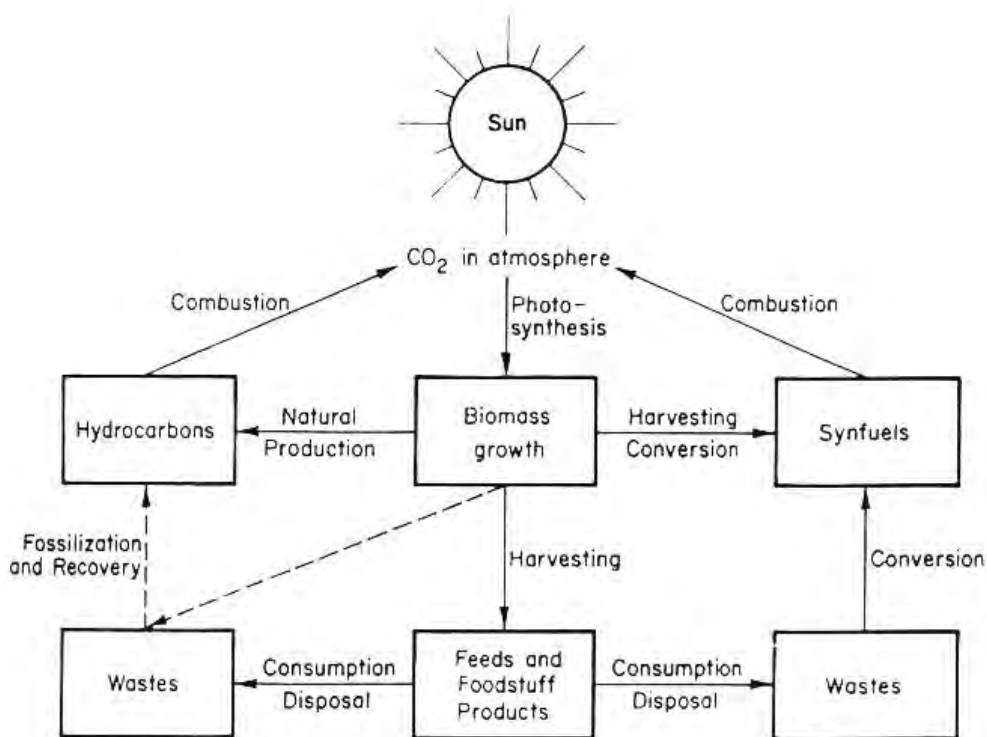
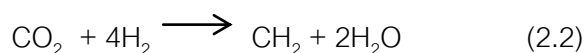


Figure 2.1 Main features of biomass energy technology

Another approach to the development of fixed carbon supplies from renewable carbon sources is to convert CO_2 outside the biomass species into synthetic fuels and organic intermediates. The ambient air, which contains about 360 ppm of CO_2 , the dissolved CO_2 and carbonates in the oceans, and the earth's large terrestrial carbonate deposits could serve as renewable carbon sources. But since CO_2 is the final oxidation state of fixed carbon, it contains no chemical energy. Energy must be supplied in a reduction step. A convenient method of supplying the required energy and of simultaneously reducing the oxidation state is to reduce CO_2 with elemental hydrogen. The end product, for example, can be methane, the dominant component of natural gas:



With all components in the ideal gas state, the standard enthalpy of the process is exothermic by -165 kJ (-39.4 kcal) per gram mole of methane formed. Biomass feedstocks could also serve as the original source of hydrogen via partial oxidation or steam reforming to an intermediate hydrogen-containing product gas. Hydrogen would then effectively act as an energy carrier from the biomass to the CO_2 to yield substitute

or synthetic natural gas (SNG). The production of other synthetic organic fuels can be conceptualized in a similar manner.

The basic concept then of biomass as a renewable energy resource comprises the capture of solar energy and carbon from ambient CO_2 in growing biomass, which is converted to other fuels (biofuels, synfuels) or is used directly as a source of thermal energy or hydrogen. One cycle is completed when the biomass or derived fuel is combusted. This equivalent to releasing the captured solar energy and returning the carbon fixed during photosynthesis to the atmosphere as CO_2 . Hydrocarbons identical to those in petroleum or natural gas can be manufactured from biomass feedstock. This means that essentially all of the products manufactured from petroleum and natural gas can be produced from biomass feedstock. Alternatively, biomass feedstock can be converted to organic fuels that are not found in petroleum or natural gas. The practical uses of biomass feedstock and the applications of biomass energy and derived fuels, however, are limited by several factors.

2.1.1 Virgin Biomass

Consider first the incident solar radiation, or insolation, that strikes the earth's surface. At an average daily insolation worldwide of about 220 W/m^2 (1676 Btu/ft^2), the annual insolation on about 0.01% of the earth's surface is approximately equal to all the primary energy consumed by humans each year. For the United States alone, the insolation on about 0.1 to 0.2% of its total surface is equivalent to its total annual energy consumption.

The most widespread and practical process for capture of this energy as organic fuels is the growth of virgin biomass. As already discussed, extremely large quantities of carbon are fixed each year in the form of terrestrial and aquatic biomass. Using the figures in Table 2.1, the energy content of standing biomass carbon; that is, the renewable, above-ground biomass reservoir that in theory could be harvested and used as an energy resource, is about 100 times the world's annual energy consumption. At a nominal biomass heating value of 18.6 GJ/dry t ($16 \times 10^6 \text{ Btu/dry ton}$) and assuming that the world's total annual coal, oil, and natural gas consumption is about 315 EJ

(1993), carbon, would be equivalent to the world's consumption of these fossil fuels. Since it is estimated that about 77 Gt of carbon, or 171 Gt of dry virgin biomass equivalent, most of which is wild and not controlled by humans, is fixed on the earth each year, it is certainly in order to consider biomass as a raw material for direct use as fuel or for conversion to large supplies of substitute fossil fuels. Under controlled conditions, dedicated biomass species might be grown specifically as energy crops or for multiple uses including energy. Relatively rapid replacement of the biomass utilized can take place through regrowth.

Table 2.1 Estimated Net Photosynthetic Production of Dry Biomass Carbon for World Biosphere

Ecosystem	Area (10 ⁶ km ²)	Mean net biomass Carbon production		Standing biomass carbon	
		(t/ha-year)	(Gt/year)	(t/ha)	(Gt)
Tropical rain forest	17.0	9.90	16.83	202.5	344
Boreal forest	12.0	3.60	4.32	90.0	108
Tropical season forest	7.5	7.20	5.40	157.5	118
Temperate deciduous forest	7.0	5.40	3.78	135.0	95
Temperate evergreen forest	5.0	5.85	2.93	157.5	79
Total	48.5		32.26		744
Extreme desert-rock, sand, ice	24.0	0.01	0.02	0.1	0.2
Desert and semi desert scrub	18.0	0.41	0.74	3.2	5.8
Savanna	15.0	4.05	6.08	18.0	27.0
Cultivated land	14.0	2.93	4.10	4.5	6.3

Ecosystem	Area (10 ⁶ km ²)	Mean net biomass Carbon production		Standing biomass carbon	
		(t/ha-year)	(Gt/year)	(t/ha)	(Gt)
Temperate grassland	9.0	2.70	2.43	7.2	6.5
Woodland and scrubland	8.5	3.15	2.68	27.0	23.0
Tundra and alpine	8.0	0.63	0.50	2.7	2.2
Swamp and marsh	2.0	13.50	2.70	67.5	14.0
Lake and stream	2.0	1.80	0.36	0.1	0.02
Total	100.5		19.61		85
Total continental	149.0		52.87		829
Open ocean	332.0	0.56	18.59	0.1	3.3
Continental shelf	36.6	1.62	4.31	0.004	0.1
Estuaries excluding marsh	1.4	6.75	0.95	4.5	0.6
Algae beds and reefs	0.6	11.25	0.68	9.0	0.5
Upwelling zones	0.4	2.25	0.09	0.9	0.04
Total marine	361.0		24.62		4.5
Grand total	510.0		77.49		833.5

A more realistic assessment of biomass as an energy resource can be made by calculating the average surface areas needed to produce sufficient biomass at different

annual yields to meet certain percentages of fuel demand for a particular country, and then to compare these areas with those that might be made available. Such an assessment for the United States could, for example, address the potential of biomass for conversion to SNG as shown in Table 2.2. For this analysis, the annual U.S. demand for natural gas is projected to reach 26.5 EJ (25.1 quad) by 2010 at an annual growth rate in consumption of 1.2% (U.S. Dept. of Energy, 1994). It is assumed that biomass, whether it be trees, plants, grasses, algae, or water plants, has a heating value of 18.6 GJ/dry t, is grown under controlled conditions in “methane plantations” at yields of 20 and 50 dry t/ha-year, and its converted in integrated biomass planting, harvesting, and conversion systems to SNG at an overall thermal efficiency of 50%. These conditions of biomass and conversion either are within the range of present technology and agricultural practice, or are believed to be attainable in the near future. Areas that are not used for productive purposes might be suitable, or possibly biomass for both energy and foodstuffs or energy and forest products applications can be grown simultaneously or sequentially in ways that would benefit both. Also, relatively small portions of the bordering oceans might supply the needed biomass growth areas, in which case, marine plants would be grown and harvested.

Table 2.2 Potential Substitute Natural Gas Production in United States from Virgin Biomass Feedstocks at Different Biomass Yields

Percent of natural gas Demand supplied	Average area required at indicated biomass yield (10 ⁶ ha)	
	20 dry t/ha-year	50 dry t/ha-year
1.42	2.02	0.81
10	14.3	5.7
50	71.2	28.5
100	142.5	57.0

This approach to the preliminary assessment of the potential of biomass energy presumes that suitable conversion processes are available for conversion of biomass to SNG. Other processes could be used to manufacture other synfuels such as synthesis gas, alcohols, esters, and hydrocarbons. The direct route alluded to in Figure 2.1 as natural production of hydrocarbons, can possibly bypass the harvesting-conversion routes. As already mentioned, some biomass species produce hydrocarbons as

metabolic products. Natural rubber, glycerides, and terpenes from selected biomass species for example, as well as other reduced compounds could be extracted and refined to yield conventional or substitute fossil fuels.

A second source of renewable carbon is the deposits and reservoirs of essentially non-energy carbon-forms ambient CO₂ and the lithospheric carbonates. The availability of such raw materials cannot be questioned, although low-cost separation and energy-efficient recovery of very small concentrations of CO₂ from the atmosphere present technological challenges. Another basic problem resides in the fact that all of the energy must be supplied by a second raw material, such as elemental hydrogen. Hydrogen would have to be made available in large quantities from a nonfossil source or the purpose of the synfuel system to produce renewable fuels would be defeated. Conceptually, there is no difficulty in developing such hydrogen sources. Hydrogen can be produced by water electrolysis and thermo chemical and photolytic splitting of water. Electrical power and thermal energy can be supplied by nonfossil-powered nuclear reactors, and by means of hydroelectric and wind systems, ocean thermal gradients, wave action, and solar-actuated devices. Hydrogen can also be manufactured from biomass and by direct action of solar energy on certain catalytic surfaces.

As already pointed out, about 16.9 Gt of dry biomass, or about 7.7 Gt of biomass carbon, would have approximately the same energy content as the total global consumption of coal, oil, and natural gas. This amount of carbon corresponds to less than 1.0% of the total standing biomass carbon of the earth. Under present conditions of controlled and natural production of fixed carbon supplies, the utilization of some of this carbon for energy applications seems to be a logical end use of a renewable raw material. Forest biomass is especially interesting for these applications because of its abundance. The expansion of controlled production of virgin biomass in dedicated energy crop systems should also be considered because this would result in new additions over the current low levels by means of marine biomass energy plantations in areas of the ocean that are dedicated to this objective. Unused croplands and federal lands might also be used for the production of herbaceous or woody biomass energy crops.

2.1.2 Waste Biomass

Another large source of renewable carbon supplies is waste biomass. It consists of a wide range of materials and includes municipal solid wastes (MSW), municipal bio-solids (sewage), industrial wastes, animal manures, agricultural crop and forestry residues, landscaping and tree clippings and trash, and dead biomass that results from nature's life cycles. Several of these wastes can cause serious health or environmental problems if they are not disposed of properly. Some wastes such as MSW can be considered to be a source of recyclables such as metals and glass in addition to energy. Thus, waste biomass is a potential energy resource in the same manner as virgin biomass.

To assess the potential impact of energy from waste biomass on supplying energy demand, it is necessary to consider the amounts of the different types of wastes generated, their energy contents, and their availabilities. Every person in the United States, for example, discards about 2.3 kg (5 lb) of MSW per day. From an energy standpoint, one short ton of MSW has an as-received energy content of about 9.5 GJ (9.0×10^6 million Btu), so about 2.2 EJ/year (2.1 quad/year) of energy potential resides in the MSW generated in the United States.

As for the amount of energy that can actually be recovered from a given waste and utilized, much depends on the waste type. The amount of available MSW, for example, is larger than the total amounts of available agricultural wastes even though much larger quantities of agricultural wastes, most of which are left in the fields where generated. The collection costs are prohibitive for most of these wastes. Note that municipal bio-solids on a dry solids basis is generated in the smallest quantity of all wastes. Its disposal, however, is among the most costly and difficult of all waste treatment operations.

Many studies have been carried out to estimate the potential of available virgin and waste biomass as energy resources. One is presented in Table 2.3 for the United States for the year 2000. The estimated energy potential of the recoverable materials is about 70% of the total recoverable energy potential and 50% of the estimated maximum

energy potential. These estimates of virgin and waste biomass energy potential are based on existing, sustainable biomass production and do not include new, dedicated biomass energy plantations that might be developed and placed in commercial operation.

The energy values are the higher heating values of the indicated biomass or derived methane. The conversion of biomass or methane to another biofuel or to steam, heat, or electric power requires that the process efficiency be used to reduce the potential energy available. These figures do not include additional biomass that could be grown as a dedicated energy crop.

Table 2.3 Potential Biomass Energy Available in United States in 2000

Energy source	Estimated Recoverable (EJ)	Theoretical Maximum (EJ)
Wood and wood wastes	11.0	26.4
Municipal solid wastes		
Incineration	1.9	2.1
Methane from landfills	0.2	1.1
Herbaceous biomass and agricultural residues	1.1	15.8
Aquatic biomass	0.8	8.1
Industrial solid wastes	0.2	2.2
Methane from municipal biosolids	0.1	0.2
Methane from farm animal manures	0.05	0.9
Miscellaneous wastes	0.05	1.1
Total	15.4	57.9

This review of the concept of utilizing biomass energy shows that when sufficient supplies of renewable carbon are available, virgin and waste biomass have the potential

of becoming basic energy resources. Presuming that suitable conversion processes are available, and that the demand for energy and established organic fuels and intermediates continues, an industry based on renewable biomass fuels and feedstock that can supply a significant portion of this demand is, at the very least, a technically feasible concept.

2.2 Structure and Chemical of Biomass

Biomass is a natural composite material and a chemical complex of cellulose, lignin, hemicelluloses, and extractives. Cellulose is the framework substance comprising 40 to 50% of wood in the form of cellulose micro fibrils, whereas hemicelluloses are the matrix substances present between cellulose micro fibrils. Lignin, on the other hand, is the encrusting substance solidifying the cell wall associated with the matrix substances. The significance of lignin as the encrusting substance can be demonstrated by examination of the lignin skeleton created by the acid removal of carbohydrates.

The roles of these three chemical substances in the cell wall are compared to those of the constructing material in the structures made from the reinforced concrete in which cellulose, lignin, and hemicelluloses correspond, respectively, to the iron core, cement, and buffering material to improve their bonding. Lignocellulosic materials are mostly cellulose, hemicellulose, and lignin in ratios of roughly 4:3:3. This can vary considerably as softwood contains typically 42 percent, 25 percent, and 28 percent of cellulose, hemicellulose, and lignin, respectively, whereas corn cobs contain about 40 percent, 36 percent, and 16 percent. Cellulosic biomass contains some protein as do all living cells, and some proposed energy feedstocks contain sufficient protein to justify recovery. In fact, edible protein is much more valuable than the fuels or chemicals designated as the main products. Ideally, biomass can feed the world, provide energy, and supply chemical feedstocks. Matching supply to demand for a multiproduct array is a formidable problem; thus a discussion should focus on one large-volume product and treat others as by-products. Trees, corn stover, and other biomasses composed mainly of structural portions of plants are relatively low in protein, and it is too costly and difficult to extract.

Cellulose is a polymer of glucose rings linked at the 1,4 positions. The 1,4 positions are also linked in starch, which has additional bonds at some of the 1,6 positions to form branches. Whereas the 1,4 links in starch are of the α type and very easily hydrolyzed, cellulose has β 1,4 links resistant to hydrolysis (Figure 2.2). Starch is a rather dynamic biochemical that serves as a food reserve that may be drawn on quickly and easily. In contrast, cellulose furnishes rigidity to plants and should maintain its integrity until death. Snails are one of the few animals to produce enzymes that attack cellulose. Other animals that feed on cellulose rely on microorganisms in their intestinal tracts to digest cellulose to smaller molecules that can be absorbed in the intestine. Rumen organisms, wood rots, and other microorganisms hydrolyze cellulose. Most are molds, but some bacteria produce cellulose enzymes.

Hemicellulose is a polymer with a linear chain of mostly xylose units jointed through 1-4 linkages plus side chains of diverse units such as arabinose, glucuronic acid, mannose, other pentoses, and hexoses (Figure 2.2). Side chains are usually initiated through 1-3 links to the linear portion. Hemicellulose is much lower in molecular weight than cellulose; roughly 100 to 200 monomers are polymerized. There is no highly ordered crystalline state as with cellulose.

Hydrolysis of hemicellulose to mono- and oligosaccharides is easily accomplished with either acids or enzymes under moderate conditions. Native cellulose resists hydrolysis because of (1) its highly ordered crystalline structure and (2) a physical barrier of lignin surrounding cellulose fibers. The 1,4- β -glucosidic linkage in cellulose may be about as easy to break as the 1-4- α -glucosidic linkage in starch if the cellulose molecules are fully hydrated and exposed and free of lignin. In other words, the primary linkage of the cellulosic polymeric chain may not be as important in causing slow and incomplete hydrolysis of cellulose as are secondary and tertiary structures of cellulosic materials.

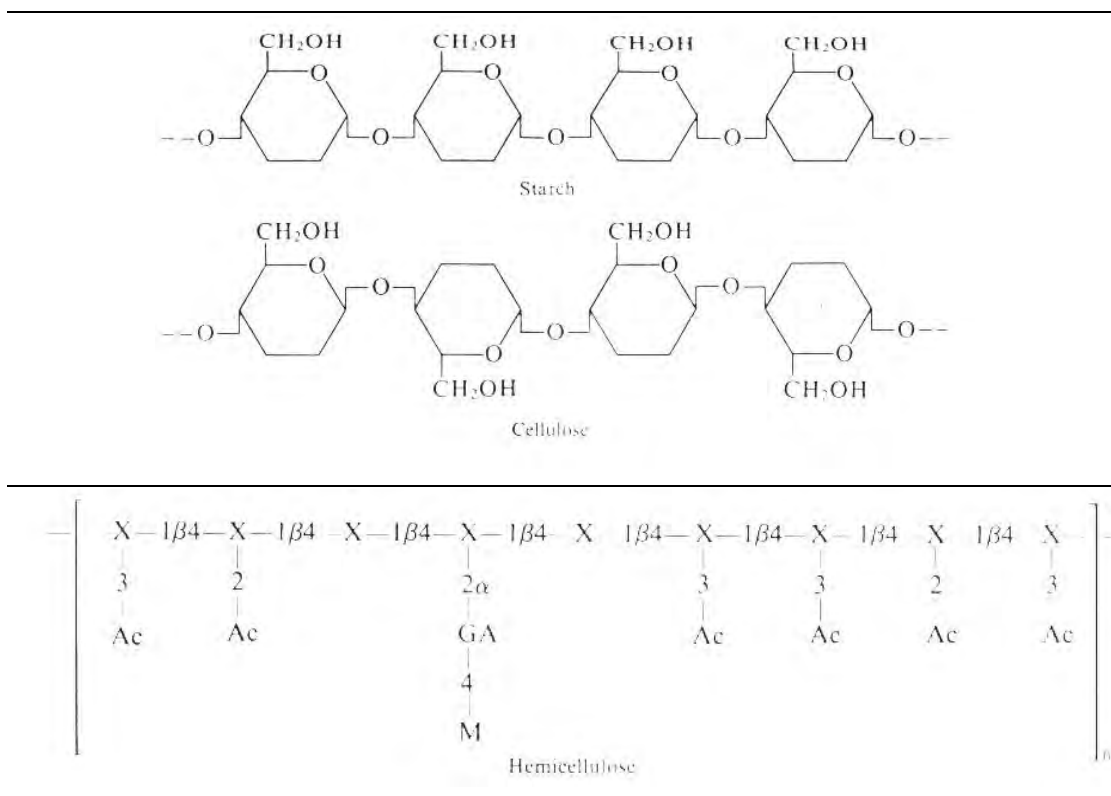


Figure 2.2 Structure of starch, cellulose, and hemicelluloses

Degree of polymerization (DP) is the number of glucose units in an average chain. Depending on its source, the cellulose DP ranges from about 1000 (cellulose in newspaper) to as high as 10,000 (in cotton). In hydrolysis with acids, the DP drops quickly and levels off at a more or less constant value of 100 to 200, corresponding to a length of 500 to 1000 Å. The easily hydrolysable portion of cellulose is often referred to as the “amorphous” region and the resistant residue, the “crystalline cellulose.” On average, cellulose is 15 percent amorphous and 85 percent crystalline. To hydrolyze crystalline cellulose, a strong acid at high temperature is needed; chemical and equipment costs can be prohibitively high. The strongly acidic conditions degrade some of the glucose into undesirable by-products.

Once the amorphous cellulose is removed, rod-shaped particles of crystalline cellulose can be obtained. In the case of cotton the particles are about 400 Å long and 100 Å wide. Further hydrolysis with strong acid can reduce particle weight by as much as 80 percent and yet the crystalline order remains. The crystalline structure of cellulose is still a subject of considerable controversy. Two major schools of thought exist. Based on the observation of chain folding in linear synthetic polymers, models of cellulose

fibrils involving folded chains have been suggested. On the other hand, models based on extended cellulose molecules are also found in the literature.

The anhydroglucose units are linked together through 1,4- β -glucosidic bonds, most of which exist in a configuration known as *Hermans form*. Through repeated Hermans β linkages, linear polymeric cellulose molecules can be built up. Variations of the normal Hermans form probably exist. With two or three such successive deflected β bonds, a loop can be formed in a cellulose polymer to produce a 180° U tern essential for chain folding. These exposed, deflected β linkages are likely to be more susceptible to hydrolytic cleavage. Therefore, the so-called amorphous regions in a cellulose fibril could be zones rich in loop bonds containing many deflected β -glucosidic linkages. After hydrolysis by a dilute acid that removes “amorphous” regions, cellulose left is of an increased “crystallinity” and is very resistant to further acid hydrolysis.

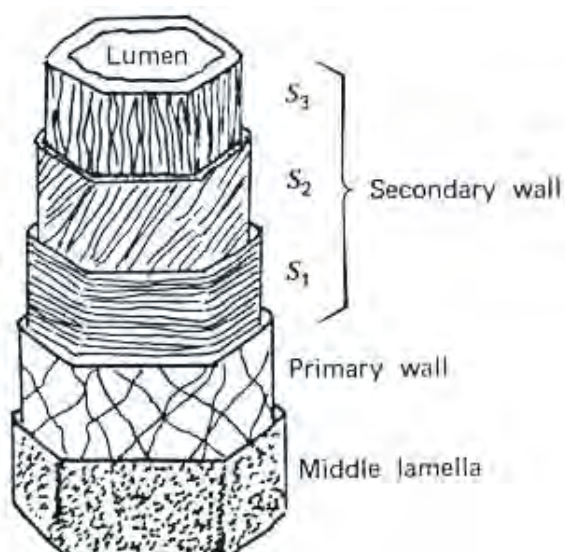


Figure 2.3 Structure of plant stalks

Native cellulose fibers exist in the cell walls of trees and other vegetative materials. The cell wall architecture is schematically depicted in Figure 2.3, which suggests the cementing role of lignin and the hindrance it creates to cellulose hydrolysis. The lumen represents space once occupied by the cytoplasm of the living cell. Surrounding the fiber is a region called the *middle lamella*, which contains mostly

lignin. The outermost layer of the fiber is called the *primary wall*, which was formed on cell division. The secondary wall, formed during the growth and maturation of the cell, is subdivided into the transition lamella (S_1), the main secondary wall (S_2), and the inner secondary wall (S_3). The middle lamella is about 1 to 2 microns thick, amorphous, and generally porous. The primary wall is usually very thin, but the secondary wall (S_1 , S_2 and S_3) thickens during cell growth and contains the majority of cellulose. Some molds send their hyphen right into the lumen for efficient digestion.

With the concepts of strong crystalline structure and lignin barrier, the difficulties of cellulose hydrolysis by either acids or enzymes are understandable. Acids are nonspecific catalysts that can attack cellulose and, to a small extent, paper. Only very strong acids can hydrolyze cellulose well, but they also promote the degradation of glucose and reduce its yield. Cellulases can convert cellulose into glucose with few by-products. Cellulase enzymes cannot easily penetrate through the lignin seal surrounding the cellulose fibers; thus the problem is nonaccessibility of cellulose to the enzymes.

The structure of a piece of cellulosic material is analogous to that of a reinforced concrete pillar with cellulose fibers resembling the metal rods and the lignin the natural cement. To obtain a significant amount of glucose from a piece of cellulosic material, the material is often pretreated. Mechanical grinding is an obvious method. Mechanical milling to reduce a piece of cellulosic material to small particles of an average size of 400 mesh can enhance the sugar production with 48 hours of contact with enzymes from about 50 to about 75 percent. Unfortunately, the cost of milling is too high. Hemicellulose is insoluble in water, soluble in dilute alkali, and very readily hydrolyzed by dilute acid. There are two types: that found in cellulose fibrils and the spongelike, amorphous material between cells.

Lignin is a very complicated polymer of a wide variety of phenolic compounds. Figure 2.4 shows a structure for lignin and its principal monomers. Ether linkages between aromatic rings are possible at several positions; thus a three-dimensional structure results. Many-OH and methoxy groups are present. Lignin is slowly decomposed by microorganisms, but the aromatic rings are opened before the ether

bonds are broken. Catalytic hydrogenation can cleave the ethers to give valuable aromatic compounds. Biological cleavage of aromatic ethers has not been observed. The resulting phenols would be toxic, so a microbial process to produce them is unlikely. After extracting hemicellulose, the solid mass could be treated with a solvent for either lignin or cellulose. Lignin is fairly soluble in butanol, xylene, and the like; however, the insoluble cellulose may retain its crystallinity and be resistant to hydrolysis.

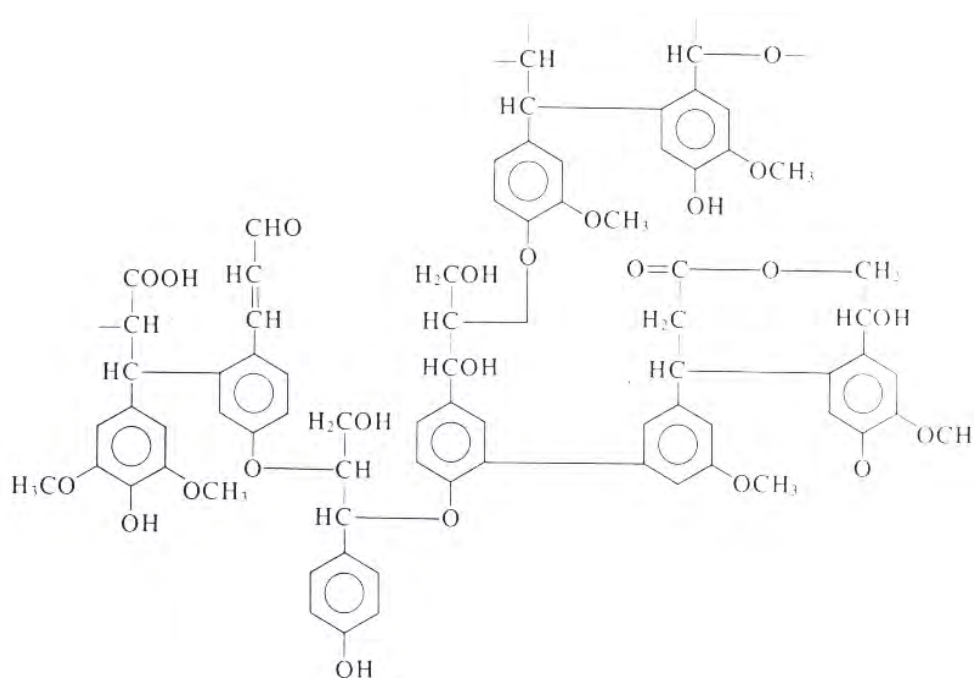


Figure 2.4 Structure of lignin

Dissolution of the cellulose instead renders it more amorphous and leads to easy hydrolysis. Ladisch has tested a number of solvents for cellulose and found several that are effective. It has not been necessary to solubilize the cellulose, and soaking in the solvent destroys enough of the crystallinity to permit ready hydrolysis so that the resulting sugar solution can be washed away from the residue of lignin.

Some perspective on the resistance of lignin to microbial attack is gained from research by Martin and Haider. Radiotracer experiments showed that only 48 percent of the carbon atoms in the aromatic rings was oxidized to CO₂ after 6 months of incubation in fertile sandy-loam soil. Carbon atoms in the side chains were more readily attacked, and 60 percent appeared as CO₂ in the same time period. Although lignin is degraded

in soil and thus has some fertilizer value, the rates even with rich mixed cultures are discouragingly slow for consideration as the basis for an industrial process. Addition of easily metabolizable substances has little effect on the rate of lignin degradation, and there are little differences in the rates of attack on lignins from various materials. Ban, Glanser-Soljan, et al. report reasonably rapid degradation of lignin with mixed culture of microorganisms. The substrate was calcium lignosulfonate from pulping of beechwood, and the culture contained at least two yeasts and two bacteria. About one-half of the lignin was destroyed in 24 hours. Several other papers report lignin degradation.

2.3 Biomass Pyrolysis

The pyrolysis of biomass is a thermal treatment which results in the production of char, liquid and gaseous products. This process is mainly carried out in the absence of oxygen. Pyrolysis is interesting, not only as an independent process leading to the production of energetically-dense products, but also as an intermediate step in a gasification or combustion process. This process is one of the most energy efficient of all the conversion process currently under investigation. Pyrolysis oil is a versatile product and has been used successfully as fuel for commercial kiln patio and in the operation of power boiler. Pyrolysis oil has already been tested by Trane Thermal in their Vortex burner and by KVB in a test boiler. Both these tests were successful. The oil has been blended and test-burned successfully with pulverized char and/or other fuel oils. Thus, pyrolysis oil from wood has been demonstrated to be an acceptable fuel oil in commercial applications. It has also been demonstrated to be a technically viable fuel for use in gas turbines.

Wood pyrolysis oil also has potential as a chemical feedstock. Plenty of research project in the field of thermochemical conversion of biomass and particularly on biomass pyrolysis have been carried out. The results of this research have proved the feasibility of this technology. Many results regarding the identification of the wide spectrum of substances produced and their physico-chemical characterizations are no available. The problems associated with the realization of the process and the utilization of the products have been made evident.

In the past few years, much effort has been focused on the optimization of the operating conditions in order to obtain the most favourable yields of products and to improve their quality. By changing the operation conditions during pyrolysis the course of the reaction and nature of final product can be changed. Pre-requirement conditions, biomass pretreatment process, technical limitations, safety and cleaning are few steps common to all dry and thermo-chemical processes involved in conversion of biomass to gaseous or liquid fuels and many other products.

2.3.1 Operational Experiences

Before entering the pyrolysis reactor the biomass feedstock e.g. straw, wood, MSW (Municipal Solid Waste) etc. must be reduced to fine particle sizes so that high heat transfer rates may be attained for shortening the residence pyrolysis time, and thereby maximizing liquid yields. Pyrolysis can be carried out with or without catalyst. Flash pyrolysis occurs at 500°C and 101 KPa pressure in the absence of a catalyst. The solid char is separated from the product fluids with cyclone separators after leaving the reaction vessel. The char is then recycled to the reactor as a heat source following its combustion with air, and rapid mixing occurs within the reactor as the suspended materials pass upwards under turbulent flow. Rapid heat transfer is thus effected, minimizing further degradation of substances formed and optimizing liquid fuel yields by way of the very short residence time achieved. The vapourized material passes to a gas/oil separation unit to be quenched rapidly from 500 to 600°C so as to prevent the large molecule oil components from cracking further to less useful end-products. Separation is carried out into pyrolytic oil, gas and water.

As stated earlier, some of the outlet gases are utilized to convey shredded feed material into the reactor, the remainder being combusted in the process heater to raise the temperature of the carrier gases, char and rotary kiln dryer. Commonly, the energy content of the pyrolysis gases is around 14 MJ/m. The percentage of oil, tar and other gases depend mainly on the type of biomass feedstock and temperature as already stated earlier. Table 2.4 gives an account of production of oil and other components of a pyrolysis plant mainly based on municipal refuse feedstock. The oil obtained from such

process is viscous, chemically complex and having low sulfur content. The gaseous pollutants emitted during pyrolysis are, usually, passed through a bag house and after burner at 650°C for atleast 0.5 second, and then exhausted through another bagther to the atmosphere. The particulate pollutant produced along the gas are usually dealt with by landfilling.

Table 2.4 Energy content of gas, oil, tar from a municipal refuse feedstock based pyrolysis plant

Nature of products	Quantity of product (% of feedstock)	Energy content MJ/kg
Char	10	19
Gas	20	15
Oil	30	25

The oils obtained *via* pyrolysis are invariably complex mixtures of hydrocarbons, ketones, aldehydes and other organic compounds, while the gases may contain carbon monoxide, carbon dioxide, hydrogen, ethylene, methane, ethane and various other hydrocarbons in smaller quantities.

At an elevated pressure (> atmospheric) and > 500°C and < 700°C, generally oil is formed. When the temperature goes beyond 700°C, the pyrolysis reactor is predominated with charcoal which can be used even for briquettes as a solid fuel. Pyrolysis of organic materials to hydrogen and carbon monoxide would enable methanol synthesis, while the pyrolytic oils could be purified and upgraded.

2.3.2 Types of pyrolysis

On the basis operating conditions, the pyrolysis process can be divided as shown in Table 2.5.

Table 2.5 Different types of pyrolysis process based on range of temperature

	(°C) pyrolysis	Fast pyrolysis	Flash pyrolysis
Operating temperature (°C)	300 - 700	600 - 1000	800 - 1000
Heating range (°C/S)	0.1 – 1.0	10 - 200	> 11000
Solid residence time (S)	600 - 6000	0.5 – 5.0	< 0.5
Particle size (mm)	5 - 50	< 1	-

2.3.2.1 Conventional pyrolysis

It is defined as the pyrolysis which occurs under slow heating rate. This condition permits the production of solid, liquid and gaseous pyrolysis products in significant proportions. A typical diagram of a conventional pyrolysis apparatus is Figure 2.5. It consists of a moving-bed reactor (inner diameter $id = 100$ mm, height $h = 500$ mm) which is placed in an electrically heated oven.

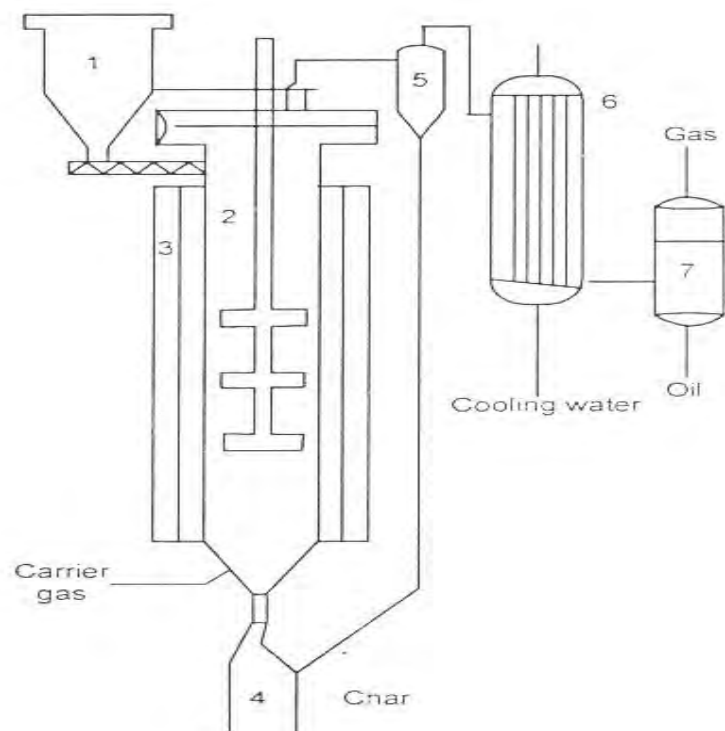


Figure 2.5 Flow diagram of the bench scale pyrolysis reactor. 1. biomass feeder, 2. moving bed reactor, 3. electric oven, 4. char collector, 5. hot cyclone, 6. heat exchanger, 7. entrainment separator

The biomass is fed to the reactor by a screw feeder and deposits on a rotating grate, where it receives a counter current gas stream which is generally introduced at the bottom of the reactor. The purpose of feeding gas is to remove the volatile product of the pyrolysis and carry them outside the reactor. The gaseous stream leaving the reactor passes through a hot cyclone where the entrained char dust is separated. The liquid product is condensed in a heat exchanger. The gas flow is measured with a gas meter and analyzed on line by chromatography. The char is extracted from the reactor through the rotating grate collected under the reactor. Typical data on chemical and elemental analysis of different biomass used in conventional pyrolysis is given in Table 2.6.

Figure 2.6 shows a typical thermogram obtained with TA 3000 where three ideal stages can be distinguished. The first, which occurred between 120 and 200°C, can be called prepyrolysis. During this stage some internal rearrangement (water elimination, bond breakage, appearance of free radical, formation of carbonyl, carboxyl and hydroperoxide groups) takes place. A small weight loss is observed, caused mainly by the release of H₂O, CO₂ and CO.

Table 2.6 Chemical and elemental analysis and heating values of tested materials (%wt)

Biomass	Hemi-cellulose	Cellulose	Lignin	Extra-actives	Ash	C	H	O	N	Moisture (%wt)	LHV MJ/kg dry biomass
Wood	19.4	47.5	24.0	7.5	1.6	47.8	5.1	45.4	0.1	33	17
Hazel Nut	24.1	27.5	40.7	3.9	1.0	44.5	5.0	49.0	0.5	10	17
Shell											
Olive husks	21.1	22.2	45.0	8.1	3.6	47.5	5.8	37.5	1.5	9	19
Corn-cobs	31.8	51.2	14.8	1.2	1.0	45.8	6.2	46.7	0.3	12	17
Wheat-straw	40.0	24.0	21.0	8.0	8.0	42.3	5.3	43.9	0.3	7	17
Lucerne-Pressed cake	45.5	13.7	21.3	10.6	7.6	45.4	5.5	39.3	2.9	8	18

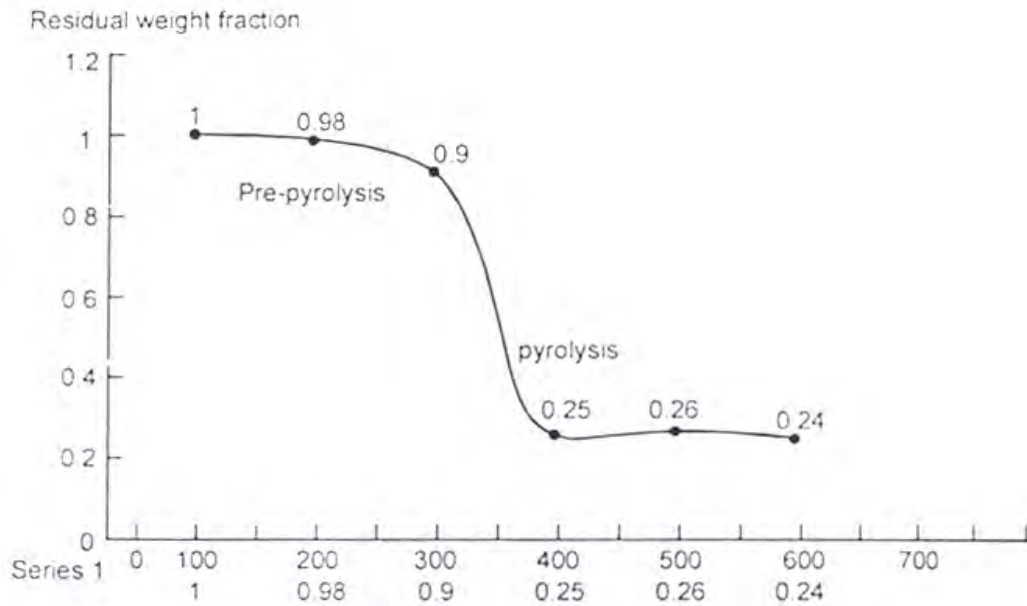


Figure 2.6 Thermogram of pyrolysis of biomass (hard wood) heating rate = 20 k/min

When a lignocellulosic material is heated at low temperature ($< 200^{\circ}\text{C}$), even for a long time period, a small weight loss occurs and no significant external modifications of the material are observed. However, after this treatment, the internal structure of the biomass is changed. Thus, the pyrolysis yield of this material will be different from the yields of material which has not received this preliminary treatment. This means that prepyrolysis is important for the progress of the whole process.

In the second stage, the biomass is subscribed to pyrolysis process. The thermochemical reaction at this stage is very fast and leads to the formation of the pyrolysis products. This reaction is generally carried out at temperature 300 and 800°C . In the third stage of this thermochemical reaction, the char decomposes at a very slow rate and the solid residue reaches an asymptotic value. This continuous devolatilization of the char, due to further cleavage of the C-H and C-O bonds, results in the carbon enrichment of the residual solid. Different rate and temperature for the three stages have been noticed when lignocellulosic materials with different chemical composition were tested. The heating rate effect can be interpreted in terms of temperature and residence time effect.

(a) Qualitative and Quantitative Nature of Yields

Table 2.7 shows the yields of pyrolysis products obtained through conventional process. The most interesting temperature range for the production, in significant amounts of the pyrolysis products, is between 350 and 550°C. The charcoal yield decreases as the temperature increases. The production of the liquid fraction has a maximum at temperatures between 350 and 450°C. At much elevated temperatures, large molecule presenting the liquid are broken down to produce smaller molecules which enrich the gaseous phase. Thus, when the temperature exceeds 500°C a rather sudden decrease of the liquid yield is noticed and gas production is enhanced. In lignin-rich biomass charcoal production is favored, but a higher pyrolysis time is required to reach the final conversion.

Table 2.7 Yields of conventional pyrolysis product (wt%)

Temperature (°C)	350	400	500	550
Biomass: Wood				
Char	29.0	26.1	22.9	21.1
Tar fraction	11.5	11.4	10.1	9.4
Aqueous fraction	34.0	33.5	33.3	31.4
Gas	25.5	28.7	32.7	36.4
Biomass: Olive husks				
Char	36.2	31.5	28.2	22.3
Tar fraction	12.2	11.5	9.2	7.4
Aqueous fraction	27.4	27.5	23.5	19.2
Gas	24.2	29.4	39.5	48.2

(i) Charcoal The nature of the charcoal obtained from various types of biomass is given in Table 2.8. The heating value of charcoal is lower than that of common coal but higher than of many other solid fuels (e.g. lignite). With ecological criteria, charcoal is a very interesting fuel due to its low ash, sulfur and nitrogen content. The bulk density of charcoal ranges from 150 to 300 kg/m³. Charcoal has also good adsorbent properties towards dyes and, consequently, it can be used as a substitute for activated carbon.

Table 2.8 Elemental analysis (wt%) and heating values (MJ/kg) of charcoal produced by conventional pyrolysis 450°C

Source of charcoal	C	H	O	N	Ash	HHV	LHV
Wheat straw	66.4	2.7	11.1	0.6	17.1	25	24
Lucerne pressed	61.6	2.9	13.8	2.4	16.3	23	22
Olive husks	64.7	5.2	11.6	2.4	7.5	28	23
Pine cones	82.9	2.7	10.6	0.2	1.7	31	30
Wood	72.2	3.0	17.4	0.4	2.6	28	27

Chlorine and sulfur content very low

(ii) Liquid Generally, the liquid fraction of the pyrolysis products consists of two phases: an aqueous phase consisting of a wide range of organo-oxygen compounds of molecular weight and a non-aqueous phase containing insoluble organics (mainly aromatics) of high molecular weight [15-17]. This phase is called bio-oil or tar and is the product of great interest. Conventional pyrolysis gives a relatively low yield of bio-oil. A wide range of organic substances are contained in the liquid fraction. The elemental analysis and the heating values of bio-oils derived by the pyrolysis of different biomass types are given in Table 2.9. The heating value of 'bio-oil' and the rather high density (930-1500 kg/m) makes it a rather energetically dense fuel. It has high oxygen content. On the other hand it contains very low amount of ash and essentially no sulfur.

Table 2.9 Elemental analysis (wt%) and heating values (MJ/kg) of bio-oil produced by conventional 450°C

Bio-oil from	H	O	N	Ash	HHV	LHV
Wheat straw	65.2	8.2	24.2	0.5	0.2	27
Lucerne pressed	64.7	5.4	25.3	3.8	0.3	27
Olive husks	64.5	7.7	19.9	3.1	0.3	30
Pine cones	66.1	7.5	23.1	0.6	0.1	27
Wood	52.3	6.7	38.4	0.2	0.1	23

Chlorine and sulfur content very low

Due to its low pH aqueous phase the bio-oil is very corrosive in nature. The bio-oil is soluble in solvent such as heptane and gas oil. This viscosity of bio-oil increases on exposure to air. This is due to polymerization. Bio-oil is unstable when it is exposed at 150°C.

Since the bio-oil has high BOD and COD, it is supposed to create environmental problems while disposing the same to nature. However, the aqueous phase can be reduced by a preliminary drying of the biomass, the residual water produced by pyrolysis, containing about 20 percent by weight of organic compounds, can be incinerated in the combustion unit of the pyrolysis plant.

(iii) Gases Carbon monoxide and dioxide, hydrogen, low quantity of methane and small amount of hydrocarbons are the main gaseous product during conventional pyrolysis. Table 2.10 shows a typical composition of gas generating during conventional pyrolysis. The heating of the pyrolysis gas is about 10 to 15 MJ/nm. Raising the temperature about 700°C shows remarkable increase in the hydrogen content which could have been caused due to gasification phenomena.

Table 2.10 Chemical composition of gaseous products of the conventional pyrolysis of hazel nut shells at different operating temperature (% vol)

Temperature (°C)	400	550	650	750	800	850
H ₂	7.3	10	18	33	37	40.5
CO ₂	25.5	20	15	16.4	11	7.6
C ₂ H ₄	0.7	1	1	0.6	0.2	-
C ₂ H ₂	0.9	4	3	12	0.4	0.1
CH ₄	13.4	13	16	13.5	10.7	8.5
CO	30.0	41	35	25.2	33.5	37.1
Organic compounds	22.5	12	10.5	8.0	7.0	5.5

2.3.2.2 Fast Pyrolysis (Ultra Pyrolysis)

In an earlier section, it has been discussed that fast heating rates minimize the final charcoal yield. Complete conversion of biomass without any charcoal production is possible by thermal degradation at very high temperature and heating rates. In addition, very high yields of olefins and other valuable hydrocarbons are predicted. This process of pyrolysis is known as fast pyrolysis or ultra pyrolysis.

Of the many traditional and novel thermochemical conversion pathways being investigated, fast pyrolysis has shown particular promising yields of high quality chemical intermediate. A thorough characterization of fast pyrolysis and an outline of specific advantages have been detailed in many earlier documents [10, 18-19]. Fundamental research has indicated that olefin yields of 10 to 15 percent by weight of the biomass feedstock can be realized and that little or no char need be formed under conditions of short vapour residence time (less than 500 ms), high reactor temperatures (greater than 700°C), rapid heating rates (thousands of degrees celsius per second) and rapid quenching of the reactor production.

Biomass Processing

The biomass is fed to the reactor entrained by a gas stream (inert gas or steam) by a specially designed feeder. The reactor consists of a spiral coiled tube ($d = 10$ mm, $l = 20,000$ mm) inserted in the furnace. In the reactor, the temperature of the steam increases rapidly and the pyrolysis of the biomass particles and a considerable reforming of tar take place. The gaseous products, with restricted amount of charcoal and residual tar, leaving the reactor are cooled in a heat exchange. After the separation of the solids the gas-flow rate is measured in a gas meter.

Table 2.11 Biomass feedstock analysis

Material	Mass % Moisture Received	Element analysis (% by mass)						Empirical Formula
		C	H	O	S	N	Ash	
Cellulose	4.01	43.32	6.32	50.34	0.001	0.02	0.03	CH _{1.75} C _{0.87}

(A vicel)								
Lignin	4.75	65.5	5.4	27.2	1.7	-	-	CH _{0.99} C _{0.31}
(Indulin)								
Birch wood	5.54	48.66	6.37	44.33	0.04	0.1	0.5	CH _{1.57} C _{0.68}

Table 2.11 shows typical data on the pyrolysis products. The high temperatures favour some secondary reactions such as cracking and tar reforming. On the hand, above 800°C partial gasification process are involved and as a consequence, an enrichment of gas production is obtained.

The composition of the gaseous streams for different pyrolysis temperatures are given in Table 2.12. The gas is rich in hydrogen and carbon monoxide. The content of methane and organic compounds decrease as the temperature increases. Generally the gas produced by fast pyrolysis is of a medium quantity of gas. However, its quality is better as compared to the gas produced by conventional pyrolysis. The char produced by fast pyrolysis is considered a marginal product, as its yield does not exceed 15 percent by weight. Due to its higher ash content, it is less valuable than the conventional pyrolysis charcoal.

Table 2.12 Yields of the products obtained by fast pyrolysis biomass: hazel nut shells

Temperature (°C)	Char (kg/kg biomass)	Gas (kg/kg biomass)	Tar (%) (kg/kg biomass)
700	0.28	0.68	7
720	0.27	0.73	6.8
750	0.24	0.79	6.1
800	0.16	0.90	4.5
850	0.11	1.21	3.7
900	0.11	1.28	2.1

2.3.2.3 Flash Pyrolysis

This pyrolysis is carried out by a fluidized bed of solid as heat carrier, over a temperature range of 400 to 650°C. The reactor is so designed that during pyrolysis the char formed is blown from the bed and the sand is retained in the bed. Special “blow-through” method of operation has been use during such practice.

Occidental research Corporation claims that by means of flash pyrolysis process, minimum electricity is consumed and the overall process of flash pyrolysis is entirely energy self-sufficient. This capable of high liquid yields from lignocellulosic materials. Yield of organic liquids from hard woods, such as poplar, or maple, agricultural wastes gives liquid yields of 40-65 percent. Pyrolysis oils produced are suitable for use as low grade liquid fuels. A medium quality gas and a reactive char are also produced.

(a) Process Technology

Flash pyrolysis is suitable for biomass, particularly saw mill dust, bark and other highly solidified biowaste. However, Occidental Research Corporation’s flash pyrolysis [9] is even very much suitable for municipal refuse. The outstanding economic feature of this biomass process is the costs associated with harvesting the material. If the biomass is available as a waste at a central facility, the supply will be limited. If the biomass is to be harvested, this can only be done economically over a restricted distance, possibly about 50 km. As a result of this limitation of supply at a site, a biomass conversion process should be economical on a small a scale, so that the plant could be located at the source of raw material supply. Products from several such conventional plants could then be shipped readily to a common site for further processing.

For the small scale pilot unit sawdust or other biomass is air dried and then hammer milled and screened to 595 μm (30 mesh) particle size. The sawdust is conveyed form a hopper by a variable speed twin screw feeder, at the end of which the biomass particles are swept off the screw discharge by a flow of recycled product gas and are conveyed into the reactor. The feed injection point is within the fluid bed itself. The reactor contains sand as the fluidized material, and the fluidizing gas is recycled product gas which has been preheated in the inlet line by controlled electric

heaters. In addition, the reactor is wrapped with heating coils allowing extra heat to be added either to the bed of sand or to free board space as desired.

Pyrolysis products are swept from the reactor to a cyclone, together with all the char formed. The char is separated in the cyclone and the product gas and vapours pass to two condensers in series. These condensers have the pyrolysis gas inside the tubes, which are vertical. Every tube has clean-out plug at the top and a condensate collection pot at the bottom. The first condenser can be operated at temperatures up to 100°C, while the second condenser uses chilled water at 0°C as a cooling medium. The gas from the condensers passes through a series of filters to remove tar mist and then discharged to fluidize the reactor and to convey feed into the reactor, while the excess is vented through a gas analyzer and gas meter as product gas.

The method of operation of the fluidized bed reactor is unique in this process. Existing fluid bed pyrolysis technology normally uses twin fluid beds, in the first of which pyrolysis occurs. The sand and char are then circulated to a second fluid bed where the char is burned and the sand heated. The hot sand is then returned to the first bed to supply the required heat of reaction. While this method of pyrolysis is used commercially e.g. for municipal waste gasified, it can have operating problems with transfer lines, and is expensive. In the reactor, the design has been carried out so that during pyrolysis the char form is blown from the bed and the sand is retained in the bed. By carefully selecting sand size, biomass particle size, bed velocity and reactor configuration, this method of operation can readily be successfully achieved. This “blown-through” method of operation has been used without problem under a variety of conditions in the continuous unit.

The residence time in the reactor is difficult to define. However, the residence is calculated as an apparent gas residence time, based on the volumetric flow rate of the total fluidizing gas at reactor conditions and the net empty reactor volume. The fact, actual vapors residence time will be less than this, because of the vapor volume generated in pyrolysis. This extra volume flow would reduce the apparent vapors residence time by about 15 percent on an average. Char residence time is not

known with any certainty, but the small char accumulation in the bed at any time suggests that it would be only slightly longer than that of the vapors.

Temperature and pressure are monitored throughout the unit, the former by means of thermocouples, and the latter by differential and absolute type gauges. Normally, a run is started by bringing the reactor to temperature with total recycle and nitrogen flowing in the system. After reaching a suitable temperature level, biomass feed is started (from 1.5 to 3.0 kg/hr) and within about 10-20 minutes the system can reach a final steady state with respect to both temperature and gas composition. For bench scale reactor, such time varied from 45 to 120 minutes and temperatures from 425 to 625°C. Reactor pressure is usually about 125 KPa absolute.

(b) Product analysis

In general, four products are recovered from flash pyrolysis. From the two condensers a fairly fluid oil is obtained which also contains most of the water produced. The "liquor" fraction varies from about 50 percent of the total liquid yield for wheat straw to about 85 percent for poplar-aspen and maple. It is a dark fluid, with an acrid smell, easily pourable and showing only one phase. It contains from 15 to 30 percent water depending on the type of feed and its moisture content. This oil appears to be stable on the self over periods of weeks if not exposed to air.

After a run, the condensers are washed with acetone, solution filtered and the acetone subsequently evaporated under vacuum to yield a "tar" fraction. Additional tar is collected in the filters which are also weighed before and after a run. If the tar amount in the filters is substantial, which is the case only at the highest temperature or for wheat straw feed, the filters are also washed with acetone and the tar recovered. All liquid products are readily soluble in acetone.

Char is collected from the char pot. This char is very reactive and precautions are required to ensure that it should not react with air when hot. The residue from the filtration of the tar fraction, that is, any acetone insoluble material recovered is also included in the char fraction. The gases produced during such process are mainly CO, CO₂ and other gases. At temperature about 550°C, there is a considerably larger gas yield. The gas produced is a medium quality gas with a higher heating value of

about 14.4 MJ/std m for the composition obtained at elevated temperature (about 500°C). This heating value increases at higher pyrolysis temperatures as CH content increases and CO content decreases. The char from clean wood shows a steady increase in carbon content and decrease in hydrogen content with temperature, with the H/C molar ratio falling from 1.19 at 425°C to 0.38 at 625°C.

H/C ratio for the organic liquid appears to be approximately constant at about 1.3 over the range of 425 to 625°C. The development process based on the thermal pyrolysis of biomass have been directed largely to gasification, either for fuel gas or synthesis gas production, and many such processes have been described. The pyrolysis of biomass to give a maximum direct yield of liquid product has received much less attention, and very few studies have been reported.

2.3.2.4 Vacuum Pyrolysis

Thermal decomposition under a reduced pressure is also an attractive approach for the conversion of biomass into chemicals and liquid fuel product. This process is carried out in a staged multiple hearth furnace at typical temperature of 350 to 450°C.

(a) Process Technology

The main reactor is a multiple hearth furnace, with six hearths 2 m high by 0.71 m in diameter. Heat transfer is provided through heating elements immersed in ceramics within each of the six metallic heating plates. The whole reactor is actually made of stainless steel.

Wood chips are fed in a continuous mode from a hopper which sits on top of the reactor. Wood chips are poured batch wise at the onset of an experiment in the hopper which is equipped with a feeding device. The hopper is hermetically sealed. Wood chips are fed at a rate of typically 1-2 kg hr⁻¹ for a period of 6 to 8 hours. Contact time of the solid feedstock in the furnace is approximately 30 minutes.

A mechanical vacuum pump draws the organic vapour and gas product from the reactor through a series of outlets provided along the external wall of the reactor. The gas vapours are received in a glass cooler which is the metallic flanges. The condensable vapours are received in a row of glass jars which serves as condensation unit at the bottom of the cooling unit. The non-condensable gases (H_2 , N_2 , CO_2 , CO , CH_4 and light hydrocarbons) are continuously received in a metallic vessel which is set under a vacuum at rattles which are attached to the main rotating shaft within the reactor. The residual char is received in a metallic vessel which is attached to the bottom of the reactor body.

(b) Product Analysis

As stated earlier, this process is carried out under vacuum in a staged multiple hearth furnace. Liquid product fractions contain oil about 45 to 50 percent by weight (moisture ash-free basis). Detailed reports are also available on characterization of vacuum pyrolysis liquid product fractions.

2.4 Gasification technology

A range of reactor configurations have been developed, as shown in Table 2.13. Figures 2.7-2.9 show the configurations of the more common gasified types. At the end of this section, Table 2.14 summarizes the key features of each reactor type, Table 2.15 summarizes the other relative advantages and disadvantages of the most common gasifier types and Tables 2.16 and 2.17 summarize performance data for most gasifier types. Each main type of gasifier configuration is described below, with significant features and limitations highlighted.

2.4.1 Downdraft

The downdraft gasifier features a co-current flow of gases and solids through a descending packed

Table 2.13 Gasifier types

Gasifier type	Mode of contact
<i>Fixed bed</i>	
Downdraft	Solid moves down, gas moves down
Updraft	Solid moves down, gas moves up
Co-current	Solid & gas move in same direction – downdraft
Counter-current	Solid & gas move in opposite directions – updraft
Cross-current	Solid moves down, gas moves at right angles
Variations	Stirred bed; two-stage gasifier
<i>Fluid bed</i>	
Single reactor	Low gas velocity; inert solid stays in reactor
Fast fluid bed	Inert solid is elutriated with product gas and recycled
Circulating bed	Inert solid is elutriated, separated and recirculated. This sometimes also refers to fast fluid bed or twin reactor systems
Entrained bed	Usually no inert solid; highest gas velocity of lean phase systems; can be run as a cyclonic reactor
Twin reactor	Steam gasification and/or pyrolysis occurs in the first reactor; char is combusted in the second reactor to heat the fluidizing medium for recirculation. Either can be any type of fluid bed, although the combustor is often a bubbling fluid bed
<i>Moving bed</i>	Mechanical transport of solid, usually lower temperature processes; includes multiple hearth, horizontal moving bed, sloping hearth, screw/auger kiln
<i>Other</i>	Rotary kiln: good gas-solid contact; careful design needed to avoid solid carry-over Cyclonic and vortex reactors: high particle velocities give high reaction rates

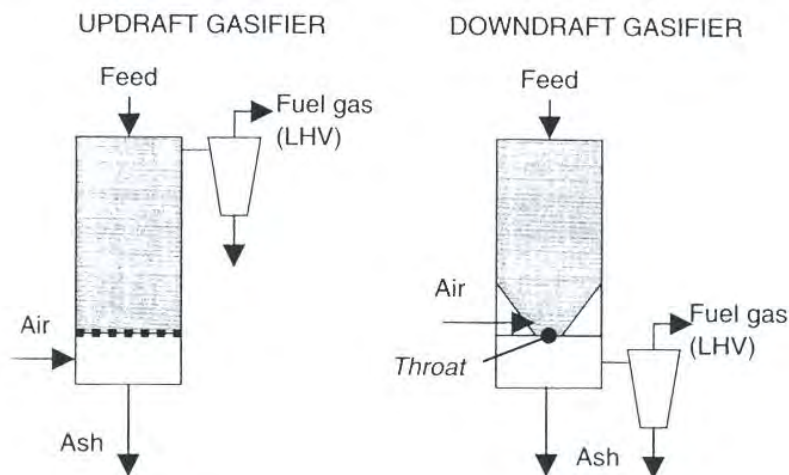


Figure 2.7 Fixed-bed gasifiers: updraft and downdraft

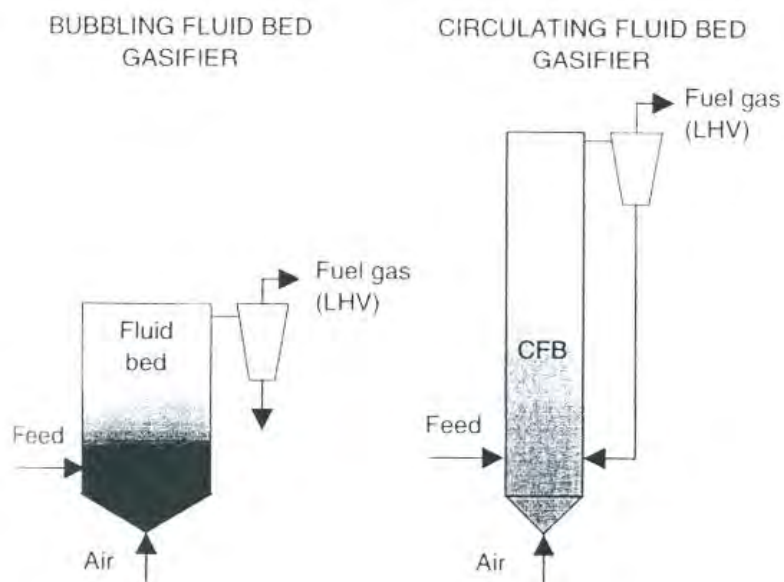


Figure 2.8 Bubbling and circulating fluid-bed gasifiers

The reaction products are intimately mixed in the turbulent high-temperature region around the throat, which aids tar cracking. Some tar cracking also occurs below the throat on a residual charcoal bed where the gasification process is completed. This configuration results in a high conversion of pyrolysis intermediates and hence a relatively clean gas.

Downdraft gasification is simple, reliable and proven for certain fuels, such as relatively dry (up to about 30 %wt moisture) blocks or lumps with a low ash content (below 1 %wt) and containing a low proportion of fine and coarse particles (not smaller

than about 1 cm and not bigger than about 30 cm in the longest dimension). Owing to the low content of tars in the gas, this configuration is generally favored for small-scale electricity generation with an internal combustion engine. The physical limitations of the diameter and particle size relationship mean that there is a practical upper limit to the capacity of this configuration of around 500 kg h^{-1} or 500 kWe.

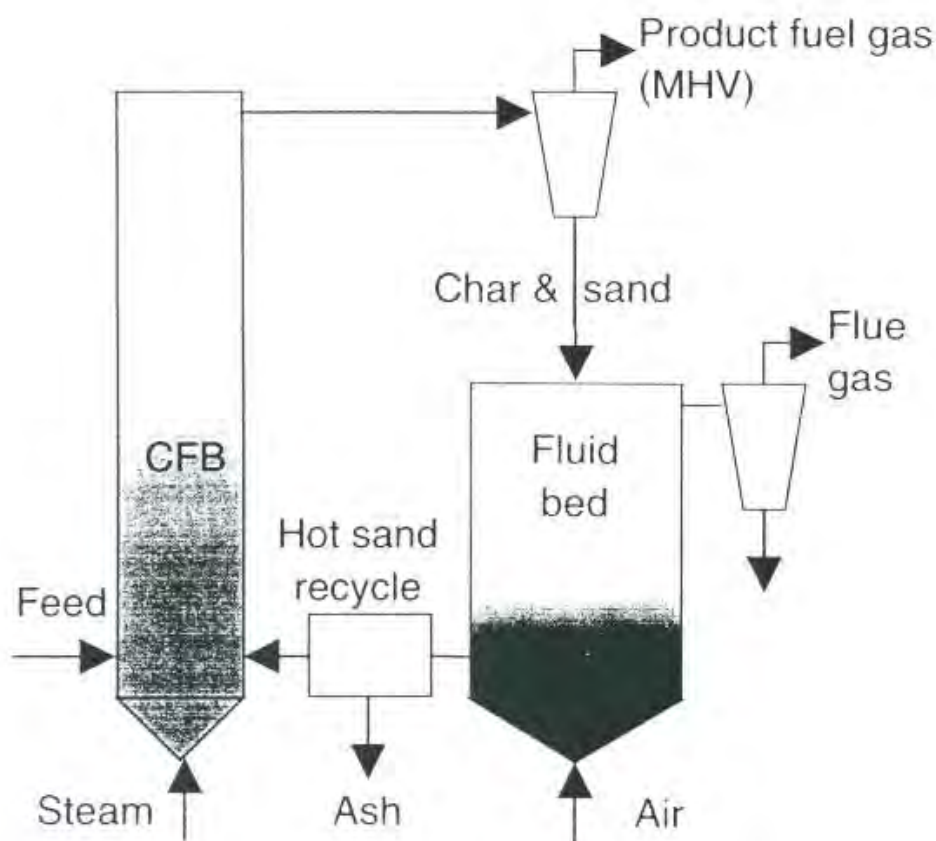


Figure 2.9 Twin fluid-be gasifier

A relatively new concept of a stratified or open-core downdraft gasifier has been developed in which there is no throat and the bed is supported on a grate. This was first devised by the Chinese for rice husk gasification and further developed by Syngas Inc. [23] from work carried out at the Solar Energy Research Institute (now the National Renewable Energy Laboratory – NREL). The concept is still widely practiced in China for rice husk gasification.

2.4.2 Updraft

The updraft gasifier arrangement is shown in Figure 2.7. The downward-moving biomass is first dried by the upflowing hot product gas. After drying, the solid fuel is pyrolyzed, giving char that continues to move down to be gasified and pyrolysis vapors that are carried upward by the upflowing hot product gas. The tars in the vapor either condense on the cool descending fuel or are carried out of the reactor with the product gas, contributing to its high tar content. The extent of this tar 'bypassing' is believed to be up to 20% of the pyrolysis products. The condensed tars are recycled back to the reaction zones where they are further cracked to gas and char. In the bottom gasification zone the solid char from pyrolysis and tar cracking is partially oxidized with the incoming air or oxygen. Steam may also be added to provide a higher level of hydrogen in the gas.

The product gas from an updraft gasifier thus has a significant proportion of tars and hydrocarbons, which contribute to its high heating value. The fuel gas requires substantial clean-up if further processing is to be performed. The principal advantages of updraft gasifiers are their simple construction and high thermal efficiency: the sensible heat of the gas produced is recovered by direct heat exchange with the entering feed, which thus is dried, preheated and pyrolyzed prior to entering the gasification zone. In principle, there is little scaling limitation, although no very large biomass gasifiers have been built.

2.4.3 Fluid bed

Fluid-bed gasifiers are a more recent development that takes advantage of the excellent mixing characteristics and high reaction rates of this method of gas-solid contacting. Although only recently applied to biomass, there are over 50 years of experience with peat. Fluid-bed reactors are the only gasifiers with isothermal bed operation. A typical operating temperature for biomass gasification is about 800-850 K. Most of the conversion of the feedstock to product gas takes place within the bed. However, some conversion to product gas continues in the freeboard section from reactions of entrained small particles and particularly from thermal tar cracking. In most

cases, carbon conversion approaches 100%, unless excessive carry-over of fines takes place, which will occur with a top-feeding configuration.

The bubbling fluid-bed gasifier tends to produce a gas with a tar content between that of the updraft and downdraft gasifiers. Some pyrolysis products are swept out of the fluid bed by gasification products, but are then further converted by thermal cracking in the freeboard region. Loss of fluidization due to bed sintering is also a commonly encountered problem, depending on the thermal characteristics of the ash, but the inherently lower operating temperature of a fluid bed and better temperature control provide an acceptable control measure. The problem is that alkali metals from the biomass ash form low-melting eutectic with the silica in the sand, resulting in agglomeration and bed sintering with eventual loss of fluidization. With biomass of high ash/inert content, it is better to use alumina or even a metallic sand such as chromate sand.

Carbon loss with entrained ash can, however, become significant and fluid beds are not economical for small-scale applications. Moreover, they incur higher operating (i.e. compression) costs. Fluid-bed gasifiers also have the advantage that they can be readily scaled up with considerable confidence. Only the fuel distribution becomes problematic in large beds, although multiple feeding is an acceptable solution. Alternative configurations such as twin bed systems and circulating fluid beds are also available to suit almost every type of feedstock or thermochemical process. In catalytic thermochemical process the bed material can be replaced by the catalyst, thereby avoiding costly impregnation techniques. Alternatively, a second catalytic reactor, as in the TPS system, or a thermal cracking reactor can be added.

Fluid beds provide many features that are not present in the fixed-bed types, including high rates of heat and mass transfer and good mixing of the solid phase, which means that reaction rates are high and the temperature is more or less constant in the bed. A relatively small particle size compared to dense-phase gasifiers is desirable and this may require additional size reduction. The ash is elutriated and removed as fine particulates entrained in the off-gas.

2.4.4 Circulating fluid bed

The fluidizing velocity in the circulating fluid bed is high enough to entrain large amounts of solids with the product gas. These systems were developed so that the entrained material is recycled back to the fluid bed to improve the carbon conversion efficiency compared with the single fluid-bed design. A hot raw gas is produced, which, in most commercial applications to date, is used for close-coupled process heat or retrofitting to boilers to recover the sensible heat in the gas. This configuration has been developed extensively for wood waste conversion in pulp and paper mills for firing lime and cement kilns and steam generation for electricity.

2.4.5 Entrained bed

In entrained-flow gasifiers no inert material is present but a finely reduced feedstock is required. Entrained bed gasifiers operate at much higher temperatures of about 1200-1500 °K, depending on whether air or oxygen is employed, and hence the product gas has low concentrations of tars and condensable gases. However, this high-temperature operation creates problems of material selection and ash melting. Conversion in entrained beds effectively approaches 100%. There is little experience with biomass in such systems.

2.4.6 Twin fluid bed

Twin fluid-bed gasifiers are employed to give a gas of higher heating value from reaction with air than from a single air-blown gasifier. The gasifier in effect is a pyrolyzer, heated with hot sand from the second fluid bed, which is heated by burning the product char in air before recirculating it back to the first reactor. Steam is also usually added to encourage the shift reaction to generate hydrogen and to encourage carbon-steam reactions. Product quality is good from a heating value viewpoint but poor in terms of tar loading from the pyrolysis process.

2.4.7 Comparison of pressurized and atmospheric operation

The relative advantage and disadvantages of pressurized gasification systems have not been fully resolved. Pressurized gasifiers have the following notable features:

- Feeding is more complex and very costly, and has a high inert gas requirement for purging.
- Capital costs of pressure equipment are much higher than atmospheric equipment, although sizes are much smaller.
- Gas is supplied to the turbine at pressure, removing the need for gas compression and also permitting relatively high tar contents in the gas. Hot gas clean-up also reduces energy losses and, in principle, is simpler and of lower cost than scrubbing systems.
- Overall system efficiency is higher due to retention of sensible heat and chemical energy of tars in the product gas.

Atmospheric gasifiers have the following notable features:

- For gas turbine applications, the product gas is required to be sufficiently clean for compression prior to the turbine. For engine applications, the gas quality requirements are less onerous and pressure is not required.
- Atmospheric systems have a potentially much lower capital cost at smaller capacities of below around 30 MWe.
- Gas compositions and heating values are not significantly different for either system.

2.4.8 Summary

A summary of the relative advantages and disadvantages is given in Table 2.14.

Table 2.14 Gasifier characteristics

Gasifier type	Characteristics
Downdraft	High residence time of solids

Simple, reliable and proven for certain fuels	Needs low-moisture fuels
Relatively simple construction	High carbon conversion
Close specification on feedstock characteristics	Low ash carry-over
Uniform-sized feedstock required	Fairly clean gas is produced
Very limited scale-up potential	Low specific capacity
Possible ash fusion and clinker formation on grate	

Updraft

Product gas is very dirty with high levels of tars	Low exit gas temperature
Very simple and robust construction	High thermal efficiency
Good scale-up potential	High carbon conversion
Suitable for direct firing	Low ash carry-over
High residence time of solids	
Relatively simple construction	

Bubbling fluid bed

Good temperature control & high reaction rates	Good scale-up potential
In-bed catalytic processing is possible	Low feedstock inventory
Greater tolerance to particle size range	Carbon loss with ash
Moderate tar levels in product gas	Good temperature control
Higher particulates in the product gas	High specific capacity
Good gas-solid contact and mixing	Can operate at partial load
Tolerates variations in fuel quality	
Easily started and stopped	

Circulating fluid bed

Good temperature control & high reaction rates	High specific capacity
In-bed catalytic processing not possible	Very good scale-up potential
Greater tolerance to particle size range	High carbon conversion
Moderate tar levels in product gas	Good gas-solid contact
Relatively simple construction and operation	

Entrained flow

Costly feed preparation needed for woody biomass	Slagging of ash
--	-----------------

High temperatures give good gas quality	Very good scale-up potential
Produces tar-free gas and little methane	High conversion
Good gas-solid contact and mixing	High specific capacity
Twin fluid bed	
MHV gas produced with air, without oxygen	Catalyst can be added to bed
Complex and hence costly design	Scale-up complex
Moderate tar levels requiring cracking or cleaning	High specific capacity
Complexity requires capacities of greater than 5 t h ⁻¹	Good gas-solid contact

2.5 Products of gasification

The products of gasification will vary according to the reactor configuration and oxidant used. Ideally, there is complete conversion of all tars, hydrocarbons and char in the gasifier to give fuel gas. However, reactor design can give rise to incomplete oxidation, the extent of which is mostly determined by reactor geometry. Typical gasifier features are summarized in Table 2.15 and were compared in Table 2.14. Product characteristics are summarized in Table 2.16 and typical gas compositions are summarized in Table 2.17.

Table 2.15 Typical gasifier characteristics (all air-blown)

Gasifier type	Reaction temp. (°C)	Exit gas temp. (°C)	Tars	Particulates	Turn-down	Scalability	Current max. (t h ⁻¹)	Min. (t h ⁻¹)	Max. (MWe*)
Fixed bed									
Downdraft	1000	800	Very low	Moderate	Good	Poor	0.5	0.1	1
Updraft	1000	250	Very high	Moderate	Good	Good	10	1	20
Cross-current	900	900	Very high	High	Fair	Poor	1	0.1	2
Fluid bed									
Single reactor	850	800	Fair	High	Good	Good	10	1	20
Fast fluid bed	850	850	Low	Very high	Good	Very good	20	2	40
Circulating bed	850	850	Low	Very high	Good	Very good	20	2	40
Entrained bed	1000	1000	Low	Very high	Poor	Good	20	5	40
Twin reactor	800	700	High	High	Fair	Good	10	2	20
Moving bed									
Multiple hearth	700	600	High	Low	Poor	Good	5	1	10
Horizontal moving bed	700	600	High	Low	Fair	Fair	5	1	10
Sloping hearth	800	700	Low	Low	Poor	Fair	2	0.5	4
Screw/auger kiln	800	700	High	Low	Fair	Fair	2	0.5	4
Other									
Rotary kiln	800	800	High	High	Poor	Fair	10	2	20
Cyclone reactors	900	900	Low	Very high	Poor	Fair	5	1	10

Table 2.16 Gasification product gas characteristics

	Capacity (t h ⁻¹)	Capacity* (MWe)	Feed	HHV (MJm ⁻³)	Gas quality	Outlet temp. (°K)
Downdraft, air	0.1-7	0.2-1.4	1	4-6	4	700-1000
Downdraft, oxygen	1-5	2-10	1	9-11	4	700-1100
Updraft, air	0.5-10	1-20	2	4-6	3	100-400
Updraft, oxygen	1-10	2-20	2	8-14	3	100-700
Single fluid bed, air	0.5-15	1-30	4	4-6	3	500-900
Single fluid bed, oxygen	2-10	4-20	4	8-14	3	700-1100

Single fluid bed, steam	1-10	2-20	4	12-18	3	700-900
Circulating fluid bed, air	2-20	4-40	3	5-6.5	2	700-1100
Circulating fluid bed, oxygen	2-20	4-40	3	10-13	3	800-1200
Twin fluid bed	1-10	2-20	4	13-20	3	750-1000
Cross-flow, air	0.1-0.5	0.2-1	2	4-6	1	600-900
Horizontal moving bed, air	0.5-5	1.10	5	4-6	2	300-800
Rotary kiln, air	1-10	2-20	5	4-6	2	600-1000
Multiple hearth	1-20	2-40	3	4-6	2	400-700
Secondary processing	-	-	-	-	5	1000-1200

* Conversion at 36% overall efficiency.

Table 2.17 Typical product gas compositions from different gasifiers

	Gas composition (dry vol.%)					HHV (MJ m ⁻³)	Gas quality	
	H ₂	CO	CO ₂	CH ₄	N ₂		Tars	Dust
Fluid bed air-blown	9	14	20	7	50	5.4	Fair	Poor
Updraft air-blown	11	24	9	3	53	5.5	Poor	Good
Downdraft air-blown	17	21	13	1	48	5.7	Good	Fair
Downdraft oxygen-blown	32	48	15	2	3	10.4	Good	Good
Multi-solid fluid bed	15	47	15	23	0	16.1	Fair	Poor
Twin fluid bed	31	48	0	21	0	17.4	Fair	Poor
Pyrolysis (for comparison)	40	20	18	21	1	13.3	Poor	Good

2.6 Carbon Materials

From a structural point of view, carbon materials, collectively, from a family of carbons. Yet, at the same time, each individual carbon possesses specific properties. Each carbon has a unique identity. This chapter considers this family of carbons in terms of related structures and how these affect porosity because the origins, extents

and characteristics of porosity are intimate functions of structure within each carbon. Activate carbons are a major part of this family of carbons. *The specific objective here is to present descriptions of structures of carbons and to asses how these structures control the characteristics of adsorption in the porosity of carbons.*

This chapter emphasizes that (apart from diamond, Figure 2.10) structures in all known carbon forms are considered as a continuous decrease in the degree of order from the single-crystal hexagonal graphite (Figure 2.11) to the most disordered (there is never total disorder) of the porous carbons and the glassy carbons with their closed (inaccessible) porosit. Within hexagonal graphite, the layers of hexagonal arrangements of carbon atoms are described as *grapheme layers*.

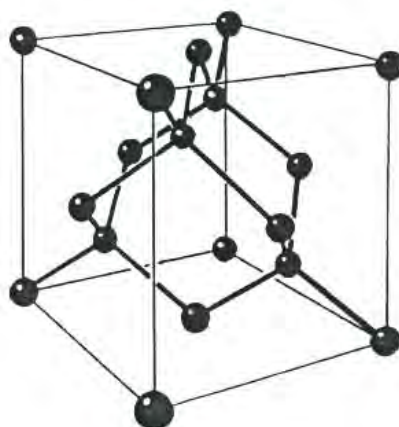


Figure 2.10 A model of the cubic unit cell of diamond. The internal carbon atoms are bonded to three other carbon atoms, with sp^3 -symmetry, as in methane.

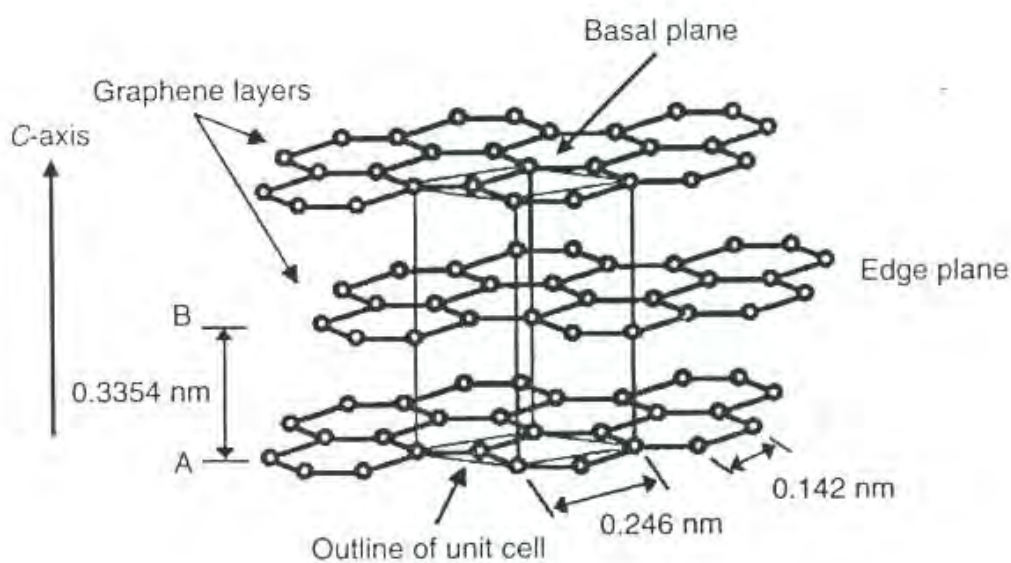


Figure 2.11 The structure of hexagonal graphite, with trigonal planar bonding within the grapheme layers

These layers do not lie immediately above and below each other but are displaced to form an ABABAB sequence. The density of hexagonal graphite is $\sim 2.25 \text{ g cm}^{-3}$. The distance between the layers is 0.335 nm (335 pm) and the distance between two bonded carbon atoms is 0.142 nm (142 pm). Within the graphitic layers, the bonding is trigonal sp^2 -hybird σ -bonds with delocalized π -bonds within the layers. The interlayer spacing of 0.335 nm, being larger than the 0.142 nm of the C-C bond, indicates no chemical bonding between the layers, the forces of attraction being limited to van der Waals forces. This distance is between the values of 0.153 and 0.132 nm for Csp^3 - Csp^3 bonding as in ethane and $Csp^3 = Csp^3$ bonding as in ethane. Resonance considerations indicate that the C to C bonding within a graphite layer has about one-third double-bond character. Such a graphite structure is referred to as AB graphite.

2.6.1 Preparation of Carbons in Solid Phase Activated carbon

Carbon forms, although from a structural point of view representing a progressive and continuous series of change, individually have quite specific methods of preparation and these have to be considered to demonstrate the several mechanisms by which carbon forms are created. Always, carbon materials result from the *carbonization* of organic materials; that is, their heat treatment in an inert atmosphere to a required temperature resulting in increases in carbon contents and decrease in contents of heteroatoms. Such carbonizations occur in the solid, the liquid and the gas phases.

In solid-phase carbonizations the parent material, almost always being a macromolecular system, naturally occurring or synthetic, essentially “decomposes” as the HTT increases, the process being accompanied by the evolution of gases and liquids of low molecular weight resulting from the decomposition processes. Consequently, the resultant carbon is a “pseudo morph” of the parent material, having more or less the same original shape but it is now of a lower bulk density (Figures 2.12).

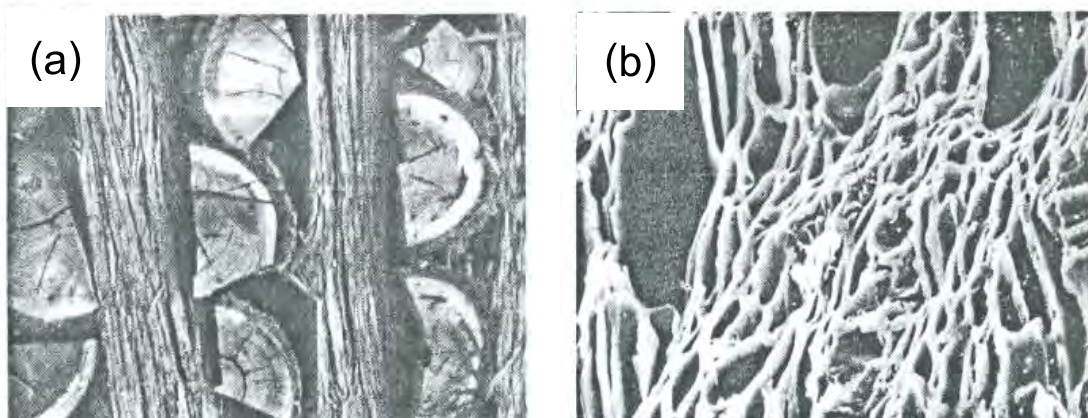


Figure 2.12 Scanning electron microscopy (SEM) photograph of (a) Photograph of stacked wood Trunks prior to carbonization (b) carbonized wood (100 x 70 m) showing that the structure of the wood has not liquefied

A solid-phase carbonization process is a progressive decomposition which will cease when the heat treatment is stopped. Increasing further the HTT results in the formation of progressively more stable intermediate structures. The structure in a carbon of a defined HTT can be considered as being “frozen” at that HTT. During the carbonization process, when the parent macromolecular system is decomposing, remaining carbon atoms of the macromolecular network move short distances (probably <1 nm) within the network to positions of greater stability (e.g. formation of six-membered ring systems), eventually creating a network of carbon atoms (with residual hydrogen bonded to it) which constitutes structure in such carbons. Different parent substances (e.g. a brown coal or coconut shell) decompose in their own distinctive ways to product a specific type of carbon. The spaces (of atomic dimensions) vacated by the evolution of the heteroatoms, the migration of carbon atoms and their co-bonding to form the network of carbon atoms constitute porosity, each porous carbon having its

own specific porous characteristics. Graphitizable carbons are never produced in solid-phase carbonizations. From the industrial point of view, lignin-cellulose precursors and coals dominate carbonizations in the solid state. The carbons produced are the *non-graphitizable, isotropic* type with considerable microporosity.

A question which now arises is how best to consider structure in such materials. The idea was introduced above that one approach is to consider such carbons to be composed of small segments of a graphene layer (defective micro-graphene layer), containing say about 20-30 carbon atoms, the layers being non-linear, enclosing five- and seven-membered ring systems with considerable strain. Such fragments of carbon material bond together in a continuous way to create a stable "macromolecular" network of carbon atoms imparting physical strength.

A microporous carbon, with a surface area of $1000\text{m}^2\text{g}^{-1}$, adsorbs nitrogen at 0.1 MPa pressure and 77°K to the extent of 10mmol g^{-1} . One gram of carbon is equivalent to 80 mmol of carbon atoms indicating that one adsorption site (pore) uses about 8 carbon atoms for the adsorption of one nitrogen molecule. This small number indicates that with such a carbon ($1000\text{m}^2\text{g}^{-1}$) all (or almost all) of the carbon atoms of its structure make up an adsorption site; that is, they are surface atoms. This feature must enter into any modeling of porosity which is undertaken.

This proportion of carbon atoms to nitrogen molecules, for example, or the dilution of the nitrogen molecule with the carbon atoms is shown in Figure 2.13 (oversimplified). The three-dimensional aspect is not considered. If the model diagram is re-considered, then the walls, containing the cages, must be composed of no more than two defective micro-graphene layers, not four or five as in the Franklin model. This is an important consideration.

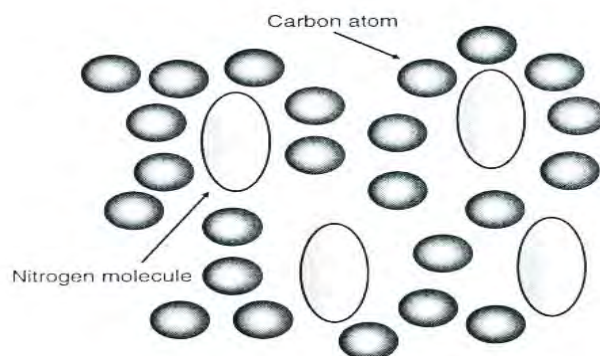


Figure 2.13 This model shows the ratio of nitrogen molecules to carbon atoms for a carbon of $1000\text{m}^{-1}\text{g}^{-1}$, filled with adsorbed nitrogen at $77\text{ }^{\circ}\text{K}$

2.6.2 Preparation of carbon in Liquid Phase

Liquid-phase carbonizations, of aromatic, pitch-like materials, lead to the formation of graphitizable carbons which, essentially, are non-porous carbons. Hence, to make a porous-activated carbon from these materials requires a reaction which will force apart the stacked graphene-type layers.

In liquid-phase carbonizations, the mechanisms are completely different from those in the solid phase. It is via liquid-phase carbonizations (but not all liquid phase) that graphitizable forms of carbon result. The explanation takes us to a quite different subject area, that of anisotropic aromatic, discotic, nematic liquid crystals (called mesophase) formed as a result as result of growth and self-assembly of the constituent polycyclic aromatic molecules of the parent material. These usually are the highly aromatic coal-tar pitches, a liquid product from the making of metallurgical coke, from aromatic pitches synthesized by the petroleum industry as well as polycyclic aromatic model compounds.



Figure 2.14 Photograph of the head of a dyke after penetrating through a coal seam

The cooled magma is in the center with metamorphosed coal adjacent on both sides. An optical micrograph of comparable spheres produced during the carbonization of anthracite is shown in Figure 2.15. On further approaching the dyke, the number of spheres increased as well as their size until they all coalesced into each other to create a mosaic structure as seen in metallurgical cokes. In order to coalesce, the spheres must have been fluid. These observations could be reproduced in the laboratory using slow rates of heating and sampling over short temperature intervals. The conclusion from the analyses of the formation and structure of these spheres was that they represented a system of aromatic, nematic, discotic liquid crystals. The aromatic molecular constituents of the coal-tar pitch undergo condensations reactions to increase in size to about 1000 amu. At this size, such molecules (termed mesogens) self-assemble with parallelism and the normal forces of surface tension between two liquid phases establish the spherical shape.

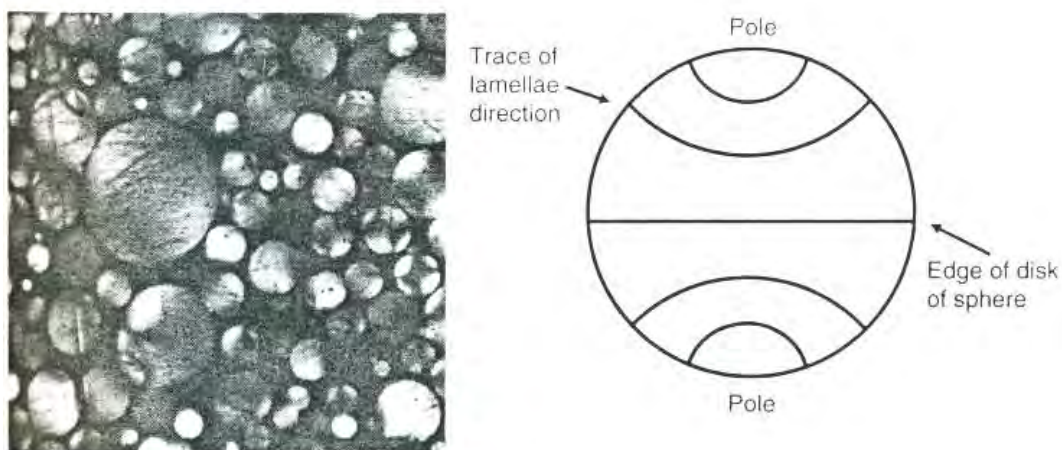


Figure 2.15, Figure 2.16 Optical micrograph of spheres of mesophase as developed during the carbonization of anthracene (left). Drawing of stacking arrangements of mesogens parallel to an equator of the sphere (right) (Marsh, unpublished results)

Structure within a sphere of mesophase is modeled in Figure 2.15 and 2.16 where the lamellar polycyclic aromatic mesogens are stacked parallel to each other to

create the anisotropy. On coalescence, these structures are maintained when the two adjoining structures merge into each other to create bulk anisotropy. Figure 2.17 (a-d) model the growth and self-assembly of mesogens during the formation of mesophase. The initial, relatively small polycyclic aromatic molecules (about 250 amu) (Figure 2.17 (a)), undergo simultaneous decomposition and condensation reactions involving the elimination of small hydrocarbon molecules, the molecular weight of the constituent molecules eventually reaching about 1000 amu when they are called mesogens (Figure 2.17 (b)).

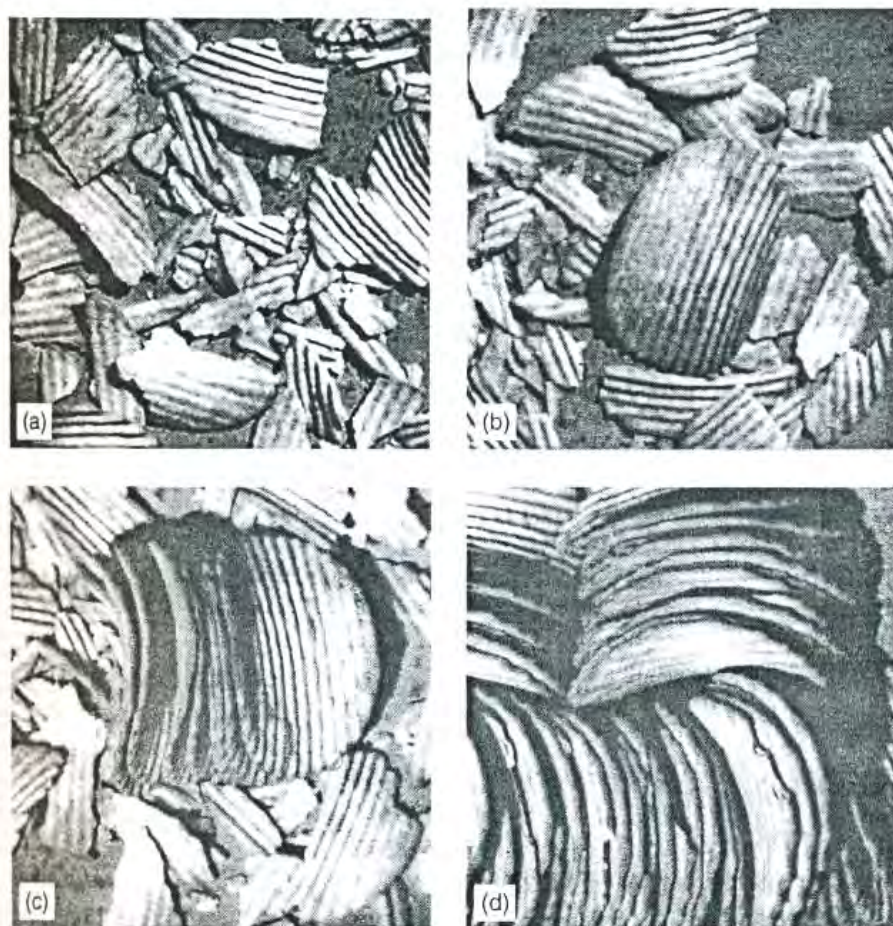


Figure 2.17 Models of anisotropic nematic aromatic discotic liquid crystals, growing from (a) an isotropic pitch to (d) an anisotropic carbon

At this stage, these M molecules self-assemble on collision, that is they “stick” together initially via polar interactions (associated with their benzenoid structures), to create laminar stacking over distances of micro/millimeters. Initially, these will be small

assemblies (Figure 2.17 (c)). Eventually, all of the carbonization system converts to mesophase (Figure 2.17 (d)), reading from top left to bottom right. This growth of mesophase is not a process of involving nucleation or crystallization or precipitation, but is one of self-assembly as is established in many biological systems. The orientation of the constituent polycyclic aromatic molecules is maintained during the subsequent carbonization process with chemical cross-linking ensuring the stability of such a structure. With feedstocks of lower aromaticity, on heating, the perfection of growth and stacking of the polycyclic molecules diminishes and carbons become less and less graphitizable until they approach the structures of the non-graphitizable carbons of solid-state carbonizations. With increasing HTT, the helium densities of these graphitizable carbons increase to about 1.8-1.9 g cm⁻³ indicating the imperfect stacking of the mesogens as well as defects within the planes of the mesogens themselves.

The structures established in graphitizable carbon, via the liquid crystal mechanism, of parallelism and cross-linking of graphene layers, prevent the formation of porosity as seen in solid-phase carbonizations, this necessitating other procedures to be adopted for activation of such graphitizable carbons.

Figure 2.18 is a diagram which attempts to include the principal stages involved in the formation of graphitizable carbons. The left-hand side of Figure 2.18 sets out the stacking of the mesogens in the mesophase, these mesogens having buckled structures with significant defects, vacancies, etc, within the graphene-like layer. With increasing HTT, the planarity increases and the defect density within the layers decreases. But then, extensive cross-linking occurs across the layers resulting in further buckling, until at about 2000 °K, the planarity of the layers becomes established leading to the production of (*hkl*) diffraction lines. At the same time, residual hydrogen is desorbed.

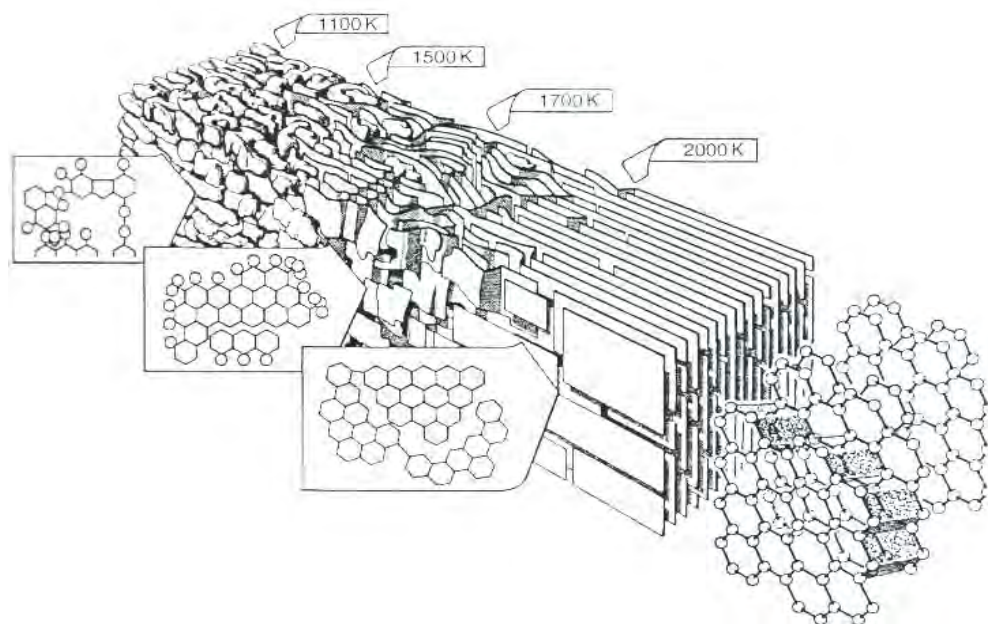


Figure 2.18 This diagram comprehensively models the structural changes which occur during the heat treatment of a graphitizable carbon

2.6.3 Preparation of Carbons in Gas Phase

Gas-phase carbonizations need careful control of the feedstocks being used. Carbo-naceous products range from the lustrous, mirror-like pyrolytic carbons to a sooty mass. The pyrolytic carbons are considered first. The feedstock can be methane, or propane or benzene, but of dominant importance is that in the carbonization process (cracking or pyrolysis) the gaseous material must be at a low relative pressure usually brought about by dilution with helium. The fragments of the pyrolyses (radicals) from the parent feedstock interact with helium. The fragments of the pyrolyses of the pyrolyses (radicals) from the parent feedstock interact with a suitable substrate and, by a mechanism involving carbon atom movement, the hexagonal lamellar structure of graphite is established. Highly orientated pyrolytic graphite (HOPG) has some of the most perfect of crystalline arrangements within the family of carbons. With a helium density of HOPG of 2.23 g cm^{-3} , porosity is absent. If a catalytic surface is present in such a pyrolysing system, for example nickel, then the carbon atoms formed at the surface interact in such a way as to produce graphic tubes or fibers of diameters of

some micrometers, and, if the conditions are appropriate, to produce carbon whiskers, diameters of <1.0 mm, of low packing density.

2.6.4 Activated carbon

Activated carbon is a processed carbon material with a highly developed porous structure and a large internal specific surface area. If you take a look at a cross section of an activated carbon particle, it looks like a beehive. It consists, principally of carbon (87 to 97%), but also contains such elements as hydrogen, oxygen, sulfur and nitrogen, as well as various compounds either originating from the raw material used in its production or generated during its manufacture.

Activated carbon has the ability to absorb various substances both from the gas and liquid phases. It is widely used for adsorption of pollutants from gaseous and liquid streams, for recovery of solvent and as a catalyst or catalyst support. In the nuclear industry, activated carbon is used for adsorption of iodine and noble gases from gaseous effluents. One of the most important fields in terms of consumption is in water and wastewater treatment. To obtain these activated carbons from cheap and readily available precursors become an interesting objective.

2.6.5 Raw materials for the production of activated carbon

The principal properties of manufactured activated carbons depend on the type properties of the raw material used. Any cheap substance with a high carbon and low ash content can be used as raw material for the production of activated carbon. In Europe the most important raw materials used for this purpose are wood (sawdust), charcoal, peat, [peat coke, certain types of hard and brown coal, and the semi-coke of brown coal. To produce activated carbon, which should exhibit high adsorption capacity and a large volume of the smallest pores (micropores), coconut shells are usually used. In the USA, brown carbons and petroleum products are widely used for manufacturing activated carbons. Source materials that have been studied for the production of activated carbon :

Bagasse	Corn cobs and corn stalks	Leather waste	Petroleum acid sludge
Beet-sugar sludges	Cotton seed hulls	Lampblack	Postassium ferricyanide residue
Blood	Distillery waste	Lignite	Petroleum coke
Bones	Fish	Molasses	Pulp-mill waste
Carbohydrates	Flue dust	Nut shells	Rice hulls
Cereals	Fruit pits	Oil shale	Rubber waste
Coal	Graphite	Peat	Sawdust
Coconut shells	Kelp and Seaweed	Polymer scrap	Wood

2.6.6 Production of activated carbon

Activated carbon is usually produced by the carbonization and activation of carbonaceous materials.

2.6.6.1 Carbonization (or pyrolysis)

The carbonaceous material that constitutes the basis for the production of activated carbon by the steam-gas method must meet certain requirements among which the most important are : (i) low content of volatile matter, (ii) high content of elemental carbon, (iii) definite porosity and (iv) sufficient strength of attrition. Of course, raw materials do not meet all these requirements simultaneously and therefore they require carbonization.

This is one of the most important steps in the production process of activated carbons since it is in the course of carbonization that the initial porous structure is formed. During carbonization most of the non-carbon elements, hydrogen and oxygen are first removed in gaseous form by pyrolytic decomposition of the starting material, and the freed atoms of elementary graphitic crystallites. The mutual arrangement of the crystallites is irregular, so that free interstices remain between them and apparently as the result of deposition and decomposition of tarry substances, these become filled or at least blocked by disorganized ("amorphous") carbon. There are three clear stages in the carbonization process: (a) loss of water in the 27-197°C range; (b) primary pyrolysis in the 197-497°C range with evolution of most gases and tars with

formation of the basic structure of the char; (c) consolidation of char structure at 497-847°C with a very small weight loss. The resulting carbonized product has only a very small adsorption capacity. Presumably, at least for carbonization at lower temperatures (400-600°C), part of the tar remains in the pores between the crystallites and on their surface. A carbon with a large adsorption capacity, however, can be produced only by activating the carbonized material under such conditions that the activation agent (steam, carbon dioxide, etc.) reacts with the carbon.

2.6.6.2 Activation

Generally, there are two main types of production of activated carbon :

- By carbonizing material with the addition of activating agents (ZnCl_2 , CaCl_2 , H_3PO_4). This method is generally known as “chemical activation”.
- By allowing the inactive carbonized product (prepared by the usual methods of carbonization) to react with oxidizing gases (steam, carbon dioxide, oxygen). This method is generally known as “physical activation”.

2.6.6.2.1 Chemical activation

For chemical activation, the common chemicals used are dehydrating agent such as ZnCl_2 , CaCl_2 , MgCl_2 and some acids such as H_3PO_4 and H_2SO_4 . The activation agent influences the pyrolytic processes so that formation of tar is restricted to a minimum and the amount of the aqueous phase in the distillate is also less than that in the normal carbonization. The activation agent also changes the chemical nature of the cellulose substance by dehydration, which decomposes the organic substances by the action of heat and prevents the formation of tar.

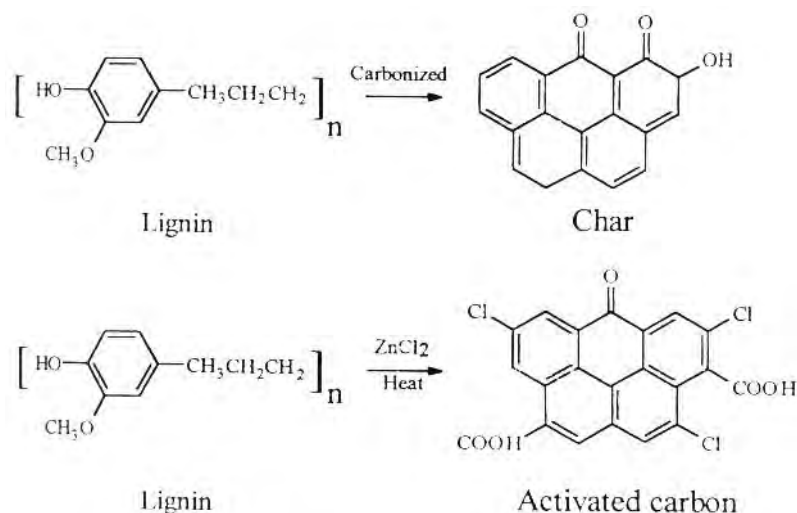


Figure 2.19 Chemical reaction of lignin with activated by ZnCl_2

Chemical activation is usually carried out at temperatures from 400-600°C. These temperatures are lower than those needed for activation with gaseous agent (physical activation). An important factor in chemical activation is the degree (coefficient) of impregnation; this is the weight ratio of the anhydrous activation salt to the dry starting material. The effect of the degree of impregnation on the resulting product is apparent from the fact that the volume of salt in the carbonized material equals the volume of pores which are freed by its extraction. For small degree of impregnation the increase in the total pore volume of the product with increase in the degree of impregnation is due to the increase in the number of small pores. When the degree of impregnation is further raised, the number of large-diameter pores increases and the volume of the smallest decreases. The most widely used activation agents are :

Aluminum chloride	Chlorine	Phosphorus pentoxide	Sodium hydroxide
Ammonium chloride	Hydrogen chloride	Potassium metal	Sodium hydroxide
Borates	Iron salt	Potassium hydroxide	Sodium oxide
Boric acid	Nickel salt	Potassium permanganate	Sulfur dioxide
Calcium chloride	Nitric acid	Potassium sulfide	Sulfuric acid
Calcium hydroxide	Nitrous gases	Phosphoric acid	Zinc chloride

2.6.6.2.2 Physical activation

The basic method of activating coal-based granules consist of their treatment with oxidizing gases (steam, carbon dioxide, oxygen) at elevated temperatures. In the activation process, carbon reacts with the oxidizing agent and the resulting carbon oxides diffuse from the carbon surface. Owing to the partial gasification of the granules or grains, a porous structure builds up inside them. The structure of the carbonization product consists of a system of crystallites similar to those of graphite bonded by aliphatic type bonds to yield a spatial polymer. The spaces between the neighboring crystallites constitute the primary porous structure of the carbon. The pores of the carbonized granules are often filled with tar decomposition products and are blocked with amorphous carbon. This amorphous carbon reacts in the initial oxidation step, and as a result the closed pores open and new ones are formed. In the process of further oxidation, the carbon of the elementary crystallites enters into reaction due to which the existing pores widen. Deep oxidation leads to a reduction in the total volume of micropores due to the burning off of the walls between the neighboring pores, and in consequence the properties and mechanical strength of the material decrease.

In the first of activation, when burn-off is not higher than 10% (which occurs at low reaction times), this disorganized carbon is burnt out preferentially and the closed and clogged pores between the sheets are freed. In the course of further activation at the second stage, carbon of the aromatic sheets is burnt. When the burn-off is less than 50%, a microporous activated carbon is obtained; when it is large than 75% (which occurs at thig reaction times), a macroporous product is obtained; and when the burn-off is between 50 and 75%, the product is of mixed structure and contains both micro- and macropores. Development of macropores due to coalescence or widening of micropores under fast reaction conditions.

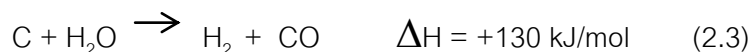
Carbon oxidation is a complex heterogeneous process encompassing the transport of reagents to the surface of the particles, their diffusion into the pores, chemisorption on the pore surface, reaction with carbon desorption of the

reaction products, and diffusion of these products to the particle surface. The concentration profile of the oxidizing agent of the granule volume, and hence the formation of the carbon porous structure, depends of the rate of the particular steps of the process. At low temperatures the rate of the chemical reaction of carbon with the oxidizing agent is small, so it is this reaction that limits the overall rate of the process. This results in a dynamic equilibrium becoming established between the concentration of the oxidizing agent in the pores and that in the interparticle spaces. In such a case the activation process yields a homogeneous product with a uniform distribution of the pores throughout the whole volume of the granule. With increase of the oxidation temperature, the rate of chemical reaction increase much faster than that of diffusion, and then the overall rate of the process becomes limited by the rate of transport of the oxidizing agent into the granule. At very high temperatures the oxidation reaction rate becomes so high that the whole oxidizing agent reacts with carbon on the external surface of the granule. In such a case significant losses of the material occur due to superficial burn-off, and a porous structure is not formed.

The rate of the oxidation process is limited by the reactivity of the initial carbonaceous material towards the oxidizing agent. The greater is the reactivity of the substrates, the lower the optimal temperature of the process at which uniform formation of pores in the granule.

- *Activation with steam*

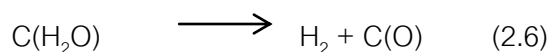
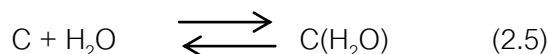
The basic reaction of carbon with water vapor is endothermic and a stoichiometric equation can be written in the form:



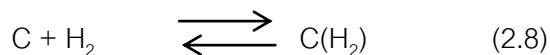
This process has been studied extensively since it dominates not only the activation reaction but also the production of water-gas. The reaction of carbon with water vapor is inhibited by the presence of hydrogen while the influence of carbon monoxide is practically insignificant. The rate of gasification of carbon by water vapor is given by the formula:

$$U = \frac{K_1 P_{H_2O}}{1 + k_2 P_{H_2O} + k_3 O_{H_2O}} \quad (2.4)$$

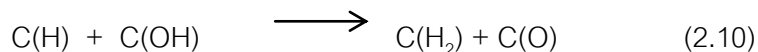
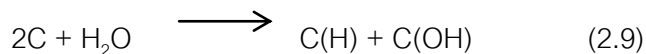
where: P_{H_2O} and P_{H_2} are the partial pressures of water and hydrogen, respectively, k_1 , k_2 , k_3 are the experimentally determined rate constants. The mechanism of reaction of carbon with water vapor can be presented with reasonable confidence by the following set of equations:



The inhibiting effect due to hydrogen may be assigned to blocking of the active centers by its adsorption.

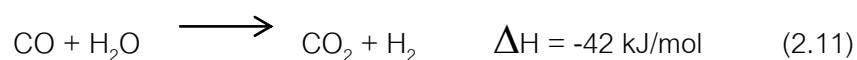


According to Long and Sykes in the first step of the reaction the adsorbed water molecules dissociate according to the scheme:

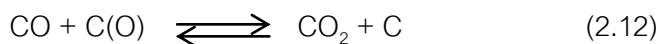


Hydrogen and oxygen are adsorbed at neighboring active sites which account for about 2% of the surface area.

The reaction of carbon and water vapor is accompanied by the secondary reaction of carbon monoxide with water vapor (the so-called homogeneous water-gas reaction) catalyzed by the carbon surface:



Explained the presence of carbon dioxide and the catalytic surface effect of carbon by the following reaction:



Activation with steam is carried out at temperatures from 750 to 950°C with the exclusion of oxygen which at these temperatures aggressively attacks carbon and decreases the yield by surface burn-off. It is catalyzed by the oxides and carbonates of alkali metals, iron, copper and other metal; the activation catalyst usually employed in practice are carbonates of alkali metals, which are added in small to the material to be activated.

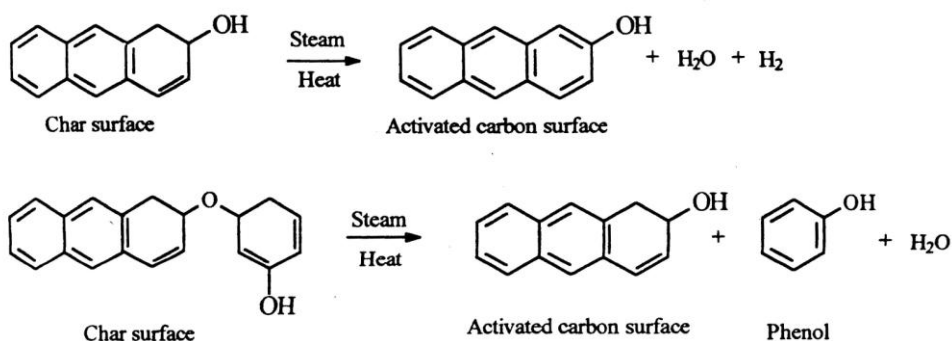


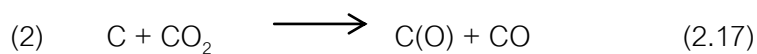
Figure 2.20 Chemical reaction of char with activated by steam

- Activation with Carbon Dioxide

The rate of carbon gasification with carbon dioxide is described by an expression analogous to that for the reaction with steam:

$$v = \frac{k_1 P_{\text{CO}_2}}{1 + k_2 P_{\text{CO}} + k_3 O_{\text{CO}_2}} \quad (2.13)$$

where : P_{CO_2} and P_{CO} are the partial pressures, and k_1 , k_2 , k_3 are the experimentally determined rate constants. Two different mechanisms of interaction of carbon dioxide with the carbon surface are proposed:



Activation with carbon dioxide involves a less energetic reaction than that with steam and requires a higher temperature 850-1100°C. The activation agent used in technical practice is flue gas to which a certain amount of steam is usually added, so that actually this is a case of combined activation. The catalyst for the reaction with carbon dioxide are carbonates of alkali metals.

- Activation with Oxygen (air)

In the reaction of oxygen and carbon both carbon monoxide and carbon dioxide are formed according to the equations:



The used of oxygen as activating agent presents particular difficulties which are due to its exothermic reaction with carbon. In this case it is difficult to avoid local overheating in the activation process. In view of its high rate, the carbon burn-off process proceeds chiefly on the surface of the granules, producing high losses of material. In many processes, oxygen activation is conducted at very low temperatures and combined with treatment with water vapor. Such a method is most convenient when materials of low reactivity are activated.

2.6.6.3 Pyrolysis and steam activation

Usually the production of activated carbons involves two stages : the carbonization of the raw materials followed by a high temperature activation, at 800-1000°C, of the resulting chars. The method used in this study combines the two stage into a single one, while the treatment temperature is considerably lower, 600-800°C. This method is preferable to the two-stage treatment from an economic point of view. During the pyrolysis and steam activation of carbon-containing materials the following main processes take place:

1. Oxidation-thermolytic conversion of the carbon material leading to the accumulation of oxygen-containing groups.

2. A thermal destruction process including the decomposition of the oxygen-containing groups accompanied by the formation of carbon oxides and water.
3. Condensation processes.
4. Deeper penetration of the water molecules and opening up of the initially closed pores into the structure of the carbon materials.

2.6.7 Molecular, Crystalline and porous structure of activated carbon

The graphite-like microcrystalline structure is the basic structural unit of activated carbon, as in the case of carbon black. The ordering of carbon atoms in an elementary microcrystallite indicates considerable similarity to the structure of pure graphite, the crystals of which consist of parallel layers of condensed regular hexagonal ring spaced 0.335 nm apart. Such interlayer spacing is diagnostic of interaction by means of van der Waals forces. The length of the carbon-carbon bond in individual layers is 0.142 nm. Each carbon atom bonds with the three adjoining ones by means of covalent bonds, and the fourth delocalized π -electron may move freely in a system of conjugated double bonds of condensed aromatic ring. The scheme of arrangement of the carbon atoms in a crystal of graphite is presented in Figure 2.21.

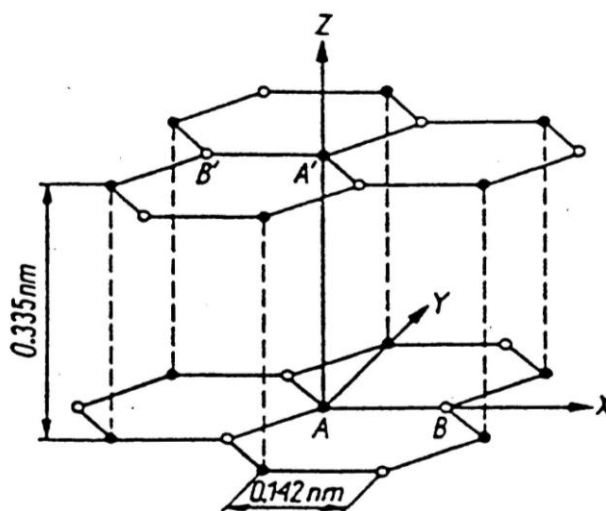


Figure 2.21 Ordering of carbon atoms in a crystal of graphite

The formation of the crystalline structure of activated carbon begins early during the carbonization process of the starting material. Thus sets of condensed aromatic ring of various numbers, which are the nascent centers of graphite-like micro crystallites, are formed. Although their structure resembles that of a crystal of graphite there exist some deviations from that structure. Thus, among other things, the interlayer distances are unequal in crystals of activated carbon and range from 0.34 to 0.35 nm. Again, the orientations of the respective layers generally display deviations. Such deviations from the ordering characteristic of graphite, called a turbostratic structure, are illustrated in Figure 2.22. Disordering of the crystal lattice may be caused to a considerable degree both by its defects (vacant lattice sites) and by the presence of built-in heteroatoms. It is resulted from the kind of the raw material used, the nature and quantity of its impurities as well as the methods and conditions of the production processes of the activated carbon.

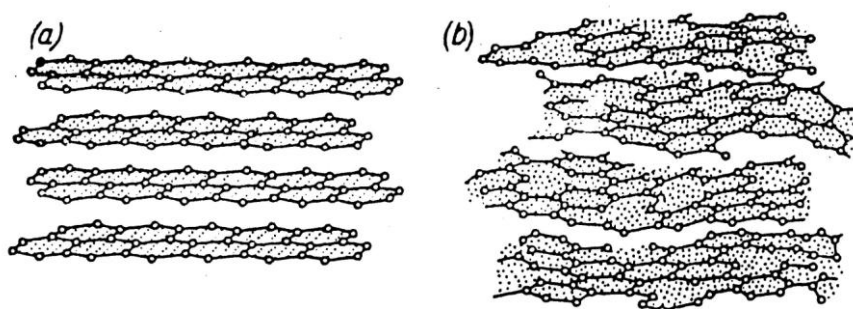


Figure 2.22 Comparison of three-dimensional crystal lattice of graphite (a) and the turbostratic structure (b)

The average activated carbons have a strongly developed internal structure (the specific surface often exceeds 1000 and sometimes even 1500 m^2/g), and they are usually characterized by a polydisperse capillary structure, featuring pores of different shapes and sizes. Bearing in mind the values of the effective radii and the mechanism of adsorption of gases, Dubinin proposed three main types of pore, namely macropores, mesopores and micropores.

Macropores are those having effective radii ≥ 100 -200 nm and their volume is not entirely filled with adsorbate via the mechanism of capillary condensation (it may occur only for a relative pressure of adsorbate of nearly one). The volumes of macropores are usually in the range 0.2-0.8 cm³/g and the maxima of volume distribution curves according to the radii are usually in the range 500-2000 nm. The values of their specific surface area not exceeding 0.5m²/g are negligibly small when compared with the surface of the remaining types of pore. Consequently macropores are not of great importance in the process of adsorption as they merely act as transport arteries rendering the internal parts of the carbon grains accessible to the particles of adsorbate.

Mesopores, also known as transitional pores, have effective radii falling in the range of 1.5-1.6 nm to 100-200 nm. The process of filling their volume with adsorbate takes place via the mechanism of capillary condensation. For average activated carbons, the volumes of mesopores lie between the limits 0.1-0.5 cm³/g and their specific surface area in the range of 20-100 m²/g. The maximum of the distribution curve of their significant contribution to adsorption, also perform as the main transport arteries for the adsorbate.

Micropores have sizes comparable with those of adsorbed molecules. Their effective radii are usually smaller than 1.5-1.6 nm and for average activated carbons their volumes usually lie between 0.2-0.6 cm³/g. The energy of adsorption in micropores is substantially greater than that for adsorption in mesopores or at the non-porous surface, which causes a particularly large increase of adsorption capacity for small equilibrium pressures of adsorbate. In micropores, adsorption proceeds via the mechanism of volume filling. For some activated carbon, the microporous structure may have a complex nature, e.g. two overlapping microporous structure : firstly one for effective pore radii smaller than 0.6-0.7 nm and termed specific micropores, and the secondly one exhibiting pore radii from 0.6-0.7 to 1.5-1.6 nm termed supermicropores.

2.6.8 Chemical nature of the surface of activated carbon

The chemical nature of activated carbons significantly influences their adsorptive, electrochemical, catalytic, acid-base, redox, hydrophilic-hydrophobic, and other properties. It is determined decisively by type, quantity and bonding of various heteroatoms, especially oxygen. Heteroatoms may be combined both with peripheral carbon atoms at the corners and edges of crystallites, and in intercrystalline spaces and even in defect zones of particular planes constituting the crystallites. Most heteroatoms are grouped at the surface of activated carbon. Apart from their different locations, the heteroatoms are strongly differentiated in terms of their chemical reactivity. Surface-bound heteroatoms are believed to adopt the character of the functional groups typical for aromatic compounds. The surface functional groups often consist of more than one type of heteroatom, e.g. oxygen and hydrogen together as $-OH$ or $-COOH$.

Surface functional groups can originate from the starting material from which a particular activated carbon is produced. Substantial quantities of oxygen can be introduced during the production process itself, e.g. during activation of carbonaceous materials by oxidizing gases, such as water vapor and air. Activated carbon used predominantly for practical purpose generally includes some percentage by weight of chemically-bound oxygen and usually much smaller quantity of hydrogen combines with surface carbon atoms either directly or through oxygen.

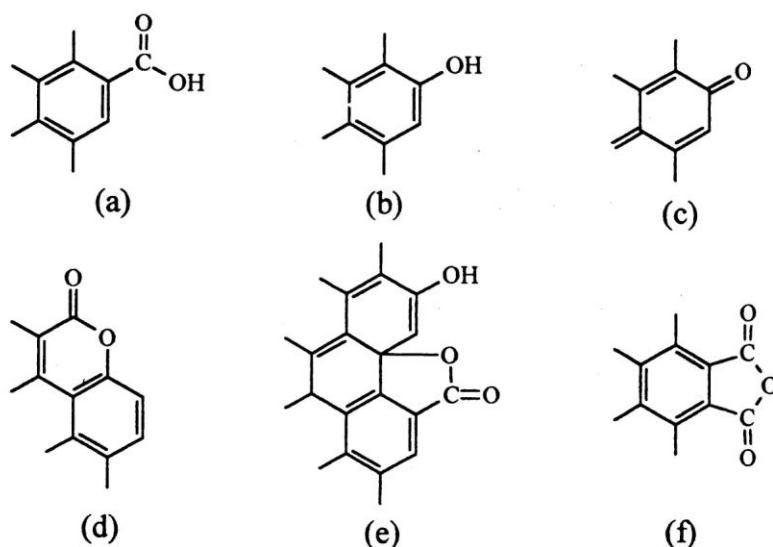


Figure 2.23 Principal types of acidic oxygen surface functional groups : (a) carboxyl, (b) phenolic, (c) quinonoid, (d) normal lactone, (e) fluorescein-type lactone, (f) anhydride originating from neighbouring carboxyl groups

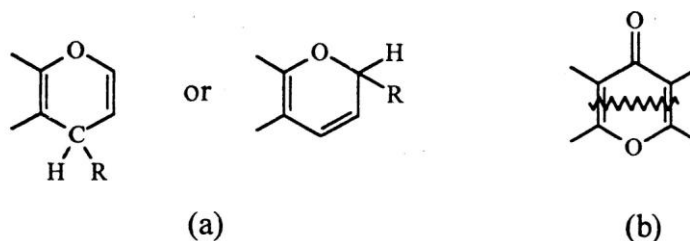


Figure 2.24 Functional groups of basic character : (a) chromene, (b) pyrone-like

Oxygen surface compounds are usually divided into two main types: functional groups of acidic nature and basic groups. The first acidic group is exemplified schematically in Figure 2.24. The later basic group is much less well-characterized compared with the first. Usually structures corresponding to chrome or pyrone-like structures are illustrated in Figure 2.25.

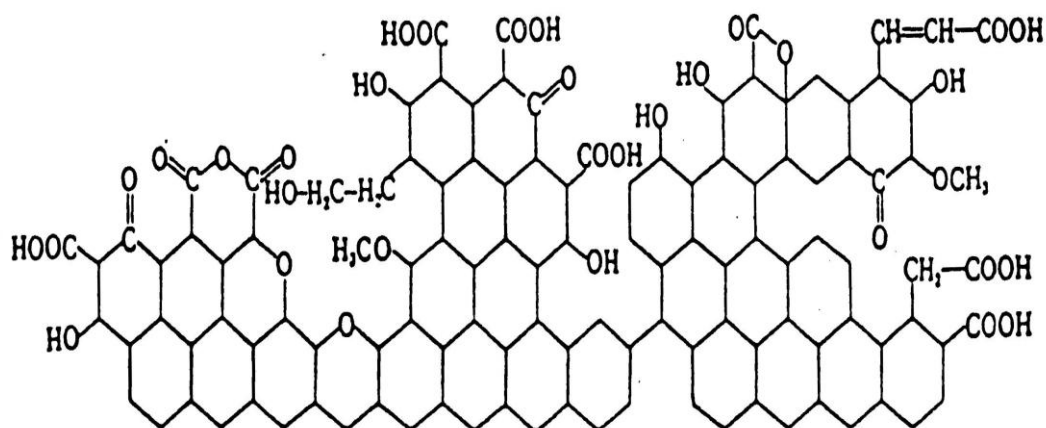


Figure 2.25 Model of fragment of an oxidized activated carbon surface

2.7 Cracking reaction

2.7.1 Thermal Cracking

Thermal cracking, where free radicals (lacking one hydrogen atom on carbon atom in the hydrocarbon molecule) are intermediate species and cracked by a β -scission mechanism. The most successful present explanation of thermal cracking of hydrocarbon is Rice free radical theory as modified by Kossiakoff and Rick. This will be called the "RK-theory" as follows to explain in the cracking of normal paraffin.

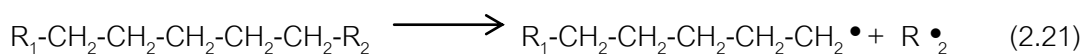
The normal paraffin molecule loses a hydrogen atom by collision and reaction with a small free hydrocarbon radical or a free hydrogen atom, thereby becoming a free radical itself. This radical may immediately crack or may undergo radical isomerization prior to cracking. Radical isomerization presumably occurs through a coiled configuration of a single radical, in which the hydrogen donor and acceptor position of hydrogen atom usually yields a more stable radical in order of tertiary > secondary > primary free radical.

Cracking of either the original or isomerized radical then takes place at carbon-carbon bond located in the β position to the carbon lacking one of hydrogen atom. Cracking at the β position gives directly an alpha olefin and primary radical (lacking one hydrogen atom on primary carbon atom); in this step no change of position of any hydrogen atom with respect to the carbon skeleton.

The primary radical derived from this step may immediately re crack at the β bond to give ethylene and another primary radical, or it may first isomerizes. In the absence of radical isomerization, only primary radical are derived from cracking reaction of normal paraffin primary radical thus give only ethylene as the olefin product. Radical isomerization reduced the amount of ethylene, but it still remains the major product. By successive re cracking, the radical ultimately are reduced to methyl or ethyl fragments. These radical then react with feedstock molecules to produce new free radicals and themselves converted to methane or ethane. Thus, cracking is propagated as chain reaction.

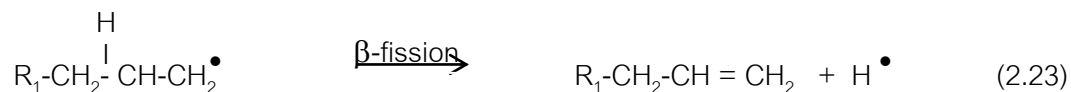
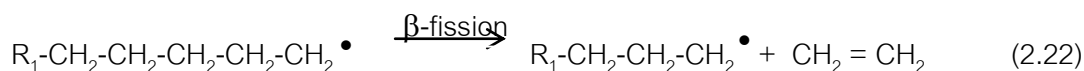
A schematic representation of polyethylene cracking is as follow;

1. Initiation Step

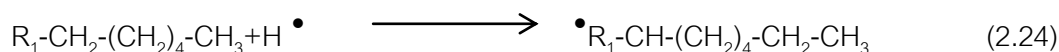


2. Propagation Step

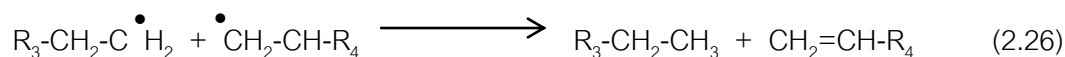
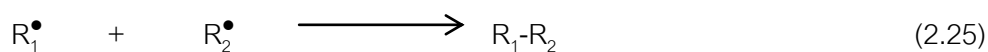
β-fission



Chain transfer



3. Termination Step



2.7.2 Catalytic Cracking

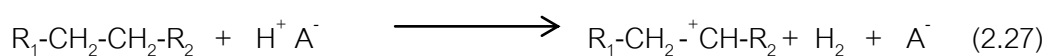
Catalytic cracking is the most important and widely used refinery process for converting heavy oil more valuable gasoline and light oil product. Originally cracking was accomplished thermally but the catalytic process has almost completely replaced thermal cracking because of more gasoline having a higher octane and less heavy oil and unsaturated gases are product.

Commercial cracking catalysts can be divided into three classes;

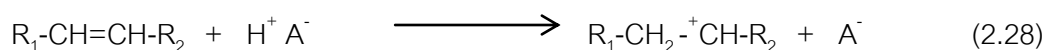
1. Acid-treated natural aluminosilicates
2. Amorphous synthetic silica-alumina
3. Crystalline synthetic silica-alumina catalysts (zeolites or molecular sieves)

Most catalysts used in commercial units today are either class (3) or mixtures of classes (2) and (3) catalysts. A major difference between thermal and catalytic cracking

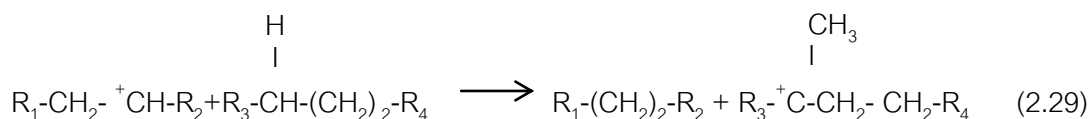
is that reactions through catalytic cracking occur via carbonium ion intermediate. Compared to the free radical intermediate in thermal cracking. Carbonium ions are longer lived and accordingly more selective than free radicals. Acid catalysts such as amorphous silica-alumina and crystalline zeolites promote the formation of carbonium ions. There are two possibilities for the initial step in the catalytic cracking of polyolefins. The first involves the simultaneous loss of a hydride ion from the polyolefins molecule and of a proton from the acidic catalyst surface. This produced a carbonium ion in combination with acid anion and molecule hydrogen:



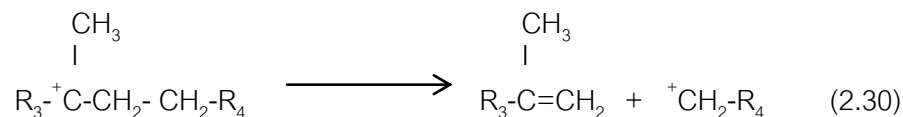
Alternatively a small amount of olefin, create by thermal cracking could initiate the reaction;



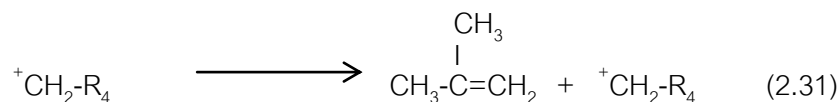
Chain propagation involves an exchange reaction in which a carbonium ion react with a polyolefins to give a new hydrocarbon and a carbonium ion of the polyolefins to be cracked (hydride transfer).



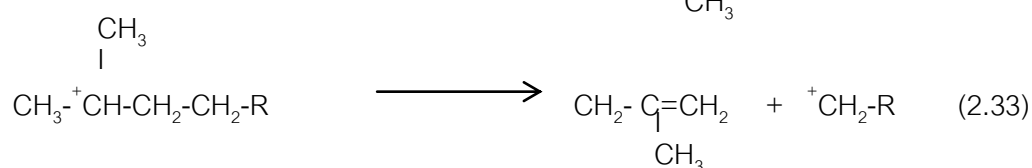
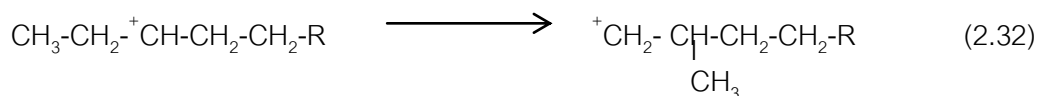
The next step is the decomposition of the activated molecule. The primary rule involved is that the carbon-carbon cleavage occurs at the position one carbon atom away from the carbonium ion, i.e. β -scission.



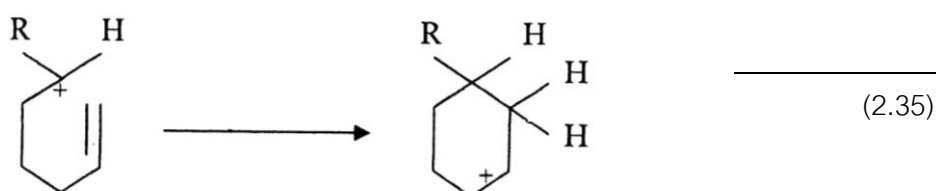
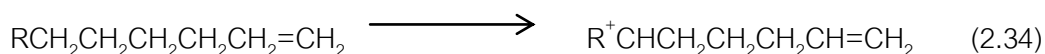
A hydride shift then converts the primary carbonium ion formed into a secondary carbonium ion;



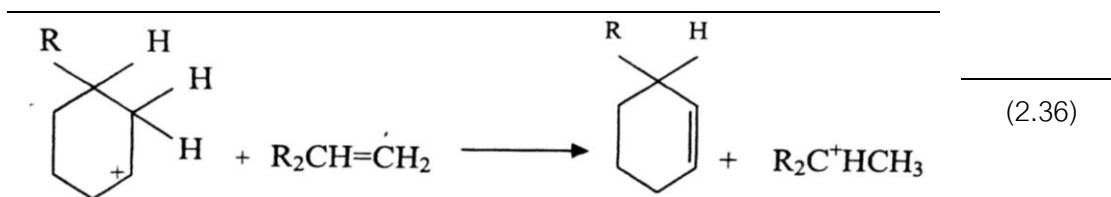
Subsequent steps involve further hydride transfer and proceed until the chain becomes so short that cracking at the β -scission is no longer a rapid reaction. Large amounts of iso-compounds are formed in catalytic cracking. This is readily explained by the rearrangement of the secondary carbonium ion:



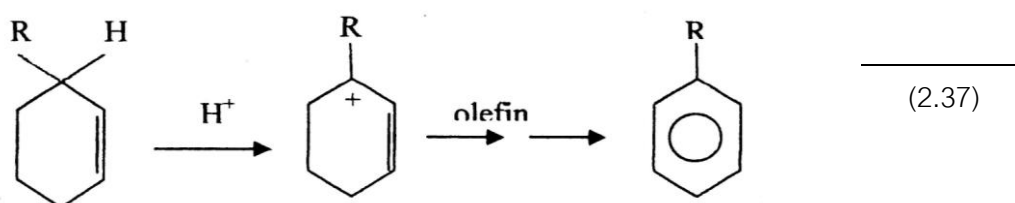
Aromatization of paraffins can occur through a dehydrocyclization reaction. Olefinic compounds formed by the beta scission can form a carbonium ion intermediate with the configuration conducive to cyclization. For example, if a carbonium ion such as that shown below is formed (by any of the methods mentioned earlier), cyclization is likely to occur.



Once cyclization has occurred, the formed carbonium ion can lose a proton, and a cyclohexene derivative is obtained. This reaction is acidic by the presence of an olefin in the vicinity (R-CH=CH_2).



The next step is the abstraction of a hydride ion by a lewis acid site from the catalyst surface to form the more stable allylic carbonium ion. This is again followed by a proton elimination to form a cyclohexadiene intermediate. The same sequence is followed until the ring is completely aromatized.



During the cracking process, fragmentation of complex polynuclear cyclic compounds may occur, leading to formation of simple cycloparaffins. These compounds can be a source of C_6 , C_7 and C_8 aromatics through isomerization and hydrogen transfer reactions.

Coke formed on the catalyst surface is thought to be due to polycondensation of aromatic nuclei. The reaction can also occur through a carbonium ion intermediate of the benzene ring. The polynuclear aromatic structure has a high C/H ratio.

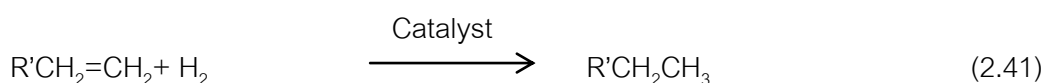
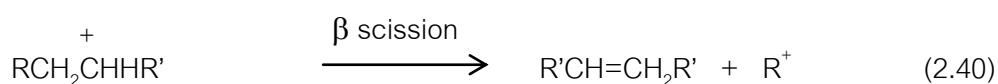
2.7.3 Hydrocracking Processing

Hydrocracking is essentially catalytic cracking in the presence of hydrogen. It is one of the most versatile petroleum refining schemes adapted to process low value stocks. Generally, the feedstocks are not suitable for catalytic cracking because of their high metal, sulfur, nitrogen, and asphaltene. The process can also use feeds with high aromatic content. Products from the hydrocracking process lack olefinic hydrocarbons. The product slate ranges from light hydrocarbon gases to gasoline to residues.

The dual-function catalyst used in hydrocracking provide high surface area cracking sites and hydrogenation-dehydrogenation sites. Amorphous silica-alumina, zeolites, or mixture of them promote carbonium ion a high iso/normal ratios. The hydrogenation-dehydrogenation activity, on the other hand, is provided by catalysts such as cobalt, molybdenum, tungsten, vanadium, palladium, or rare earth elements. As with catalytic cracking, the main reactions occur by carbonium ion and beta scission, yielding two fragments that could be hydrogenated on the catalyst surface. The main hydrocracking reaction could be illustrated by the first step formation of a carbonium ion over the catalyst surface:



The carbonium ion may rearrange, eliminate a proton to produce an olefin or crack at a beta position to yield to an olefin and a new carbonium ion. Under an atmosphere of hydrogen and in the presence of a catalyst with hydrogenation-dehydrogenation activity, the olefins are hydrogenated to paraffinic compounds. This reaction sequence could be represented as follows:



As can be anticipated, most products from hydrocracking are saturated. For this reason, gasoline from hydrocracking units have lower octane ratings than those produced by catalytic cracking units; they have a lower aromatic content due to high hydrogenation activity, products from hydrocracking units are suitable for jet fuel use. Hydrocracking also produces light hydrocarbon gases (LPG) suitable as petrochemical feedstock. Other reactions that occur during hydrocracking are the fragmentation

followed by hydrogenation (hydrogenolysis) of the complex asphaltenes and heterocyclic compounds normally present in the feeds. Hydrocracking reaction conditions vary widely, depending on the feed and the required products. Temperature and pressure range from 400 to 480°C and 35 to 170 atmospheres, respectively. Space velocities in the range of 0.5 to 2.0 hr⁻¹ are applied.

2.8 Basic Principles of Catalysis

In the study of reacting chemical system, two considerations are of importance. The first is chemical thermodynamics, the second is reaction kinetics. The thermodynamics of the system determines the maximum attainable yield of products under specified conditions. It is a fundamental principle of thermodynamics that changes in Gibbs free energy G , enthalpy H and entropy S depend only upon the initial and final states of the systems, and not upon the path taken to move from one to the other. The kinetic parameters, rate coefficient k , activation energy E , order of reaction. These parameters depend on the sensitivity on the path followed, and the introduction of a catalyzed pathway changes not only the values of these parameters, but also their significant. Classical kinetics based on collision theory is then really on little help, and theoretical discussion has necessarily to be based on the absolute rate theory. It must first be emphasized, and this is another implication of our definition, that a catalyst can increase the rate only of a reaction that is already thermodynamically as are unanalyzed reactions. Catalyst decreases the activation energy of a reaction. This must mean that catalyzed reaction proceeds by a new and energetically more favorable pathway.

It is possible to divide catalytic systems into two distinct categories, homogeneous catalysis and heterogeneous catalysis. With heterogeneous catalysis, concerns with the specific chemical properties of the surface of the chosen substance. These of course reflect the chemistry of the bulk solid, and some useful insight into the catalytic activities of surfaces is gained from knowledge of the bulk properties of the solid. Table 2.18 presents a preliminary classification of solids into group. This table may be in part interpreted using the qualitative concept of compatibility between catalyst, reactants, and products.

Table 2.18 Classification of heterogeneous catalysts

Class	Function	Example
Metals	Hydrogenation Dehydrogenation Hydrogenolysis	Fe, Ni, Pd, Pt, Ag
Semiconducting oxides and sulphides	Oxidation Dehydrogenation Desulphurization	NiO, ZnO, MnO ₂ , Cr ₂ O ₃ , Bi ₂ O ₃ -MoO ₃ , WS ₂
Insulator oxides	Dehydration	Al ₂ O ₃ , SiO ₂ , MgO
Acids	Polymerization Isomerization Cracking Alkylation	H ₃ PO ₄ , H ₂ SO ₄ , SiO ₂ -AlO ₃ , zeolites

This table also shows that transition metals are especially good catalyst for reaction involving hydrogen and hydrocarbon. This is because these substances readily adsorb at the surfaces of metals, in a manner to be described in more detail below, and except in a few cases the reaction does not precede below the surface.

2.8.1 Metal Catalyst

For a molecule to react catalytically as a metal surface, it must first be chemisorbed. When two molecules react, at least one and probably both must be chemisorbed. Chemisorptions is an essential step in the preparation of a molecule for reaction: indeed a chemisorbed molecule sometimes resembles the product into which it will be transformed more than does the free molecule. The effect of chemisorptions can also be very like that of raising a molecule to its first electronically excited state; physical adsorption on the other hand has little direct relevance to catalysis.

For metals, relationships have been sought between collective properties and catalytic behavior. The metallic state was generally described by the simple band model or the Pauling valence structure theory, in metal the valence shell is formed by s or d

band. The main-group elements with their s bands are typical electron donors and form strong bonds with electron acceptors such as sulfur or oxygen; stable sulfides and oxides are formed. These metals are therefore not suitable as catalysts. In contrast the transition metals with their d bands are excellent catalysts. It is noted worthy that both hydrogenations and oxidations can be carried out with d-block elements.

Figure 2.26 describe the electronic structure of the transition metals with the aid of the band model. According to this model the metal is a collective source of electrons and electron holes. In a row of the periodic table, the metals on the left have fewer d electrons to fill the bands. There are two regions of energetic states, namely, the valence band and the conduction band with mobile electrons or position holes. The potential energy of the electrons is characterized by the Fermi level, which corresponds to the electrochemical potential of the electrons and electron holes.

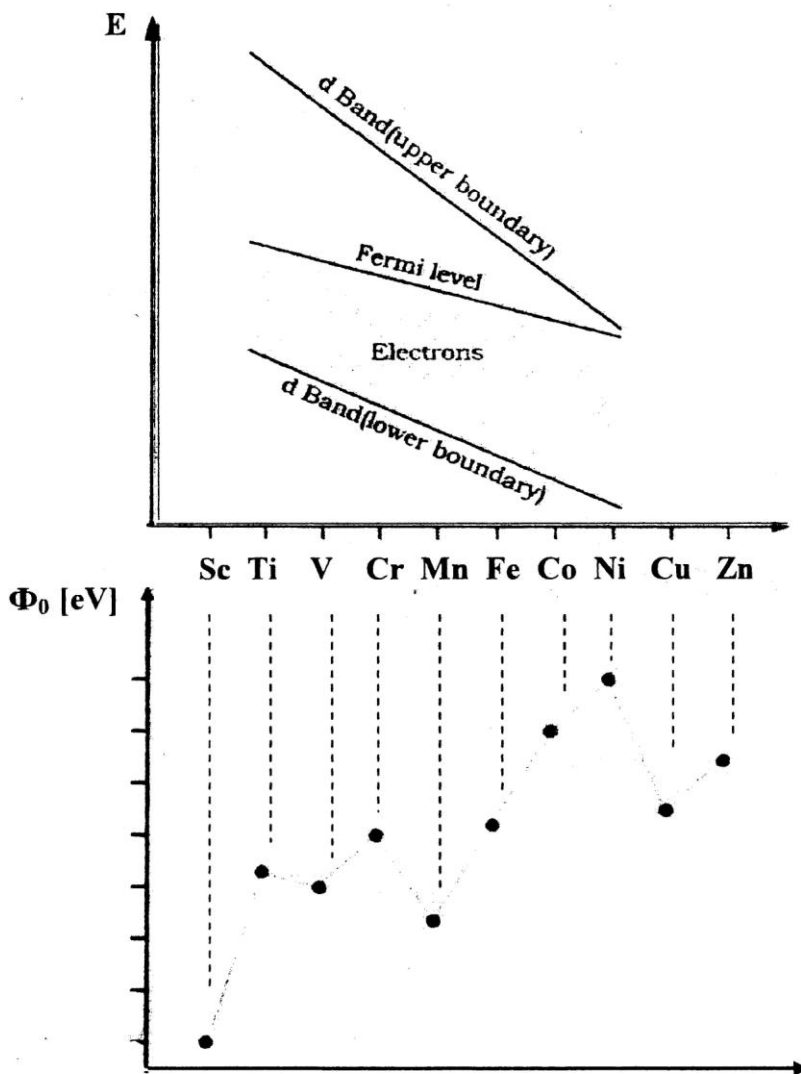


Figure 2.26 Electron density of the 3rd band and work function Φ of the transition metals of the fourth period

The position of the Fermi level also indicates the number density of electrons in the band model. The energy required to transport an electron from the edge of the Fermi level into vacuum corresponds to the work function Φ (Figure 2.27a). For the d-block metals, the work function is around 4 eV and therefore in the UV range.

A certain number of free levels or d-holes are available for bonding with adsorbents. The lower the Fermi level, the stronger the adsorption. How do donors and acceptors function in the band model. In the surface layer, the free electrons or holes allow molecules to be bound to the surface, whereby the strength of binding depends on the position of Fermi level. An acceptor removes electron density from the conduction

band of the metal as a result of which the Fermi level drops to E_F and the work function $\phi_A > \phi_O$ (Figure 2.27b). A donor donates electrons to the conduction band of the metal, and the work function becomes corresponding lower: $\phi_A < \phi_O$ (Figure 2.27c).

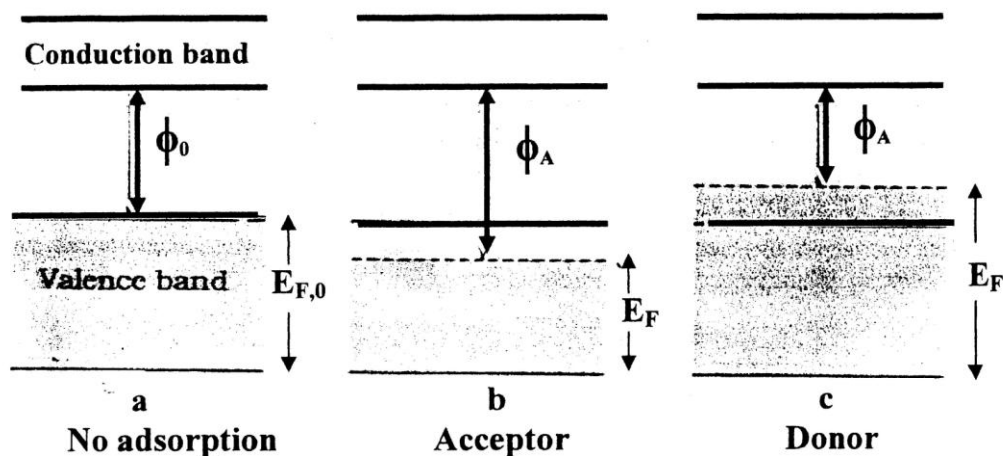


Figure 2.27 Acceptor and donor function according to the band model a) No adsorption ; b) Acceptor ; c) Donor, $E_{F,0}$ = Fermi level ; E_F = Fermi energy

Metals normally have a narrow d band. The catalyst properties are strongly influenced by the occupational density of the electrons in this band. In many cases a direct relationship has been found between the catalytic activity of transition metals and the electronic properties of the unfilled d bands. This is shown by the general trend of the rate of adsorption along the transition metal rows. For molecular species it was found that the rate of dissociative adsorption on the noble metals increase from right to left as a function of the d-band occupation. Besides the electron occupation of the d bands, another description can be used for obtaining correlations, namely, the valence bond theory of metals. The bonding in transition metal is partially due to unpaired electrons in bonding d orbital. The contribution of these d electrons to the valence bonding was termed “percentage d character” of the metallic bonding by Pauling, who made a distinction between three types of d orbital in transition metals.

- Bonding d orbital involved in covalent d s p hybrid bonds
- Metallic (free) d orbital

2.8.2 Catalyst support

The early concept of a support or a carrier was of a substance that provided a means of spreading out an expensive catalyst ingredient such as platinum for its most effective use, or a means of improving the mechanical strength of the inherently weak catalyst. However, the carrier may actually contribute catalytic activity, depending on the reaction and reaction condition, and it may react to some extent with other catalyst ingredient during the manufacturing process. It can also help stabilize the catalytically active structure. The carrier may be used as pellets or powders to be impregnated, a powdered carrier may be incorporated into a mixture to be precipitated, or the carrier may itself be precipitated from the solution in manufacturing process.

Some substance such as colloidal alumina or silica may play a double role, acting as a binding agent in catalyst manufacturing and as a carrier in the ultimate product. Alumina in the gamma form is intrinsically weakly acidic, but such a substance may be a truly inert carrier for many reactions. In other cases it can be used by itself as a catalyst, as in dehydration of an alcohol. High area carrier is sometimes loosely referred to as active carrier in contrast to low area inert carrier, but this usage may be misleading.

The selection of a carrier is based on its having certain desirable characteristics. In addition to possible chemical effects certain physical properties are important:

1. Inertness to undesired reaction
2. Desirable mechanical properties, including attrition resistance, hardness, and compressive strength
3. Stability under reaction and regeneration conditions
4. Surface area (high surface area is usually, but not always, desirable)
5. Porosity, including average pore size and pore-size distribution (high area implied fine pores, but relatively small pores, such as less than 2 nm, may become plugged in catalyst preparation, especially if high loadings are sought.)

2.8.3 Co precipitation method

In a common procedure an aqueous metal salt solution is contacted with an aqueous alkali, ammonium hydroxide or ammonium carbonate, to cause the precipitation of an insoluble metal hydroxide or carbonate. These can be readily converted to oxides by heating. The starting compounds are generally chosen because of their availability and high water solubility, and in some cases to avoid introducing elements that may be deleterious in the final catalyst or that may cause difficulties in subsequent processing. For example, acids evolved from a chloride during calcining can be highly corrosive. Halogens remaining in the final catalyst may cause an undesired acidic functionality and sodium compounds may enhance sintering.

Control of air and water pollution is also an important factor. NO_2 from nitrates must be removed, e.g., by scrubbing with aqueous alkali; many heavy metals are more or less toxic and cannot be simply discharged. If the final catalyst is to be a supported metal, sulfate may be undesirable, since it can be reduced to a sulfide, which is a common poison for metal catalysts. The metal nitrate salt is often preferred because it usually is highly water-soluble, generally available, and cheap, but NO_x control is required. An organic compound such as a formate or oxalate may be used, although these are more expensive and organic fragments from their decomposition on heating may adsorb on the catalyst to cause partial inactivation. Also, the average ultimate metal particle size may be considerably different if it is formed by decomposition of a compound rather than by reduction of an oxide. Sulfates and chlorides are generally water-soluble, but the anions must usually be removed by washing, and disposal of waste water may be a problem. A preferred base is usually ammonium hydroxide since it leaves no cation residue, but it may complex with some metals and keep them in solution.

If a relatively crystalline precipitate is formed, the size of the crystal may affect the ultimate particle size of a supported metal catalyst. Thus, fine crystals may be desired to produce high surface area of a supported metal catalyst, but crystals that are too fine may be difficult to filter. The size of such crystals may be controlled by a variety of techniques. In a multicomponent catalyst, crystals may be smaller if the metals are truly coprecipitated rather than precipitated in sequence. Crystal size may also be

affected by temperature and by stirring, since this affects nucleation and the degree of supersaturation. Ripening, in which a precipitate is allowed to stand for a period, can allow for recrystallization in which small and/or amorphous particles dissolve and crystalline particles grow. This may convert a gelatinous precipitate to a more crystalline and filterable solid.

2.8.4 Impregnation

Two methods of contacting may be distinguished. The support is sometimes dipped into an excess quantity of solution, whereupon the uptake is the sum of solution occluded in the pore plus material adsorbed onto the pore surface. If two or more compounds are present, they are frequently adsorbed on the support surface in a ratio different from that of the solution; this must be taken into account. Moreover, material may be dissolved from the support into the treating solution. More precise control is achieved by a technique termed dry impregnation or impregnation to incipient wetness, which is commonly used industrially. A batch of support is tumbled and sprayed with a solution of appropriate concentration, corresponding in quantity to the total known pore volume of the support, or slightly less. This allows accurate control of the amount of the active ingredient that will be incorporated into the catalyst, but the maximum loading obtainable in a single impregnation is limited by the solubility of the reagent. The resulting catalyst is then usually dried and calcined.

In a few cases, the active ingredient may be fixed inside by immersing the impregnated catalyst in a reagent to cause precipitation, occur oxide supports such as alumina and silica are readily wetted by aqueous solutions. Capillary forces then ensure that liquid is sucked into the entire porous structure. Because of capillary pressure, even pores closed at one end are nearly filled, and the solution of gas in the liquid assists the process. If the support is not readily wetted, e.g., a carbon that is highly graphitized or without chemisorbed oxygen, an organic solvent may be used or the support may be impregnated under vacuum. These procedures are somewhat more costly to use in the plant than incipient impregnation.

2.9 Literature Reviews

Many research have been studied on the thermal decomposition of organic mater occurring in the absence of air and oxygen. Thermal decomposition in an oxygen deficient environmental can also be considered to be ture pyrolysis as long as the primary products of the reaction are solid or liquid. The products pyrolytic process can be gaseous, liquid and solid.

For example, in 1998, Aik Chong Lua and Jia Guo [6] conducted the preliminary tests to investigate the influences of different operating parameters, such as initial material size, inert gas flow rate, heating rate, pyrolysis temperature and hold time, on the properties of the pyrolyzed chars from oil palm waste. Te reported that the optimum conditions for pyrolysis were found to be for 0.5-1.0 mm material sized at a final temperature of 850°C for 3.5 hour hold time, heating rate of 10°C min⁻¹ and a nitrogen flow rate of 150 Nml min⁻¹. From this condition, chars from extracted oil palm fibers with a maximum surface area could be developed into effective absorbents of activated carbon. Three years later, in 2001, P.R. Bonelli et al. [20] examined changes in chemical and surface characteristics of Brazil nut shells (*Bertholletia excelsa*) due to pyrolysis at different temperatures. The result showed that the pyrolysis of Brazil nut shells leads to significant changes in chemical and textural morphological char-acteristic of lignocellulosic waste that depend markedly on temperature. Release of volatile matter brings about the opening-up of residual cellular structure and consequently, the development of porosity. At the highest temperature (850°C), union of larger pores seems to occur and micropores development becomes strongly predominant. The structure of these pyrolyzed chars were characterized with Elemental Analyzer, Surface Area Analyzer, X-ray Spectrometer and Scanning Electron Microscope. Within the same year, S.Yorgun et al. [3] studied the flash pyrolysis experiments of sunflower (*Helianthus annuus* L.) press oil cake were performed in tubular transport reactor at atmospheric pressure under nitrogen atmosphere. The reactor at atmospheric pressure under nitrogen atmosphere. The effects of pyrolysis temperature, particle size and sweep gas flow rate on the yields of products were investigated. The highest liquid yield of ca. 45% was obtained at a final pyrolysis temperature of 550°C with a particle size of 0.425-0.85 mm, and nitrogen flow rate of 300 cm³ min⁻¹. The liquid obtained shows a maximum

oxygen content at the conditions of maximum liquid yield. The heating value of the bio-oil is 33.7 MJ kg^{-1} which is very close to those of petroleum fractions. The liquid product may be used as a source of low-grade fuel directly, or it may be upgraded to higher quality liquid fuels. The next year, Hasan Ferdi [21] studied the pyrolysis experiments on sunflower (*H. annuus* L.) - pressed bagasse were performed in a fixed-bed tubular reactor under a nitrogen atmosphere. The highest bio-oil yield of 52.10 wt% was obtained at a final pyrolysis temperature of 550°C with particle size of 0.224-0.425 mm with the heating rate of 5°C S^{-1} , and nitrogen flow rate of 50 ml min^{-1} . The highest overall conversion of 79.01 wt% was obtained at the final temperature of 700°C with a nitrogen flow rate of 400 ml min^{-1} . The bio-oil was a mixture of aliphatic and aromatic hydrocarbons having an empirical $\text{CH}_{1.68}\text{O}_{0.165}\text{N}_{0.059}$, H/C molar ratio 1.68 and O/C molar ratio 0.165 at optimum conditions. It was concluded that the liquid product may be better used as a source of chemical feedstock, or it may be upgraded to higher quality liquid fuels. And Rolando Zanzi et al. [5], investigated the rapid pyrolysis of birch and some agricultural residues (olive waste and wheat straw in untreated and in palletized form) at high temperature ($800\text{-}1000^\circ\text{C}$) has been studied in a free-fall reactor at pilot scale. The conditions are of interest for gasification in fluidized beds. Because rapid pyrolysis is the first step in gasification and combustion in fluidized bed reactors, knowledge on rapid pyrolysis may contribute to development of gasification and combustion models in fluidized bed reactors. The higher treatment temperature has led to more tar cracking resulting in higher yield of gaseous products and lower yields of tar. When the pyrolysis temperature was increased from 800°C to 1000°C the char yield decreased. The temperature influences the heating rate. At higher temperature, the heating rate is higher. A similar result, a decrease of the char yield and increase of the gas yield, was obtained when smaller particles of wood and olive waste were used in the reactor. The heating rate for the smaller particles also decreases.

In 2003, Ozlen Onay and co-worker [23] studied the pyrolysis experiments have been conducted on a sample of rapeseed to determine particularly the effects of pyrolysis temperature, heating rate, particle size and sweep gas flow rate on the pyrolysis product yields and their chemical composition of rapeseed. They found that the oil yield was obtained as 49% at a final pyrolysis temperature of 550°C , particle size

range of 0.6-1.8 mm with a heating rate of $30^{\circ}\text{C min}^{-1}$. The oil yield only reached 51.7% with the experiments under sweeping gas atmosphere (nitrogen flow rate of $100\text{ cm}^3\text{ min}^{-1}$). Employing the higher heating rate of $300^{\circ}\text{C min}^{-1}$ breaks mass transfer limitations and the oil yield reach a maximum of 68%, increasing by 32%, at the final pyrolysis temperature of 550°C , particle size range of 0.6-1.25 mm and sweeping gas flow rate of $100\text{ cm}^3\text{ min}^{-1}$.

Furthermore, in flash pyrolysis conditions, the maximum liquid product yield of 73% was obtained at final pyrolysis temperature of $550\text{-}600^{\circ}\text{C}$ particle size range if 0.6-1.25 mm and sweeping gas flow rate of $100\text{ cm}^3\text{ min}^{-1}$. It can be managed that the increasing of 45% of oil yield in flash pyrolysis conditions compared to that of slow pyrolysis. Fast pyrolysis technologies are receiving considerable attention because they can produce a more dense and easily transportable fuel compared to origin feedstocks. The pyrolysis oil conceivably can be used as a chemical feedstock for other processes.

In 2005, Haiping Yang et al. [22] studied concerns the various gaseous products released during the pyrolysis of palm oil wastes. The influence of temperature was investigated by repeated experiments at 250, 280, 300, 325, 355, 400 and 450°C .

The result showed that the temperature has a significant influence on the pyrolysis of palm oil wastes, particularly on the distribution of gaseous products. The different patterns of the rate of pyrolysis and profile for evolution of gas at low ($<355^{\circ}\text{C}$) and high temperatures ($>355^{\circ}\text{C}$) indicate that different reaction pathways are involved. The experimental study using TGA-FTIR and thermodynamic modeling both indicate similar results: the total yields of gas increase with temperature at the expense of char residue. The large amounts of H_2 produced above 355°C are thus reasonably postulated. Simulations of thermodynamic equilibrium indicate that H_2 , CO_2 , CH_4 and CO are the main gaseous products. They confirmed that H_2 is produced only at high temperatures. The yields of H_2 and CO increased with temperature and have maximum yields of 45 and 30 mol%, respectively, at temperatures higher than 900°C . The yields of H_2O , CO_2 and CH_4 decrease if the temperature increase and because essentially zero at high temperature ($>800^{\circ}\text{C}$).

Recently, in 2006, Hasan Ferdi Gercel and co-werker [21] studied the effects of pyrolysis temperature, heating rate, particle size and sweep gas flow rates on the yield of the products from olive baggasse. Pyrolysis runs were performed using pyrolysis temperatures between 350°C and 550°C with heating rate of 1.0 and 50°C min⁻¹. The particle size and sweep gas flow rates varied in the range 0.2-1.8 mm and 50-200 cm³ min⁻¹, respectively. The bio-oil obtained at 500°C was analyzed and at this temperature the liquid product yield was the maximum. The higher treatment temperature led to lower bio-oil yields and higher gas yields. The bio-oil was a mixture of aliphatic and aromatic hydrocarbons having an empirical formula of CH_{1.62}O_{0.25}N_{0.03}. Also FTIR analysis showed that the bio-oil composition was determinted by oxygenated species. The high oxygen content is reflected by the presence of mostly oxygenated fractions such as carboxyl and carbonyl groups produced by pyrolysis of the cellulose and phenolic and methoxy groups produced by pyrolysis of the lignin.

Lately, in 2007, O. Eylem et al. [9] studied the trends in yields and product compositions of slow pyrolysis and fast pyrolysis were determined and compared with each other. Slow pyrolysis of tobacco residues with particle of between 0.425 and 0.85 mm were conducted in a fixed bed tubular reactor with a heating rate of 7°C min⁻¹ for various pyrolysis temperatures (400, 500, 550 and 700°C) and various nitrogen flow rates (50, 100, 200 and 400 cm³ min⁻¹). From the results of the experiments, it can be concluded that the yields of volatile pyrolysis products depend on the final pyrolysis temperature, type of pyrolysis and heating rate. The maximum oil yield was obtained as ~ 27% at the pyrolysis temperature of 550°C with the sweeping gas flow rate of 100 cm³ min⁻¹ by slow pyrolysis. Increasing heating rate up to 300°C min⁻¹ caused 10% increase of liquid yields (~30%). The result of the yields where as higher temperatures up to 550°C favor liquid yields. Pyrolysis of tobacco residues leads to three phases (solid, liquid and gaseous) whose yields strongly depend on temperature and heating rate. It is proved that different pyrolysis technique caused difference in product quantity and quality. High temperature (>700°C) was favorable for the evolving of hydrogen-rich gases, while medium temperature (500-600°C) was recommendable for a higher generation of liquid oil and charcoal with a large BET surface area and fine pore size.

In 1999, Bhabendra K. Pradhan and co-worker [10] studied the effect of different oxidizing agent treatments on the surface properties of activated carbons. The identification of the function groups on activated carbons prepared under different conditions are important from its application point of view. Most of the time a specific functional group plays a significant role in imparting character of carbon. The objectives of the present work therefore is to assess how the surface chemistry and the texture of the activated carbons change after their treatment with different oxidizing agents viz. , HNO_3 , H_2O_2 and $(\text{NH}_4)_2\text{S}_2\text{O}_8$. The results of characterization of activated carbons are predominantly microporous and they retain this character even after oxidation with different oxidizing agents and heat treatment. The adsorption capacity of activated carbons is decreased by oxidation, the decrease being minimum in the case of HNO_3 and maximum in the case of H_2O_2 and the adsorption capacity of granular activated carbons is more than that of activated charcoal cloth. In the case of $(\text{NH}_4)_2\text{S}_2\text{O}_8$ the sample retained its microporosity to some extent and have the stronger acidic groups. The removal of surface oxygen groups by heat treatment results in the regeneration of its pores and hence the adsorption capacity. These findings can be useful when these activated carbons used for removal of inorganic and organic pollutant from aqueous phase as well as for organic vapor adsorption.

In 2001, Li-Yeh Hsu and Hsisheng Teng [23] investigated the influence of different chemical agents on the preparation of activated carbons from bituminous coal. Activated carbons were prepared by chemical activation from bituminous coal with three chemical agents, ZnCl_2 , H_3PO_4 and KOH . They found that ZnCl_2 and H_3PO_4 , which are acidic, are not suitable for preparing high-porosity carbon from bituminous coal, while carbons with very high porosity can be produced with bases such as KOH .

In 2005, Lu Chunlan et al. [12] studied the influence of pre-carbonization of petroleum cokes on the properties of the activated carbon precursors and final carbons activated with KOH . TG-DTG study revealed the decomposition of volatile species and volatile species and FTIR analysis identified the presence of C-O, C-O-Cm C-O-H and some alkyl groups on the surface of petroleum cokes pre-carbonized at studied temperatures. Increasing the pre-carbonization temperature decrease noticeably the

amount of thus surface species, which act as the active sites in the chemical activation with KOH. XRD results indicated that a disorder occurred after carbonization at 500°C and a transition of gradually getting ordered in the pre-carbonized petroleum cokes. Happened with increasing pre-carbonization temperature from 500, 800, to 1200°C. The precursors pre-carbonization at 800 and 1200°C are more difficult to be activated with KOH than the fresh sample without vi pre-carbonization and the precursor pre-carbonized at 500°C. The decreases in the BET surface area and N₂ adsorption capacity coincided with the reduction in the functional species on the precursor surface with the increase of the pre-carbonization temperature.

In 2006, Aik Chong Lua et al. [13] studied the influence of pyrolysis conditions on pore development of oil-palm-shell activated carbons. Physical activation normally involves two stages pyrolysis and activation. During pyrolysis, the starting materials are carbonized in an inert atmosphere, which is usually nitrogen at temperature from about 400-800°C to produce chars with rudimentary pore structures. These chars are then activated in oxidizing gases such as carbon dioxide, steam or just air at temperature of about 800-1000°C to produce the final activated carbons: The shells were first subjected to a pyrolysis process and the resulting chars were then treated under a physical activation process in the presence of carbon dioxide. The influences of the operating pyrolysis parameters on the activated carbon were investigated in particular. These parameters included the pyrolysis temperature and hold time, the volume flow rate of the purging gas (N₂) and the process heating rate. All the char were subjected to fixed activation conditions, i.e., CO₂ activated at 900°C, 30 min hold time, CO₂ flow rate of 100 cm³/min and heating rate of 10°C/min under a nitrogen flow rate of 150 cm³/min. The specific pore surface area and the micropore volume of the activated carbon were used as the criteria for selecting the optimum pyrolysis parameters. The optimum conditions for pyrolysis were a temperature of 600°C, hold time of 2 hours, nitrogen flow rate of 150 cm³/min and heating rate of 10°C/min that yielded the activated carbon with the highest BET surface area. The activated carbon prepared under these optimum conditions had a BET surface area of 519 m²/g and a micropore area and volume of 475 m²/g and 0.215 cm³/g, respectively.

In 2007, Y. Onal et al. [14] studied the effect of activation temperature on the activated carbon samples prepared from sugar beet bagasse that in an industrial waste was investigated by chemical activation with $ZnCl_2$. The result showed that the determined surface area of the activated carbons was $1697 \text{ m}^2/\text{g}$ at 500°C . These activated carbons are essentially microporous. Increase in the activation temperature up to 500°C leads to development of microporous structure and mesoporous structure starts to develop after this temperature. The maximum activation yield is observed as 37% at 500°C . The yields of the chars, which impregnated with $ZnCl_2$, change scarcely in the temperature range of $600\text{-}900^\circ\text{C}$. In this temperature range; the surface area and pore volume of the activated carbon decrease.

Within the same year, Yanping Guo and David A.Rocksraw [15] studied the activated carbons with high surface area and strong acidic surface chemistry properties as well as low ash content can be prepared from rice hull by one-step H_3PO_4 activation at relatively low temperatures. A threshold activation temperature exists for the development of porous structure on carbons prepared from rice hull by H_3PO_4 activation. This temperature is 300°C for the process investigated in this study. The activated carbons tend to be microporous under the studied activation in particular the contribution of the silica component. Low activation temperature favors the formation and retention of acidic groups on the surface of H_3PO_4 activated rice-hull based activated carbons. The acidic surface groups consist of both temperature-sensitive and temperature insensitive contributions. The temperature-sensitive groups are primarily carbonyl-containing groups of varying acidic strengths and silanol groups; while the temperature-insensitive one are mainly phosphorus-containing groups and groups containing Si-O bond, and to a less degree, carbonyl-containing groups with different acidic strengths.

Biomass as a source of renewable energy presents at least one main advantage over fossil fuels: lower emission of carbon dioxide and other greenhouse gases. In particular, hydrogen production from biomass from fuel cells application is very attractive and this process has been optimized in fluidized bed and fixed bed conditions. The catalyst has to be strong enough to resist attrition in addition of having a

similar density as the biomass to be fluidized and fixed bed in the same conditions. Biomass steam gasification leads to a mixture containing water, hydrogen, carbon oxides and small amount of methane and higher hydrogen by catalytic light hydrocarbons reforming with water and carbon dioxide. Both are present in the mixture and both can be used as oxidants.

For economic reasons nickel catalyst is the most suitable choice among metals like Co, Fe, Pt, Ru and Rh. Ni on Al_2O_3 or MgO favours syngas production with high H_2/CO molar ratio but, when used at high temperatures, sintering of nickel particles and carbon deposition occurs.

For example, in 2000, C.Courson et al. [16] studied the optimum condition of biomass gasification in fluidized bed by the use of metallic nickel as active phase grafted on olivine. Natural olivine ($(\text{Mg}, \text{Fe})_2 \text{SiO}_4$) has been chosen as catalyst support because of its activity in biomass steam gasification and tar cracking, its high attrition resistance. After impregnation of nickel oxide on olivine and calcinations at 900, 1100 or 1400°C, different interactions between the precursor and the support have been revealed by X-ray diffraction, scanning electron microscopy and transmission electron microscopy coupled to energy dispersive X-ray spectroscopy. The most promising catalyst determined after these different characterization studies contained 2.8 wt% of Ni and was calcined at 1100°C. It exhibited strong nickel-olivine interaction but the grafted nickel oxide particles stayed reducible under catalytic test conditions.

Already at 750°C, this catalyst presented a high activity in dry-reforming (95% methane conversion) and steam-reforming (95% methane conversion) and steam-reforming (88% methane conversion) and yield in syngas (80% and 75% CO yield, respectively). An excess of water content in steam-reforming inhibited the catalytic activation which could be retrieved by addition of a reducer like H_2 .

In 2002, C.Petiti et.al. [17] studied the preparation of nickel oxide upon natural olivine is obtained by impregnation with a nitrate salt. The type of interaction of nickel oxide with olivine is different depending upon the synthesis method and the calcinations temperature. For calcinations at 1100°C the effects of the amount of NiO and the number of impregnation have been studied. At a high temperature of calcinations (1400°C), NiO

is integrated into the olivine structure and the amount of free iron increases. Integrated NiO on olivine is non reducible, resulting in an inactive catalyst. At lower calcinations temperatures grafted NiO is formed a species which is reduced under catalytic test conditions without aggregation of particles. A single impregnation of nickel (5.5 wt% of NiO) gives a stable catalyst activated directly under reaction conditions ($\text{CH}_4 + \text{CO}_2$) yielding 96% CO and 76% H_2 . Catalysts with lower amounts of NiO or a double impregnation of nickel salt lead to a less stable system. This system is promising for the catalytic gasification of biomass to $\text{CO} + \text{H}_2$, in fluidized bed, given its high attrition resistance and the presence of nickel particles strongly linked to the support.

In 2004, M.Piana and co-worker. [30] studied a new sol-gel synthetic route has proven effective in the production of pure LiMPO_4 (with Fe or Mn as the active transition metal M). The amorphous precursors allow the production of powders with submicrometric agglomerates of nanocrystalline domains that are smaller than those prepared by solid state synthesis with the same thermal treatments. With this new route, it is also possible to produce a very homogeneous carbon dispersion in the phosphate phase by simply adding, for example, carbon black in the solution before gelation. The crystallization temperature of the precursors is low and comparable to that found in other similar syntheses, which allows a lower annealing time or temperature. Such synthetic improvements lead to a constant increase in specific capacity of LiFePO_4 samples. On the contrary, LiMnPO_4 samples show extremely poor electrochemical performance, which is in agreement with previous data from the literature. The observed results for LiMnPO_4 are justified by the strong cooperative Jahn-Teller distortion at the Mn^{3+} ions, which causes an extreme instability of the crystalline charged phase MnPO_4 . The synthesis is defined as promising because the preparation conditions, thus the properties of the products, can be further optimized.

In 2005, Krzysztof J.Ptasinski [31] investigated the Olivine as tar removal catalyst for biomass gasifiers. Calcination of olivine with air at 900°C for different treatment times of 1/5/10 hours, could improve its activity significantly towards tar removal. Calcination time of 10 hours is observed to be the optimal for tar conversion among the tested calcinations times. Further increase of calcinations time to 20 hours, however, dose not

improve the conversion, rather similar conversion is observed. This activity could be related to the segregation of iron at the surface of olivine due to calcinations. Visually a color change of olivine from typical pale green to brown-red is observed after calcinations. The BET-surface area of olivine is less than $0.5 \text{ m}^2 \text{ g}^{-1}$ and hence olivine can be regarded as non-porous. The iron segregation at the surface of olivine is found to be non-uniform. Also the oxidation state of iron changes due to calcinations. The contribution of the crystalline hematite increases with increase in the calcinations time of olivine. For higher treatment times, concentration of iron at the surface increases, thus increasing the possibility of higher reduction due to presence of H_2 as a product gas. Although the exact correlation between catalytic activity of olivine and calcinations is not understood yet, it is obvious that the activity is related to the presence of iron at the olivine surface and appearance of iron (III) phases. Besides catalytic activity towards tar reduction, olivine is also observed to be highly attrition resistant and thus can be a prospective candidate as an in-bed catalyst for fluidized bed biomass gasifiers.

In 2007, Lei Wang and Dianzeng Jai [32] prepared and characterized of nano-size LiFePO_4 by low heating solid-state coordination method and microwave heating. Compared with the complicated conventional furnace heating procedures, this method presents a more preferable and faster way of nano- LiFePO_4 synthesis. In the heating process, suitable citric acid addition led to the formation of homogenous nano-particles with the diameter of 40-50 nm and good crystalline phase, which improved the cycling performance of LiFePO_4 . Charge-discharge testing indicated that the sample with 2.5 nmol citric acid addition possessed satisfactory electrochemical capacity of 123 mAhg^{-1} at the 50th cycle. The excellent cycle life and stability as well as the fast and efficient method make the process feasible commercially. The whole synthesis process, performed without any solvent, is economic and environmentally benign.

In 2007, C. Courson et al [33] investigated Ni/olivine catalyst, previously developed for biomass gasification and tar removal during fluidized bed steam gasification of biomass, was tested in a fixed bed reactor in toluene steam reforming as a tar destruction model reaction. The influence of the catalyst preparation parameters (nickel precursor, calcinations temperature and nickel content) and operating

parameters (reaction temperature, steam to carbon S/C ratio and space-time) on activity and selectivity was examined showing a high toluene conversion and a low carbon formation compared to olivine alone. The results study performed on this optimized catalyst, with 3.9 wt% of Ni, as a function of operating parameters demonstrates that, for a reaction temperature higher than 650°C, total toluene conversion is obtained and carbon formation is negligible. The main gaseous reaction products are H₂ and CO which are having proportions in good agreement with thermodynamic equilibrium. The total amount of carbon formed on the N1100 catalyst decreased with an increase in reaction temperature. Reducing space-time about two orders of magnitude, gave the same conversion when the temperature was raised from 560 to 800°C. In the range of studied S/C ratios, from 1.1 to 3.4, no influence on toluene conversion or CO and CO₂ selectivities was observed, although the amount of carbon formed on the Ni/olivine catalyst decreased from 180 to 30 $\mu\text{g}/(\text{g}_{\text{cat}} \cdot \text{hC}_{\text{conv}})$. The catalyst stability resulting from resistance towards carbon formation can be explained on the base of the particular structure of the reduced catalyst which can be described as Ni-Fe/Mg/olivine system. Both factors-the presence of Ni-Fe alloys and basic MgO oxide are beneficial for limiting carbon formation. The importance of Ni/olivine catalyst was clearly demonstrated by the comparison with olivine alone: higher activity, higher selectivity to H₂ and CO, and lower carbon deposition.

And Robert C. Brown et al. [34] studied steam reforming of tar compounds over Ni/Olivine catalysts doped with CeO₂. Producer gas from this process usually contains unacceptable levels of tar. Tar can cause operational problems in downstream processes by blocking gas coolers, filter elements and engine suction channels. Most producer gas applications require removal of at least part of the dust and tar before the gas can be used. Olivine was used as a substrate for various catalyst formulations designed to steam reform tar to gas. Three catalysts were prepared by wet impregnation, yielding the following compositions: 3.0% NiO/Olivine, 3.0% NiO/olivine doped with 1.0% CeO₂ and 6.0% NiO/olivine. Benzene and toluene were selected as model compounds of biomass tar. Catalytic steam reforming of these compounds was performed in a bench scale fixed bed reactor at temperatures between 700 and 830°C using a molar ratio of steam/carbon (S/C) equal to 5. The effect of catalyst composition

on tar conversion and yields of various product gases were determined. The result showed that the steam reforming of benzene and toluene were investigated for Ni/olivine and Ni/olivine doped with CeO_2 catalyst was particularly effective compared to the other two NiO/olivine formulations in terms of both catalytic activity and coking resistance. Cerium oxide is thought to promote the catalytic activity of nickel and resist the deposition of the carbon. CeO_x ($x = 1.5$ or 2) produced during the catalyst reduction, which also existed in the steam reforming environment. The promotion effect of cerium oxide on the nickel catalyst for steam reforming of benzene is probably through a redox mechanism. The lower valence state cerium might adsorb water and dissociate it, the resulting species $-\text{O}$ or $-\text{OH}$ transferring to the nickel and reacting with surface carbon species to form carbon monoxide, carbon dioxide and hydrogen gases.

The obtained researches are useful for the study focuses on the optimum pyrolysis condition of physic nut (*Jatropha Curcas* L.) waste as a source of chemicals production should become more attractive within the biorefinery concept. The current situation resembles the early days of the development of a chemicals industry from coal and coke or the later development of the early petrochemical industry. Chemical and engineering knowledge is now far more advanced, so technical advances will occur more rapidly when economics dictate a change. Major technical opportunities exist to develop catalytic biomass pyrolysis processes and subsequent catalytic transformation of the bio-oils and gases produced.

CHAPTER III

EXPERIMENTS

The objective in this research is divided into three parts. Firstly, the pyrolysis conversion of Physic nut (*Jatropha curcas* Linn.) waste to fuel products was carried out in a fixed bed reactor. The effect of different pyrolysis operating parameters, such as pyrolysis final temperature, hold time, and heating method on the quality and quantity of the pyrolyzed products were investigated. Secondly, the activated carbons from pyrolyzed physic nut waste char were produced via with physical and chemical activations. The effects of activation temperature, activation time, particle size of solid char, and type and concentration of activation agents were investigated. The characteristic of activated carbon were evaluated. The last objective of this research is to synthesis olivine and Ni/olivine as catalysts for tar reduction to upgrading products to more quality fuels. The catalytic activity of catalyst was investigated in a fixed bed reactor over glycerol waste as long chain hydrocarbon.

3.1 Biomass raw material

The raw material was prepared from Physic nut waste from Chiang Rai province that were left after extraction of oil from biodiesel Production process The raw material is shown in Figure 3.1.



Figure 3.1 Physic nut (*Jatropha curcas* Linn.) residue.

3.2 Chemicals

1. Potassium dihydrogen phosphate (KH_2PO_4)	Sigma-Aldrich
2. Disodium phosphate (Na_2HPO_4)	Fluka
3. Methylene blue ($\text{C}_{16}\text{H}_{18}\text{N}_3\text{SCl} \cdot 3\text{H}_2\text{O}$)	Fluka
4. Cobolt nitrate ($\text{Co}(\text{NO}_3)_2 \cdot 6\text{H}_2\text{O}$)	Sigma-Aldrich
5. Ferric citrate n-hydrate ($\text{FeC}_6\text{H}_8\text{O}_7 \cdot n\text{H}_2\text{O}$)	Fluka
6. Hydrochloric acid (HCl)	Merck
7. Potassium hydroxide (KOH)	Fluka
8. Phospheric acid (H_3PO_4)	AJAX
9. Nickel nitrate ($\text{Ni}(\text{NO}_3)_2$)	Merck
10. Paradium nitrate ($\text{Pd}(\text{NO}_3)_2$)	Fluka
11. Lithium Phosphate (Li_3PO_4)	Sigma-Aldrich
12. Methanol (CH_3OH)	Merck
13. Chloroform-D (CHCl_3)	Merck
14. Iodine (I_2)	Sigma-Aldrich
15. Sodium thiosulfate ($\text{Na}_2\text{O}_3\text{S}_2 \cdot 5\text{H}_2\text{O}$)	Merck
16. Potassium iodine (KI)	Fluka
17. Potassium iodate (KIO_3)	Fluka
18. Strach, Soluble potato	AJAX
19. Sodium hydroxide (NaOH)	Fluka
20. Nitrogen gas (N_2)	TIG
21. Oxygen gas (O_2)	TIG
22. Hydrogen gas (H_2)	TIG
23. Air zero	TIG
24. Mixed gas	TIG

3.3 Pyrolysis reactor and other apparatus

The fixed bed reactor was a vertical heater. The system consisted essentially of a quartz tube reactor (height = 400 mm, inside diameter = 12 mm, and wall thickness = 0.5 mm) with a sample retainer made of quartz wool, a cooling system for the separation of water and condensable organic vapors (tar), and a gas cleaning / drying system followed by gas-measurement devices. The bed could be operated maximum 1100°C. Air flew into the bed, which was controlled by using a mass-flow meter. The fixed bed pyrolysis, which was used in this work and a schematic of the experimental setup, are show in Figure 3.2.

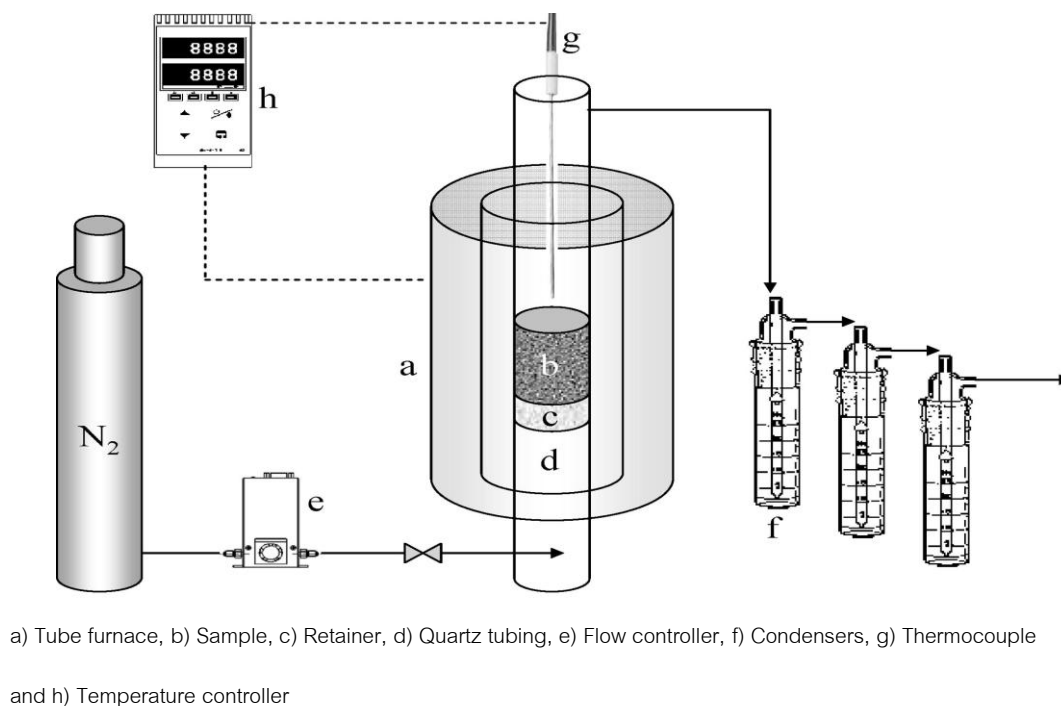


Figure 3.2 Schematic of the pyrolysis reactor setup

3.4 Apparatus used in this research included

1. UV / VIS Spectrophotometer : SPECORD S100 ; Analytikjena.
2. Microscope : OLYMPLUS SZ40 ; E for L INTERNATIONAL Co., Ltd.

3. Viscometer : KU-2 ; BROOKFIELD.
4. Balance : AB 204-S ; Metter Teledo.
5. Gel Permeation Chromatography (GPC) : RID-10A ; SHIMADZU.
6. Vacuum oven (0-300°C) : Medell 100-800 ; Memmert.
7. Vacuum pump : WJ-20 ; SIBATA.
8. Fisher Stirring Hotplate ; Fisher Scientific Col, Ltd.
9. Electric Automatic Drying System : OD-10 ; Shin-ei Co., Ltd.
10. Laboratory test sieve : MESH NO. 8, 16, 20, 35 and 40 ; ENDECOTTS Ltd.
11. Gas liquid Chromatography : GC 2010 ; SHIMADZU.
12. Varian Gas Chromatography : CP 3800 ; Thai Unique Co., Ltd.
13. Electric Furnace : D2804 ; Lilienthal / Berman Co., Ltd.
14. pH-meter : UB100 ; DENVER Instrument Co., Ltd.
15. Thermo gravimetric analyzer (TGA) : TGA / SDTA 851^e ; Metter Toledo.
16. Sampling bag (1L) ; Cole-Parmer, U.S.A.
17. Automatic Bomb Calorimeter : AC-350 ; Leco.
18. Nuclear magnetic resonance spectroscopy (NMR) : DPX 300 ; Bruker Biospin.
19. Surface area analyzer : ASAP 2020 ; Micromeritics Instrument Corporation.
20. Scanning electron microscope (SEM) : JSM E410 ; JELO.
21. Fourier-transform infrared spectroscopy (FT-IR) : System 2000 FT-IR ; PERKIN ELMER.
22. CHNS/O analyzer : PE 2400 Series II ; PERKIN ELMER.
23. X-ray diffraction (XRD) : AXS diffractometer ; Bruken.
24. Particle size analyzer : Malvern Instrument 2000.
25. Online gas analyzer : MRU GmbH ; SWG 200⁻¹

3.5 Experimental Part I: Pyrolysis of physic nut waste

3.5.1 Pyrolysis process: effect of pyrolysis temperature and time and particle size of physic nut waste

The various parameters including temperature, time, size of raw material were investigated in order to determine the optimum condition for the production of the fuel products from pyrolysis process. Experiment is shown in Figure 3.3. The procedures are described as follows :

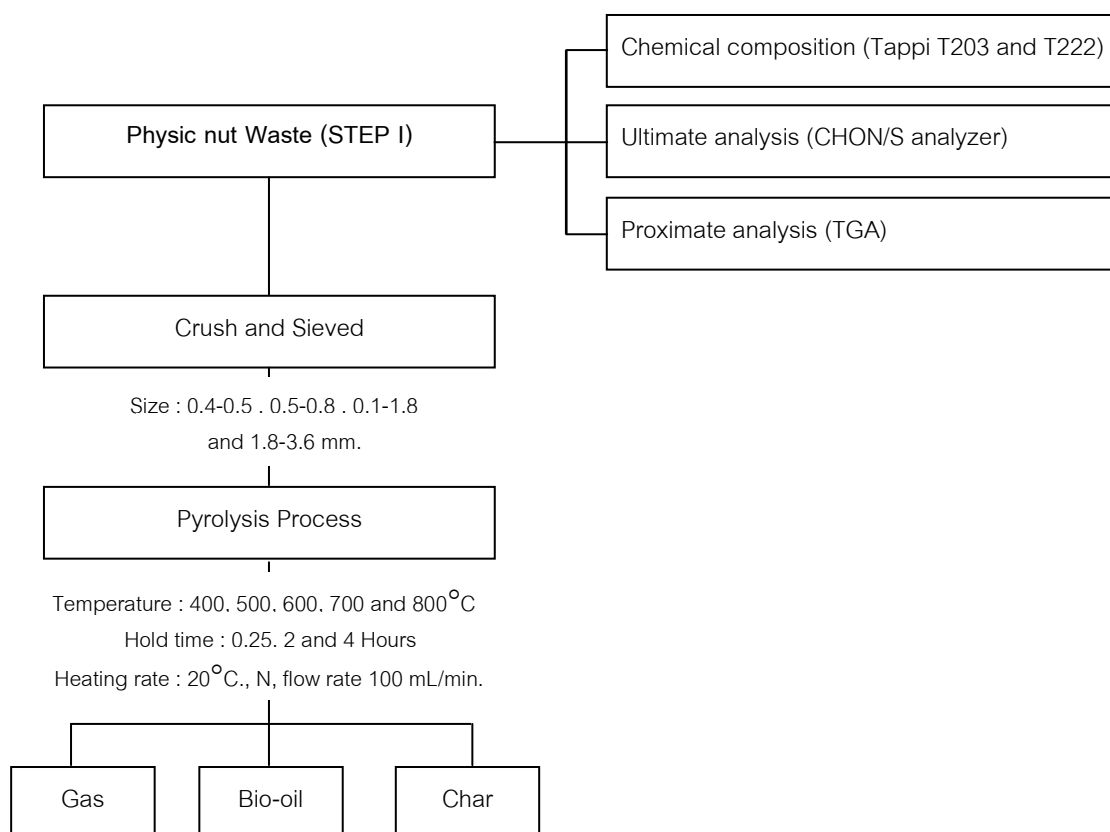


Figure 3.3 Flow chart of screening test for selected optimum condition

Extracted physic nut wastes (grain mill with Hatz engine) from local operation were first dried at 60°C for 24 hours to reduce their moisture content. The dried samples were crushed and sieved to different size fractions (0.425-0.5, 0.5-0.85, 0.85-1.8 and 1.8-3.6 mm). The chemical contents of physic nut waste sample were further identified using Tappi T203 and T222 standard methods.

For every trial, approximately 5.5 g of sample was placed into the reactor. Prior to heating, inert gas (high purity nitrogen) was provided from the bottom of the reactor at 100 mL/min to maintain the pyrolysis atmosphere. The ceramic tube furnace was then heated at a heating rate 20°C/min to the final pyrolysis temperature of 400, 500, 600, 700 and 800°C, respectively, each with hold times of 0.25, 2, and 4 hours, then left to natural cool down before disassembled to recover char samples. Finally, the % yield (solid, liquid, and gas), % ash, % volatile matter and % fixed carbon of solid products were analyzed following ASTM.

3.5.2 Pyrolysis process: effect of heating method

After screening test, favorable operating conditions will be used for further investigation on in-depth pyrolysis process. Pyrolysis of physic nut residues was conducted under isothermal (fast) and dynamic (slow) heating conditions in a vertical fixed bed type reactor. The influences of final pyrolysis temperatures and hold time on the quality and quantity of the pyrolyzed products were also studied (Figure 3.4). The system consisted of a quartz tube reactor (height = 300 mm., i.d. = 12 mm., and o.d. = 13 mm.) with a sample retainer made of quartz frit at the bottom end and a three stage condensers for the collection of water and condensable organics (tar) followed by gas-measurement devices. The reactor is heated by a tubular ceramic furnace equipped with a PID temperature control and K-type thermocouple placed at the center. In each run, approximately 10 grams of sample material was used and the system was purged with 2 L/min of N₂ for 15 min to ensure inert conditions in the bed.

For dynamic cases, the physic nut waste was placed into the reactor prior to heating and the temperature was raised with 20°C•min⁻¹ from ambient to final temperature of 500, 700 or 900 °C. Experiments were carried out in three different hold times, namely, 15 min, 30 min and 60 min. For isothermal pyrolysis trials, the reactor was preheated to a final temperature of 500, 700 or 900°C and instantaneous decomposition started as soon as waste sample was rapidly inserted into the reactor. The retention time was kept at 15 min. After each run, char left in sample retainer was carefully weighed, liquid product was collected in cold traps maintained at 0°C. Non-condensable gas was analyzed by online gas analyzer (MRU GmbH, SWG 200-1) which

capable of continuous real time quantification of CO, CO₂, C_xH_y (as CH₄) and H₂ by using thermal conductivity detector (TCD) and non-disperse infrared detector (NDIR). Solid and liquid yields were calculated on a dry basis from the measured weight of each fraction. Yields of identified gas were calculated based on conversion of measured mole (vol.) to mass of that particular gas species.

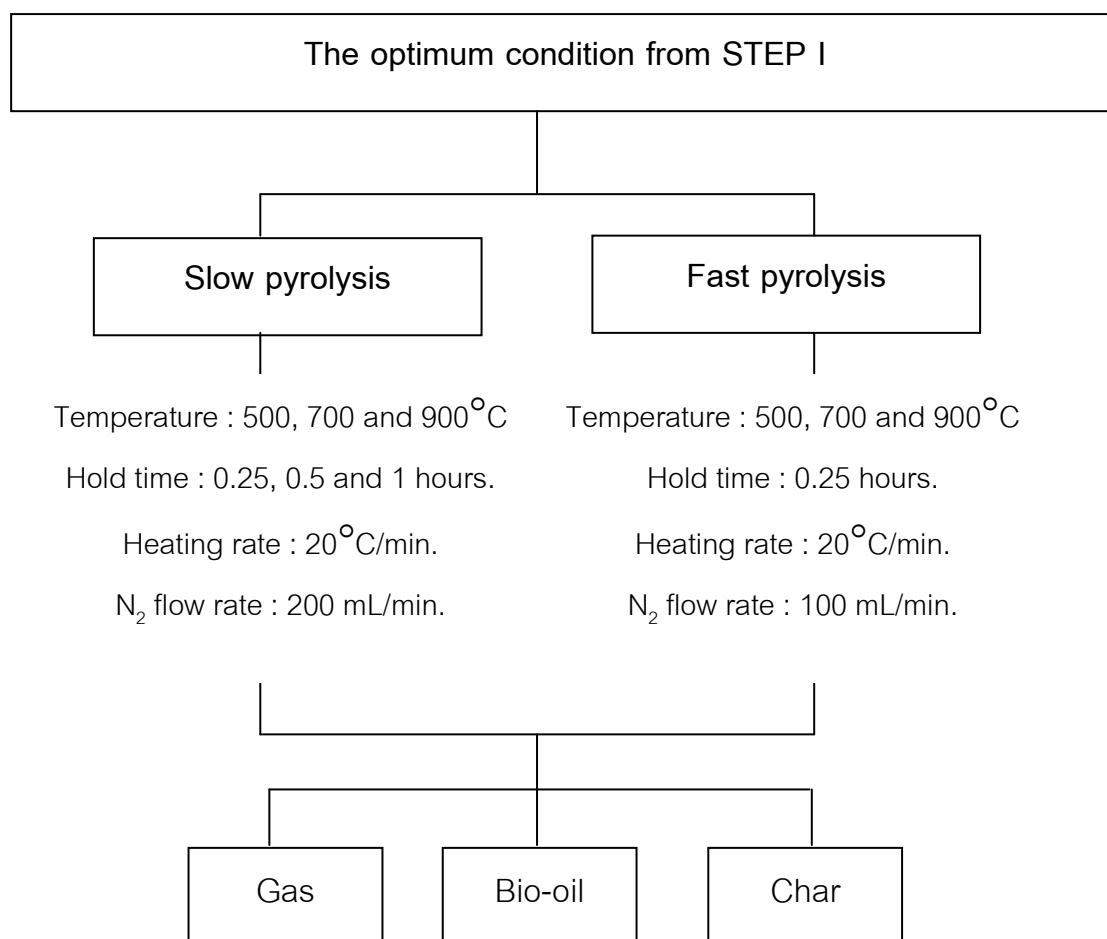


Figure 3.4 Flow chart of different pyrolysis processes for selected optimum condition

3.5.3 Characterization of products from pyrolysis process

3.5.3.1 Characterization of solid char

After pyrolysis, the solid char was removed, crushed, and sieved to a uniform size, ranging from 0.43-0.5 mm, and then kept in a desiccators for further used. Major elemental components of the solid were analyzed using a CHNS/O analyzer (Perkin Elmer PE2400 series II). Fixed carbon, volatile, and ash analyses were carried out using a thermogravimetric analyzer.

3.5.3.2 Characterization of bio-oil

After completing the pyrolysis reaction the reactor was cool down to room temperature and the bio-oil was collected from the condensers. These liquid products contained an aqueous phase and oil phase (tar, pyrolytic oil or bio-oil), which were separated. The solvent part of the oil phase, which dissolved in dichloromethane was extracted in a rotary evaporator and the quality of bio-oil was established. The bio-oil selected for characterization were those obtained at the pyrolysis conditions, which gave the maximum oil yield.

For this purpose, spectroscopic and chromatographic methods were used. Elemental analysis was performed on a Perkin Elmer PE 2400 series II. Fourier transform infrared spectroscopic analysis of the bio-oil was performed on a Perkin Elmer system 2000 FT-IR spectrometer to determine its functional groups. Oil was dissolved in 100 mL of acetone solution, and 1 mL of solution was added on to a KBr pellet. The pellet was heated at 50°C for 10 minutes to allow acetone to be fully vaporized to minimize the interference of transmittance caused by acetone. A thin film of organics was, thus, on the KBr pellet and adsorbed IR spectra. The spectra were recorded from a wave number of 400-4000 cm⁻¹.

The ¹H-NMR spectra of the bio-oil were obtained at a hydrogen frequency of 300 MHz using a Bruker Biospin DPX-300 instrument. The chemical classification and composition of the bio-oil were determined by gas chromatography coupled with a mass selective detector (SHIMADZU 2010). The oven program consisted of 2 minutes of isothermal at 40°C and then a ramp to 100°C at 1 minute, followed by 0.2 minute of isothermal at this temperature. The oven was continuously heated to 105°C at 2°C/min, and then it was heated to 250°C at 30°C/minute and maintained for 2 minutes. Helium was taken as a carrier gas at a 1.2 mL/minute constant flow rate. The injector was pulsed splitless at 200°C ; pulsed pressure and time were set at 25.0 psi for 1 minute, purge flow and time were set at 50.0 mL/minute for 0.25 minute, and gas sever flow and time were set at 20 mL/minute for 3 minutes.

The density, viscosity, pH value and heating value of physic nut waste bio-oil were measured. The density was measured with a density measurement bottle.

Viscosity of a liquid is the measurement of its internal friction which resists the flow of the fluid. The viscosity of bio-oil was measured according to the ASTM D445. The pH was measured with a digital pH meter (DENVER Instrument, Model UB 100).

Calorific value of bio-oil was measured by means of an Oxygen bomb calorimeter (Leco model AC-350). The solids content in the pyrolysis oil were measured as ethanol insoluble portion. A certain amount of oil was weighed (5-10 grams) and dripped into a beaker containing 50-100 ml ethanol solvent and agitated by magnetic stirrer. The insoluble portion remained on the dried filter paper was weighed out. Some characteristic properties of pyrolysis oil was evaluated in accordance with the American Standards for Testing and Materials (ASTM) guidelines for petroleum products and analysis methods.

3.5.3.3 Characterization of producer gas

When pyrolyzing the physic nut waste, the furnace was heated to the selected temperature (400-800°C) from the ambient temperature at 20°C/minute. With temperature increasing, the waste sample decomposed and volatiles were purged out by N₂. Following that, the condensable volatiles were collected in the ice-water condenser, whereas those non condensed parts were filtered and cleaned through a quartz wool filter. The gas generated in the course of pyrolysis trial was sequentially collected using a gasbag for every 5 minutes. The initial gas-sampling time started as the furnace temperature reached 200°C and continued for every 5 minute until the pyrolysis was completed. Then it was immediately analyzed using micro-GC. (Varian, CP-3800) with thermal conductivity detectors (TCD). Channel A with molecular sieve 5A column (MS-5A) was set 90°C for determination of H₂, CO, and CH₄. Channel B with Porapak Q (PPQ) was set at 60C for checking CO₂, C₂H₄, and C₂H₆. The gas-bags were cleaned by N₂ purge and vacuumed after each trial of gas sampling. Micro gas chromatography (GC) has been used to analyze qualitatively and quantitatively the gas components from physic nut waste conversion because of the following advantages : small amount of sample ($\times 10^{-6}$ cm³) needed, short retention times (~ 180 seconds), high accuracy, speed, and profitability.

After each trial, the furnace was cooled instantly. Gas yield was calculated by combining all the gases collected in the whole temperature range and was converted from volume to weight percentage at ambient temperature and atmospheric pressure (the volume of 1 mol gas equals 24.45 L at 1 atm and 25°C).

3.6 Experiment Part II: Preparation and characterization of activated carbon from pyrolyzed physic nut waste char

After pyrolysis, the char was removed, crushed, and sieved to a uniform size, ranging from 0.43-0.5 mm, and then kept in a dessicator for further chemical (via KOH and NaOH) and physical (via CO₂) activation methods.

3.6.1 Physical Activation by oxidizing gas

Temperature and activation time which have an effect on the activation process were studied in order to determine the optimum conditions for producing activated carbon. Experiment scheme of the production of activated carbon from Physic nut waste was shown in Figure 3.5. The procedure were described as follows.

3.6.1.1 The effect of activation temperature

In this work, four different temperatures (400, 500, 600, and 700°C) were studied for activation process. Ten grams of Physic nut waste char with particle size of 0.43-0.5 mm was loaded into a tubular reactor. Then the reactor was passed with CO₂ at the bottom. Then CO₂ was allowed to flow though from the bottom to the top at the flow rate of 100 mL/min. Next, the reactor was heated to the desired temperature. The CO₂ was charged continuously on, passing up though the reactor of each fixed temperature and 1 hour of reaction time. Finally, bulk density, iodine number, methylene blue number and B.E.T. surface area of obtained activated carbon were characterized.

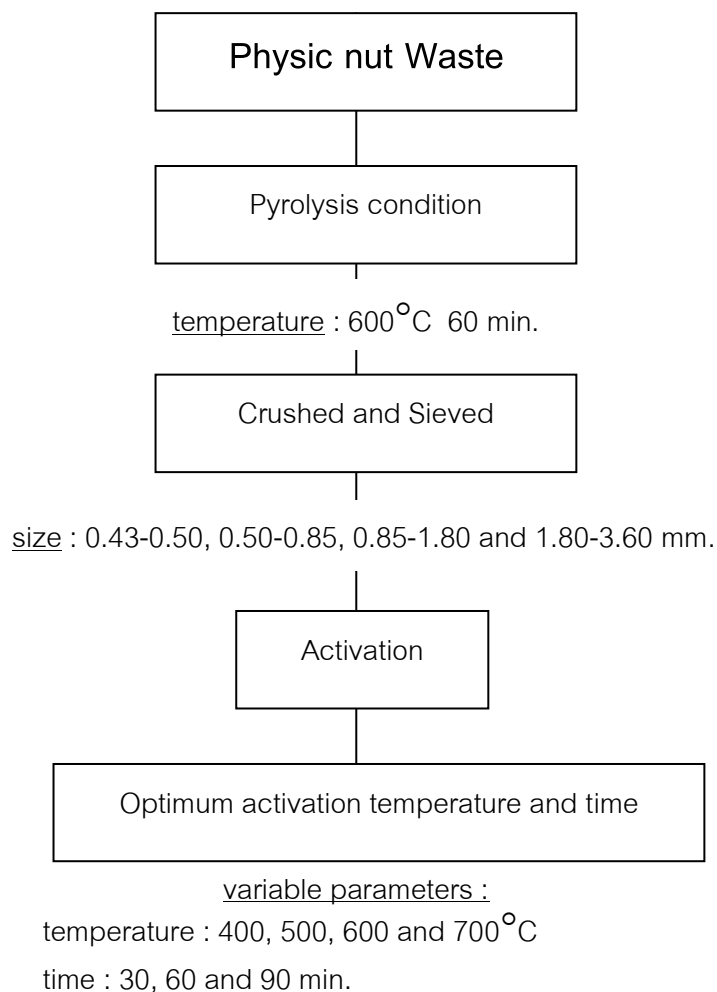


Figure 3.5 Experiment scheme of the production of activated carbon from Physic nut waste by oxidizing gas in a fixed bed reactor

3.6.1.2 The effect of activation time

Different activation times of 30, 60 and 90 minutes were studied for CO₂ activation. 10 grams of Physic nut residue char with particle size of 0.43-0.5 mm was loaded into the reactor. Then the reactor was passed with CO₂ at the bottom and was allowed to flow through from the bottom to the top at the flow rate of 100 mL/min. Next, the reactor was heated until the temperature was increasing and being fixed at 600°C. The CO₂ was continued passing up through the reactor for varying reaction time of 30, 60 and 90 minutes. Finally, bulk density, iodine number, methylene blue number and B.E.T. surface area of obtained activated carbon were characterized..

3.6.2 Chemical activation with alkaline solution

The variables, which have an effect on the activation process such as: temperature, activation time, concentration of KOH, size of char and type of alkaline solution were studied in order to determine the optimum conditions for producing activated carbon. Experimental schemes of the production of activated carbon from Physic nut waste char via chemical activation were shown in Figure 3.6 respectively. The procedures were described as follows:

3.6.2.1 The effect of concentration of KOH activation

The different concentrations of potassium hydroxide (KOH) at char : KOH ratio 1:1, 3:1, 5:1, 7:1 and 10:1 by weight were studied to determine the optimum concentration for soaking for preparation of activated carbon. Firstly, 10 grams of Physic nut waste (0.43-0.50 mm. of particle size) was soaked in different concentrations of KOH, then dried and loaded into a reactor. The reactor was passes with nitrogen gas at the bottom. Nitrogen gas was then allowed to flow though from bottom to the top at the flow rate of 100 mL/min. Secondary, the reactor was heated until the temperature in the tube rising and being fixed at the final temperature of 700^oC. The nitrogen gas was continued on, passing up through the tube reactor for 1 hrs of each experiment. Finally, the product was characterized by bulk density, iodine number, methylene blue number, B.E.T. surface area.

3.6.2.2 The effect of temperature for activation

The different temperatures were studied in this work of activation. They were 500, 600 and 700^oC. The sample 10 grams of Physic nut residue with particle size of 0.43-0.5 mm were soaked in the char : KOH ratio 1:1, then dried and loaded into a reactor. Then the reactor was passes with nitrogen gas at the bottom. Nitrogen gas was then allowed to flow though from bottom to the top at the flow rate of 100 mL/min. Next, reactor was heat to the desired temperature (500, 600 and 700^oC). The nitrogen gas was continued on, passing up though the reactor for each fixed temperature and for 1 hour of reaction time. The product was characterized by bulk density, iodine number, methylene blue number, B.E.T. surface area.

3.6.2.3 The effect of time of activation

Different reaction times of 0.25, 0.5 and 1 hour were studied for activation. First, ten grams of Physic nut waste char with particle size of 0.43-0.5 mm were soaked in char : KOH ratio of 1:1, then dried and loaded into a tubular reactor. The procedure of operation was the same as the former experiment. The reactor was passes with nitrogen gas at the bottom. The nitrogen gas was then allowed to flow though from the bottom to the top at the flow rate of 100 mL/min. Then, the reactor was heated until the temperature was increased and being fixed at the temperature 700°C. The nitrogen gas was continued on, passing up though the reactor for varying reaction time of 0.25, 0.5 and 1 hour. All products at different condition were characterized by same techniques as mentioned earlier.

3.6.2.4 The effect of size of Physic nut residue char

The sizes of Physic nut residue char of 0.43-0.50, 0.50-0.85, 0.85-1.80 and 1.80-3.60 mm were studied to determine the suitable size for preparation of activated carbon. Ten grams of Physic nut waste char with varying particle size of 0.43-0.50, 0.50-0.85, 0.85-1.80 and 1.80-3.60 mm were soaked in char : KOH ratio 1:1, then dried and loaded into a quartz reactor. The procedure of operation was the same as the former experiment. The reactor was passed with N₂ gas at the bottom. The N₂ gas was then allowed to flow though from the bottom to the top at the flow rate of 100 mL/min. The reactor was heated until the temperature was increased and being fixed at the temperature 700°C. The nitrogen gas was continued passing up though the tube reactor for 1 hour. Finally, the product was characterized by same techniques as mentioned earlier.

3.6.2.5 The effect of reagent for alkaline solution

The two different alkalines as KOH and NaOH were studied to compare the effect on the activated carbon. For 10 grams of Physic nut waste char (0.40-0.5 mm of particle size) was soaked in different alkalines at char: alkaline ratio of 1:1. The activation was proceeded as the former experiment. The tube reactor was connected to nitrogen tank. Next, the bed was heated until the temperature in the tube increased and being fixed at the final temperature of 700°C. The nitrogen gas was continued on,

passing up through the tube reactor for 1 hour of each experiment. Finally, the product was characterized by same techniques as mentioned earlier.

3.6.3 Characterization of activated carbon

3.6.3.1 Chemical characterization

Elemental analysis of activated carbon was carried out using a CHNS/O analyzer (Perkin Elmer PE 2400 series II). Fixed carbon, volatile, and ash analyses were carried out using a thermogravimetric analyzer. When the sample was heated under an inert atmosphere to 850°C, the weight loss during this step is a volatile component. The gas atmosphere is then switched to air to burn off fixed carbon, while the temperature is reduced to 800°C. Finally, any residue left after the system is cooled to room temperature is considered as ash. An X-ray diffractometer was used to investigate the surface inorganic components of the prepared activated carbons over 2θ ranging from 10° to 70°. The X-ray patterns were recorded under the scan rate of 0.1°/min. The surface organic functional groups were studied by Fourier transform infrared spectroscopy (Perkin Elmer System 2000 FT-IR). The spectra were recorded from a wavenumber of 400-4000 cm^{-1} .

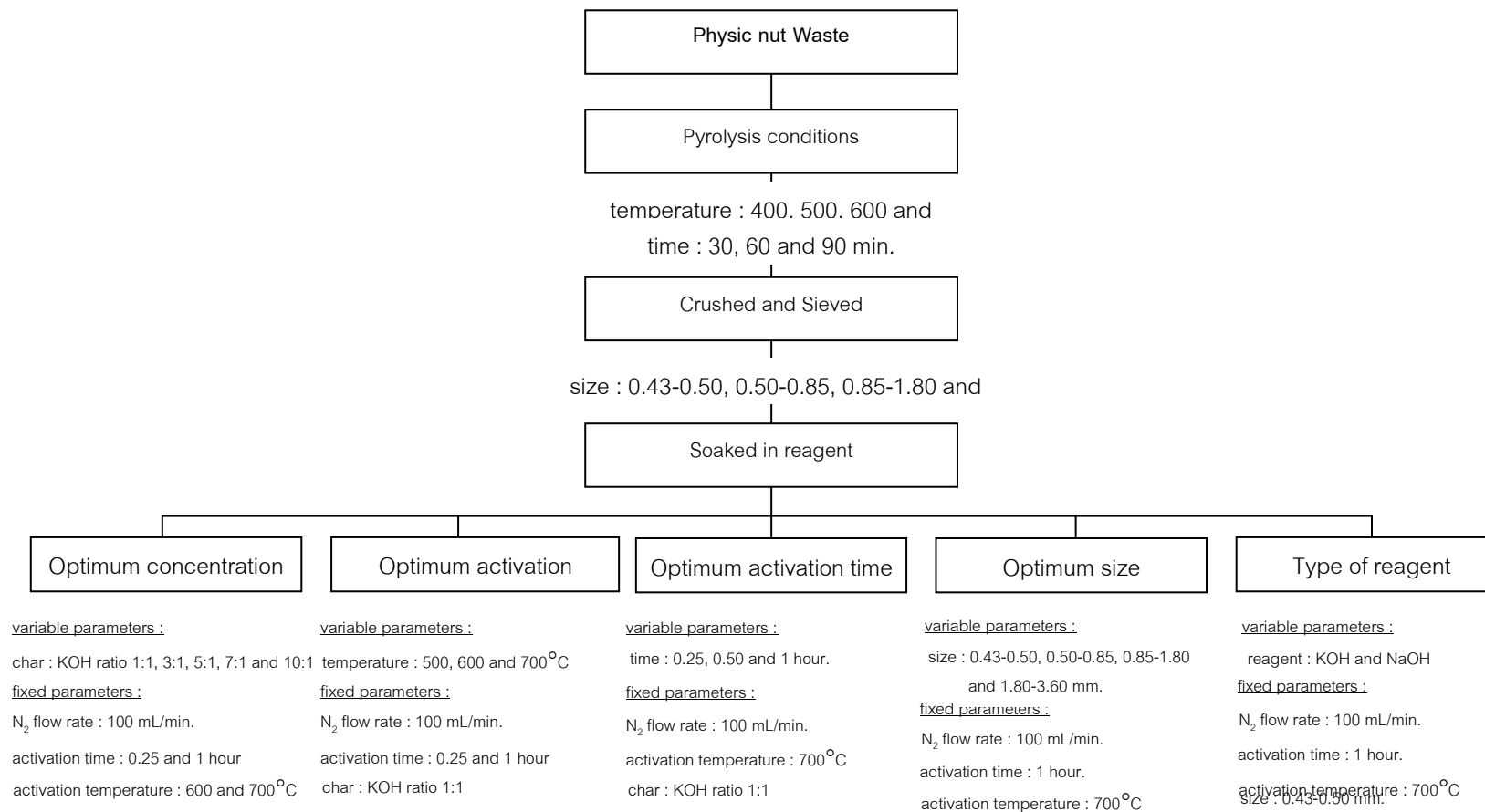


Figure 3.6 Experiment scheme of the production of activated carbon from Physic nut waste by alkaline solution in fixed bed reactor

3.6.3.2 Textural characterization

The surface area and the porous texture of activated carbons were characterized using adsorption of nitrogen at -196°C with the accelerated surface area and porosimetry system (ASAP 2020 : Micro Merities). The N_2 adsorption-desorption isotherms were used to determine the following parameters : surface area (using the Brunaver-Emmett-Teller (BET) equation), total pore volume, total micropore volume, and total mesopore volume.

The surface characteristics of samples were analyzed using scanning electron microscopy (JSH 5410, JELO). The instrument was operated under gold field emission with the accelerating voltage of 2500. Scanning was performed in situ on a carbon powder.

3.7 Experiment Part III: Synthesis and catalytic activity of catalyst

3.7.1 Synthesis of olivine support

Olivine (LiFePO_4) was prepared by a co-precipitation method using Li_3PO_4 , phosphoric acid ($0.85 \cdot \text{H}_3\text{PO}_4 \cdot 0.15\text{H}_2\text{O}$) and ferric citrate n-hydrate ($\text{FeC}_6\text{H}_8\text{O}_7 \cdot n\text{H}_2\text{O}$) as starting materials. Lithium phosphate (1M) were dissolved in 200 ml of deionized water. Ferric citrate n-hydrate (1M) was dissolved in 500 ml of deionized water (boiling water), and the two solutions were combined and concentrated on the hot plate until a wet powder with high viscosity was formed. The wet powders were placed in an oven and heated at 140°C for 2 hours. The dried powders were grounded before firing at a heating rage of $10^{\circ}\text{C}/\text{minute}$ under Ar up to $500\text{-}1000^{\circ}\text{C}$, held for 24 hours, and the sample were then air quenched to obtain crystallized LiFePO_4 . The synthesized olivine catalyst was crushed to particle size between 20-30 mesh.

3.7.2 Synthesis Ni/Olivine catalyst

The Ni/Olivine catalyst was prepared by wet impregnation of Phosphor olivine (LiFePO_4) with an excess of nickel and salt solution, followed by drying in vacuum oven at 110°C for 8 hours. After drying, the catalyst samples were calcined under air at 800°C for 2 hours and then reduced at 500, 600, 700, 800 and 900°C under H_2 gas for 4 hours.

These different ways of preparation a series of Ni/Olivine catalysts was described in Figure 3.7.

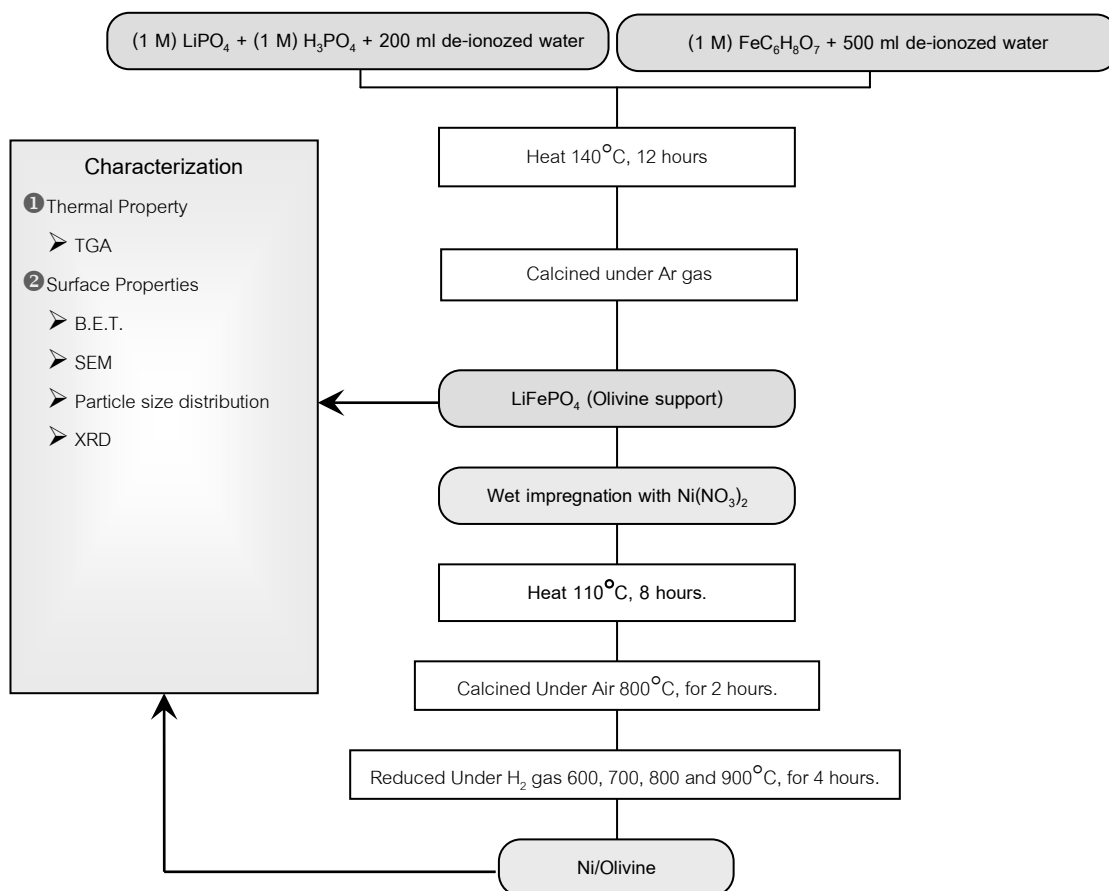


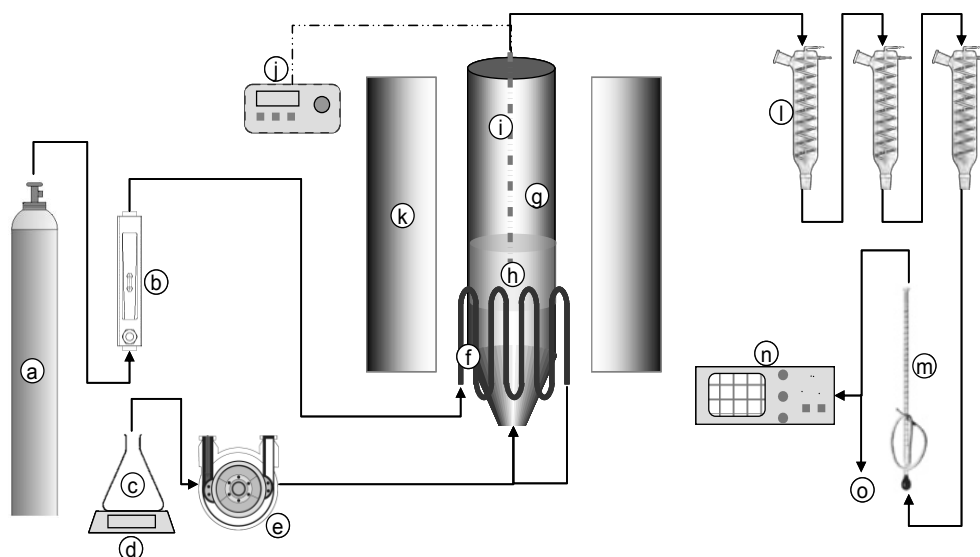
Figure 3.7 The experiment procedure of catalyst synthesis

3.7.3 Characterization of Olivine and Ni/Olivine

The thermogravimetry (TGA/SDTA 851e, Mettler Telleo) was performed to investigate the thermal stability of the hydrothermally synthesized LiFePO_4 support. Particle size of olivine, and Ni/Olivine were characterized with laser scattering (Malvern Instrument 2000). The BET-surface area was determined by means of N_2 decompositions on Micrometrics ASAP-2000 equipment. Phase and microstructure were characterized by X-ray diffraction (XRD) on Bruker AXS diffractometer using $\text{Cu K}\alpha$ radiation and by scanning electron microscopy (SEM) on a JEOL : JSM 5410 microscope apparatus coupled the energy dispersive X-ray spectroscopy (EDXS), respectively.

3.7.4 Catalytic activity of olivine and Ni/olivine catalysts

Steam reforming of waste glycerol as a linear long chain hydrocarbon from biodiesel production process to evaluate the performance of prepared catalysts is conducted. The schematic of glycerol reforming process is shown in Fig. 3.8. The experiments were carried out in a fixed bed quartz reactor (23 cm length × 2.2 cm i.d.). Catalyst with 8.14×10^{-4} mol of active metal mixed with 40 g of silicon carbide bed which equivalent to 8.5 cm of static bed height was placed on quartz wool retainer supported by mesh at the center of reactor. Total time for each experiment was 15 min during which glycerol was pumped into the reactor at the feed rate of 1 g/min by the use of a peristaltic pump placed at the bottom of the reactor. The N₂ carrier gas with a flow rate of 2 l/min was passed through air pre heater section which utilized heat from the furnace before mixing with fed glycerol where reaction started. The temperature of reaction was set at 700°C by the use of feedback temperature controller. Product stream was passed through cold traps to remove any condensable component. The exit sampling gas was analyzed by online gas analyzer (MRU GmbH model SWG 200-1) equipped with non-disperse infrared (NDIR) detector for CO, CO₂, C_xH_y (as CH₄) and thermal conductivity (TCD) detector for H₂ contents. Output flow rate was measured by bubble flow meter as well as electronic flow meter.



a) Nitrogen cylinder, b) Rotameter, c) Glycerol, d) Heating plate, e) Peristaltic pump, f) Air preheater, g) Quartz reactor, h) Catalyst bed, i) Thermocouple, j) Temperature controller, k) Furnace, l) Condensers, m) Bubble flow meter, n) Online gas analyzer, o) Bypass to exhaust

Figure 3.8 Schematic of the catalytic reforming system setup for linear long chain hydrocarbon

CHAPTER IV

DISTRIBUTION AND CHARACTERIZATION OF PRODUCTS FROM VARIOUS PYROLYSIS OPERATIONS

4.1 Biomass Raw Materials

Physic nut waste used in this study was obtained from an oil-extraction process using a twin screw extruder and sieved to the particle size of 0.43–0.50, 0.50–0.85, and 0.85–1.80 mm, respectively. The average proximate and elemental analyses of this material are shown in Table 4.1. This waste may be considered as a good candidate for conversion to activated carbon because of its relatively high carbon content and low ash, although its large portion of volatiles suggests that the substantial formation of liquid products through the pyrolysis process could be expected.

Table 4.1 Chemical characteristics of physic nut waste used as raw material for pyrolysis

Proximate analysis (wt%)		Ultimate analysis ^a (wt%)		Composition (wt%)	
Volatile	55.40	Carbon	45.50	Hemicellulose	17.47
Fixed carbon	37.20	Hydrogen	7.20	Cellulose	56.31
Ash	6.30	Nitrogen	4.00	Lignin	23.91
Moisture	0.68	Oxygen ^b	43.30		

^a Moisture and ash free. ^b By difference.

4.2 Results and discussion of the experiments

4.2.1 Thermal Degradation of Physic Nut Waste

Thermo-gravimetric analysis of the physic nut residue revealed that major thermal decomposition occurred around 250–450°C as shown in Figure 4.1.

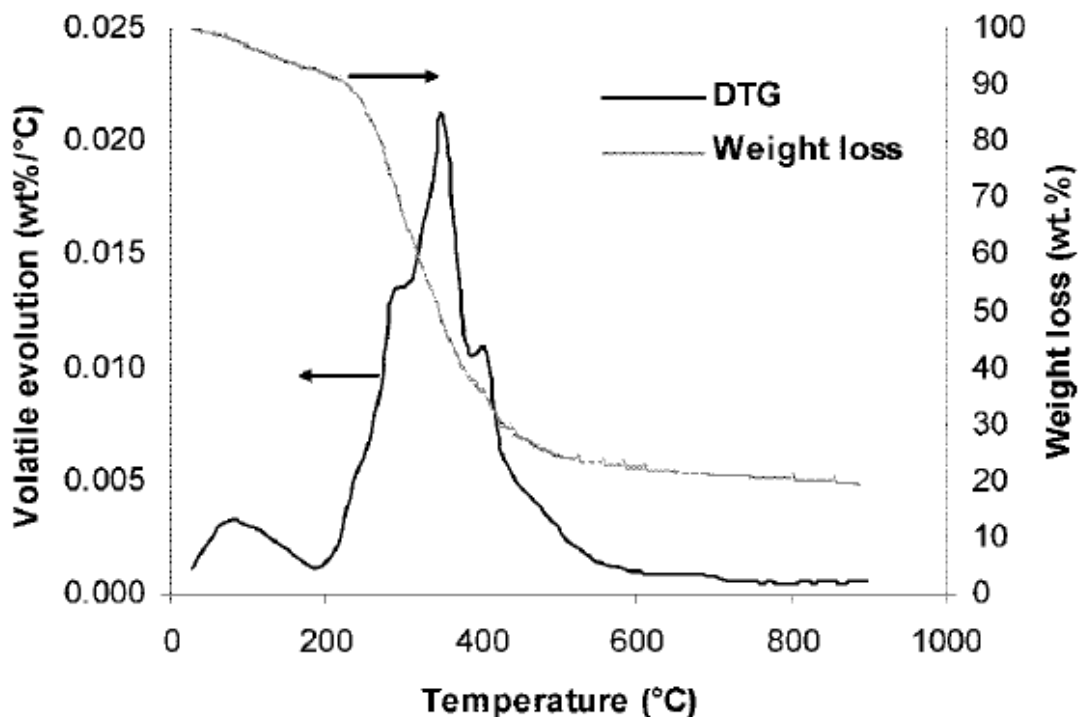


Figure 4.1 Pyrolytic thermogravimetric analysis of the residue showing weight loss and DTG plots

Generally, biomass consists of hemicellulose, cellulose, lignin, and extractives. From pyrolytic differential thermogravimetric (DTG) curves, initial weight loss corresponds to moisture removal, followed by a second degradation event around 200–400°C, where the evolution of light volatile compounds occurs from the degradation of cellulose and hemicelluloses. Degradation of lignin slowly takes place in a wide temperature range and lasts to higher temperatures. Thermal degradation of these individual components may be superimposed to simulate the overall degradation of the original biomass.

4.2.2 Pyrolysis yields

Thermal degradation of biomass results in solid, liquid, and gas products with the relative quantity mainly depending upon process parameters, such as sample size, reaction temperature, residence time, and reacting gas environment.

The product distribution from the pyrolysis of physic nut waste with a particle size of 0.85–1.80 mm is displayed in Figure 4.2. The effect of the hold time on the apparent product yield was not significant because the shortest time of 15 min used in this work was appreciably long enough compared to typical devolatilization rates of biomass, in that most of the primary pyrolytic reactions were complete by that time. In addition, from previous thermogravimetric analysis, major decomposition processes of physic nut waste would have been over at the lowest tested temperature of 400°C.

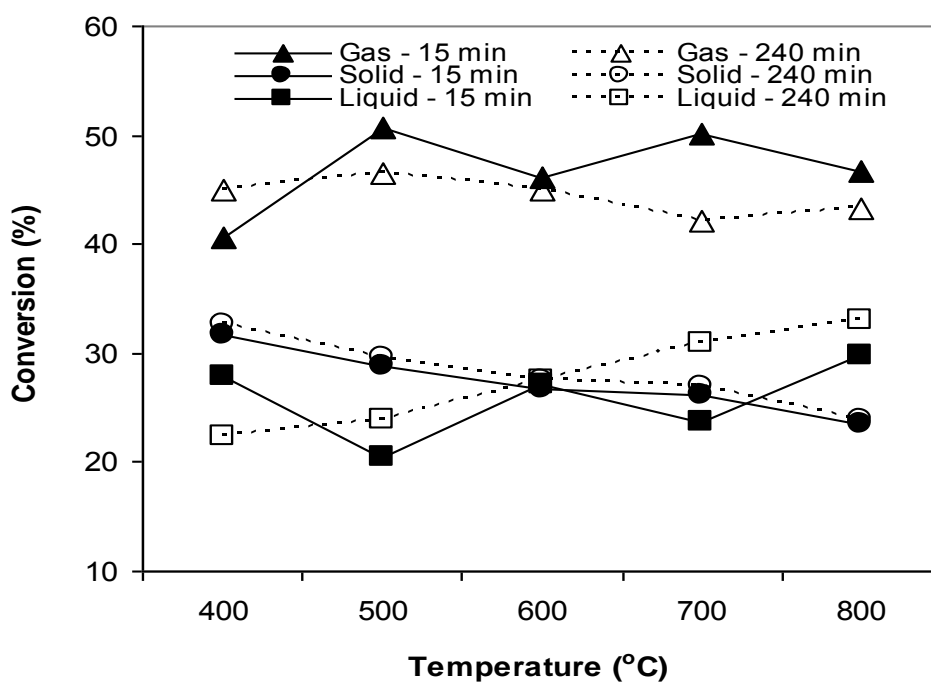


Figure 4.2 Product distribution from the pyrolysis of physic nut waste using hold times of 15 and 240 minutes

Hence, a slow change of product yield is mainly resulting from secondary reactions at higher temperature. Yields of solid slowly decrease with temperature because of subsequent decompositions of the solid matrix at higher temperature, probably to liquid products, resulting in higher liquid yields at those conditions.

Generally yields of gas are highest, while solid yields are greater than liquid products, except at some high-temperature conditions. Particle size exhibits less influence on the product quantity at higher temperatures as noticed from Figure 4.3, for the data on char yields. Char yields from a larger particle size of 0.85–1.80 mm were 5–15% lower than that of 0.43–0.50 mm at 400°C, while the gap was narrower at higher temperatures.

Generally, in view of heat- and mass-transfer limitations, the result should be opposite because larger particles may not be heated evenly and would require more time for mass transport through the particle. However, this is a slow-heating process as described earlier; therefore, these limitations are not applied. Thus, the variation on char yield may result from the non uniformity of raw material, typical for bio-based material, such as physic nut waste. The chemical composition of small-particle waste may somewhat be different from that of larger ones.

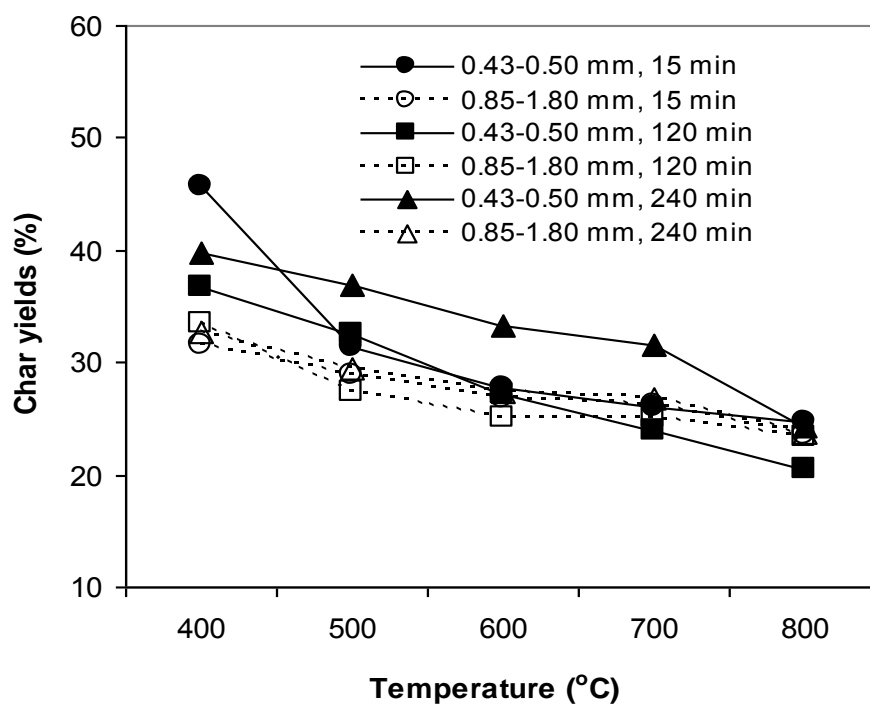


Figure 4.3 Char yields from the pyrolysis of physic nut waste

The waste sample was generated from the crushing of whole seed including its shell; therefore, larger particles tend to include more shell fraction, while the greater cake portion belongs to smaller particles. At a lower reaction temperature, some of the more stable components in small particles may not be readily decomposed, while at

higher temperatures, most of these constituents can be thermally devolatilized, leaving a comparable amount of char.

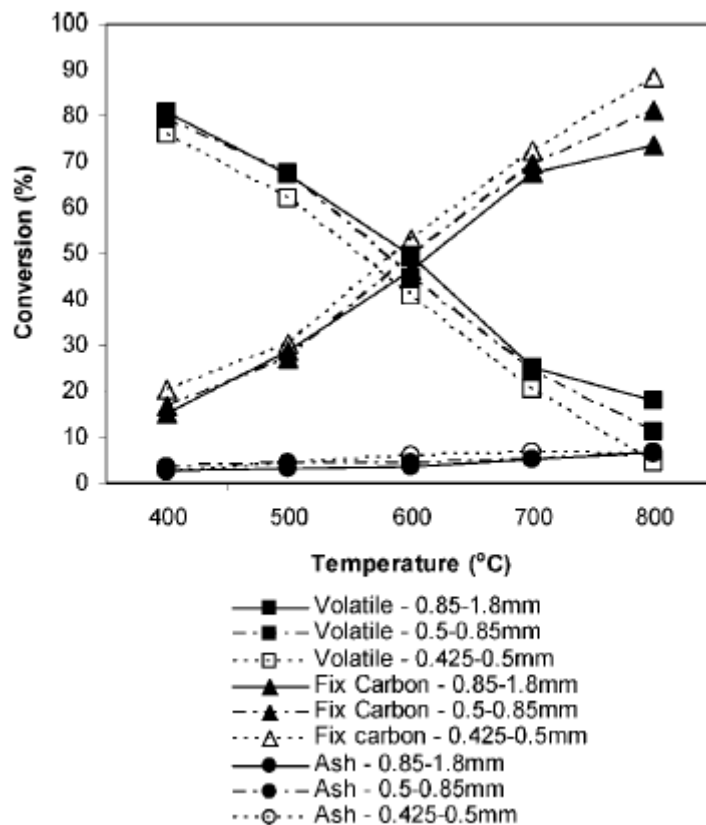


Figure 4.4 Components in char from the pyrolysis of physic nut waste using a hold time of 15 minutes

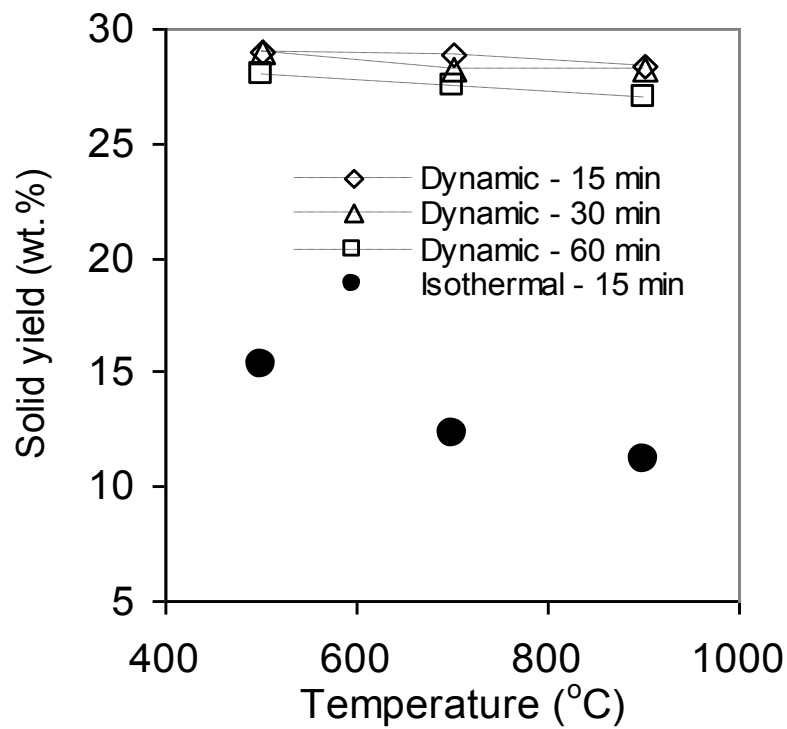
Char yields from a larger particle size of 0.85–1.80 mm were 5–15% lower than that of 0.43–0.50 mm at 400°C, while the gap was narrower at higher temperatures. Generally, in view of heat- and mass-transfer limitations, the result should be opposite because larger particles may not be heated evenly and would require more time for mass transport through the particle. However, this is a slow-heating process as described earlier; therefore, these limitations are not applied. Thus, the variation on char yield may result from the nonuniformity of raw material, typical for bio-based material, such as physic nut waste. The chemical composition of small-particle waste may be somewhat different from that of larger ones. The waste sample was generated from the crushing of whole seed including its shell; therefore, larger particles tend to include

more shell fraction, while the greater cake portion belongs to smaller particles. At a lower reaction temperature, some of the more stable components in small particles may not be readily decomposed, while at higher temperatures, most of these constituents can be thermally devolatilized, leaving a comparable amount of char.

For the production of high-quality activated carbon, a greater surface area along with higher fixed carbon content is preferable. Although similar in quantity, the quality of chars obtained at different operating conditions is different in terms of fixed carbon, volatiles, and ash contents as displayed in Figure 4.4. Smaller particles tend to yield char with high fixed carbon and low in volatiles when compared at the same reaction temperature. The highest char fixed carbon value of 88.24% was obtained by pyrolysis of 0.43–0.50 mm particles at 800°C for 15 min with relatively low volatiles of 4.30%. Higher pyrolysis temperatures may be applied to obtain a greater fixed carbon content, but the cost of operation at high temperature as well as greater carbon burn off and the possibility of pore closure from sintering would limit such effort.

The effect of heating pattern and reaction temperature on product yields is shown in Figure 4.5. Generally, rapid pyrolysis resulted in greater changes on product yields at different temperature when compared with those of slow conversion processes. For slow heating, solid yields were much higher than those obtained from isothermal runs and decreased slowly with temperature within the range of less than 2.0 wt%. The effect of hold time at final temperature was insignificant on solid yields from this process. Larger drop on solid yields with increased temperature was obtained by isothermal experiments but still accounted for less than 4.0 wt% changes. It may be suggested from these results that pyrolysis processes on formation and decomposition of solid are mainly rapid primary reactions and this fraction plays minor role on subsequent secondary reactions during the overall conversion. This also explains small changes on solid yields with temperature for dynamic runs. During slow heating process, all samples were subjected to similar temperature history (identical heating rate) and not on final temperature. Since pyrolysis reactions start early at temperature around 400–500°C, major rapid primary reactions related to solid yields should already take place and mostly finish by the time that reaction temperature increased to final set point for higher temperature experiments. Hence, small reduction on solid yields at higher temperature

resulted from insignificant slower secondary decomposition reactions. On the other hand, historical temperature profile for rapid heating at different reaction temperature is different and pyrolysis reactions occur mainly at that particular set point results in larger difference on yields.



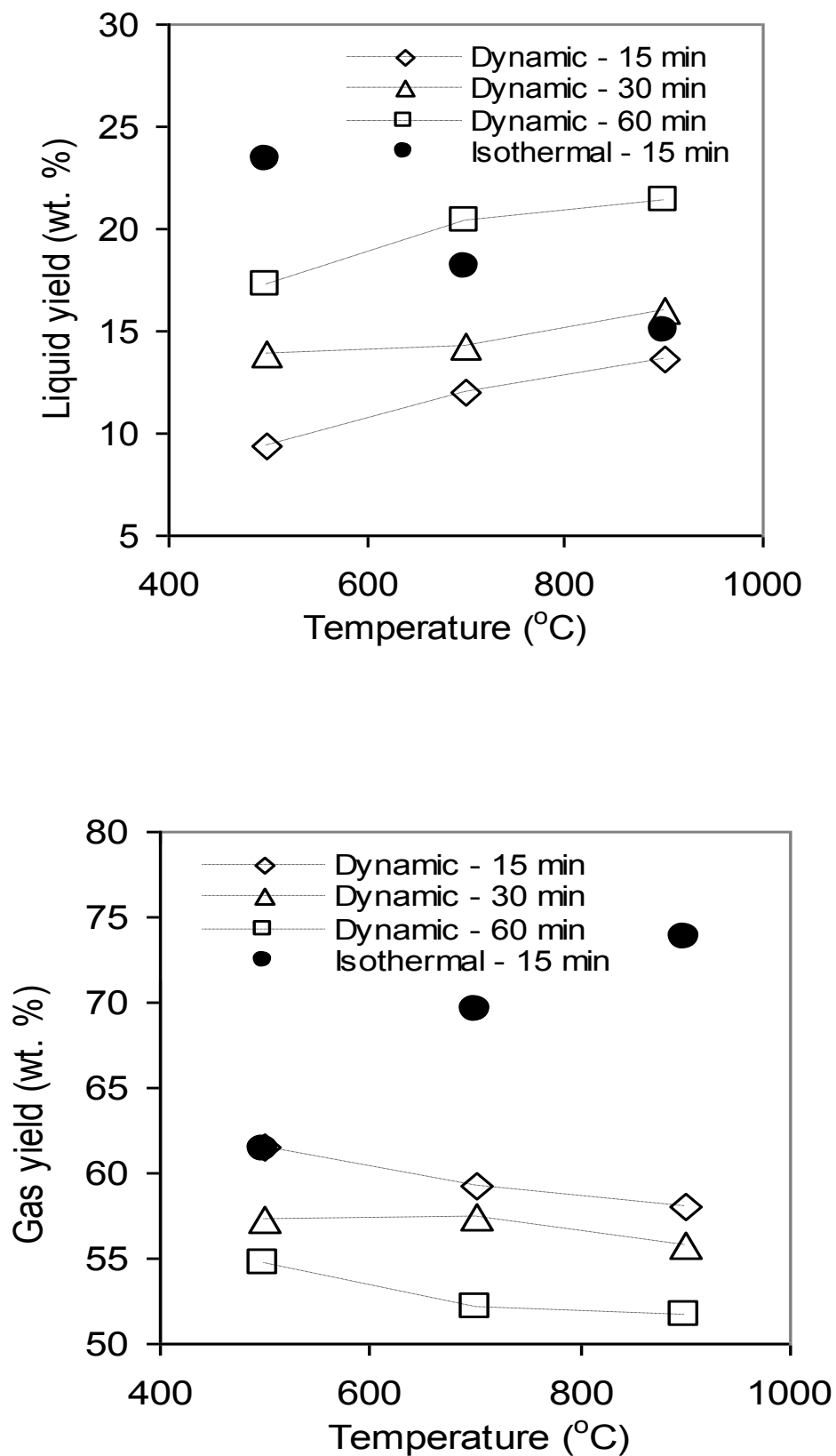


Figure 4.5 Product yields from dynamic and isothermal heating of physic nut wastes

Gas and liquid yields from slow pyrolysis of physic nut displayed opposite trend from those of rapid experiments. For slow pyrolysis, liquid yields increased with temperature while continuous drop on liquid product was obtained from rapid runs. Obviously, decomposition reactions of liquid products resulted in higher gas yields for isothermal trials. During dynamic heating, higher temperature increased the formation of liquid products at the expense of lower gas yields. Generally, gas is major product from pyrolysis of physic nut with yields of more than 50 wt% to as much as 73 wt% at any operating conditions.

4.2.3 Influence of pyrolysis conditions on solid-char

“Char” is used collectively to represent the solid residue that remained after pyrolysis. Appreciable amount of char with high fixed carbon left after pyrolysis is an important factor to determine optimum operating condition. Results of the proximate analyses of chars obtained from pyrolysis of physic nut waste at different conditions are given in Figure 4.6.

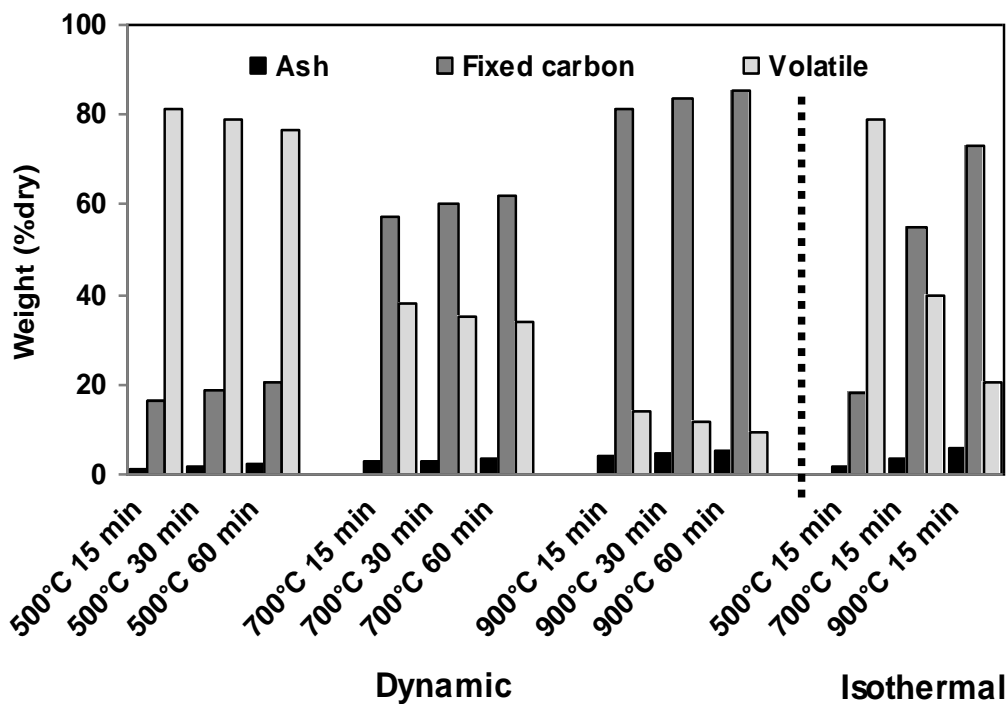


Figure 4.6 Proximate analysis of char from dynamic and isothermal heating of Physic nut wastes

As expected, an increase in temperature results in char with higher fixed carbon and decrease in volatile matter. As the pyrolysis temperature increased from 500 to 900°C, the volatile content of the chars correspondingly decreased from 76.50-81.10 to 9.80-14.40%. The fixed carbon content increased sharply from 16.34-20.28% at 500°C to 57.25-62.20% at 700°C and rose continually to 81.10-85.40% at 900°C. Elemental analysis of char shows similar trend of higher portion of carbon content and lower amount of other elements with temperature (Figure 4.7). The devolatilization during pyrolysis resulted in the char to be predominantly carbon. Losses in hydrogen and oxygen correspond to the scission of weaker bonds within char structure favored by the higher temperature.

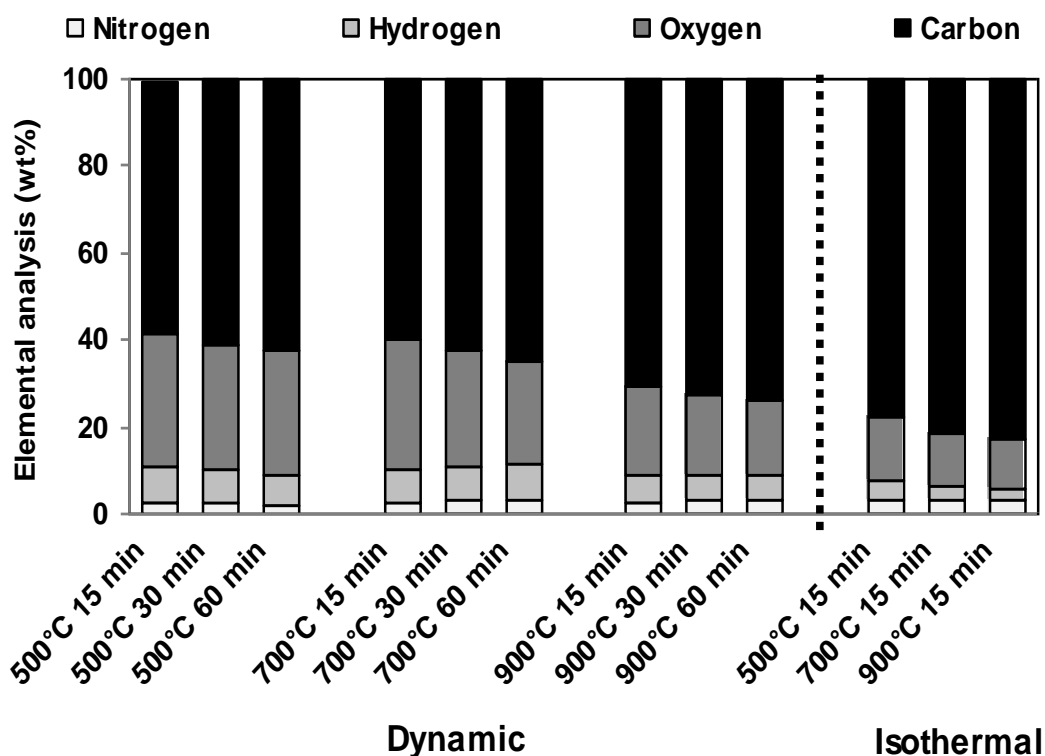


Figure 4.7 Elemental analysis of char from dynamic and isothermal heating of Physic nut wastes

Decreasing trends in the volatile content of chars were also observed when the hold time was increased for a particular final temperature. For the hold time increased, larger amount of volatile matters were released, hence the decreasing volatile content thus leaving char with high fixed carbon content. Mode of heating did not show significant effect on fixed carbon and volatile contents. However, char from rapid pyrolysis had higher carbon content and lower amount of oxygen and hydrogen compared to one produced from slow pyrolysis. It was thought that remaining of inorganic substance, e.g. carbonate, after isothermal heating in a short period of time might be the cause for higher amount of carbon.

The effects of pyrolysis temperature, hold time and method of heating on the BET surface area, mesopore area and mesopore volume of chars are shown in Table 4.2. BET surface areas increased progressively with increased pyrolysis temperature and exposure time which was explained with the burn-out of carbon that led to the development of porosity.

Char obtained from rapid pyrolysis condition had lower surface area and pore volume than ones attained from slow pyrolysis approximately 15-19%. The highest surface area of char was achieved at pyrolysis temperature of 900°C for an exposure time of 60 min.

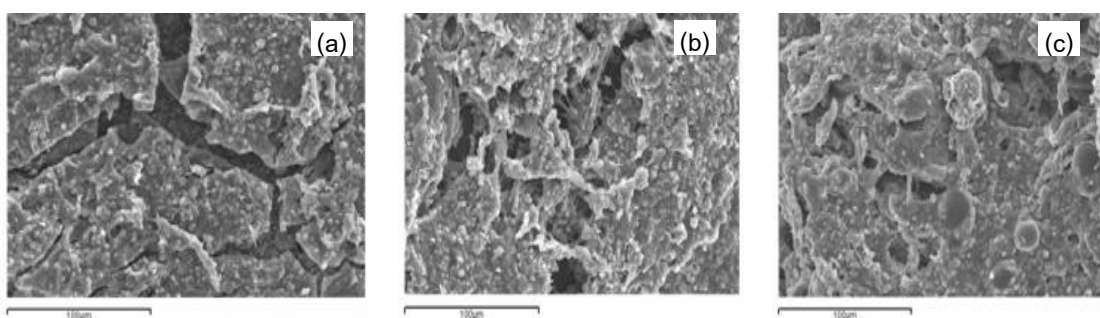
Table 4.2 Surface area and porosity characteristics of chars

Temperature (°C)	Hold time (min)	BET (m ² ·g ⁻¹)	Total volume (cm ³ ·g ⁻¹)	Mesopore area (m ² ·g ⁻¹)	Mesopore volume (cm ³ ·g ⁻¹)
Dynamic heating					

500	15	140.54	0.274	124.04	0.093
500	30	154.63	0.315	131.18	0.099
500	60	171.85	0.352	142.62	0.104
700	15	188.32	0.386	153.90	0.110
700	30	197.91	0.497	178.47	0.118
700	60	202.37	0.545	185.51	0.123
900	15	199.13	0.512	180.22	0.120
900	30	215.82	0.607	189.92	0.128
900	60	217.55	0.628	192.38	0.131
Isothermal heating					
500	15	114.38	0.204	100.23	0.074
700	15	154.16	0.295	129.76	0.096
900	15	169.79	0.332	134.45	0.102

Pyrolysis conditions: nitrogen flow rate = $2 \text{ L} \cdot \text{min}^{-1}$.

SEM was applied to characterize the shape and the size of the char particles, as well as their porous surface structure. Figure 4.8 shows SEM images of physic nut chars produced under different conditions. At a low temperature of 500°C under dynamic heating, surface of char showed cracked and pitted morphology (Figure 4.8 a). At 700°C , the presence of small pores on the surface explained that char was starting to develop an elementary pore network (not shown).



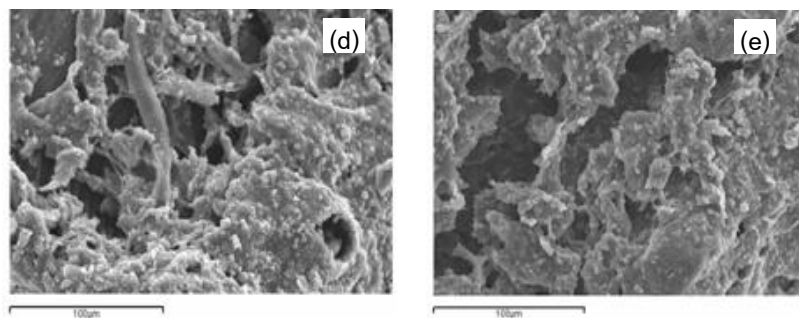


Figure 4.8 SEM of chars: dynamic heating at (a) 500°C –15 min, (b) 900°C –15 min, and (c) 900°C –60 min; and isothermal heating at (d) 500°C –15 min, and (e) 900°C –15 min

After 900°C, surface morphological change was evident. Porous structure and opening pores on the surface was developed, thus char possessed high surface area. Increasing exposure time at a particular pyrolysis temperature also increased the surface area. This trend was less pronounced at high temperature suggesting that decomposition reactions would have been rapid at such high temperature and mostly finished in short time. The SEM image of char pyrolyzed at 900°C for 60 min (Figure 4.8 c) exhibited relatively smooth in some regions as well as open pores were being seal off indicating initial stage of sintering at high exposure time. The char particles obtained after isothermal heating were slightly different as seen in Figure 4.8 d-e. While a gradual release of volatile compounds occurred as the temperature increased during dynamic heating; the fast volatile release throughout isothermal condition produces relatively substantial internal overpressure and the coalescence a more open structure (Figure 4.8 d). Partial smooth surface of char particles were also observed at a higher pyrolysis temperature of 900°C under isothermal heating.

Fewer functional groups were detected as observed from the FTIR spectra of the char shown in Figure 4.9, indicating that the surface function groups of physic nut waste significantly experienced chemical changes during pyrolysis. The spectrum displays the following peaks. The absorption peaks around wavenumber of 3500-3000, 1512, and 1383 cm^{-1} are indicative of the existence of amine groups. The spectrum also displays the adsorption peaks at wavenumber of 3600-3200, 1641, and 1270 cm^{-1} , corresponding to carboxyl groups. The phosphonate groups show some characteristic absorption peaks around wavenumber of 1159 cm^{-1} (P-O stretching) and 1055 cm^{-1} (P-OH stretching).

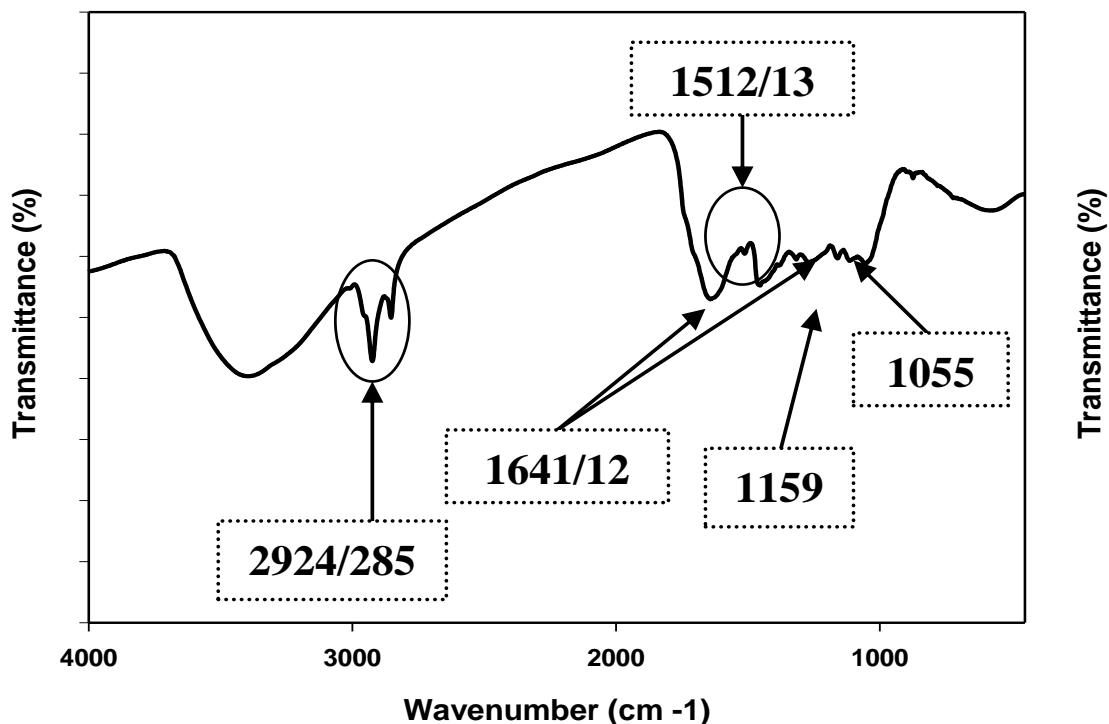


Figure 4.9 FTIR spectra of the char pyrolyzed from physic nut waste

X-ray diffractometer was used to record X-ray diffraction spectra from char sample by scanning over the angular 2θ range of $10\text{-}70^\circ$ and intensity at various degrees was displayed in Figure 4.10. There are two broad diffraction peak around $2\theta = 23^\circ$ and $2\theta = 43^\circ$ in a spectrum which confirm the structure of the graphitic basal planes of char crystallite in the low angle region ((002) peak of graphite) and radial spread of crystalline structures in high angle region ((100) peak of graphite) [19]. Hence the chars obtain are believed to be in the form of graphite.

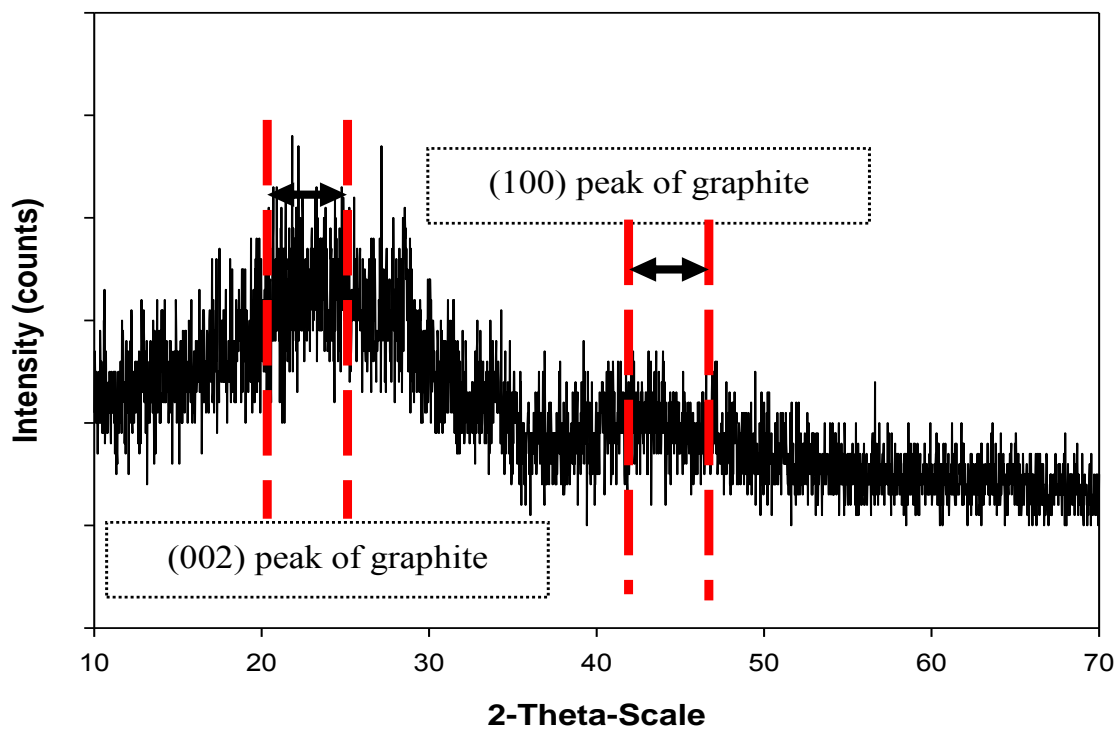


Figure 4.10 X-ray diffraction pattern of the char pyrolyzed from physic nut waste

4.2.4 Influence of pyrolysis conditions on gas

Generally, gas is major product from pyrolysis of physic nut with yields of more than 50 wt% to as much as 73 wt% at any operating conditions. More detail on gas production is exhibited in Figure 4.11 for isothermal experiment at 900°C. Measured gas concentrations are reported as percentages of carbon or hydrogen in feed material that are converted to carbon or hydrogen in specified gas species.

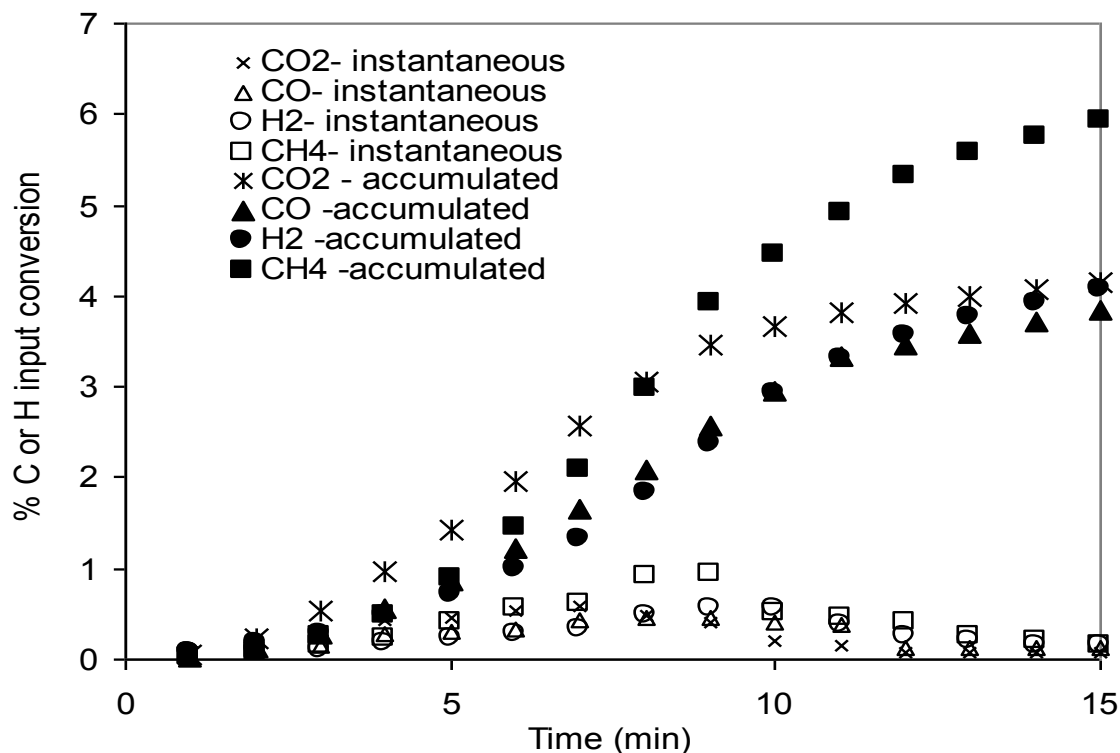


Figure 4.11 Gas produced from isothermal heating of physic nut wastes at 900°C

Due to distance from reactor to gas analyzer, there is around one minute lag time for response on gas measurement. As a result, it may be seen from this figure that gas production started immediately as soon as raw material was inserted into the reactor vessel. Most of gas was formed within 15 minutes with CO₂, CO, CH₄, and H₂ as major gas species. However, from material balance, relatively large fraction of gas species is still unaccounted for which probably be those C₂-C₄ hydrocarbons. Comparisons between gas production profile of H₂ and CH₄ via isothermal and dynamic experiments are displayed in Figure 4.12 and 4.13, respectively. As expected, rapid heating resulted in large production of gas in short time while much slower gas release was typical pattern for dynamic runs due to gradual rise in reaction temperature.

Ratio of H₂ to CO and lower heating value (LHV) of gas product which are important parameters with respect to gas utilization viewpoint are shown in Figure 4.14. LHV of product gas is determined from heat content of each measured gas which is:

$$\text{LHV (MJ/Nm}^3\text{)} = 0.126 \times [\text{CO}] + 0.108 \times [\text{H}_2] + 0.358 \times [\text{CH}_4] \quad (4.1)$$

where $[CO]$, $[H_2]$, and $[CH_4]$ are volume (molar) percentage of these gas species, respectively.

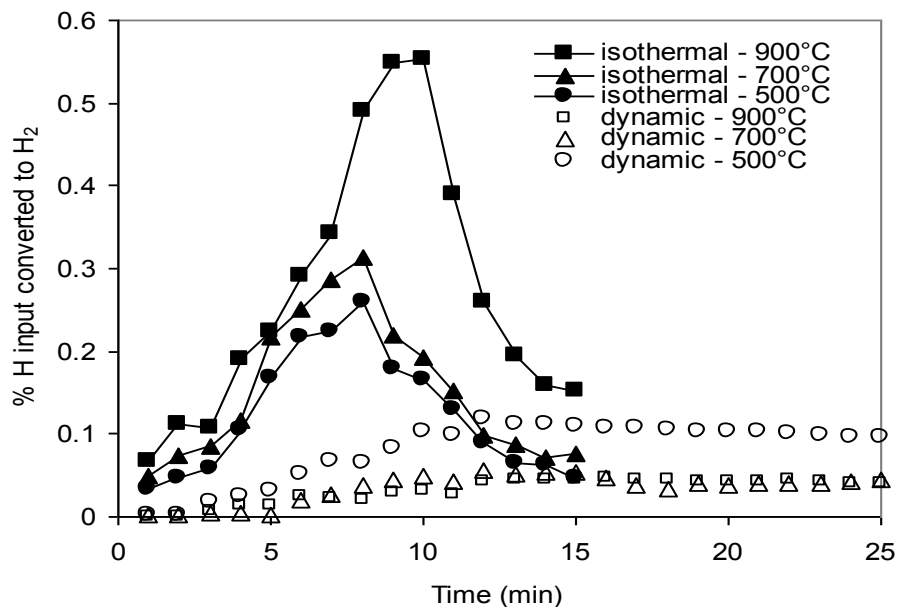


Figure 4.12 Hydrogen gas produced from isothermal and dynamic heating of physyc nut wastes

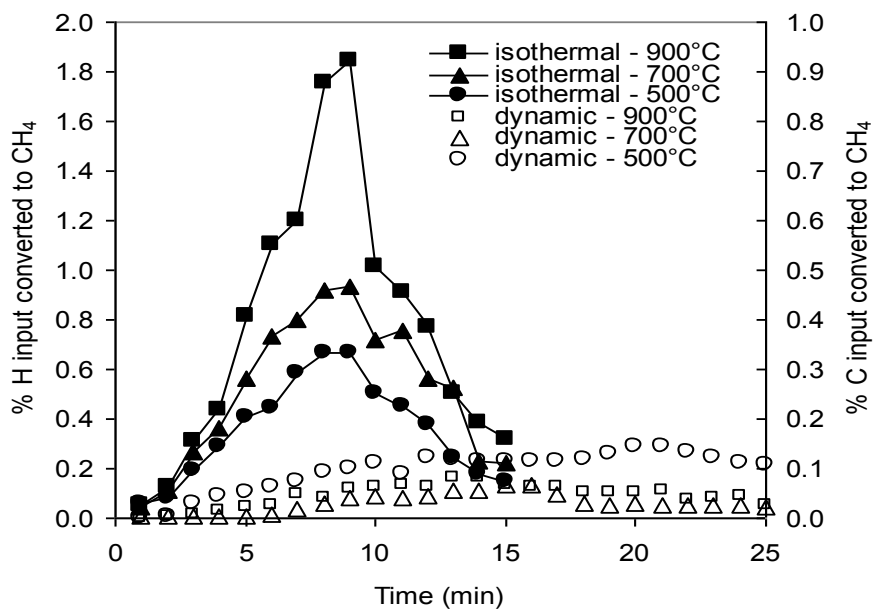
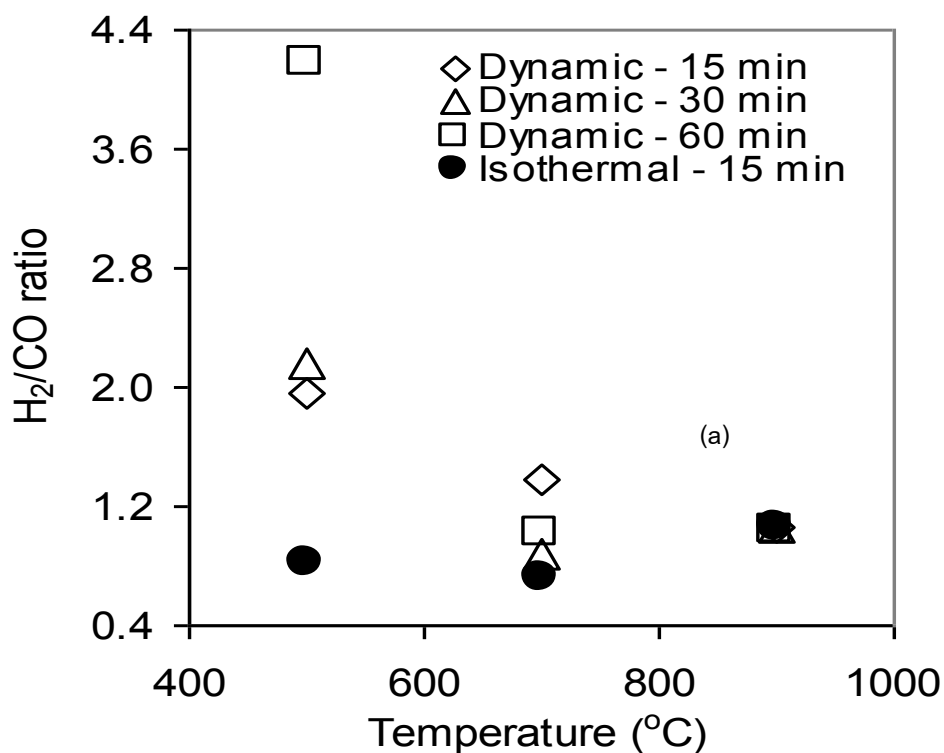


Figure 4.13 Methane produced from isothermal and dynamic heating of physyc nut wastes

At lower temperature, H_2/CO ratios of gas from dynamic runs were higher than isothermal experiment while these data were quite similar for runs at higher temperature. Since gas yields and LHV's were also higher at low temperature for dynamic runs, lower reaction temperature would be appropriate for slow heating operation to obtain enriched H_2 gas. Since ratios were indifferent for isothermal trials while gas productions were much higher at high temperature, factors including LHV and other operational constraints have to be considered when selecting optimal process temperature in this case. Note that LHV's of gas from any runs were relatively high (more than 3.7 MJ/Nm^3) indicating that these gases are at least suitable for power production without need for auxiliary fuels.



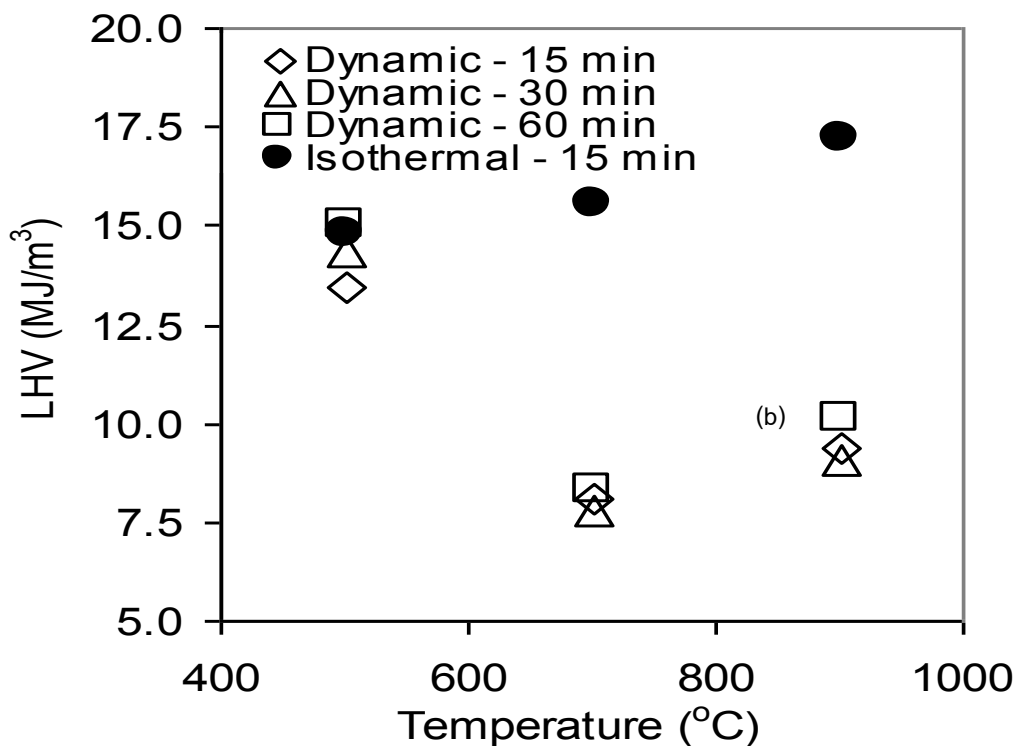


Figure 4.14 (a) H₂/CO and (b) lower heating value (LHV) of product gas

Table 4.3 is a summary of overall product distribution as well as other important product gas characteristics obtained from this work. In the table, carbon and hydrogen conversions are determined from total amount of carbon or hydrogen in feed that end up as carbon containing gases (CO, CO₂, and CH₄) or hydrogen containing gases (CH₄, H₂) as detectable by gas analyzer, respectively. Cold gas efficiency (η_{gas}) is a parameter that is defined as:

$$\eta_{\text{gas}} (\%) = \frac{\text{LHV}_{\text{gas}} \times Y_{\text{gas}}}{\text{LHV}_{\text{raw material}}} \times 100\% \quad (4.2)$$

Where Y_{gas} is yield of product gas per kilogram of fed raw material (Nm³/kg) and $\text{LHV}_{\text{raw material}}$ may be measured by bomb calorimeter.

Table 4.3 Effect of reaction temperature, hold time, and mode of heating on product distribution and gas characteristics.

Temperature (°C)	Dynamic heating									Isothermal		
	500			700			900			500	700	900
Hold time (min)	15	30	60	15	30	60	15	30	60	15	15	15
Solid (%wt)	29.0	28.9	28.4	28.9	28.3	28.2	28.0	27.5	26.9	15.3	12.3	11.2
Liquid (%wt)	9.5	11.9	13.6	13.8	14.3	16.0	17.2	20.4	21.4	23.4	18.2	15.0
Gas* (%wt)	61.5	59.2	58.0	57.3	57.4	55.8	54.8	52.1	51.7	61.3	69.5	73.8
LHV (MJ/m ³)	13.4	14.4	15.0	8.1	7.8	8.3	9.4	9.1	10.1	14.8	15.5	17.2
H ₂ /CO	2.0	2.2	4.2	1.4	0.9	1.0	1.1	1.1	1.0	0.8	0.7	1.1
C conversion to gas (wt. %)	10.4	14.2	20.8	10.8	18.1	20.3	14.3	18.9	25.6	12.6	16.9	22.7
H conversion to gas (wt. %)	9.7	15.3	25.0	5.6	7.7	9.8	7.8	10.0	15.2	11.2	15.4	25.5
Cold gas efficiency, η_{gas} (%)	8.0	12.4	19.4	4.8	7.5	9.0	7.0	8.9	13.5	10.5	14.6	22.6
Gas yield, Y_{gas} (Nm ³ /kg)	0.12	0.17	0.25	0.12	0.19	0.21	0.15	0.19	0.26	0.14	0.18	0.26

*by difference

As seen from this table, carbon and hydrogen conversion increased with hold time and temperature. Up to around a quarter of carbon or hydrogen in feed might be transformed to product gases at some operating conditions. Since these experiments were pyrolysis, cold gas efficiencies were relatively low when compared with typical gasification process, ranging from 4.83% to 22.55% at most. Longer hold time and higher reaction temperature resulted in greater cold gas efficiency with maximum value occurred at 900°C for isothermal process though the overall economic analysis of the process has to be carried out to suggest the optimal condition since pyrolysis is mainly endothermic and operation at high temperature is energy intensive process.

4.2.5 Influence of pyrolysis conditions on liquid product

The liquid products from pyrolysis are mostly oxygenated complex mixtures of hundreds of individual substance that can be grouped into many various chemical classes [11]. FT-IR spectra of the liquid product obtained from either isothermal or dynamic pyrolysis of physic nut waste are quite similar as shown in Figure 4.15. The O-H stretching vibrations between 3200 and 3450 cm^{-1} indicates the presence of phenols and alcohols. The band at the about 3100 cm^{-1} may indicate the presence of hydrocarbon groups bound to aromatic rings.

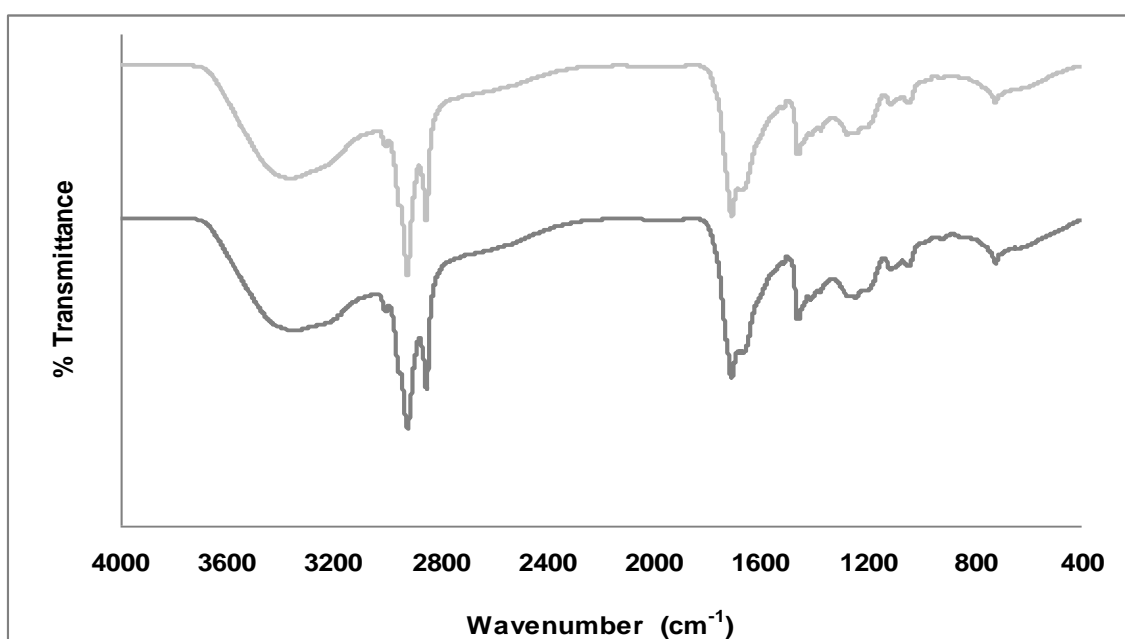


Figure 4.15 FT-IR spectra of liquid product: (a) dynamic heating at 700°C for 60 min and (b) isothermal heating at 700°C for 15 min

The C-H stretching vibrations between 2800 and 3000 cm^{-1} and deformation vibrations between 1350 and 1475 cm^{-1} indicate the presence of alkane. The C=O stretching vibrations with absorbance between 1680 and 1780 cm^{-1} represent the presence of ketone or aldehyde. The presence of both O-H and C=O stretching vibrations also indicates the presence of carboxylic acids and derivatives. The absorbance peaks between 1575 and 1675 cm^{-1} represent C=C stretching vibrations which indicate the presence of alkenes and aromatics [12-15].

Liquid products were further processed and analyzed for fatty acid methyl esters. The relative distribution of fatty acids was determined as percent of chromatographic peak area of following derivative acids: palmitic acid (C16:0:C₁₆H₃₂O₂), oleic acid (C18:1:C₁₈H₃₄O₂), and lignoleic acid (C18:2:C₁₈H₃₂O₂). Example of the distribution of fatty acids in liquid product produced from both isothermal and dynamic heating was shown in Figure 4.16. It was found that the content of fatty acid was not influenced by hold time, mode of heating, or temperature (not shown). Overall, contents of these components were in the range of 19.05-19.82% for palmitic acid, 45.03-45.77% for oleic acid, and 34.24-35.94% for lignoleic acids. Nevertheless, the results indicated that carbon chain length of liquid product from pyrolysis of physic nut waste is greater than that of diesel fuel and within the range of gas oil. It may be use on slow speed, heavy machinery but further cracking and refining of this product are required in order to utilize it in place of gasoline or diesel.

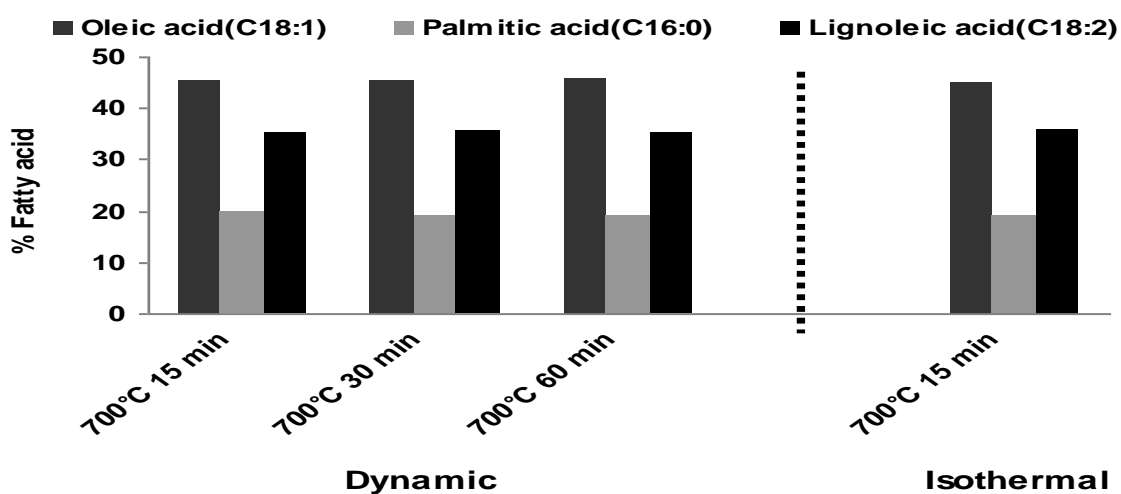


Figure 4.16 Relative distribution of fatty acids in liquid product

The characteristics of bio-oil samples were determined and the results are given in Table 4.4. Viscosity of the bio-oils was related to fatty acid chain length and number of unsaturated bonds. The bio-oil contained a heavy fraction as reflected by its high density. The high flash point suggested that the bio-oil can be safely stored at room temperature. The calorific value of bio-oil were 24.30 MJ/kg (dynamic condition), 21.24

MJ/kg (Isothermal condition). Calorific value indicates that the energy content of the bio-oils were very close to those of petroleum functions.

The average chemical composition of bio-oil from dynamic and isothermal conditions analyzed were $\text{CH}_{1.68}\text{O}_{0.24}\text{N}_{0.05}$ and $\text{CH}_{0.90}\text{O}_{0.19}\text{N}_{0.05}$, respectively. The bio-oils were characterized by lower oxygen content than that of the original feedstock. The decrease in the oxygen content of the bio-oils (18.6 – 21.20%) compared to the original feedstock (43.30%) is important because the high oxygen content is not attractive for the production of transport fuels.

Table 4.4 Properties of the bio-oil product

Properties	Methods	Bio-oil (Dynamic) ^a	Bio-oil (Isothermal) ^b
Density, 15°C (kg/m ³)	ASTM D 1298	1050	1080
Water Content (w/w %)	ASTM D 1744	None	None
Viscosity, 50°C (cSt)	ASTM D 88	54	49
Flash point (°C)	ASTM D 93	75	71
Heating value (MJ/kg)	ASTM D 3286	24.30	21.24
pH value		3.5	3.7
Ultimate analysis (w/w %)	Methods	Bio-oil (Dynamic) ^a	Bio-oil (Isothermal) ^b
Carbon	ASTM D 482	65.90	71.70
Hydrogen	ASTM D 3177	9.20	5.40
Oxygen	By difference	21.20	18.60
Nitrogen		3.70	4.30
H/C molar ratio	Calculation	1.68	0.90
C/H molar ratio	Calculation	0.24	0.19
Empirical formula	Calculation	$\text{CH}_{1.68}\text{O}_{0.24}\text{N}_{0.05}$	$\text{CH}_{0.90}\text{O}_{0.19}\text{N}_{0.06}$

^a Obtained at 700°C with dynamic condition, retention time at 15 minutes

^b Obtained at 700°C with isothermal condition, retention time at 15 minutes

The bio-oil usually contains some of organic acids such as formic and acetic acids, which cause the oils to have a pH of between 3.0 and 4.5. The pH of bio-oils in this study were found to be around 3.5 and 3.7 obtained from pyrolysis at 700°C with different heating method and retention time at 15 minutes (maximum oil yield). The acidity causes the pyrolysis oils to be corrosive to mild steel, aluminum, etc. Aldehyde also contribute to the low pH. Thus for application of bio-oil in the sophisticated engine, it needs some chemical treatment for lowering the acidity.

The molecular weight distribution (MWD) can provide the initial clue regarding the composition of the water-insoluble fraction (WIF) at different conditions (isothermal and dynamic heating). In this work, the MWD of Physic nut residue was determined via GPC. The weight average molecular weight (M_w) and the number average (M_n) molecular weight of the WIF from isothermal heating process and dynamic heating process are shown in Table 4.5. The ratio of M_w and M_n is also presented, in terms of polydispersity, which is a measure of the molecular weight homogeneity of the samples. The M_w and M_n values confirm that WIT from pyrolysis are mainly composed of trimers and tetramers of hydroxyl-phenyl, guaiacyl and syringyl compounds [47].

Table 4.5 Molecular weight distribution (MWD) of the water-insoluble fraction (WIF)

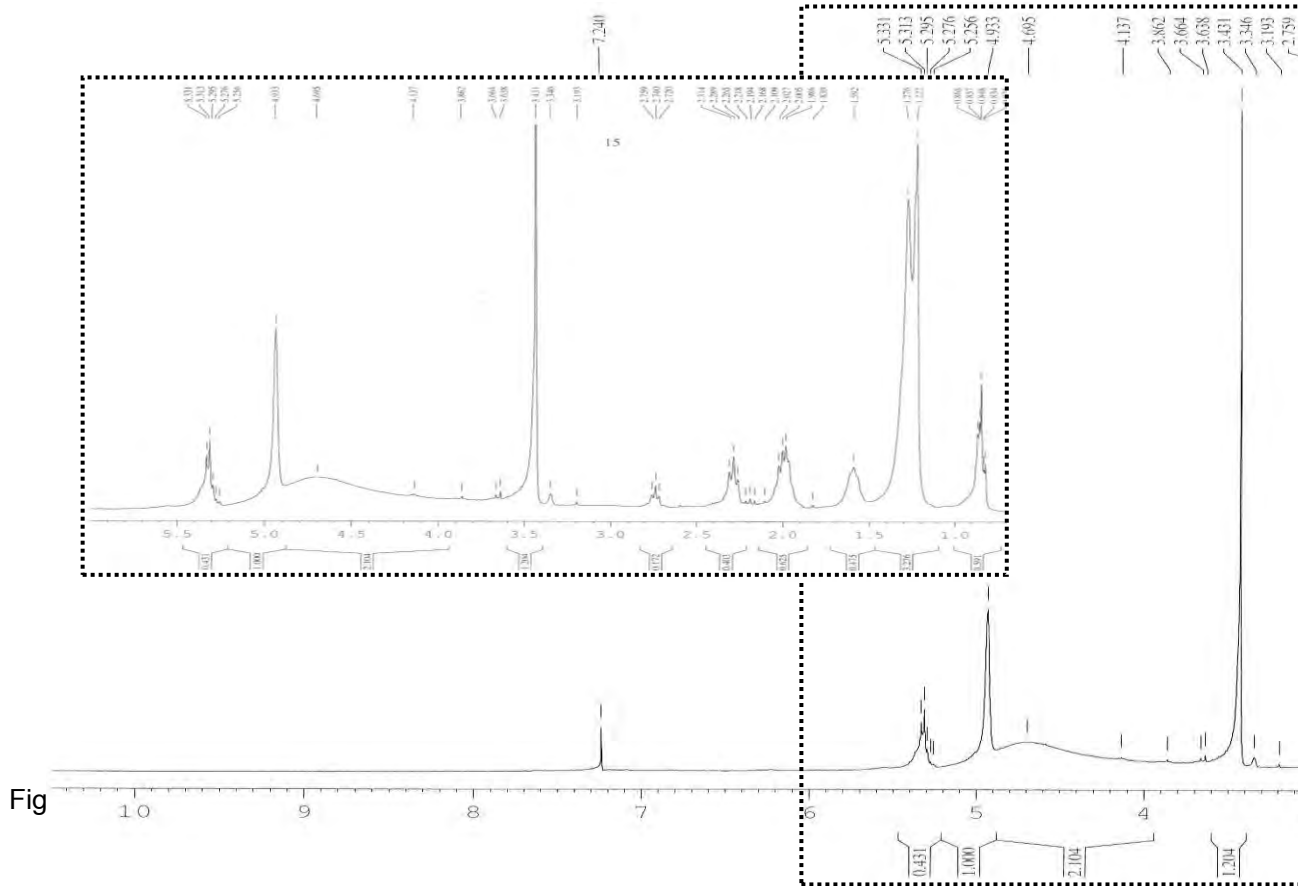
Conditions of Bio-oil	Molecular weight (g/mol)		Polydispersity, M_w/M_n
	Weight average, M_w	Number average, M_n	
Isothermal heating	161,036	76,464	2.106
Dynamic heating	174,005	82,017	2.122

^1H NMR spectra were applied to all of the bio-oils, the results are given in Table 4.6 and Figure 4.17 (isothermal heating) and 4.18 (dynamic heating). ^1H NMR spectra of bio-oils indicate that the aromaticity of the bio-oil from isothermal pyrolysis (1.67%) is greater than that from dynamic pyrolysis (0.77%). For all bio-oils and subfractions ^1H NMR spectra, ring joining methylene, and methoxy protons can be detected between the ranges of 3.3–4.5 ppm and these protons are dominant in the bio-oil from static pyrolysis and its methanol subfraction with respect to others (Table 4.6).

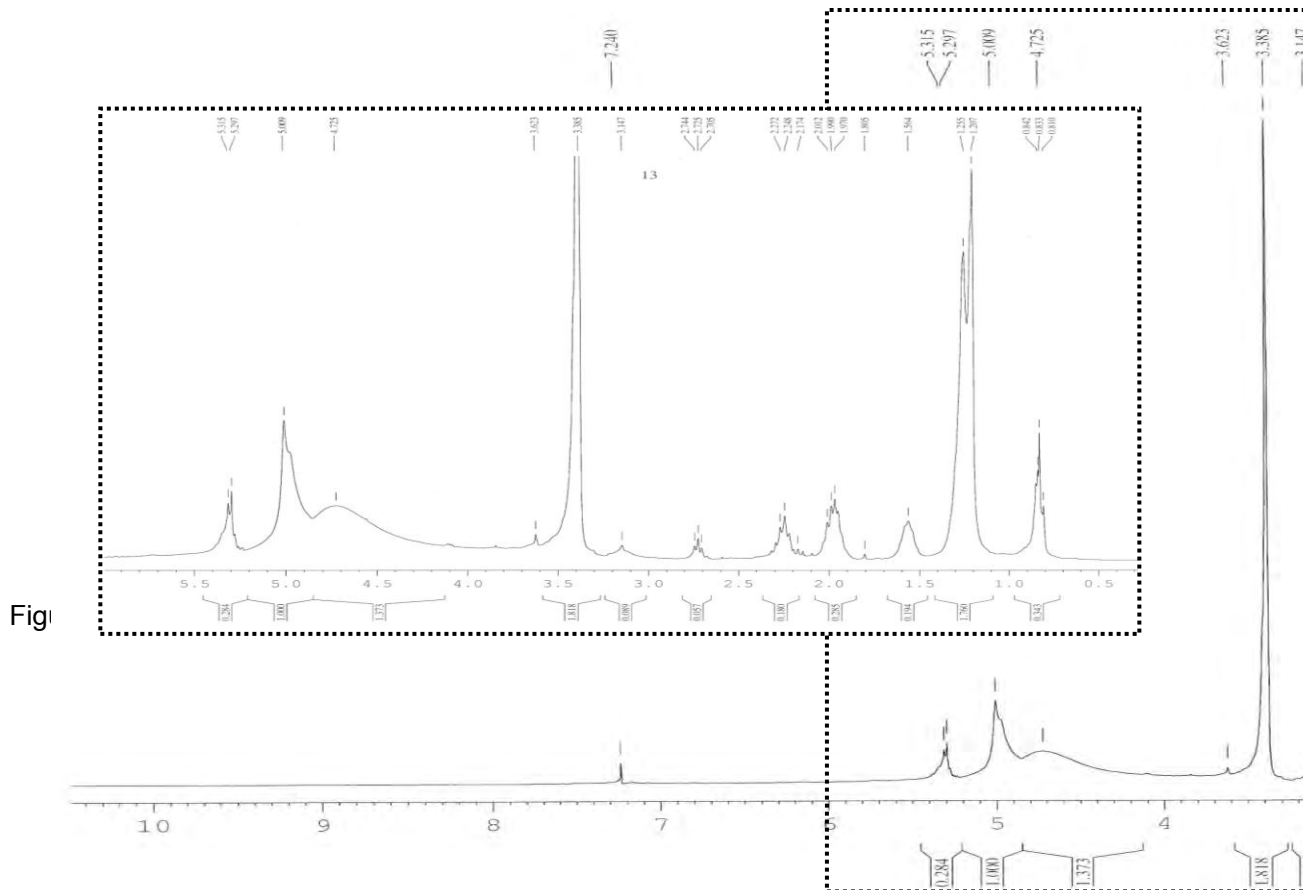
Table 4.6 Results of ^1H NMR spectra for bio-oil of different pyrolysis condition at 700°C

Type of hydrogen	Chemical shift (ppm)	Isothermal heating	Dynamic heating
Aromatics	6.5-9	1.67	0.77
Phenolic OH or olifinic proton	5.0-6.5	13.92	17.39
Ring-joint methylene (Ar-CH ₂ -Ar)	3.3-4.5	32.18	43.22
CH ₃ , CH ₂ , CH α to an aromatic ring	2.0-3.3	10.00	7.52
CH ₂ , CH β to an aromatic ring (naphthenic)	1.6-2.0	4.62	2.63
β -CH ₃ , CH ₂ and CH γ or further from an aromatic ring	1.0-1.6	31.86	23.83
CH ₃ γ or further from an aromatic ring	0.5-1.0	5.75	4.64

The protons in α position to an aromatic ring of the bio-oil from steam pyrolysis are seen to be higher than the other bio-oils. Naphthenic protons CH₂ and CH in the position of β to an aromatic ring can be observed in all bio-oils and their subfraction, which are in different amounts. β -CH₃, CH₂ and CH γ or further from an aromatic ring proton (centered at 1.25 ppm) of the oils and their subfractions are higher than the other protons. They are related to the aliphatic chain bonded to the aromatic ring. CH₃ γ or further from an aromatic ring proton are seen for all bio-oils and their subfractions [50].



Fig



Fig

CHAPTER V

PRODUCTION OF ACTIVATED CARBON

5.1 Raw materials

In this experiment physic nut residue were used for the production of activated carbon by pyrolysis in one stage. They were crushed and sieved to four particles with various size of 0.43-0.50, 0.50-0.85, 0.85-1.80 and 1.80-3.60 mm before being treated. The proximate analysis of physic nut waste is shown in Table 5.1

Table 5.1 Proximate analysis of physic nut residue

Physic nut waste sizes (mm)	BD (g/cm ³)	M (wt%)	On dry basis		
			% Ash	VM (wt%)	FC (wt%)
0.43-0.50	0.5521	4.01	2.28	80.28	17.44
0.50-0.85	0.5470	4.35	2.05	80.66	17.29
0.85-1.80	0.5160	4.32	1.59	83.21	15.20
1.80-3.60	0.5002	4.37	2.28	83.67	14.05

BD = Bulk density, M = Moisture, VM = Volatile matter and FC = Fixed carbon

5.2 Carbonization processes

The 0.43-0.50 mm of physic nut waste was pyrolyzed before activation with oxidizing gas and alkaline solution. The carbonization was carried out in a fixed bed furnace. The studied condition was temperature range of 400 to 800°C and each temperature being varied retention time from 15 to 240 minutes. The proximate analysis of Physic nut waste char is presented in Table 5.2.

Table 5.2 Proximate analysis of Physic nut waste char at different temperature and times

Temp (°C)	Time (min)	Y (wt%)	M (wt%)	Ash (wt%)	VM (wt%)	FC (wt%)
400	15	45.76	0.66	1.50	79.20	18.86
	120	39.74	0.71	1.37	79.33	18.82
	240	36.64	0.64	1.24	81.06	17.35

500	15	36.95	0.61	3.28	65.01	30.70
	120	32.55	0.69	3.40	67.39	29.51
	240	31.35	0.59	2.71	68.69	28.49
600	15	33.27	0.51	3.93	33.32	62.44
	120	27.71	0.61	3.40	34.08	61.75
	240	27.12	0.54	3.23	35.64	60.81
700	15	31.66	0.47	4.41	15.22	79.32
	120	26.12	0.54	4.29	16.13	79.14
	240	23.87	0.48	4.05	19.71	75.90
800	15	24.23	0.46	4.87	4.34	90.01
	120	21.69	0.49	4.78	6.29	88.06
	240	20.43	0.44	4.69	11.57	83.11

Y = Yield of char, M = Moisture, VM = Volatile matter and FC = Fixed carbon

From volatile matter, fixed carbon and yield in Table 5.2, the optimum condition for pyrolysis of physic nut residue was 800°C for 15 minutes because the characteristic of physic nut waste char at this condition contained low volatile matter (approximately 4 wt%) which was appropriated for activation. The pyrolyzed physic nut waste was 24.23% yield, 4.87% ash and 90.01% fixed carbon. The physic nut waste char prepared at this condition would be used in the next activation steps.

5.3 Activation Processes

5.3.1 Physical activation by oxidizing gas

The amount of 10 g of 0.43-0.50 mm of physic nut waste char was used in each batch. The reactor was heated to the final temperature of 400, 500, 600 and 700°C before the physic nut waste char sample was charged into the reactor. After charging, the CO₂ excess was passing up through the reactor at a fixed flow of 100 mL/min, for 30, 60 and 90 minutes. The results of this experiment are shown in Table 5.3 and Figures 5.1-5.5.

Table 5.3 Characteristics of activated carbon from Physic nut residue at different temperatures and times (size 0.43-0.50 mm, 10 g, CO₂ 100 mL/min)

Temp (°C)	Time (min)	Y (%)	On dry basis			
			BD (g/cm ³)	Ash (%)	MB (mg/g)	IA (mg/g)
400	30	49.35	0.25	6.71	97.12	414.31
	60	51.12	0.24	6.12	122.24	465.54
	90	48.09	0.23	6.47	123.54	481.38
500	30	47.44	0.23	7.90	110.26	483.70
	60	46.35	0.23	7.43	128.56	482.21
	90	43.32	0.22	8.31	157.45	510.76
600	30	45.18	0.21	10.51	111.52	485.33
	60	39.30	0.21	9.35	162.09	526.68
	90	38.71	0.20	10.01	145.77	509.82
700	30	35.26	0.20	10.81	119.91	473.99
	60	34.03	0.20	10.99	127.20	420.23
	90	29.27	0.19	13.22	132.18	447.56

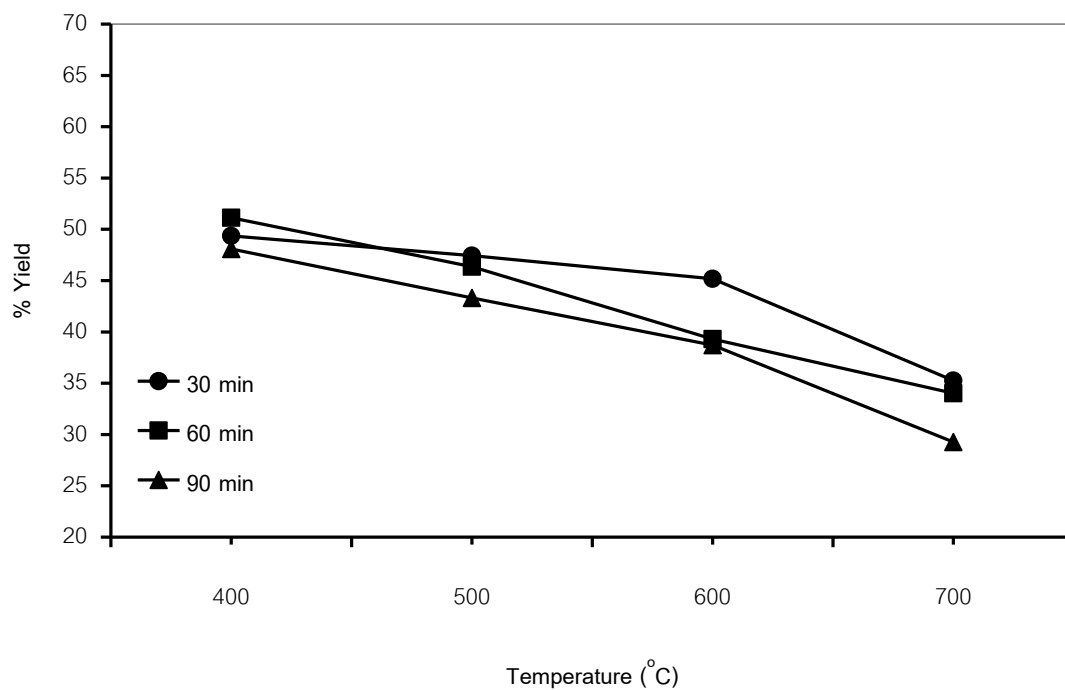


Figure 5.1 Effect of activation temperature and time on % yield

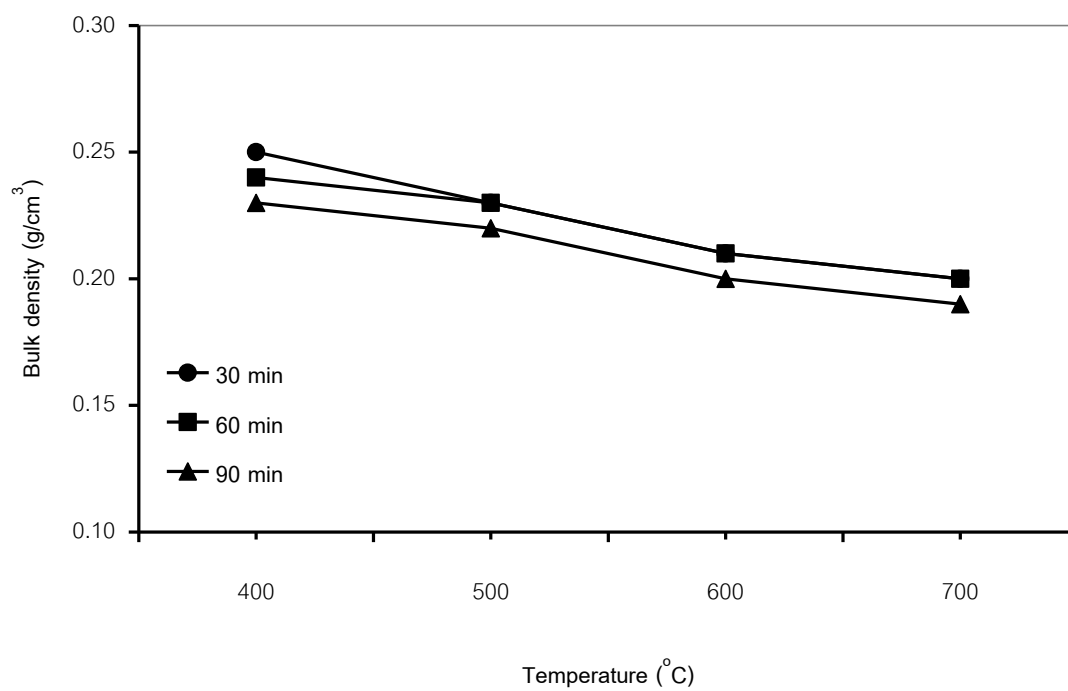


Figure 5.2 Effect of activation temperature and time on bulk density

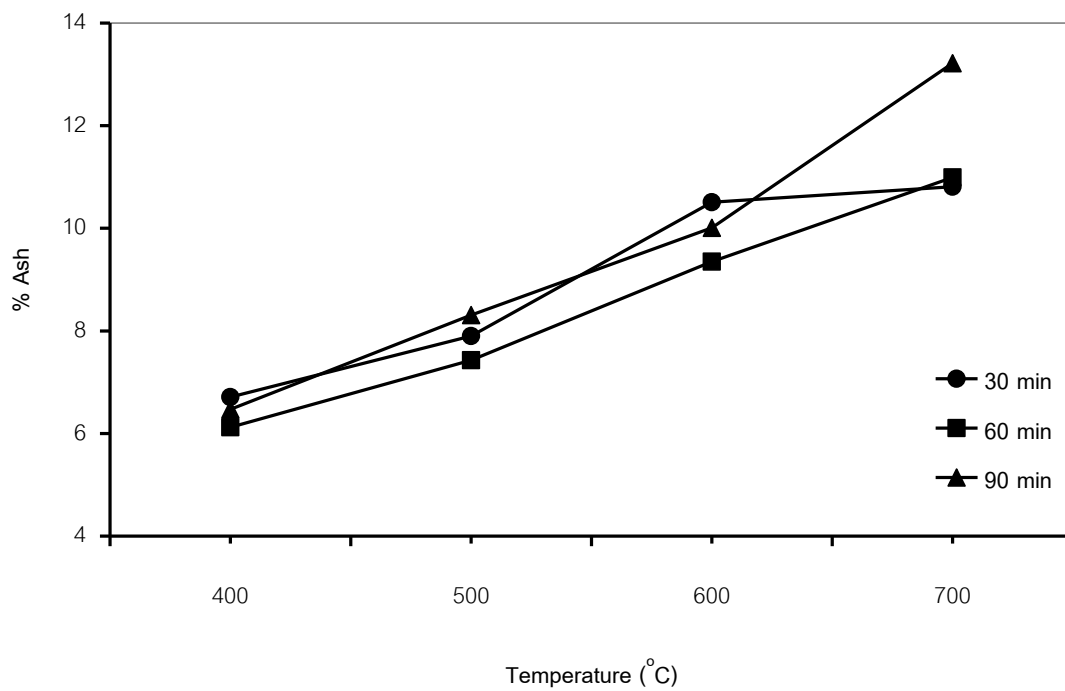


Figure 5.3 Effect of activation temperature and time on % ash

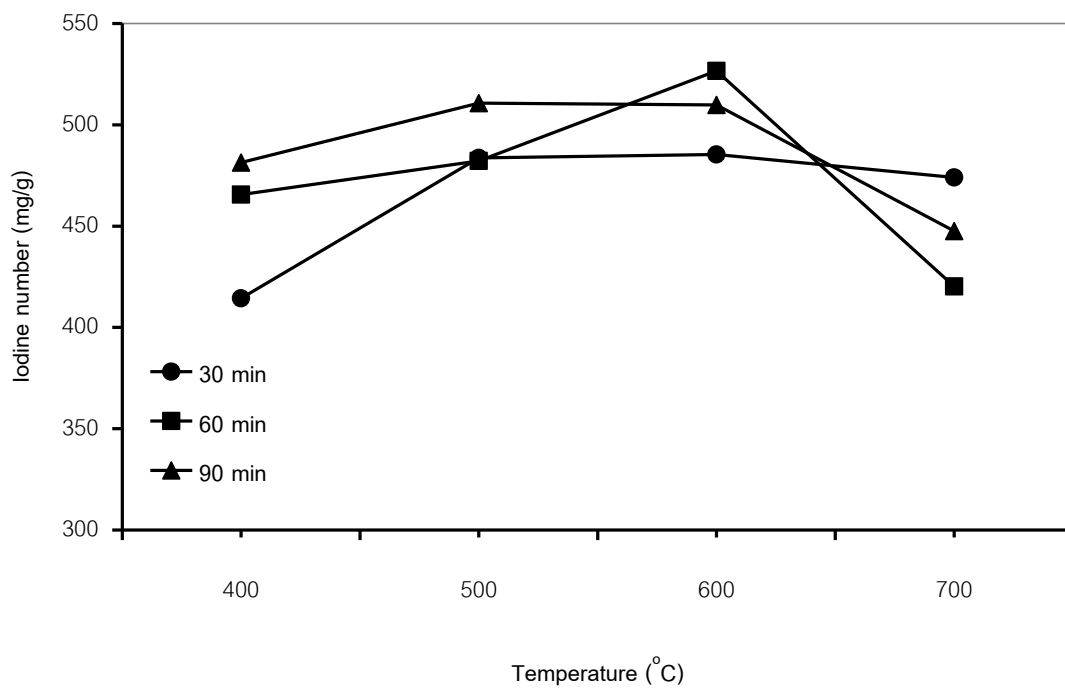


Figure 5.4 Effect of activation temperature and time on iodine number

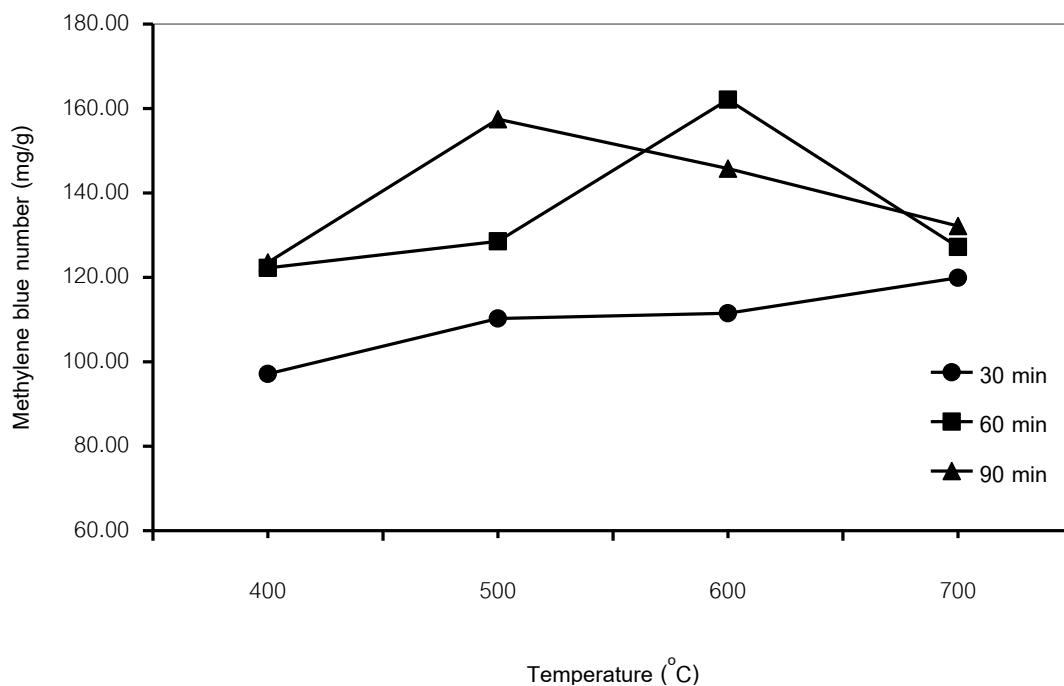


Figure 5.5 Effect of activation temperature and time on methylene blue number

From Table 5.3 and Figures 5.1, the % yield decreased when the temperature increased from 400 to 700°C, for 30, 60 and 90 minutes. The decrease of % yield can be attributed to the loss of volatile matter with the increase of temperature and the porosity development in granules. From the reasons, ash would increase (Figure 5.3) with an increase temperature. The % ash in first stage (400-500°C) between 30 and 60 minutes increase slowly because only the volatile matter at the surface is removed, hence the % ash is rather constant. When time is increase to 90 minutes, the % ash would increase quickly. But when the temperature increase from 500 to 700°C for 30 and 60 minutes, the % ash in this stage would increase faster than % ash in the first stage (400-500°C). The % ash at 500 to 700°C for 90 minutes increase the fastest of all.

From the Figure 5.2, the bulk density decreases slowly with increasing temperature from 400 to 500°C and then decreased quickly as temperature increase from 500 to 700°C for 30, 60 and 90 minutes. This is because at high temperature, porosity is highly developed.

Figure 5.4 and Figure 5.5 shows that the iodine number and the methylene blue number increase when the temperature increases from 400 to 600°C for 60 and 90 minutes and then drop at 700°C. In the first stage (400-500°C), the iodine number

increase slowly because the diffusion of volatile matter hinders the presentation of carbon dioxide into the surface of physic nut waste; as a result, the development of porosity is less. When the temperature increase from 500 to 600°C, iodine number increases quickly, because most of volatile matter is diffused from granules in the first stage, so the carbon dioxide penetrates easily into the surface of physic nut residue; as a result, the high development of porosity. When the temperature increases from 600 to 700°C, the iodine number and methylene blue number decreased because micropores would have coalesced, resulting in mesopores and time thus reducing those values. From these results, the optimum temperature for activation by carbon dioxide gas is 600°C for 60 minutes because this level contains high iodine number, high methylene number but moderate temperature. The activated carbon with the yield of 39.30% had bulk density of 0.21 g/cm³, ash of 9.35%, iodine number of 526.68 mg/g and methylene blue number of 162.09 mg/g.

5.3.2 Chemicals activation by alkaline solution

5.3.2.1 The effect of concentration of potassium hydroxide

The concentration of potassium hydroxide solution at char : KOH ratio (by weight) 1:1, 3:1, 5:1, 7:1 and 10:1 were prepared. The 10 g of 0.43-0.5 mm of physic nut waste char were soaked by these different solutions for studying the influence of concentration of solution on characteristics of prepared activated carbon. After drying the char was loaded into reactor and heated at 600°C for 0.25 hour by passing nitrogen gas though the reactor. The results of this experiment were shown in Tables 5.4 and Figures 5.6-5.10.

Table 5.4 Effect of KOH concentration (600°C, 0.25 hour, N₂ flow rate 100 mL/min)

Concentration (char : KOH)	Y (%)	BD g/cm ³	Ash (%)	MB (mg/g)	IA (mg/g)	B.E.T. m ² /g
1 : 1	65.56	0.17	3.55	101.03	431.27	133.27
3 : 1	68.49	0.19	3.34	97.52	345.63	99.98
5 : 1	68.01	0.19	4.26	73.43	320.99	91.22

7 : 1	69.75	0.21	5.19	59.99	297.04	82.01
10 : 1	71.12	0.21	3.60	32.67	249.20	N/A

From Tables 5.4 and Figures 5.6-5.7, the % yield and bulk density of activated carbon from Physic nut waste decreased when the concentration of potassium hydroxide increased and reached the minimum at char : KOH ratio 1 : 1. Potassium hydroxide reacted more with char and volatile matter diffused quickly out of the surface of particles (and substituted -H group by -OH group). % Ash was around 3.5-3.2 % by weight with no significant trend with concentration of KOH.

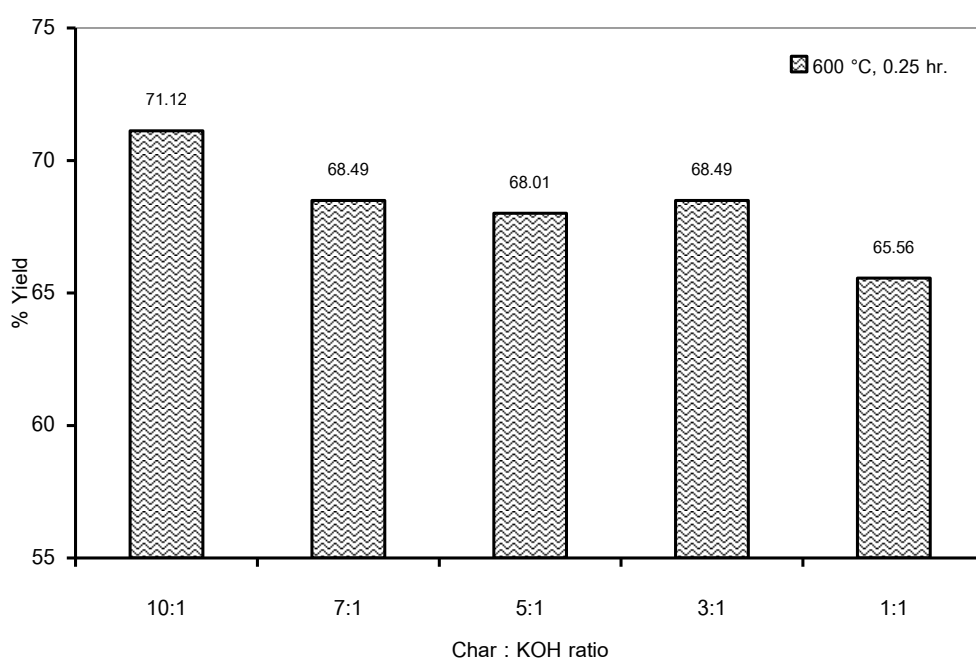


Figure 5.6 Effect of char : KOH ratio time on % yield at 600°C for 0.25 hour

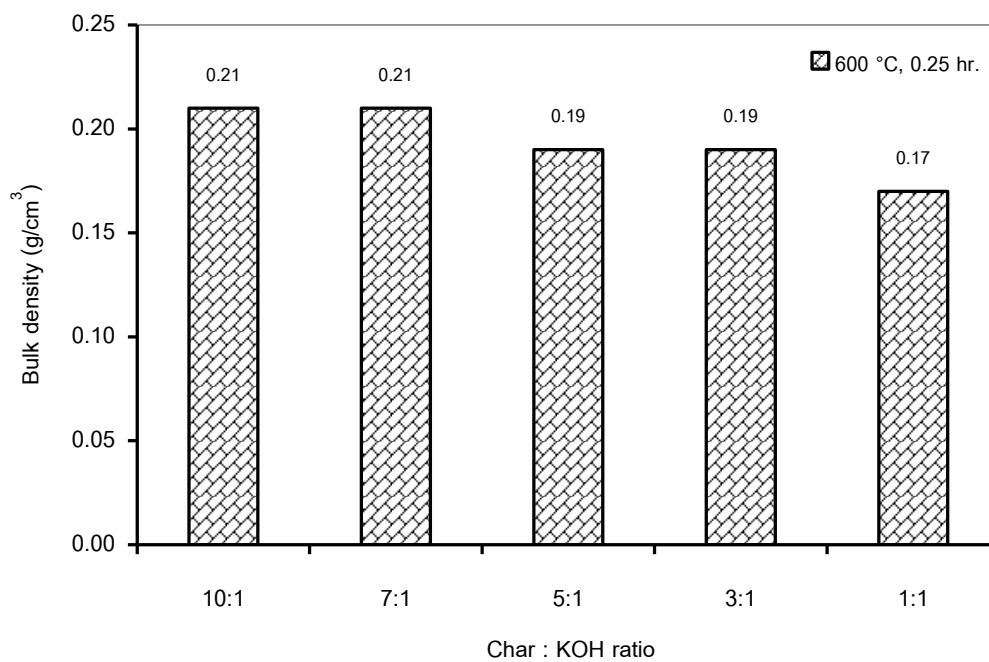


Figure 5.7 Effect of char : KOH ratio time on bulk density at 600°C for 0.25 hour

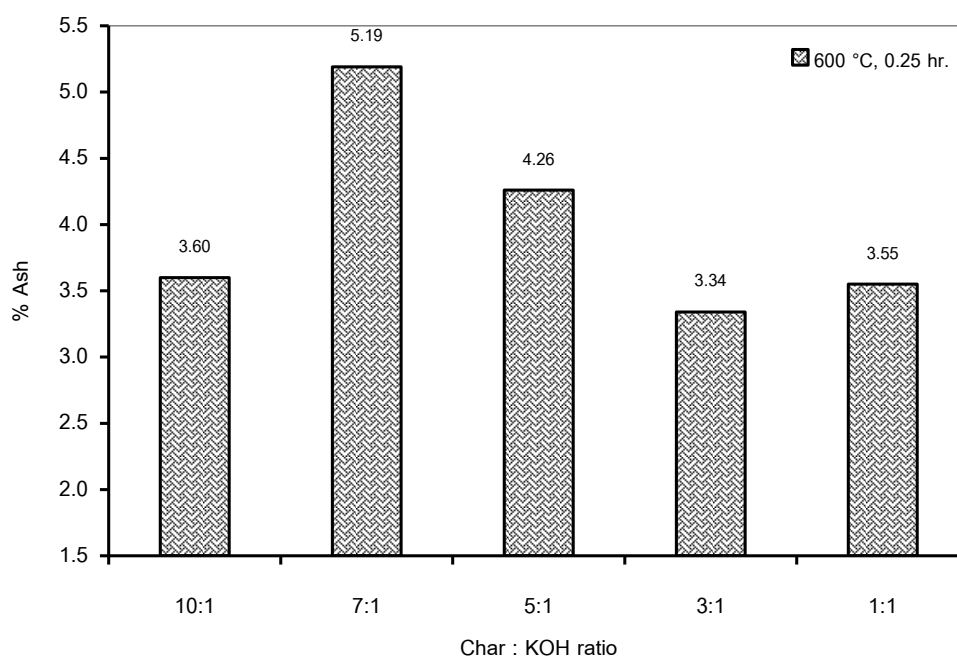


Figure 5.8 Effect of char : KOH ratio time on % ash at 600°C for 0.25 hour

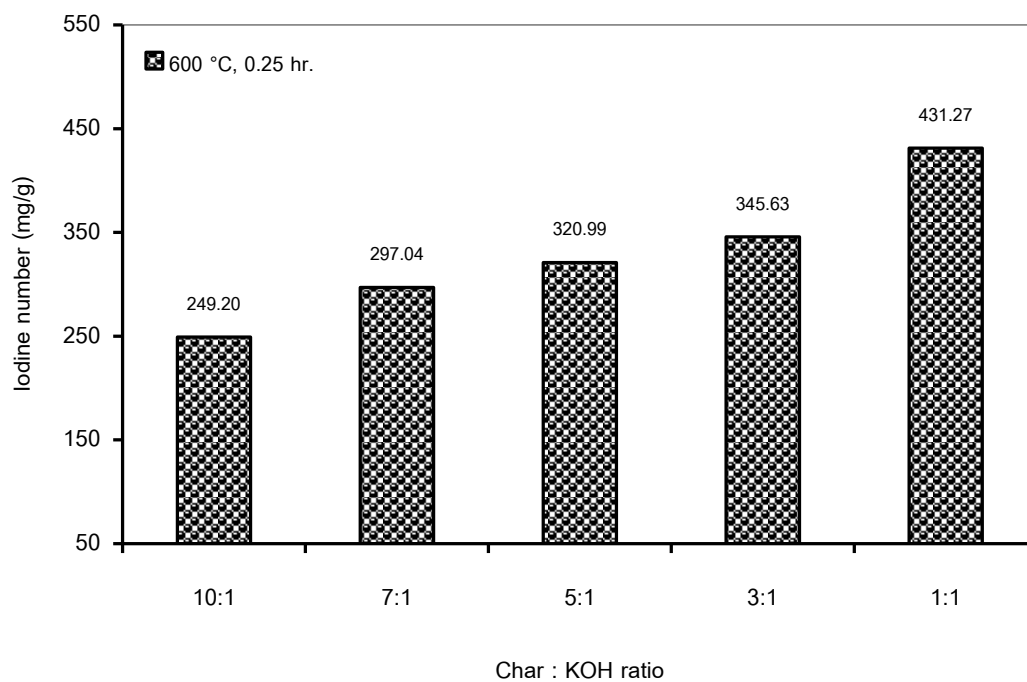


Figure 5.9 Effect of char : KOH ratio time on iodine number at 600°C for 0.25 hour

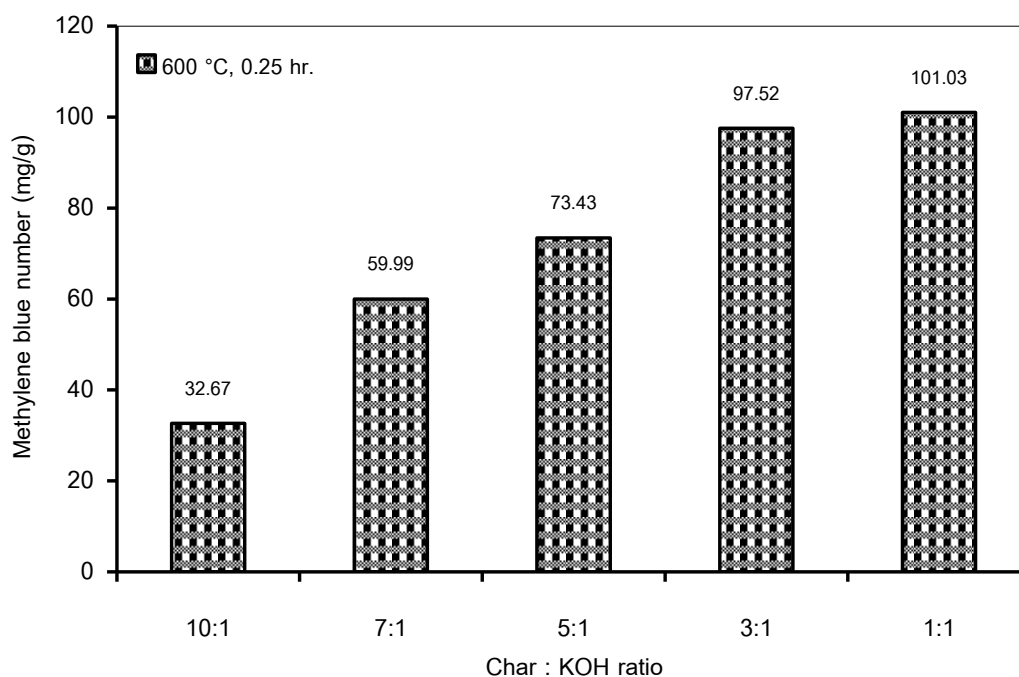


Figure 5.10 Effect of char : KOH ratio time on methylene blue number at 600°C for 0.25 hour

The iodine number, methylene blue number and B.E.T. surface area would increase when the concentration of potassium hydroxide solution increased. They reached the maximum at char : KOH, 1 : 1. It confirmed that the more reaction took

place, the more porosity developed ; as the result % yield and bulk density decreased while iodine number, methylene blue number and B.E.T. surface area increased.

From these results, the optimum concentration of KOH was at 1 : 1 char : KOH ratios because at this condition the activated carbon had highest iodine number of 824.12 mg/g, methylene blue number of 187.94 mg/g and B.E.T. surface area 767.30 m²/g. The effect of temperature and time for activation will be further investigated.

5.3.2.2. The effect of temperature for activation

Ten grams of 0.43-0.5 mm of Physic nut residue char were soaked in 1 : 1 of char : KOH ratio and then were dried. These samples were used for each batch. The nitrogen gas was then allowed to flow through the tube reactor. The quartz tube reactor was heated until the temperature in the tube reactor was raised and fixed at the final temperature 500, 600 and 700°C. The nitrogen gas was continued, passing through the tube reactor for 0.25 hr. The results of these experiments are shown in Tables 5.5 and Figures 5.11-5.15.

Table 5.5 Effect of temperature (1:1, 0.25 hour, N₂ flow rate 100 mL/min)

Temperature (°C)	Y (%)	BD g/cm ³	Ash (%)	MB (mg/g)	IA (mg/g)	B.E.T. m ² /g
500	66.23	0.19	3.76	99.84	311.07	90.01
600	65.56	0.17	3.55	101.03	431.27	133.27
700	59.03	0.16	3.22	144.56	586.21	551.23

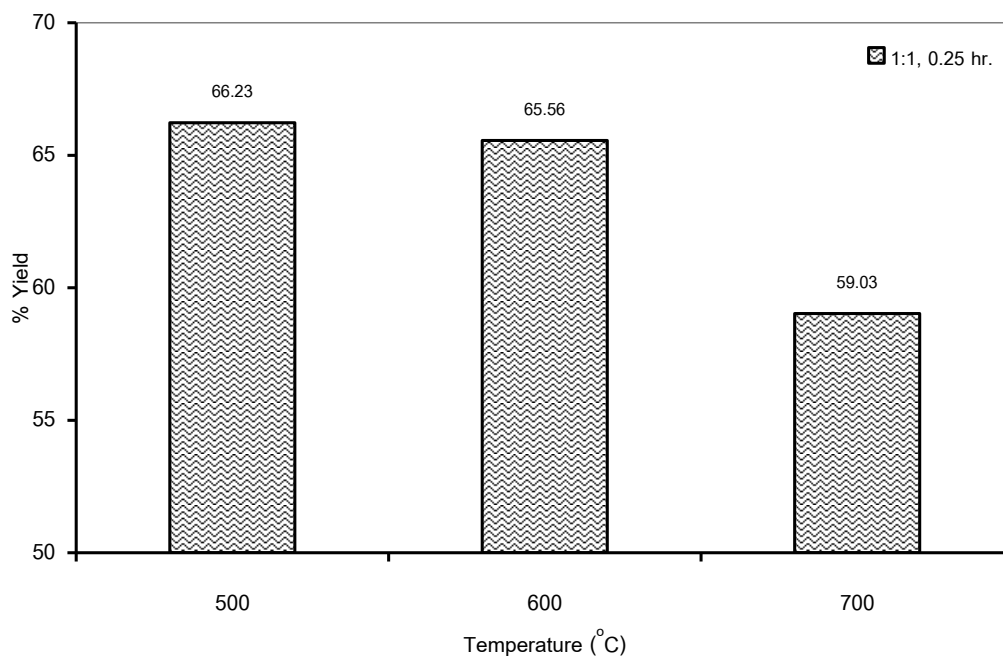


Figure 5.11 Effect of activation temperature on % yield at difference time and char : KOH ratio

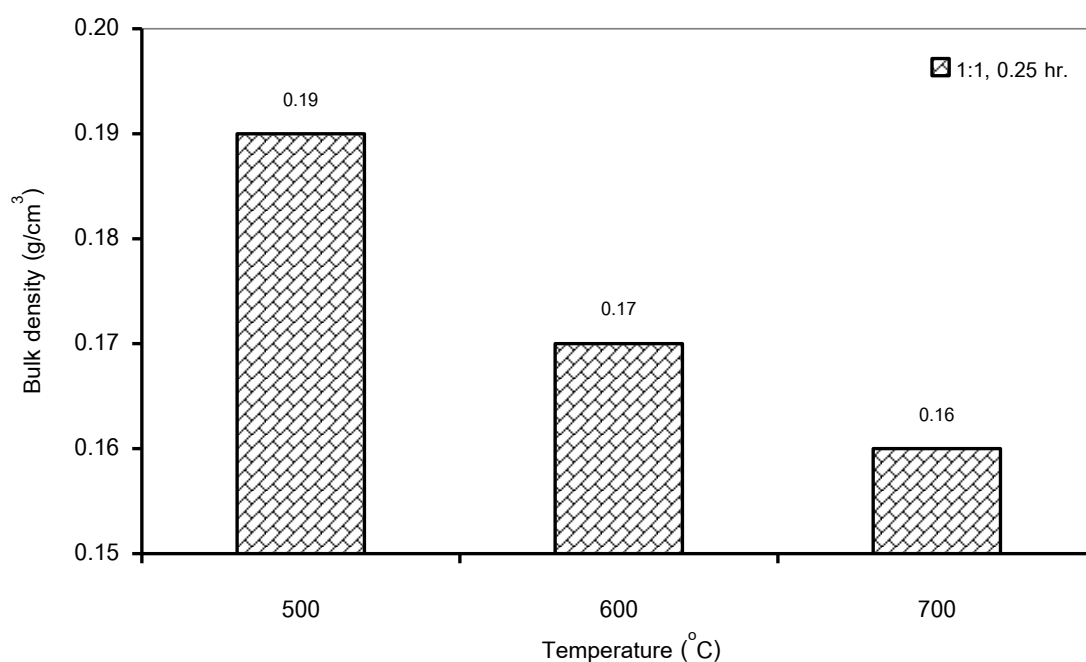


Figure 5.12 Effect of activation temperature on bulk density at difference time and char : KOH ratio

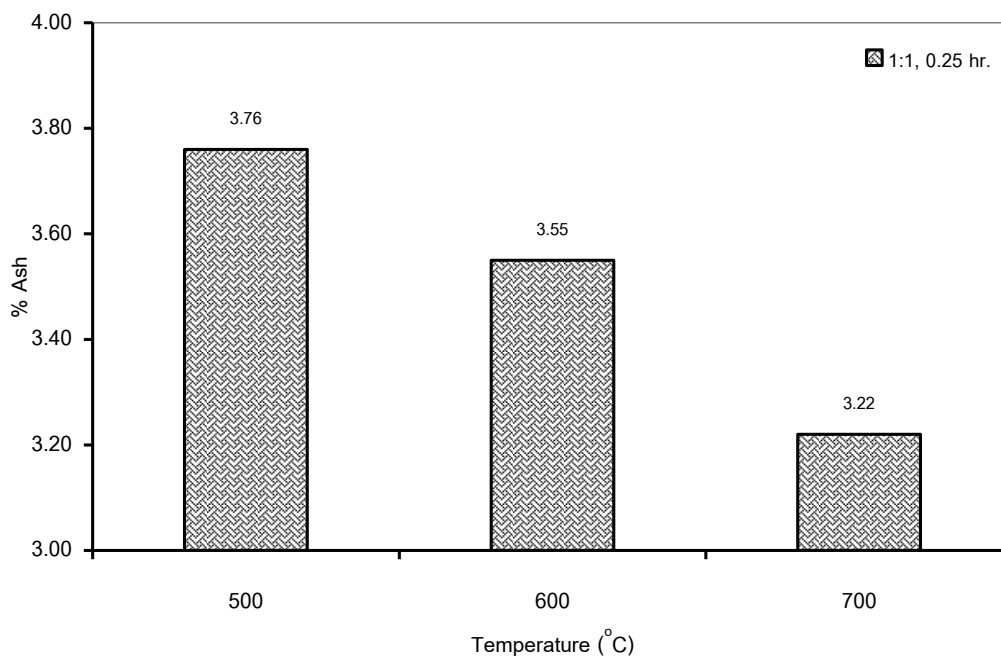


Figure 5.13 Effect of activation temperature on % ash at difference time and char : KOH ratio

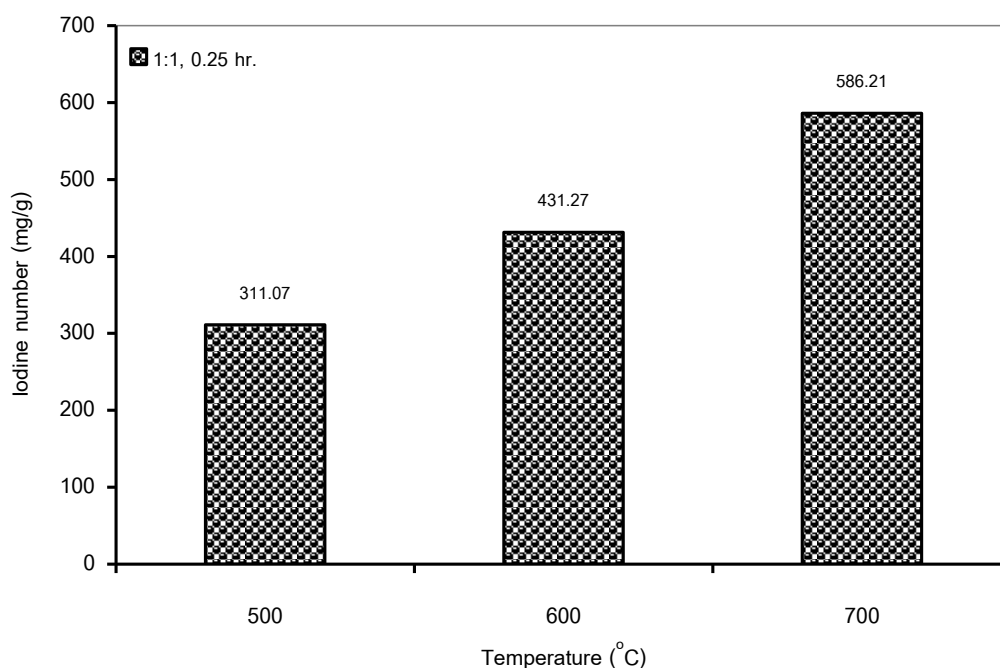


Figure 5.14 Effect of activation temperature on iodine number at difference time and char : KOH ratio

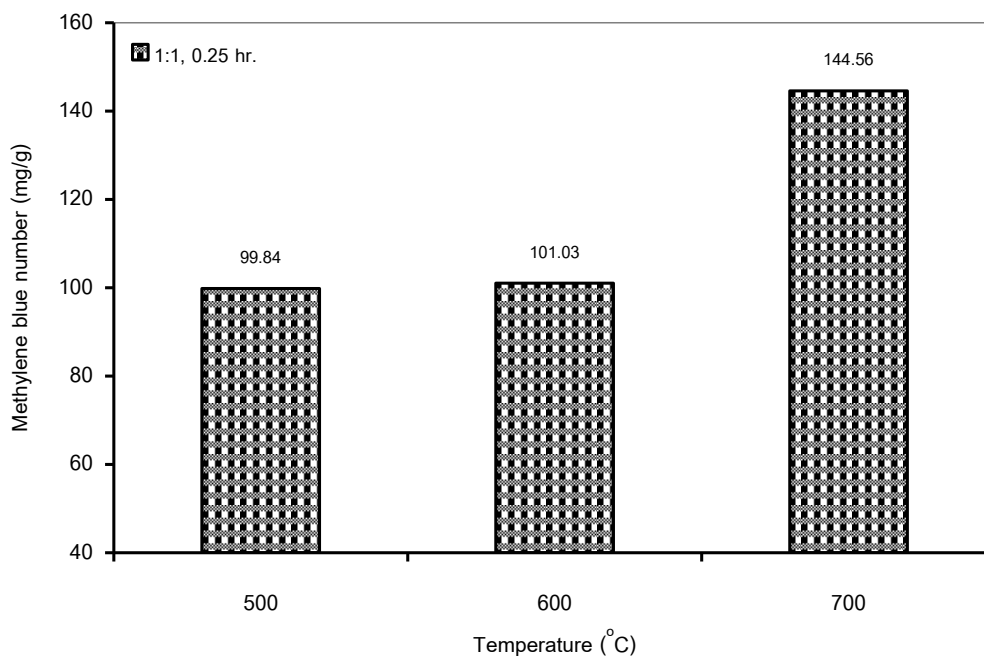


Figure 5.15 Effect of activation temperature on methylene blue number at difference time and char : KOH ratio

From Tables 5.5 and Figures 5.10-5.15, the % yield and the bulk density of activated carbon from Physic nut waste decrease conformably as activation temperature increased. % Yield decreased slowly at lower temperature and the sudden drop after 600°C. This is because at high temperature loss of volatile matter was greater than that at low temperature therefore led to the increasing of porosity development ; as a result, the weight of activated carbon decreased. The change in the % yield of Physic nut waste was less than 1% from 500 to 600°C, 6-7% from 600 to 700°C and bulk density from Physic nut residue decreased totally 9.52%.

Tables 5.5 and Figures 5.14-5.15, showed that when the activation temperature increased from 500 to 700°C , the iodine number and methylene blue number increased continuously and had a trend to be at the highest at 700°C for activated carbon from Physic nut waste. The B.E.T. surface area increased as the iodine number, because tar like matter and potassium hydroxide deposited in pores were removed or volatilized well from 600 to 700°C, which generated porosity. The higher activation temperature, the more removal potassium hydroxide results, therefore the iodine number and the methylene blue number increased quickly (see slope in Figures

5.14 and 5.15). The % change of iodine number was about 46.93% from 500 to 700°C, and 30.94% for methylene blue number.

From these results, the optimum temperature was 700°C for 1 : 1 char : KOH ratios because at this condition activated carbon have the highest iodine number of 586.21 mg/g, methylene blue number of 144.56 mg/g and B.E.T. surface area 551.23 m²/g. The effect of activation time will be further reported.

5.3.2.3 The effect of time for activation process

The 10 grams physic nut waste char with a particle size of 0.43-0.5 mm were soaked in potassium hydroxide solution at char : KOH ratio of 1 : 1 and then was dried. Then it was treated at 700°C for 0.25, 1 and 4 hours in a tube reactor under nitrogen gas. The results of this experiment were shown in Table 5.6 and Figures 5.16-5.20.

Table 5.6 Effect of times (1:1, 700°C, N₂ flow rate 100 mL/min)

Times (hours)	Y (%)	BD g/cm ³	Ash (%)	MB (mg/g)	IA (mg/g)	B.E.T. m ² /g
0.25	59.03	0.16	3.22	144.56	586.21	551.23
0.50	57.98	0.17	3.41	161.37	680.58	N/A
1.00	56.54	0.16	2.89	187.94	824.12	767.30

Figure 5.16 the % yield of Physic nut residue char decreases slightly and conformably with increasing in the time from 0.25 to 0.5 hour (about 1.78% change), and continuously decreased from 0.5 to 1 hour (2.48% change). The volatile matter outside and inside the particle of char were gasified itself by using potassium hydroxide as catalyst. The gaseous product, volatile matter, and potassium hydroxide in majority diffused out of the particle in the beginning time more slowly than longer activation time (from 0.5 to 1 hour) which less remained volatile matter being deeper in the particle diffused out only. The % bulk density of physic nut waste char (Figure 5.17) did not changed significantly with time. These phenomena showed that porosity developed quickly in 1 hour.

Table 5.6 and Figures 5.19-5.20 showed that an increase of activation time could cause an increase of iodine number and methylene blue number. It is because volatile matter and moisture have enough time to incorporate during longer activation time (0.5-1 hour) thus make micropores and mesopores increase in the carbon structure. It is found that iodine number and methylene blue number tend to increase 17.41% and 14.14% respectively

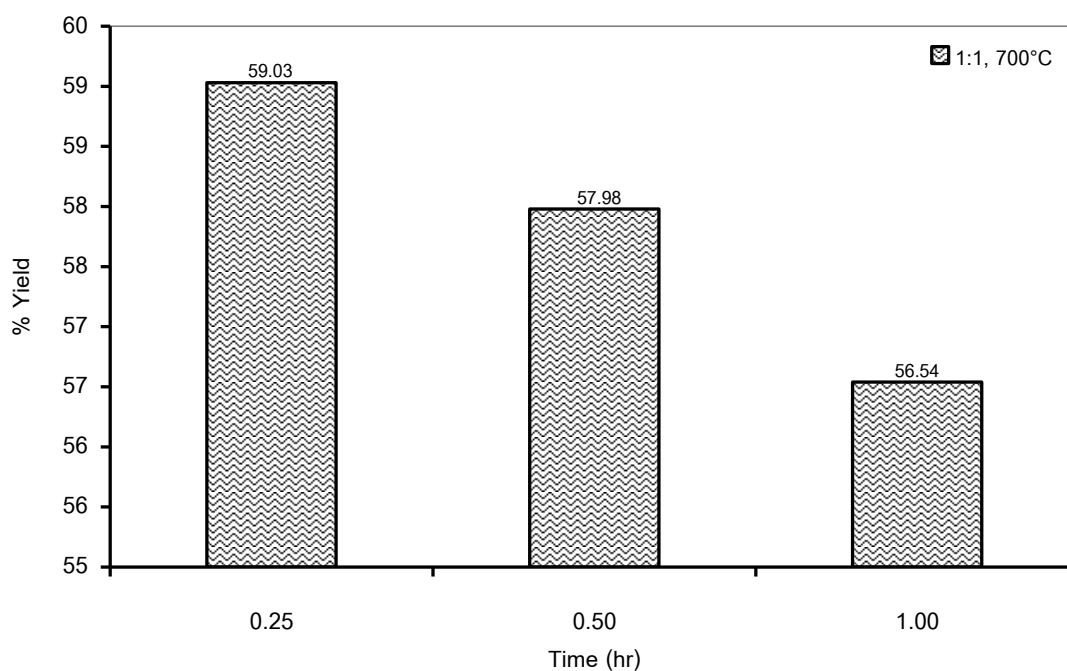


Figure 5.16 Effect of activation time on % yield (char : KOH ratio 1 : 1, 700°C, size 0.43-0.50 mm)

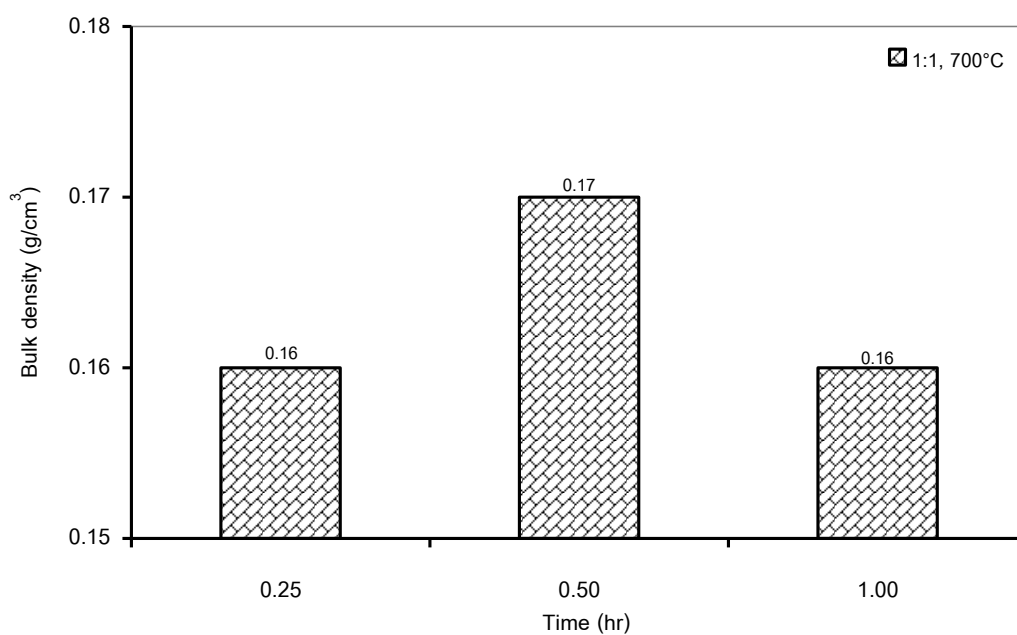


Figure 5.17 Effect of activation time on bulk density (char : KOH ratio 1 : 1, 700°C, size 0.43-0.50 mm)

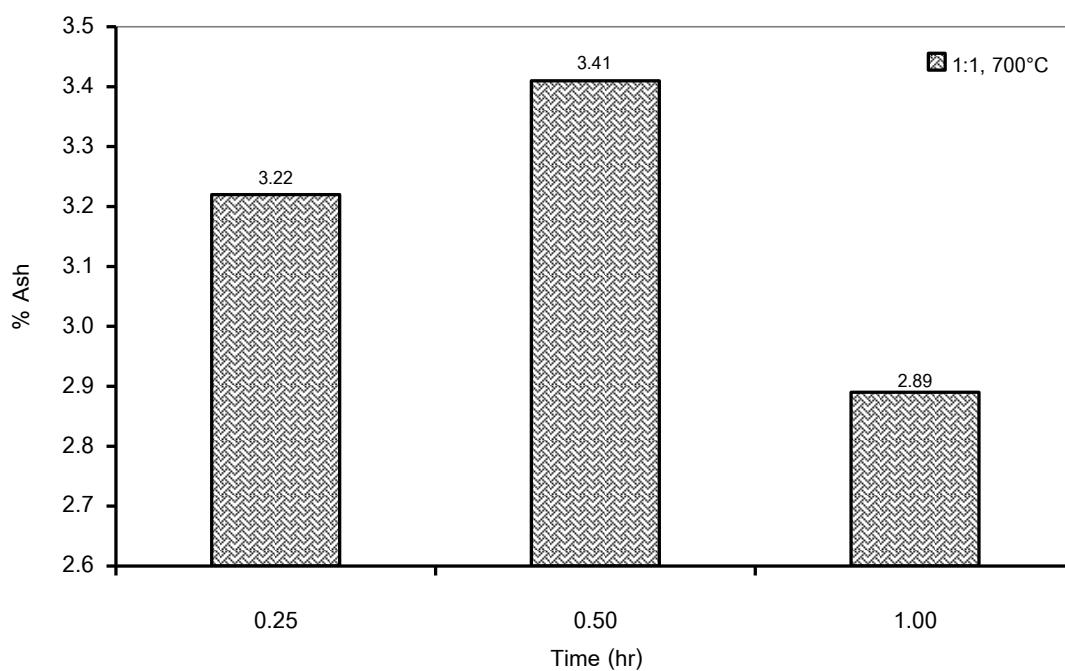


Figure 5.18 Effect of activation time on % ash (char : KOH ratio 1 : 1, 700°C, size 0.43-0.50 mm)

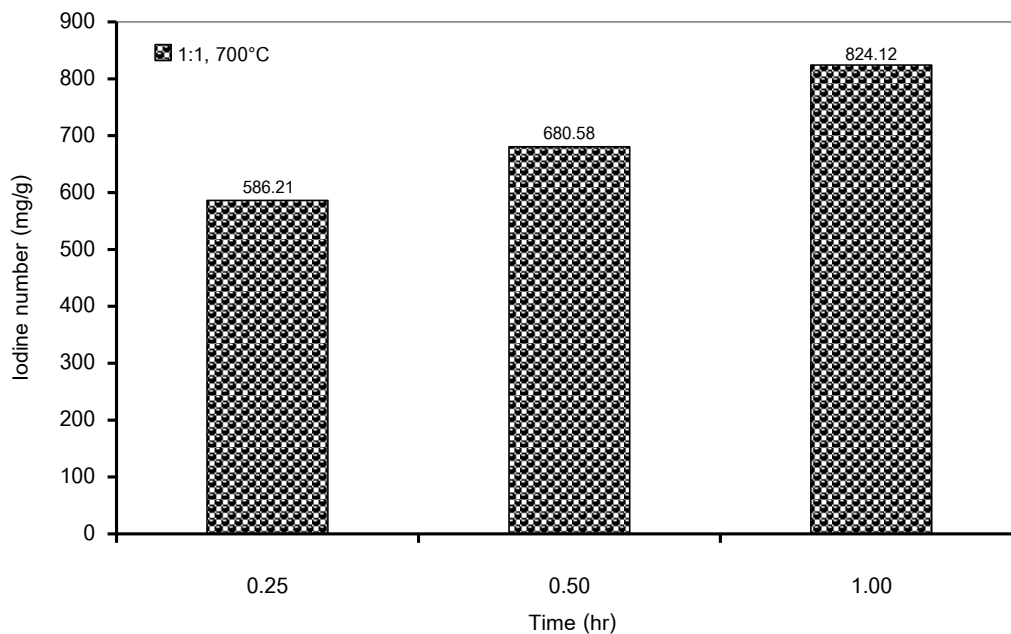


Figure 5.19 Effect of activation time on iodine number (char : KOH ratio 1 : 1, 700°C, size 0.43-0.50 mm)

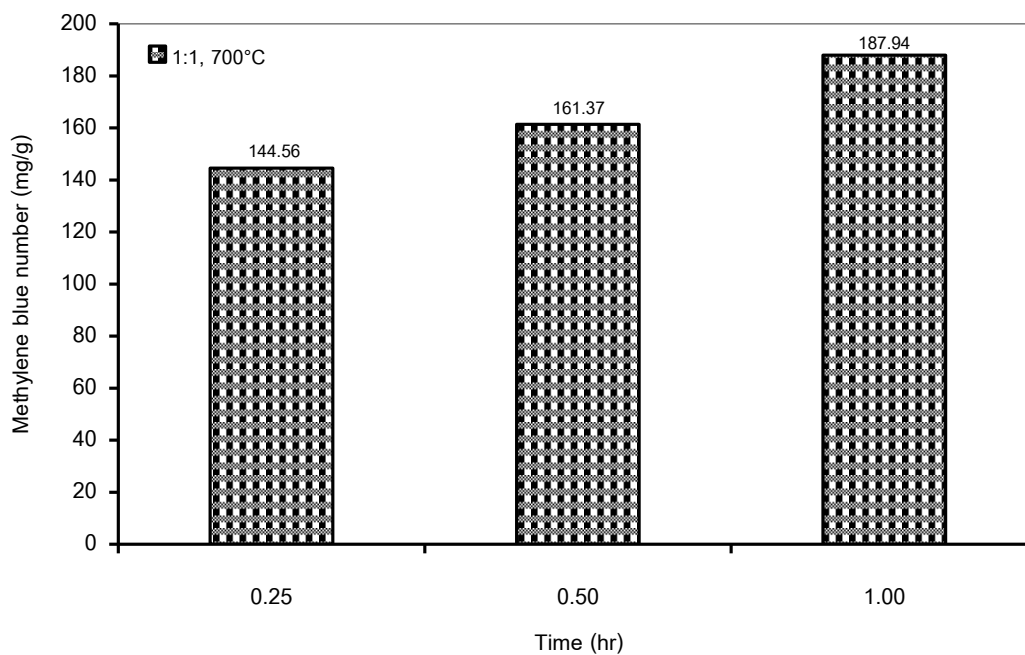


Figure 5.20 Effect of activation time on methylene blue number (char : KOH ratio 1 : 1, 700°C, size 0.43-0.50 mm)

The iodine number, methylene blue number and B.E.T. surface area are increased in the same trend. The high increasing rate covered in the range of 0.25 to 1

(from 586.21 to about 824.72 mg/g for IA, 144.56 to about 187.94 mg/g for MB and to 551.23 to about 767.30 mg²/g for specific surface area). It could be explained in the same way as % yields that volatile matter and potassium hydroxide diffused out rapidly especially at the external surface, as a result, micropores developed quickly in the form of surface area as well.

From these results, the optimum activation time was 1 hour at 700°C with char : KOH ratio of 1 : 1 because at this condition activated carbon has highest iodine number of 824.72 mg/g, methylene blue number of 187.94 mg / g and B.E.T. surface area 767.30 m²/g. The effect size of char will be further investigated.

5.3.2.4 The effect of size of Physic nut waste char for activation

The influence of particle size was determined for different four sizes of Physic nut waste char. They were 0.43-0.50, 0.50-0.85, 0.85-1.80 and 1.80-3.60 mm and soaked in 1 : 1, char : potassium hydroxide ratio solution. The mass of 10 g of each sample of the Physic nut waste char was carried out at 700°C while nitrogen gas was passed though the bed for 1 hour. The results of this experiment were show in Table 5.7 and Figures 5.21 – 5.25.

Table 5.7 Effect of particle size (1:1, 700°C, N₂ flow rate 100 mL/min)

Particle size (mm)	Y (%)	BD g/cm ³	Ash (%)	MB (mg/g)	IA (mg/g)	B.E.T. m ² /g
0.43-0.50	56.54	0.16	2.89	187.94	824.12	767.30
0.50-0.85	57.23	0.17	2.66	158.39	770.10	624.01
0.85-1.80	60.16	0.18	2.59	135.68	689.31	589.25
1.80-3.60	70.89	0.20	2.42	127.03	656.88	540.49

The % yields (Figure 5.21) and bulk density (Figure 5.22) had increased as the increasing of particle from 0.43-0.50 mm in upward again at 1.80-3.60 mm, especially % yield (from 56.54 to 70.89%). On the contrary, the iodine number (Figure 5.24), methylene blue number (Figure 5.25) and B.E.T. surface area decreased with increasing of particle size approaching at the minimum at 1.80-3.60 mm.

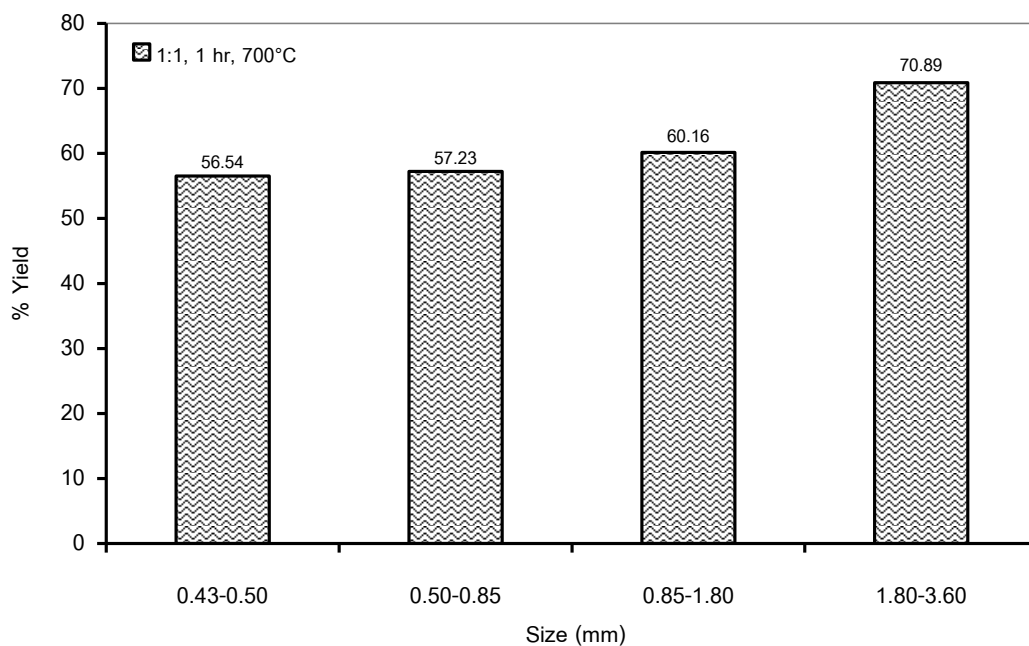


Figure 5.21 Effect of particle size on % yield (char : KOH ratio 1 : 1, 700°C)

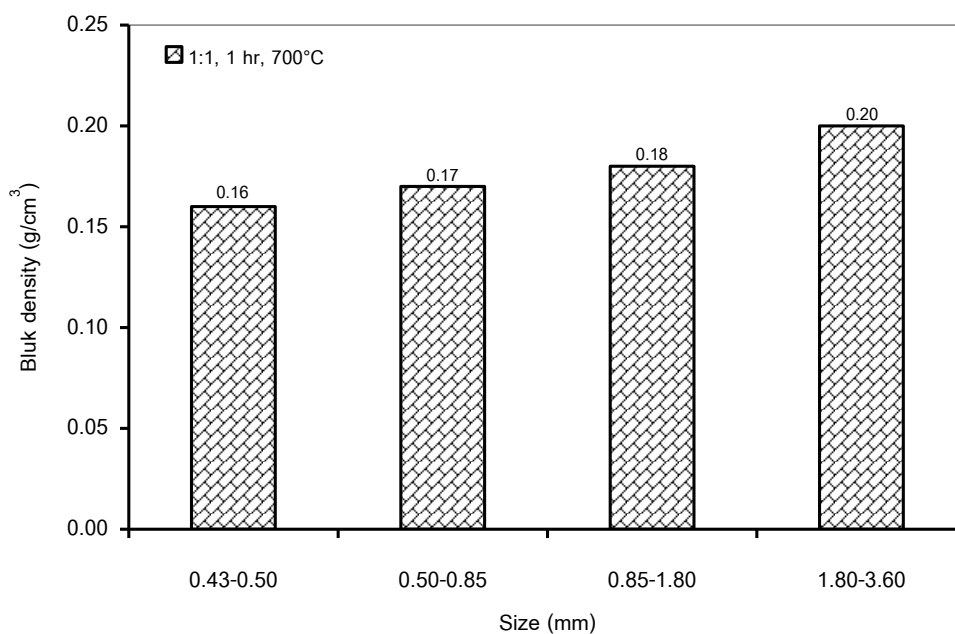


Figure 5.22 Effect of particle size on bulk density (char : KOH ratio 1 : 1, 700°C)

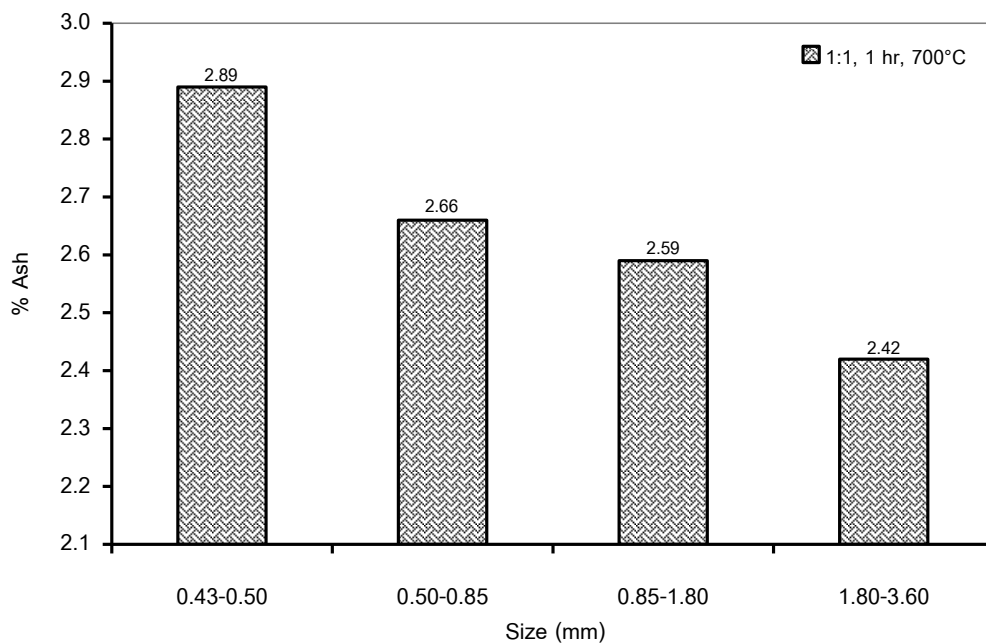


Figure 5.23 Effect of particle size on % ash (char : KOH ratio 1 : 1, 700°C)

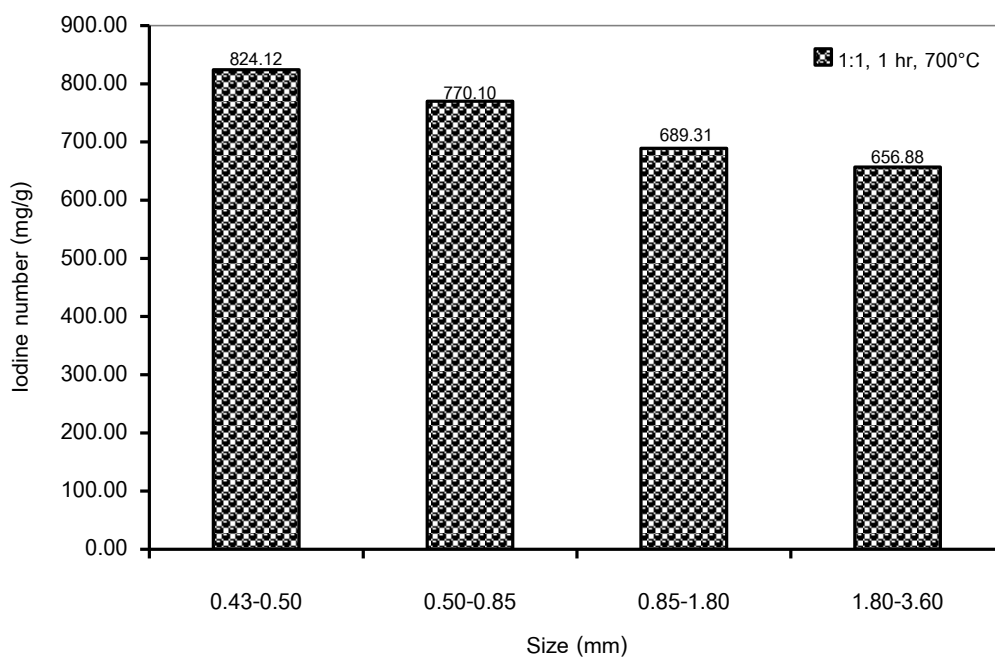


Figure 5.24 Effect of particle size on iodine number (char : KOH ratio 1 : 1, 700°C)

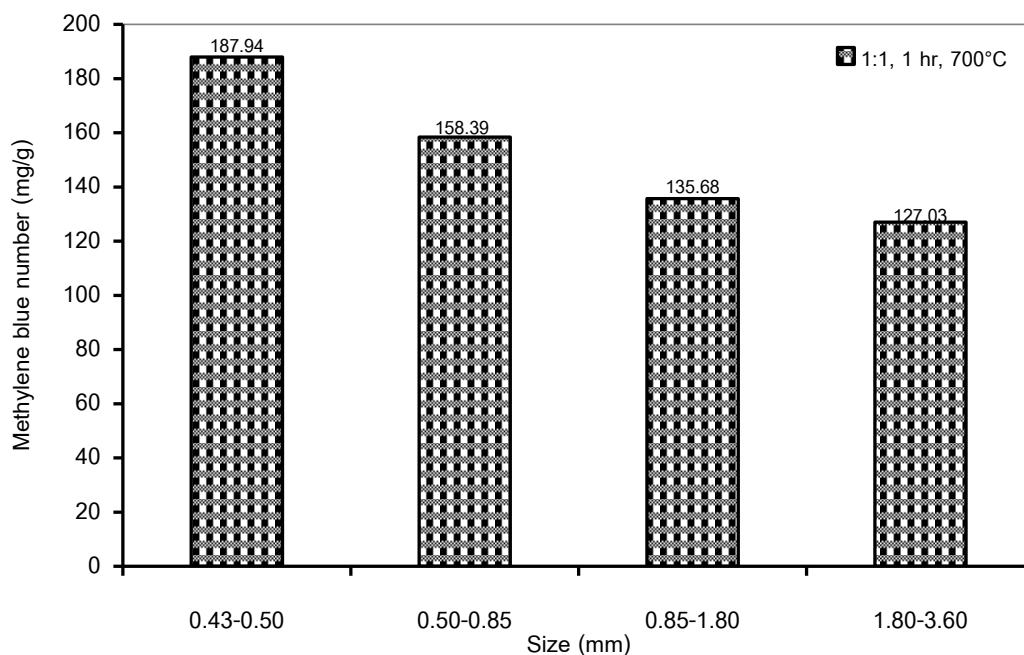


Figure 5.25 Effect of particle size on methylene blue number (char : KOH ratio 1 : 1, 700°C)

The particle size of 0.43-0.50 mm seemed appropriate for flowing of nitrogen gas and caused very well vaporization of potassium hydroxide and diffusion out of volatile matter from the surface of the particle and the bed, so the characteristic of the activated carbon was the best at this size.

The particle size of 1.80-3.60 mm was bigger about two times than the one of the optimum. They arranged themselves by packing loosely and causing big gaps between particles. The nitrogen gas could flow out rapidly without contact all of the particles or sometimes occurring a channeling was observed; low development of porosity causing higher % yield, bulk density but lower iodine number, methylene number and B.E.T. surface area.

From these results, the optimum size of Physic nut waste char for activation was 0.43-0.50 mm. The characteristic of activated carbon from 0.43-0.50 mm char activated with char : KOH of 1 : 1 at 700°C for 1 hour gave the highest iodine number, methylene number and B.E.T. surface area. Its properties were yield of 56.54%, bulk density of 0.16 g/cm³, iodine number of 824.12 mg/g, methylene blue number of 187.94 mg/g, B.E.T. surface area of 767.30 m²/g.

5.3.2.5 The effect type of alkaline solution for activation process

The different reagents as potassium hydroxide and sodium hydroxide were studied to determine the suitable reagent for activation. The mass of ten grams of Physic nut residue char (0.43-0.5 mm) were soaked in different reagent at char : reagent ratio 1 : 1 and then were dried. These samples were used for each batch. The reactor was heated until the temperature in the tube furnace increased and being fixed at the final temperature 700°C. The nitrogen gas was passing up through the tube reactor for 1 hour. The results of this experiment were shown in Table 5.8.

Table 5.8 Effect of alkaline solution (1:1, 1 hour, 700°C, N₂ flow rate 100 mL/min)

Alkaline solution	Y (%)	BD g/cm ³	Ash (%)	MB (mg/g)	IA (mg/g)	B.E.T. m ² /g
KOH	56.54	0.16	2.89	187.94	824.12	767.30
NaOH	61.11	0.19	2.67	117.80	376.43	400.52

The result showed that the iodine number, methylene blue number and B.E.T. surface area of activated carbon with KOH as activating agent were higher than NaOH. It is because NaOH is stronger alkaline than KOH. It could react with char more violent internally and caused larger pores than using KOH. Meanwhile, KOH reacted at surface another resulted in a large number of small pores.

Comparing between NaOH and KOH, the experimental results showed that KOH was more suitable as a reagent for alkaline solution activation. The characteristic of activated carbon gave the highest iodine number and methylene blue number. Properties were at yield of 56.54%, bulk density of 0.16 g/cm³, iodine number of 824.12 mg/g, methylene blue number of 187.94 mg/g, B.E.T. surface area of 767.30 m²/g.

Table 5.9 Comparison of physical activation with chemical activation

Description	Physical activation	Chemical activation	
		By NaOH	By KOH
Raw materials	Physic nut waste	Physic nut waste	Physic nut waste

Pyrolysis condition	800°C, 15 min.	800°C, 15 min.	800°C, 15 min.
Activation	600°C, 60 min.	700°C, 60 min.	700°C, 60 min.
Activating agent	CO ₂	NaOH	KOH
Size of char	0.43-0.50 mm	0.43-0.50 mm	0.43-0.50 mm
% Yield	39.30	61.11	56.54
Iodine number	526.68 mg/g	376.43 mg/g	824.12 mg/g
Methylene blue number	162.09 mg/g	117.80 mg/g	187.94 mg/g
B.E.T. surface area	529.01 m ² /g	400.52 m ² /g	767.30 m ² /g

Table 5.9 showed the comparison properties of activated carbon obtained by physical and chemical activates. % Yield, B.E.T. surface area, iodine number and methylene blue number of activated carbon from CO₂ gas fallen between those activated with NaOH and KOH. In case of using oxidizing gases, it seemed that the gases were too strong oxidizing for the soft material as Physic nut residue, which normally, has lots of cavities inside. Meanwhile as strong alkaline, NaOH caused high reaction inside the char, as a result, the larger pore size appeared in activated carbon which corresponded to the lower iodine number. In case of using KOH, it seemed appropriate for char physic nut waste activation, it gave the high iodine number which corresponded the high B.E.T. surface area.

Generally, the wood surface has a relatively smooth structure with some pores and occasional crevices and also covered with silica agglomeration. However, in this work, the physic nut residue was obtained from an oil-extraction process using a twin screw extruder; thus, there was rupturing of wood tissues in the waste structure. During pyrolysis, the char may be evolved through a liquid phase. The surface showed relatively smooth regions as well as cracked and pitted morphology. The presence of small pores on the surface showed that char was starting to develop an elementary pore network (Figure 5.26 (a)). From parts b–d of Figure 5.26, it can be clearly seen that physical and chemical activation resulted in a porous structure and the opening of pores on the surface of all activated carbon. According to the International Union of Pure and Applied Chemistry (IUPAC), pores on activated carbons are classified by their sizes into three groups: macropores having an average diameter of greater than 50 nm,

mesopores with a diameter of 2–50 nm, and micropores having an average diameter of less than 2 nm. Nitrogen adsorption isotherms of the physic-nutwaste- activated carbons indicated that they were mainly mesopores. The different pore structures of the activated carbon prepared from either physical (using CO_2) or chemical (using KOH and NaOH) activation are observed, which depend upon different reaction mechanisms. Activation with CO_2 at 400°C mainly developed pores of a similar shape and size and evenly distributed throughout the particle. The mesopores seemed to directly expose the surface of the activated carbon. On the contrary, in char activated by KOH and NaOH, pores are irregular, of different shapes and sizes, and the macropores seem to be connected to mesopores, especially for the KOH-activated case. The KOH molecule is smaller than that of NaOH; thus, it diffused faster into the pores of the carbon. Consequently, the reaction with KOH was faster than that with NaOH, aiding in the creation of the porous structure.

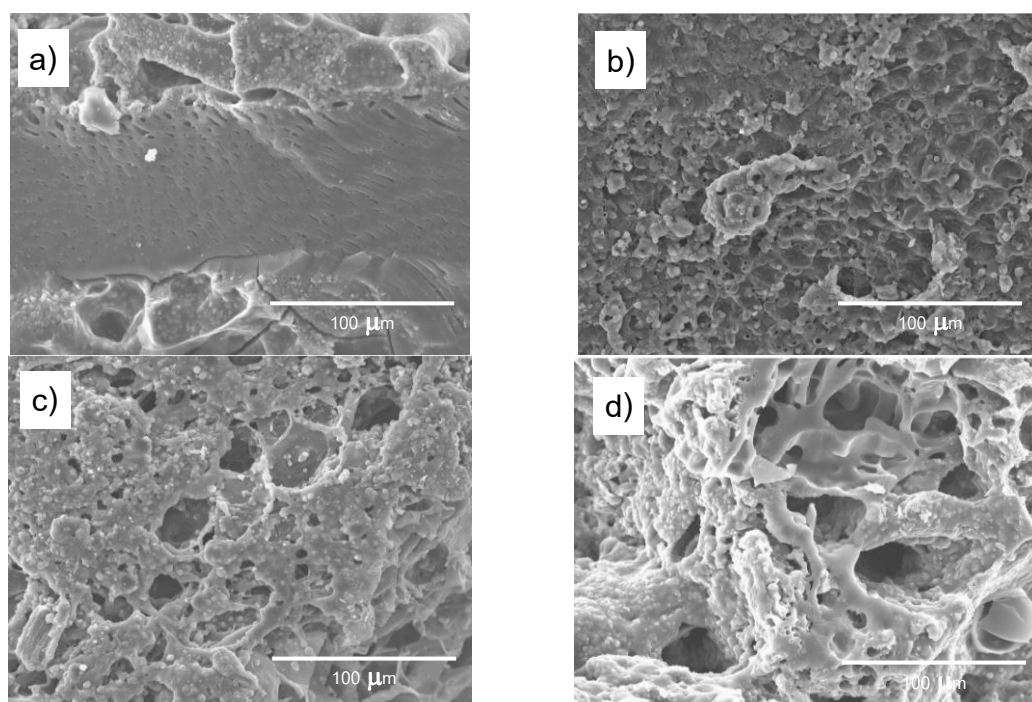


Figure 5.26 The scanning electron micrograph of activated carbon using different activation methods: a) without activation(Char), b) CO_2 activation, c) NaOH activation, and d) KOH activation

The adsorption capacity of activated carbon depends upon porosity as well as the chemical reactivity of functional groups at the surface. This reactivity creates

an imbalance between forces at the surface as compared to those within the body, thus leading to molecular adsorption by the van der Waals force. Knowledge on surface functional groups would give insight to the adsorption capability of the produced activated chars. FTIR spectra were collected for qualitative characterization of surface functional groups of porous carbons activated by both physical and chemical methods. Figure 5.27 shows that the functional groups of activated carbon differ significantly from those of pyrolyzed char. The spectrum from char at 3393 cm^{-1} indicated the presence of the -OH group of phenol. The methylene group is detected by -CH stretching at a wavenumber of 2924 cm^{-1} . The aldehyde group of -O-CH_3 is found around 2853 cm^{-1} . Strong bands at 1641 cm^{-1} indicate C-O stretching of carboxyl or carbonyl groups. Methyl or amine groups are shown by a peak around $1385\text{--}1380\text{ cm}^{-1}$. The band from 1200 to 1000 cm^{-1} is the fingerprint of syringyl units. Aldehyde and derivatives of benzene are detected by peaks at 875 and 761 cm^{-1} . FTIR spectra of char activated by different methods are quite similar. The peak around 2920 cm^{-1} is thought to be of the methylene group. The aldehyde group is also detected by a peak at 2848 cm^{-1} . The band around $1590\text{--}1500\text{ cm}^{-1}$ is assigned to ring vibration in a large aromatic skeleton generally found in carbonaceous material, such as activated carbon. Peaks around $1450\text{--}1320\text{ cm}^{-1}$ are an indication of the presence of pyrones and aromatic groups. For carbon prepared by NaOH activation, the strong bands located around 1010 and 832 cm^{-1} are attributed to asymmetric and symmetric stretching of the Si-O band.

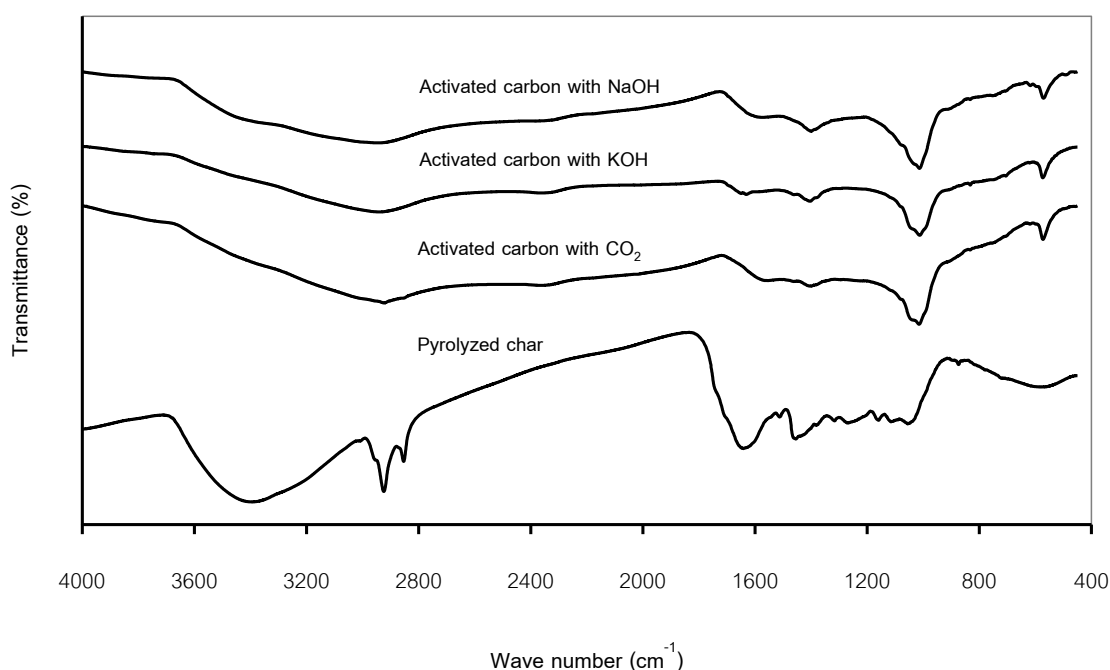


Figure 5.27 FTIR spectra of pyrolyzed char and activated carbons

It is generally accepted that pore structure development is influenced by many factors, including inorganic impurities and the initial structure of the carbon precursor. Therefore, the XRD was obtained for all samples in this study and displayed in Figures 5.28. The appearance of a broad peak centered at the 2θ angle of 28° in the X-ray diffractograms of pyrolyzed char and activated carbon indicated the presence of silica. Diffractograms of carbon activated by KOH, NaOH, as well as CO_2 were quite similar, while the graphitic basal planes at a 2θ angle of 43° could only be seen in the spectrum of pyrolyzed char but not in the activated carbon samples.

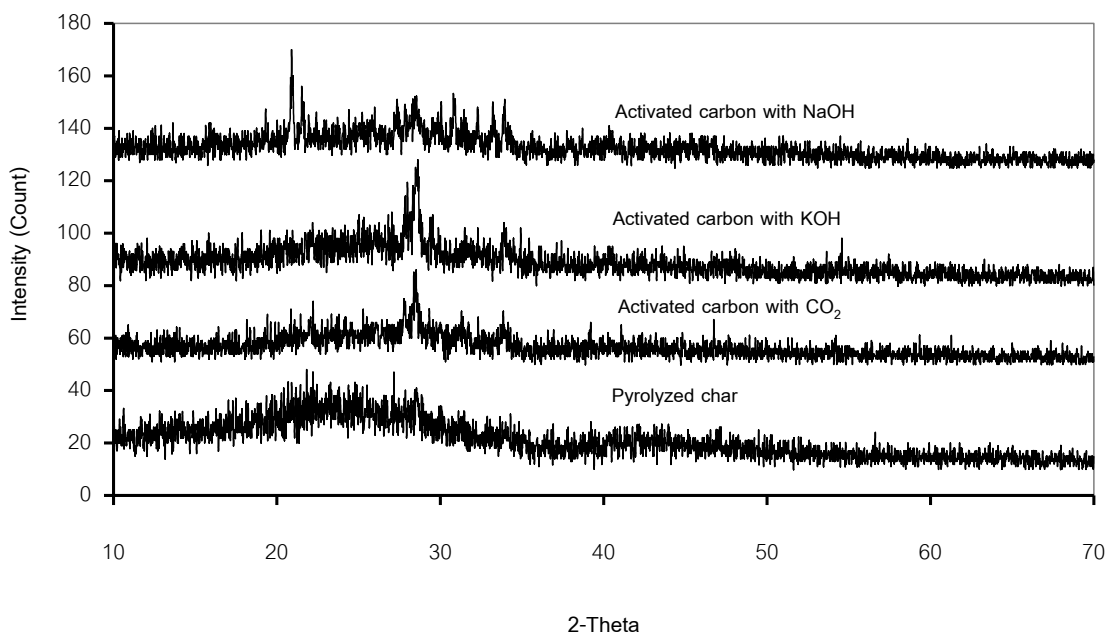


Figure 5.28 X-ray diffraction analysis of pyrolyzed char and activated carbons

5.4 Comparison of this work with other works

The comparison of this work with other works was divided into three cases. The first case is the comparison with R. Zanzi et al. (2001) who used olive waste as raw materials and CO_2 as oxidizing agent. The second case is the comparison with A.P. Carvalho et al. (2003) which used KOH as activating agent but with different raw materials. And last one is the comparison with Yun Su Park et al. (2006), who used

NaOH as activating agent but different raw materials. The characteristics of activated carbon obtained were expressed in Tables 5.10 – 5.12, respectively.

Table 5.10 Comparison of this work with R. Zanzi et al. (2001) (similar activation procedure but different raw materials)

Description	This work	R. Zanzi et al. (2001)
Raw materials	Physic nut waste	Olive waste
Pyrolysis condition	800°C, 15 min.	800°C, 15 min.
Activation	600°C, 60 min.	600°C, 60 min.
Activating agent	CO ₂	CO ₂
Size of char	0.43-0.5 mm	0.43-0.5 mm
% Yield	39.30	25.00
Iodine number	526.68 mg/g	405.00 mg/g
Methylene blue number	162.09 mg/g	137.00 mg/g
B.E.T. surface area	529.01 m ² /g	390.00 m ² /g

R. Zanzi et al. (2001) produced the activated carbon from olive waste by 2 steps : carbonization and activation by using carbon dioxide gas. The optimum condition for activation was at 600°C for 60 min and reported by B.E.T. surface area of 390 m₂/g, iodine number of 405.00 mg/g and methylene blue number 137.00 mg/g. In this work with similar activation processes, the higher iodine number (526.68 mg/g) and methylene blue number (162.09 mg/g) of activated carbon are obtained 600°C for 60 min. This is probably due to different raw material and agent. Higher flow rate of CO₂ used in this work might allow more violent activation process.

Table 5.11 Comparison of this work with A.P. Carvaloho et al. (2003) (same activation agent but different raw materials)

Description	This work	A.P. Carvaloho et al. (2003)
Raw materials	Physic nut waste	Cork waste
Pyrolysis condition	800°C, 15 min.	900°C, 30 min.
Activation	700°C, 60 min.	600°C, 60 min.
Activating agent	KOH	KOH

Char : KOH ratio	1 : 1	1 : 1
Size of char	0.43-0.50 mm	0.40-0.70 mm
% Yield	56.54	51.00
Iodine number	824.12 mg/g	738.00 mg/g
Methylene blue number	187.94 mg/g	189.00 mg/g
B.E.T. surface area	767.30 m ² /g	773.00 m ² /g

A.P. Carvaloho et al. (2003) produced the activated carbon from Cork waste through chemical activation by using KOH as activating agent. It was found that the optimum condition for activation was at 1 : 1 of ratio char : reagent temperature at 600°C for 60 min and particle size < 0.70 mm. The properties of obtained activated carbon was a 51.00 % yield, 738.00 mg/g of iodine number, 189.00 mg/g methylene blue number and 773.00 m²/g B.E.T. surface area. In this work, the activated carbon from Physic nut waste was produced using the same activating agent (KOH). It was found that the optimum condition for activation was at 1 : 1 of ratio char : reagent temperature at 700°C for 60 minutes and particle size range of 0.43-0.5 mm. The properties of obtained activated carbon was in the same ranges with Carvaloho et al. with a little bit higher % yield.

From Table 5.11, it was found that activated carbon obtained in this work gave higher iodine adsorption than that of A.P. Carvaloho et al. while methylene blue number and B.E.T. surface area were quite similar. This is probably because of different scale of porosity. Porosity of activated carbon from of A.P. Carvaloho et al. could be in very small scale (supercapillaries) which allow less amount of iodine to insert. Meanwhile, N₂, which used for measuring B.E.T. surface area, has smaller size thus could diffuse into porosity inside particles much easier. Besides, it could be because of different raw material. In this study, physic nut residue has structure with existing porosity (Figure 5.36). When activated, it would expand the existing porosity or create new porosity in some part (Figure 5.38). Meanwhile, the porosity of activated carbon from coke waste would be new ones rather than expansion of the existing ones.

Table 5.12 Comparison of this work with Yun Su Park et al. (2006) (same activation agent but different raw materials)

Description	This work	Yun Su Park et al. (2006)
Raw materials	Physic nut waste	Walnut shell waste
Pyrolysis condition	800°C, 15 min.	600°C, 120 min.
Activation	700°C, 60 min.	700°C, 120 min.
Activating agent	NaOH	NaOH
Char : NaOH ratio	1 : 1	1 : 2
Size of char	0.43-0.50 mm	0.60-1.18 mm
% Yield	61.11	66.00
Iodine number	376.43 mg/g	N/A
Methylene blue number	117.80 mg/g	N/A
B.E.T. surface area	400.52 m ² /g	603.00 m ² /g

Yun Su Park et al. (2006) prepared the activated carbon from Walnut shell waste, through chemical activation by using NaOH as activating agent. It was found that the optimum condition for activation was at 1 : 2 of ratio char : reagent temperature at 700°C for 120 minutes with char particle size of 0.60-1.18 mm. The properties of obtained activated carbon was a 66.00% yield and 603.00 m²/g B.E.T. surface area.

From Table 5.12, it can be seen that B.E.T. surface area of activated carbon from walnut waste was higher. This is because of different raw materials. Walnut shell waste contains high quantity of fixed carbon and higher density than Physic nut waste. When activated with NaOH, it would create new porosity. Meanwhile using Physic nut waste as raw materials, porosity on surface already existed. When NaOH was used for activation, it would rather expand the pores than developing new ones.

Besides, it was found that this might effect from ratio of char : NaOH used for activation. It is clear that more than 2 times of NaOH was used in Yun Su Park's work. Therefore, it is possible that the higher ratio of NaOH used in activation of Walnut shell waste would result in building more porosity.

CHAPTER VI

SYNTHESIS AND CATALYTIC REFORMING PROPERTIES OF OLIVINE AND Ni/OLIVINE CATALYSTS

6.1 Physical and thermal characteristics of olivine and Ni/olivine catalysts

LiFePO_4 olivine compounds synthesized by co-precipitations appeared visually in yellowish color and moist. The TGA/DTA result of the LiFePO_4 precursor performed at heating rate of $10^\circ\text{C min}^{-1}$ in nitrogen gas at 20 ml min^{-1} flow rate was shown in Figure 6.1. While the broaden endothermic peaks attributed to water evaporation was found at temperatures between 60°C and 160°C , the small endothermic peak at 250°C was caused by organic compound decomposition. Whereas the peak exhibited at 500°C is due to the crystallization of LiFePO_4 . This result corresponded well with the continuous weight loss since ambient temperature to $\sim 550^\circ\text{C}$. The observed initial weight loss before 160°C , the step weight loss between 170°C and 270°C , and the final weight loss from $450\text{-}550^\circ\text{C}$ corresponded to the elimination of absorbed water, decomposition of organic compounds, and crystallization of phosphate, respectively. From these results, it suggests that the precursor should be calcined at higher temperature than 550°C to obtained LiFePO_4 crystallized phase.

The olivine calcined at various temperatures appeared in different color (Figure 6.2). The yellowish color of olivine calcined at 500°C was quite similar to the fresh olivine. At higher calcination temperatures, the powders turned into gray, purple, and finally black at calcination temperature of 1000°C where the powder sample also melted.

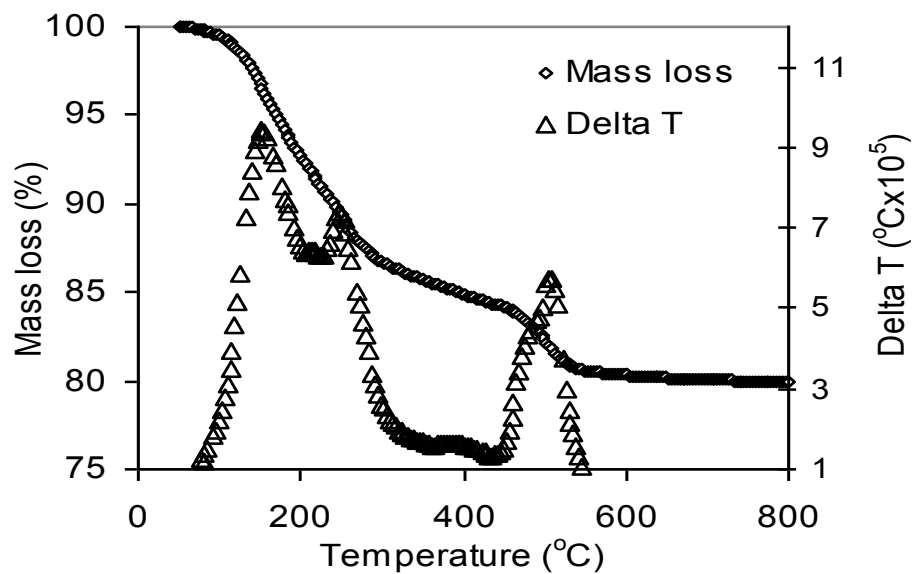


Figure 6.1 TGA and DTG curves for the LiFePO_4 olivine

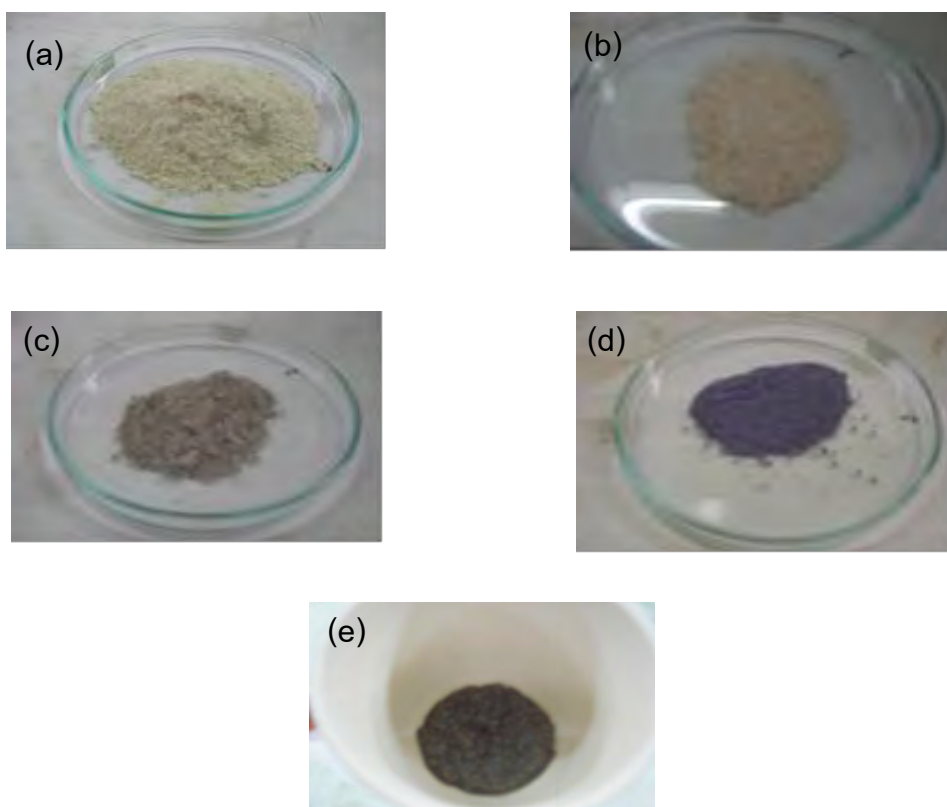


Figure 6.2 The photograph of the (a) fresh LiFePO_4 , (b) LiFePO_4 calcined at 500°C , (c) LiFePO_4 calcined at 700°C , and (d) LiFePO_4 calcined at 900°C

6.2 Phase analysis

The olivine calcined at various temperatures appeared in different color. The yellowish color of olivine calcined at 500°C was quite similar to the fresh olivine. At higher calcination temperatures, the powders turned into gray, purple, and finally black at calcination temperature of 1000°C where the powder sample was melted. This indicated the phase transformation of olivine with heat treatment which was agreed well with the results from the XRD analysis showed in Figure 6.3.

It was found that olivine phase did not formed in the sample heat-treated at 500°C as expected, which is in consistent with TGA/DTG results showed in Figure 6.3. As the calcination temperature increased, the diffraction peaks corresponding to the olivine structure emerged which indexed on an orthorhombic olivine structure type (space group: Pmnb). No second phase is found. For sample calcined at 900°C, all diffraction lines attributed to the LiFePO_4 olivine phase become prominent, an enhanced degree of crystallinity have been realized, which are evident from the sharp diffractograms of increased intensity. However, a minor impurity phases were also detected which might be because a higher sintering temperature accelerated the crystal phase transformation process, thus miscellaneous reaction might occur. XRD of the Ni/LiFePO₄ catalyst calcined at 800°C, with a support calcined at 700°C, shows that the olivine phase is maintained along with trace amount of phases related to Ni (Ni, NiO, Ni(OH)₂, Ni(NO₃)₂·6H₂O). It was thought that the nickel containing particles decreased in size or more probably their insertion into the olivine structure. As expected, after reduction process, signals of NiO and other intermediate phases related to Ni became less pronounced while intensity lines of Ni phase were amplified.

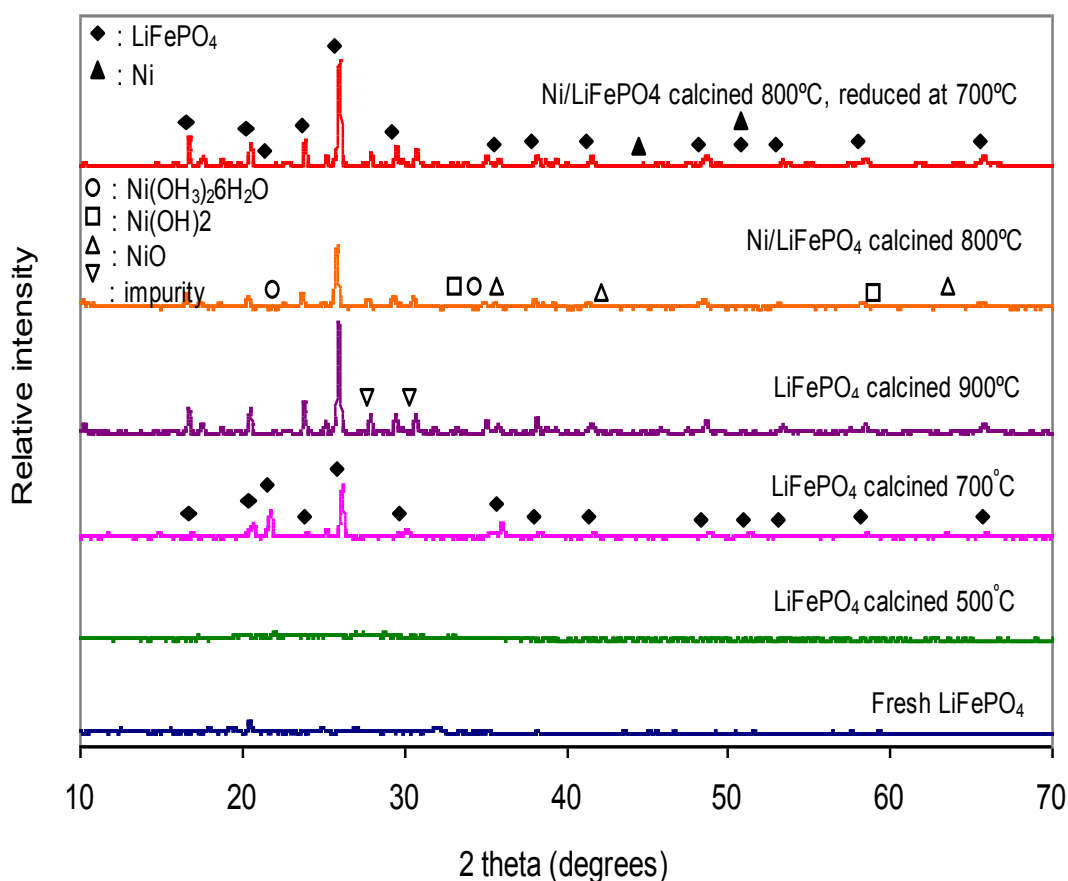


Figure 6.3 XRD patterns of fresh LiFePO_4 , LiFePO_4 calcined at 500, 700, and 900°C, Ni/LiFePO_4 calcined at 800°C (with LiFePO_4 calcined at 700°C) and Ni/LiFePO_4 calcined at 800°C and reduced at 700°C (with LiFePO_4 support calcined at 700°C)

6.3 Microstructure analysis

The SEM of the fresh olivine shows porosity of this material (Figure 6.4). Due to hygroscopic in nature, soft agglomeration of 96 μm in size was form with BET surface area of 1.94 m^2g^{-1} (Table 6.1). The particle size of calcined LiFePO_4 is bimodal where the popular peak around smaller particle size is about 56.16, 20.37, and 58.22 μm for samples calcined at 500, 700 and 900°C, respectively. The BET surface of the LiFePO_4 calcined at 500, 700 and 900°C, were 3.11, 5.28 and 2.09 m^2g^{-1} . The enhancement of the BET surface may attribute to the decrease of particle size after calcinations, and the obvious improvement of the total surface area of LiFePO_4 calcined at 700°C could be

ascribed to the formation of porous structure in LiFePO_4 material itself. After calcination at 900°C , the porosity observed on fresh olivine disappears, more compact grains are formed as evidenced by a larger particle size ($58.22\ \mu\text{m}$) and lower surface area ($2.09\ \text{m}^2\text{g}^{-1}$).

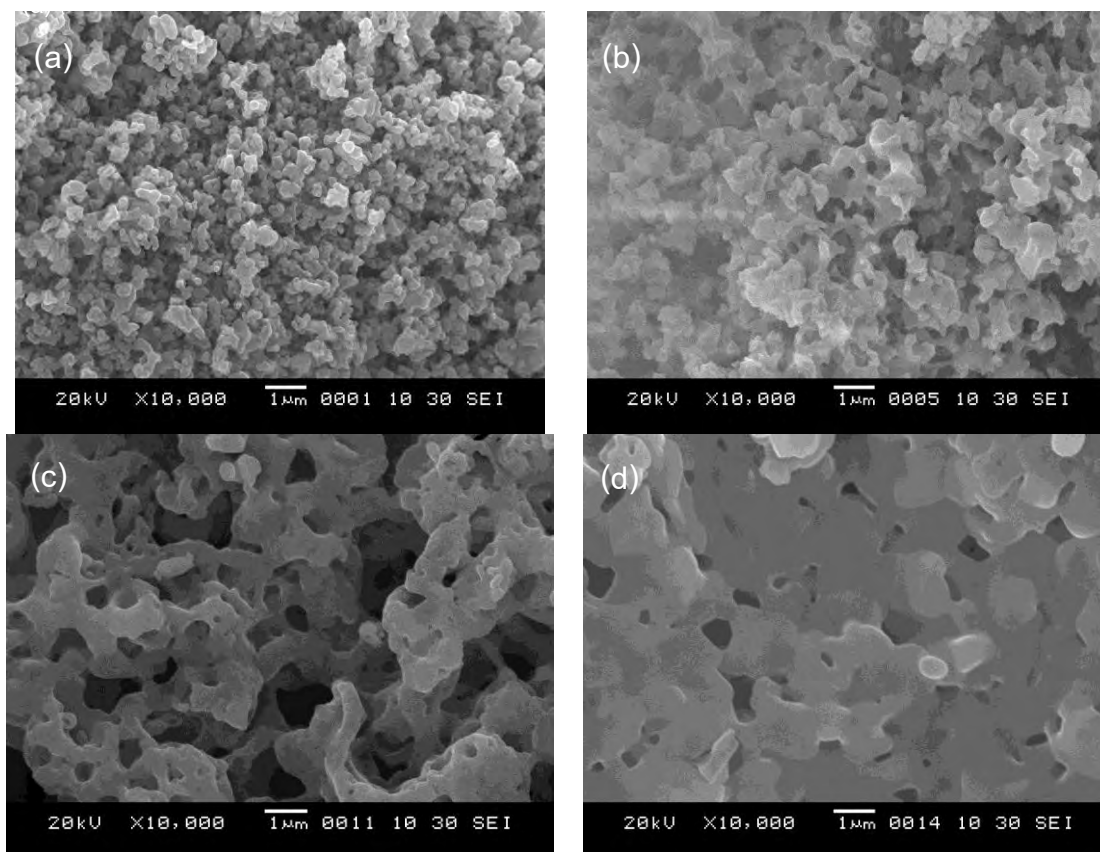


Figure 6.4 SEM photographs of (a) Fresh LiFePO_4 /olivine and LiFePO_4 calcined at (b) 500°C , (c) 700°C and (d) 900°C

On the SEM of the Ni/olivine catalyst calcined at 800°C (Figure 6.5), a deposit of individual and cluster of grains (probably NiO) with size between $1\text{-}5\ \mu\text{m}$ can be observed. Ni/olivine catalyst showed grain growth of LiFePO_4 compared to before impregnation with nickel salt, which was due to the second heat treatment at 800°C after impregnation. Calcination at 800°C of Ni/olivine catalyst with support calcined at 900°C (not shown) led to the formation of a very smooth surface of the support with a less deposition and insertion of Ni crystallites into the olivine structure.

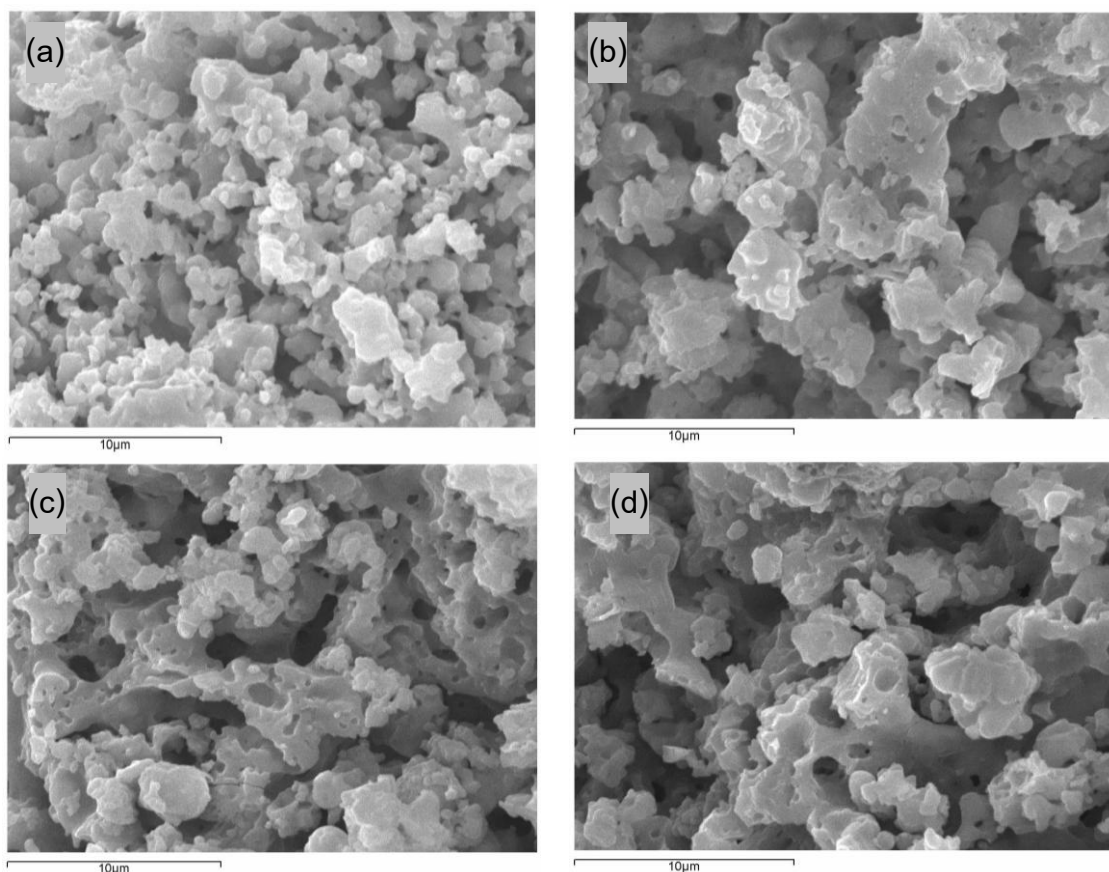


Figure 6.5 SEM photographs of Ni/LiFePO₄ (with LiFePO₄ support calcined at 700°C) (a) calcined at 800°C before reduction, (b) after reduction at 600°C, (c) at 700°C, (d) at 800°C

This confirmed by EDX analysis. The elements of catalysts with olivine support calcined at 700°C contained 8.12% Ni, 41.98% P, and 49.12%Fe. Whereas, the one with support calcined at 900°C had lower amount of nickel, 5.39%. Smooth surface with a smaller surface area structure might cause a lower degree of Ni deposition. The reduction of Ni/Olivine powders was then performed on only catalyst with support calcined at 700°C (sample 7). The reduction at 600-800°C was successful in which catalyst reduced at 700°C (sample 10) had the highest surface area and nickel content, while one reduced at 900°C was melted down to the crucible.

Table 6.1 Particle size, BET surface area, and element of olivine and Ni/olivine catalysts

Formulation code	BET (m ² g ⁻¹)	Particle size distribution			EDX analysis		
		D10	D50	D90	(%Ni)	(% P)	(%Fe)
[1] LFP	1.94	10.21	96.26	455.59	-	44.34	53.51
[2] LFP-500	3.11	7.85	56.16	217.94	-	40.36	55.78
[3] LFP-700	5.28	6.39	20.37	64.31	-	39.23	58.08
[4] LFP-900	2.09	8.66	58.22	236.18	-	38.88	58.06
[5] LFP-1000	n/a	n/a	n/a	n/a	n/a	n/a	n/a
[6] LFP-500-Ni-800	2.28	8.11	159.26	753.77	6.35	44.45	48.33
[7] LFP-700-Ni-800	4.06	11.08	84.58	340.44	8.12	41.98	49.12
[8] LFP-900-Ni-800	1.13	27.69	298.55	803.99	5.39	39.87	51.21
[9] LFP-700-Ni-800-600R	5.64	1.61	8.18	22.63	7.93	40.15	43.68
[10] LFP-700-Ni-800-700R	6.63	1.65	9.44	27.85	8.08	42.23	48.77
[11] LFP-700-Ni-800-800R	6.49	1.49	7.39	20.95	7.49	38.60	42.19
[12] LFP-700-Ni-800-900R	n/a	n/a	n/a	n/a	n/a	n/a	n/a

LFP = LiFePO₄, n/a = powders were melt

LFP-X-Ni-Y-ZR = LiFePO₄- calcination temp. of olivine – Ni impregnation – calcination temperature of Ni/olivine – reduction temp of Ni/olivine

6.4 Catalytic steam reforming of glycerol using olivine and Ni/olivine catalysts

From synthesis results, the Ni/olivine calcined at 800°C and then reduced at 700°C with the olivine support calcined at 700°C (LFP-700-Ni-800-700R) was chosen for further test. The catalytic activity was compared with those obtained from olivine calcined at 700°C (LFP-700) and thermal reforming (without catalyst). Due to residual moisture of 13.6 wt% in glycerol feed, these reactions were carried out as steam reforming processes without addition of water. Overall product distributions as well as carbon and hydrogen conversions are displayed in Figure 6.6.

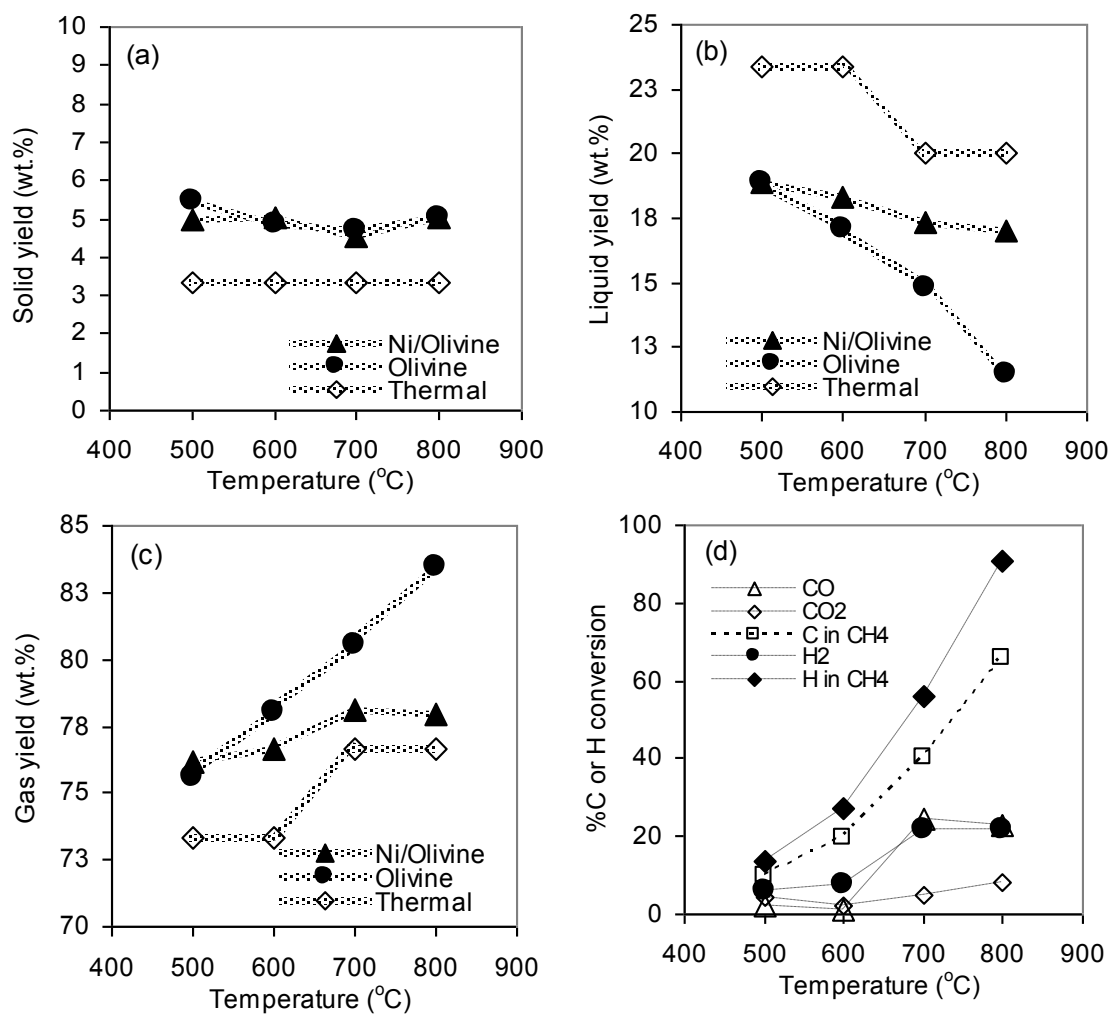
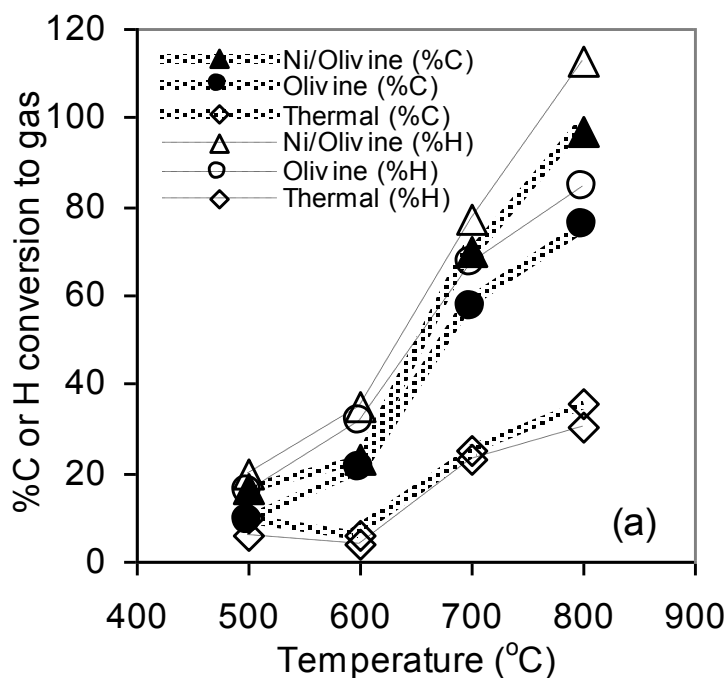


Figure 6.6 (a) Solid, (b) liquid, (c) gas yield from catalytic reforming of glycerol waste, and (d) gas produced using Ni/Olivine catalyst (LFP-700-Ni-800-700R)

Solid yields from reforming reaction were relatively low (under 6.0 wt% at any operating conditions, Figure 6.6 (a)) because boiling point of glycerol is fairly low and would evaporate as soon as entering into hot reaction zone resulted in domination of homogeneous gas phase reactions which favor product gas formation. Reaction temperature showed little effect on solid yields. Almost constant solid yields from blank (thermal) runs were probably mainly alkali salts from feed material. Increase in solid yields from catalytic tests was most likely from carbon deposit which also implied activity of prepared catalysts on reforming process. Invariable increase in solid yields when compared with blank runs at any temperature suggests carbon loading capacity of active metal sites on catalyst surface may be reached. Lower liquid yields resulted in higher gas yields as seen in Figure 6.6 (b-c). Gas is major product from this reforming process accounting more than 73.0 wt% at any trials though thermal reforming alone

was also responsible for rather high gas formation and olivine appeared to have greater effect on enhancing gas production than Ni/Olivine catalyst. As expected, major gas species were found to be CO, CO₂, C_xH_y (as CH₄), and H₂, Figure 6.6 (d).

Using catalysts resulted in superior selectivity of preferred gas species (CO and H₂) as shown in Figure 6.7. Greater amount of carbon and hydrogen in waste glycerol were converted to CO, CO₂, C_xH_y (as CH₄), and H₂ with addition of olivine or Ni/olivine especially at higher temperature. At 800°C, using Ni/Olivine would result in conversion of most carbon and hydrogen in raw material to these gases while only around 35% were measured for thermal runs. From Figure 6.7 (b), enhancement of CO and H₂ production was significant with addition of olivine or Ni/olivine, these two gases are collectively called syn-gas which may be further utilized as important reactants for production of several high valued fuel or chemical feedstock.



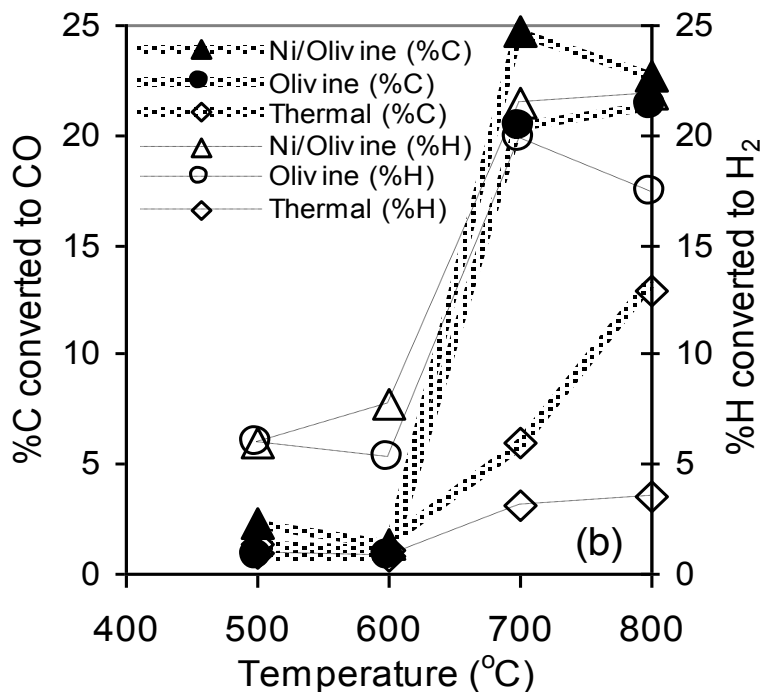


Figure 6.7 Conversion to gas products from catalytic and thermal reforming of glycerol waste: a) total conversion and b) conversion to CO or H₂

Lower heating value (LHV) and H₂ to CO ratio of produced gas are good indicators of product quality. LHV of product gas increased with temperature (Figure 6.8(a)) to maximum value of 4.65 MJ/m³ for run with Ni/olivine at 800°C while thermal reforming yielded gas with only 2.07 MJ/m³ heat content. Data on H₂ to CO ratio are fluctuated at low temperature for olivine and Ni/olivine experiments which probably due to low gas yields at those conditions where small measurement error may result in unexpected low or high ratio. When more gas was formed at higher temperature, the ratio were around 0.4 to 1.4 with higher values for runs with olivine or Ni/olivine. Since H₂/CO ratio of 1.0 is enough for methanol synthesis, using prepared olivine or Ni/olivine as steam reforming of waste glycerol at 700 or 800°C would not required additional process for H₂ enrichment.

Effect of the amount of olivine or Ni/olivine addition was shown in Figure 6.9 for experiments at 600°C. Higher amount of catalytic materials resulted in grater gas production and LHV up to 0.75 g of catalyst (for Ni/olivine). This is probably due to limitation on kinetic of reforming reactions at this relatively low temperature which

differed from runs at higher temperature (greater reaction rates) where almost complete conversion may be attained at any quantity of catalysts. Further work with longer residence time should be made in order to confirm this case.

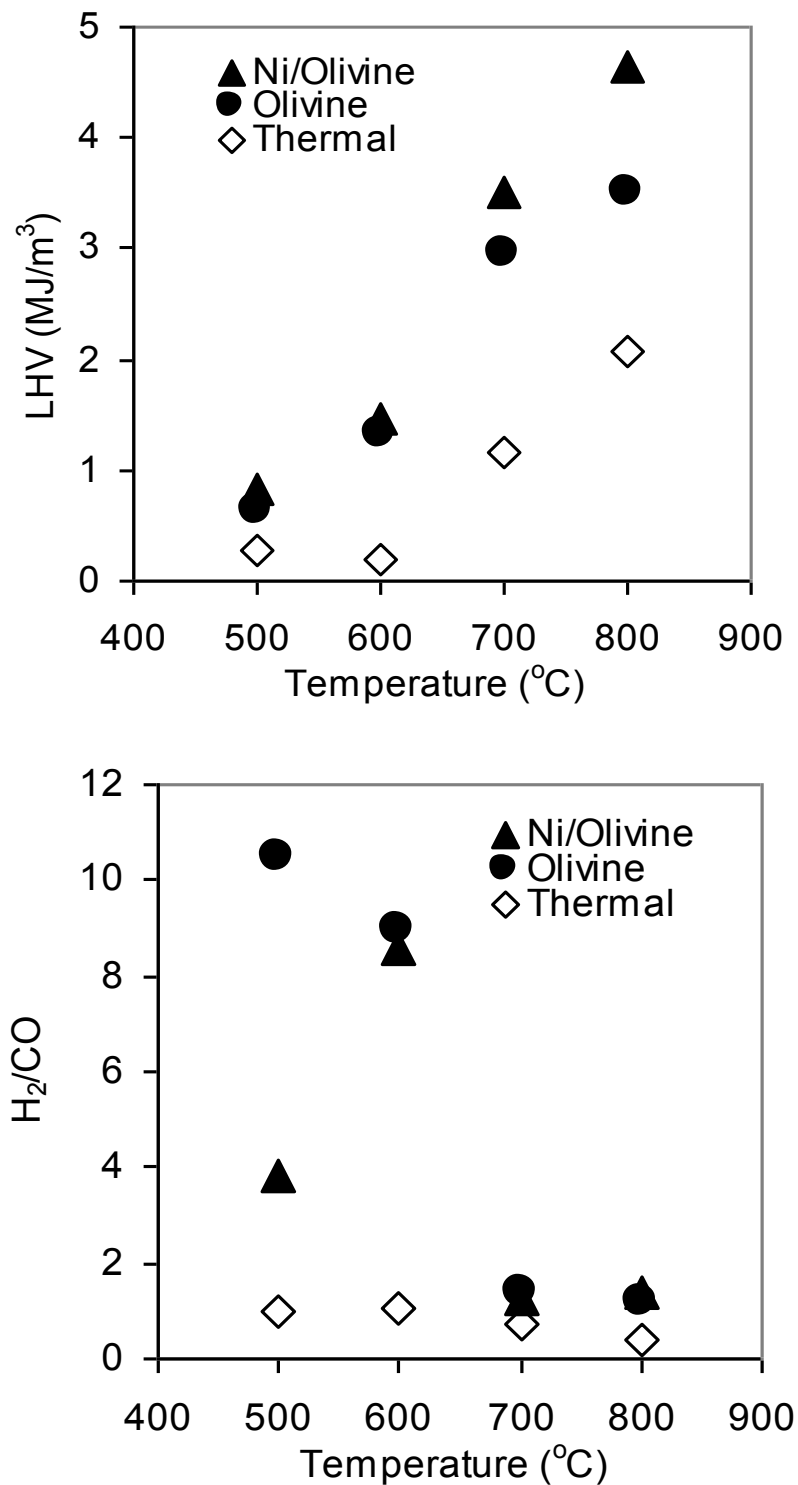


Figure 6.8 Quality of product gas: (a) lower heating value (LHV) and (b) H₂/CO

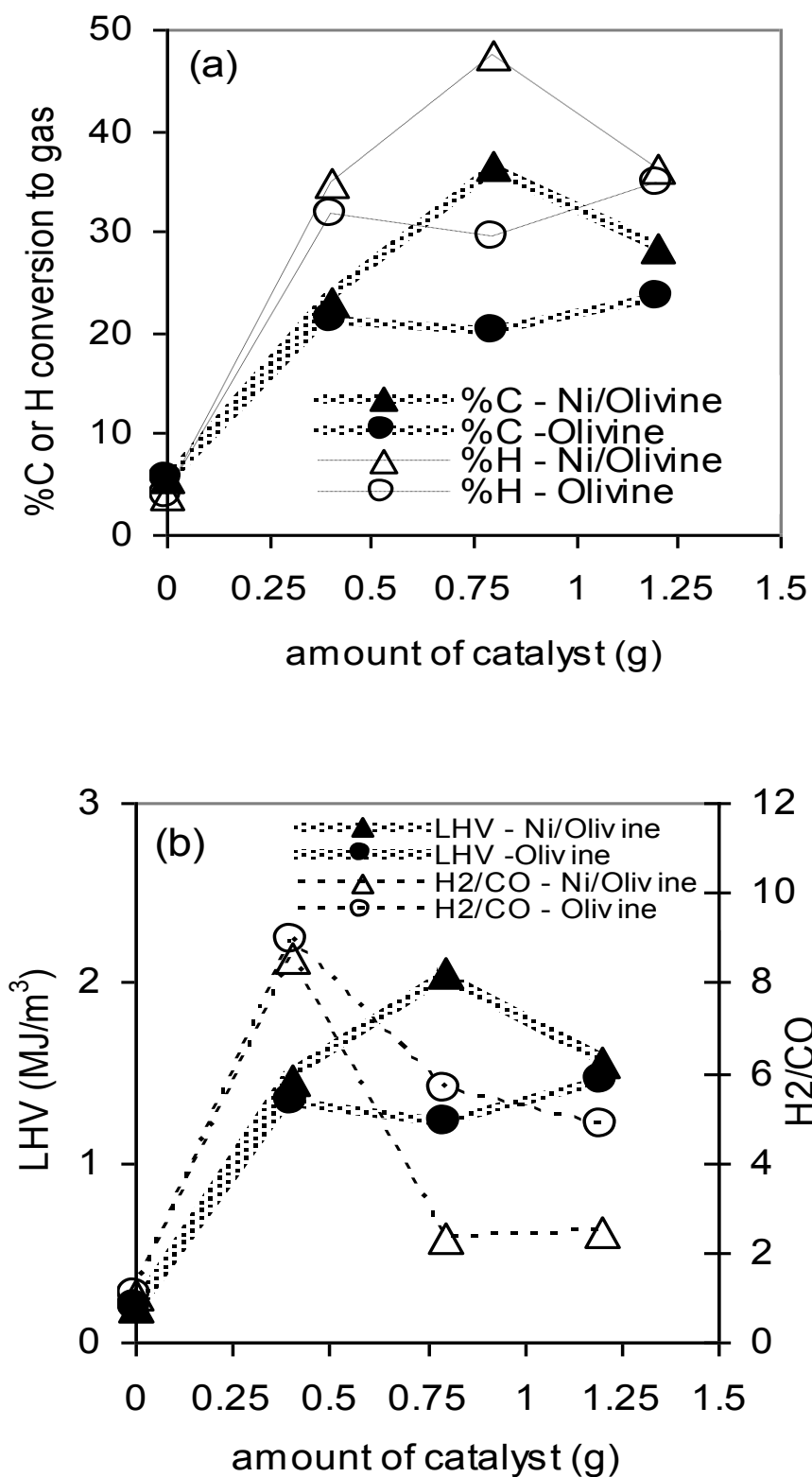


Figure 6.9 Effect of catalyst content on (a) conversion to gas and (b) LHV and H₂/CO of product gas from catalytic reforming of glycerol waste at 600°C

Table 6.2 is summary of results from several runs at various temperatures. Almost 46% and 60% cold gas efficiencies may be achieved at 800°C using olivine and Ni/olivine catalysts, respectively while thermal conversion generated around 11% at similar condition.

Table 6.2 Effect of reaction temperature and type of catalysts on product distribution and gas characteristics

Catalyst	Ni/olivine ¹				Olivine ²				w/o catalyst (Thermal)			
	500	600	700	800	500	600	700	800	500	600	700	800
Temperature (°C)												
Solid (wt.%)	4.96	5.00	4.51	5.04	5.47	4.84	4.68	5.04	3.33	3.25	3.39	3.27
Liquid (wt.%)	18.85	18.33	17.37	17.02	18.92	17.11	14.80	11.50	23.33	22.80	19.84	19.95
Gas ³ (wt.%)	76.19	76.67	78.12	77.94	75.60	78.05	80.53	83.46	73.34	73.95	76.77	76.78
LHV (MJ/m ³)	0.83	1.45	3.50	4.65	0.62	1.34	2.95	3.52	0.28	0.20	1.16	2.07
H ₂ /CO	3.81	8.56	1.26	1.40	10.50	8.96	1.41	1.19	1.00	1.05	0.75	0.40
C conversion to gas (wt. %)	16.40	22.93	69.77	97.04	9.06	21.27	57.37	75.74	9.64	5.69	24.90	35.32
H conversion to gas (wt. %)	19.81	34.70	77.26	112.90	15.94	31.72	67.02	84.51	6.19	3.80	23.30	30.16
Cold gas efficiency, η_{gas} (%)	8.74	14.88	38.80	59.50	6.50	14.12	33.84	45.82	3.17	1.71	11.20	10.73
Gas yield ⁴ , Y_{gas} (Nm ³ /kg)	1.91	1.86	2.01	2.32	1.90	1.91	2.08	2.36	2.05	1.55	1.75	0.94

¹LFP-700-Ni-800-700R, ²LEF-700, ³by difference, ⁴Exclude nitrogen

In general, addition of olivine or Ni/olivine significantly improves both quality and quantity of product gases as noticed from better gas yield, LHV, H₂/CO ratio, and, cold gas efficiency with greatest enhancement attained with nickel catalyst. In real practice, from economic point of view, olivine without nickel may be sufficient for effective reforming of waste glycerol due to high cost of nickel and its vulnerability on various metal poisoning substances.

CHAPTER VII

CONCLUSIONS

The feasibility of producing fuel products from pyrolysis of physic nut (*Jatropha curcas* Linn.) waste was demonstrated. The objective in this research is divided into three parts. The first experiment was undertaken to pyrolyze Physic nut waste in a fixed bed reactor to fuel products; solid char, liquid bio-oil, and producer gas. Then the activated carbons from pyrolyzed physic nut waste char were produced via with physical and chemical activations. Finally, the catalytic performance of synthesized olivine and Ni/olivine catalysts were investigated over glycerol waste as long chain hydrocarbons to evaluate the possibility of upgrading products to more quality fuels.

From the first part of experiment, pyrolysis of physic nut waste were investigated in fixed-bed tubular reactor. Particularly, the influences of final pyrolysis temperature (500, 700 and 900°C), retention time (15 min, 30 min and 60 min), and mode of heating (slow and rapid) on product yields were studied. An in-depth analysis of the properties of the solid and liquid products generated at different pyrolysis conditions was performed for a better understanding of the mechanism of physic nut waste pyrolysis and to determine its possibility of being a potential source of renewable fuel and chemical feedstock. The results showed that solid, liquid, and gas products were in the ranges of 26.94-29.04, 9.43-21.36, 51.70-61.54 wt% for slow pyrolysis, while those attained from rapid condition were 11.16-15.25, 15.00-23.43, and 61.32-73.84 wt%, respectively. Rapid pyrolysis resulted in greater changes on product yields at different temperature. Char yields were much higher from slow pyrolysis. The effect of hold time was insignificant on char yields which suggested key rapid primary reactions started around 400-500°C on the overall thermal conversion operation. B.E.T. surface areas increased progressively with increased pyrolysis temperature and exposure time. Char obtained from rapid pyrolysis condition had lower surface area and pore volume than ones attained from slow pyrolysis. The maximum liquid product of 21.35% was observed at the pyrolysis temperature of 900°C for 60 min under dynamic heating and 61.54% under isothermal heating at 500°C. Liquid yields increased with temperature for slow

pyrolysis while continuous drop on liquid product was obtained from rapid runs. Functional groups of liquids from any processes are quite similar. The liquid product mainly consisted of several fatty acids such as oleic acid, palmitic acid and lignoleic acid in the range of 15-19%, 40-45%, and 25-34%, respectively. Carbon chain length of liquid product from pyrolysis of physic nut waste is within the range of gas oil. Gas is major product from pyrolysis of physic nut with yields greater than 50 wt% at any operating conditions. Most of gas was formed within 15 minutes with CO₂, CO, CH₄, and H₂ as major gas species. Mode of heating displayed significant effect to the product distribution, LHV and H₂/CO ratio. Mole ratio of H₂/CO close to unity was found in the case of pyrolysis at 900°C for both slow and rapid trials. The LHV obtained from slow processes were 7.8-15.0 MJ/Nm³ while those from rapid runs were 14.8-17.2 MJ/Nm³. LHV of gases from any runs were relatively high indicating their suitable for power production without need for additional fuels though cold gas efficiencies were relatively low which is typical for pyrolysis process.

The suitable pyrolysis condition was 800°C for 15 minutes with 90.01% fixed carbon, 24.23% yield, 4.34% volatile matter and 4.87% ash. The activation step was derived in two methods; physical activation by carbon dioxide gas and chemical activation by alkaline solution (potassium hydroxide and sodium hydroxide). Studied variables in this research were activation temperature, activation time and particle size of Physic nut waste char and also the ratio of char : alkaline solution.

From the results of the second part of experiment, carbon contents of activated materials were 80.4–90.3%, depending upon the activation method, and notably higher than preactivated char. It was found that the activated carbon prepared by physical activation of the pyrolyzed physic nut residue at 600°C for 60 minutes displayed best combination of yield (39.30%), bulk density of 0.21 g/cm³, ash of 9.35%, iodine number of 526.68 mg/g and methylene blue number of 162.09 mg/g. Whereas the suitable condition for chemical activation using both KOH and NaOH as activating agent were achieved from physic nut waste with particle size range of 0.43-0.5 mm activated with a ratio of activating agent/char equal to 1.0, and carbonized at 700°C for 60 minutes. Porous carbon activated by KOH has highest iodine number of 824.72 mg/g, methylene blue number of 187.94 mg/g and B.E.T. surface area of 767.30 m²/g. The properties of

porous carbon activated by NaOH showed inferior properties with iodine number of 376.43 mg/g, methylene blue number of 117.80 mg/g and B.E.T. surface of 400.52 m²/g area.

The final part of this work was to study the synthesis of olivine catalyst by a co-precipitation method and its evolution with calcinations temperature. Olivine is an interesting support for nickel, giving a system with high attrition resistance and strong linking with nickel, therefore the nickel/olivine catalyst was then synthesized via impregnation method. These two catalysts were later used for *in-situ* steam reforming of waste glycerol to investigate their efficiencies on this thermal conversion process for production of quality syn-gas and syn-fuel.

The Ni/LiFePO₄ powders were successfully synthesized by a co-precipitation and wet impregnation methods. LiFePO₄ olivine was obtained via co-precipitation of Li₃PO₄, phosphoric acid and ferric citrate n-hydrate. Calcination of olivine with Ar for 24 hours at 700°C resulted in a single-phase and well-crystallized olivine. Lower calcination temperature of 500°C did not yield crystallized olivine; while higher calcination temperature of 900°C led to smooth support surface with lower surface area. After impregnation and calcination at 800°C, nickel compounds were formed on the Ni/LiFePO₄ catalyst surface as high as 8 wt% for one with an olivine support calcined at 700°C. After reductions at 600-900°C, Ni/LiFePO₄ catalyst calcined at 800°C and then reduced at 700°C with the olivine support calcined at 700°C (LFP-700-Ni-800-700R) had the highest surface area and nickel content, thus was chosen for further catalytic activity test. Ni/olivine displayed excellent *in-situ* gasification/reforming capability when tested with glycerol waste. Complete conversion of carbon and hydrogen in waste material to product gas, high LHV, good cold gas efficiency as well as superior selectivity of preferred gas species (CO and H₂) with acceptable H₂/CO ratio may be achieved with this prepared catalyst at 800°C. Nevertheless, olivine alone which exhibited acceptable reforming ability may be adequate due to high cost of nickel and its susceptibility on various metal poisoning substances.

Based on the results of this study, pyrolysis appears to be a practical process to produce renewable fuel and chemical feedstock from physic nut waste.

REFERENCES

- [1.] Peter, Q., Harrie, K., Hubert, S. Energy from Biomass, World bank technical paper 422 (March 1999): 2-10.
- [2.] Daniel, M.K., George, F., Jun-ichiro, H., Chun-Zhu, L. Volatilisation of alkali and alkaline earth metallic species during the pyrolysis of biomass: differences between sugar cane bagasse and cane tash. Bioresource Technology 96 (2005): 1570-1577.
- [3.] Tsai, W.T., Chen, H.P., Hsieh, M.F., Sun, H.F., Chien, S.F. Regeneration of bleaching earth by pyrolysis in a rotary furnace. Journal of Analytical and Applied Pyrolysis 63 (2002): 157-170.
- [4.] Babu, B.V., Sheth Pratik, N. Modeling and simulation of reduction zone of downdraft biomass gasifier: Effect of char reactivity factor. Energy Conversion & Management 47 (2006): 2602-2611.
- [5.] Khiari, B., Marias, F., Zagrouba, F., Vaxelaire, J. Use of a transient model to simulate fluidized bed incineration of sewage sludge. Journal of Hazardous Materials B135 (2006): 200-209.
- [6.] Aik, C.L., Jia, G. Preparation and characterization of chars from oil palm waste. Carbon 36 (1998): 1663-1670.
- [7.] Fang, H., Weiming, Y., Xueyuan, B. Investigation on caloric requirement of biomass pyrolysis using TG-DSC analyzer. Energy Conversion and Management 47 (2006): 2461-2469.
- [8.] Certin, E., Gupta, R., Moghtaderi, B. Effect of pyrolysis pressure and heating rate on radiata pine char structure and apparent gasification reactivity. Fuel 84 (2005): 1328-1334.
- [9.] Mermoud, F., Salvador, S., Van de Steene, Golfier, F. Influence of the pyrolysis heating rate on the stern gasification rate of large wood char particles. Fuel 85 (2006): 1473-1482.

- [10.] Certin, E., Moghtaderi, B., Gupta, R., Wall T.F. Influence of pyrolysis conditions on the structure and gasification reactivity of biomass chars. Fuel 83 (2004): 2139-2150.
- [11.] Guerrero, M., Ruiz, M.P., Alzueta, M.U., Bilbao, R., Millera, A. Pyrolysis of eucalyptus at different heating rates: studies of char characterization and oxidative reactivity. J. Anal. Appl. Pyrolysis 74 (2005): 307-314.
- [12.] Gerhartz, H., Yamamoto, Y.S., Campbell, F.T. Activated carbon. Ullmann's Encyclopedia of Industrial Chemistry A5 (1996): 124-140.
- [13.] Marit, J., Frank, D. Activated carbon from yellow poplar and white oak by H_3PO_4 activation. Carbon 36 (1998): 1085-1097.
- [14.] Senthilkumar, S., Kalaamani, P., Porkodi, K., Varadajan, P.R., Subburaam, C.V. Adsorption of dissolved reactive red dye from aqueous phase onto activated carbon prepared from agricultural waste. Bioresource Technology 97 (2006): 1618-1625.
- [15.] Jaguaribe, E.F., Medeiros, L.L., Barreto, M.C.S., Araujo, L.P. The performance of activated carbons from sugarcane bagasse, babassu, and coconut shells in removing residual chlorine. Brazilian Journal of Chemical Engineering 22 (2005): 41-47.
- [16.] Onur, Y., Cem, K.I., Mithat, Y., Mehmet, S., Jale, Y. Conversion of leather wastes to useful products. Resources, Conservation and Recycling 49 (2007): 436-448.
- [17.] Alejandro, A., Natalia, M., Nestor, T., Hugo, S., Cristina, D. Activated carbon briquettes from biomass materials. Bioresource Technolgy 98 (2007): 1635-1641.
- [18.] Bruce, C.G., and James, R.K. Chemistry of Catalytic Processes. New York: McGraw-Hill, 1979.
- [19.] Jan, F., Jesper, A., Ulrik, H., and Benny, G. " Formation, Decomposition and Cracking of Biomass Tars in Gasification", DTU, MEK-ET-2005-05, April 2005, ISBN 87-7475-326-6.

- [20.] Bonelli, P.R., Della, R.P.A., Cerrella, E.G., Cukierman, A.L. Effect of pyrolysis temperature on composition, surface properties and thermal degradation rates of Brazil Nut shells. Bioresource Technology 76 (2001): 15-22.
- [21.] Savgi, S., Ilknur, D., Hasan, F.G. Olive bagasse(*Olea europea L.*) pyrolysis. Bioresource Technology 97 (2006): 429-436.
- [22.] Haipig, Y., Rong, Y., Hanping, C., Dong Ho, L., David Tee, L. and Chuguang, Z. Mechanism of Palm oil waste pyrolysis in a Packed Bed. Energy & Fuels 20 (2006): 1321-1328.
- [23.] Li-yeh, H., Hsisheng, T. Influence of different chemical reagents on the preparation of activated carbons from bituminous coal. Fuel Processing Technology 64 (2000): 155-166.
- [24.] Budinova, T., Ekinci, E., Yardim, F., Grimm, A., Bjornborn, E., Minkova, V., Goranova, M. Characterization and application of activated carbon produced by H₃PO₄ and water vapor activation. Fuel Processing Technology 87 (2006): 899-905.
- [25.] Eduard, E.I., Marcelo, E.D., Thomas, D., Nolgen, G., Claude, M. Hydrogen production by sequential cracking of biomass-derived pyrolysis oil over noble metal catalysts supported on ceria-zirconia. Applied Catalysis A : General 323 (2007): 147-161.
- [26.] Pengmei, L., Zhenhong, Y., Chuangzhi, W., Longlong, M., Yong, C., Noritatsu, T. Bio-syngas production from biomass catalytic gasification. Energy Conversion and Management 48 (2007): 1132-1139.
- [27.] Lillo-Rodenas, MA., Cazorla-Amoros, D., Linales-Solano, A. Understanding chemical reactions between carbons and NaOH and KOH : an insight into the chemical activator mechanism. Carbon 41(2) (2003): 267-75.
- [28.] Lillo-Rodenas, MA., Juan-Juan, J., Cozorla-Amoros, D., Lineres Solano, A., About reactions occurring during chemical activation with hydroxide. Carbon 42(7) (2004): 1371-5.

- [29.] Ahmadpour, A., Do, D.D. The preparation of activated carbons from coal by chemical and physical activation. *Carbon* 34 (1996): 471-479.
- [30.] Koltypin, M., Aurbach, D., Nazar, L., Ellis, B. More on the performance of LiFePO_4 electrodes-The effect of synthesis route, solution composition, aging, and temperature. *Journal of Power sources* 174 (2007): 1241-1250.
- [31.] Coll, R., Salvadó, J., Farriol, X. and Montané, D., Steam reforming model compounds of biomass gasification tars: conversion at different operating conditions and tendency towards coke formation, *Fuel Process. Technol.*, Vol. 74 (2001): 19-31.
- [32.] Devi, L., Ptasinski, K. J. and Janssen, F. J. J. G., A review of the primary measures for tar elimination in biomass gasification processes, *Biomass Bioenergy*, Vol. 24 (2003): 125-140.
- [33.] Sutton, D., Kelleher, B. and Ross, J. R. H., Review of literature on catalysts for biomass gasification, *Fuel Process. Technol.*, Vol. 73 (2001): 155-173.
- [34.] Wang, T. and Chang, J., Lv, P. and Zhu, J., Novel Catalyst for Cracking of Biomass Tar, *Energy Fuels*, Vol. 19 (2005): 22-27.
- [35.] Dominko, R., Bele, M., Gaberscek, M., Remskar, M., Hanzel, D., Goupil, J.M., Pejovnik, S. and Jamnik, J., Porous olivine composites synthesized by sol-gel technique, *J. Power Sourc.*, Vol. 153 (2006): 274-280.
- [36.] Courson, C., Makaga, E., Petit, C. and Kiennemann, A., Development of Ni catalysts for gas production from biomass gasification. Reactivity in steam- and dry-reforming, *Catalysis Today*, Vol. 63 (2000): 427-437.
- [37.] Reed, A.R. & William, P.T., Thermal processing of biomass natural fibre wastes by pyrolysis. *International Journal of Energy Research*, 28 (2004): 131-145.
- [38.] Kang, B.-S., Lee, K.H., Park, H.J., Park, Y.-K. & Kim, J.-S., Fast pyrolysis of radiata pine in a bench scale plant with a fluidized bed: Influence of a char separation system and reaction conditions on the production of bio-oil. *Journal of Analytical and Applied Pyrolysis*, 76 (2006): 32-37.
- [39.] Horne, P.A. & Williams, P.T., Influence of temperature on the products from the flash pyrolysis of biomass. *Fuel*, 75 (1996): 1051-1059.

- [40.] Bridgwater, A.V., Principles and practice of biomass fast pyrolysis processes for liquids. Journal of Analytical and Applied Pyrolysis, 51 (1999): 3-22.
- [41.] Maggi, R. & Delmon, B., Comparison between 'slow' and 'flash' pyrolysis oils from biomass. Fuel, 73 (1994): 671-677.
- [42.] Encinar, J.M., Beltrán, F.J., Ramiro, A. & González, J.F., Pyrolysis/gasification of agricultural residues by carbon dioxide in the presence of different additives: influence of variables. Fuel Processing Technology, 55 (1998): 219-233.
- [43.] Garivait, S., Chaiyo, U., Patumsawad, S. & Deakhuntod, J., Physical and chemical properties of Thai biomass fuels from agricultural residues. Proc. of the 2nd Joint Int. Conf. on Sustainable Energy and Environment, Bangkok, (2006) 541.
- [44.] Sricharoenchaikul, V., Pechyen, C., Aht-Ong, D. & Atong, D., Preparation and characterization of activated carbon from the pyrolysis of physic nut (*Jatropha curcas* L.) waste. Energy and Fuels, 22 (2008): 31-37.
- [45.] Demirbas, A., Effect of temperature on pyrolysis products from four nut shells. Journal of Analytical and Applied Pyrolysis, 76 (2006): 285-289.
- [46.] Pechyen, C., Atong, D., Aht-Ong, D. & Sricharoenchaikul, V., Investigation of pyrolyzed chars from physic nut waste for the preparation of activated carbon. Journal of Solid Mechanics and Materials Engineering, 1 (2007): 498-507.
- [47.] Tsai, W.T., Lee, M.K. & Chang, Y.M., Fast pyrolysis of rice husk: Product yields and compositions. Bioresource Technology, 98 (2007): 22-28.
- [48.] Onay, O. & Koçkar, O.M., Slow, fast and flash pyrolysis of rapeseed. Renewable Energy, 28 (2003): 2417-2433.
- [49.] Onay, O. & Koçkar, O.M., Fixed-bed pyrolysis of rapeseed (*Brassica napus* L.). Biomass and Bioenergy, 26 (2004): 289-299.
- [50.] Ate, F., Pütün, E. & Pütün, A.E., Fast pyrolysis of sesame stalk: yields and structural analysis of bio-oil. Journal of Analytical and Applied Pyrolysis, 71 (2004): 779-790.
- [51.] Onay, O., Fast and catalytic pyrolysis of pistacia khinjuk seed in a well-swept fixed bed reactor. Fuel, 86 (2007): 1452-1460.

BIOGRAPHY

Mister Chiravoot Pechyen was born in Bangkok, Thailand, on 23rd March, 1980. He received the Bachelor of Science degree majoring Polymer Science from Materials Technology Programme in Faculty of Science, Ramkhamhaeng University in 2002 and Master of Science degree majoring in Applied Polymer Science and Textile Technology from Materials Science Programme in Faculty of Science, Chulalongkorn University in 2005 (GPA 3.55 from 4.00).

He stated working as a supervisor in Research and Development (R&D) unit at Thai Composite Co.,Ltd. right after he had graduated. Science 2006, he has continued study toward his Doctoral degree at Department of Materials Sciences, Faculty of Science, Chulalongkorn University. He has interested in renewable energy as well as developing energy from plastic waste, agricultural waste, biomass, biopolymer composite waste, nano technology and potential study of renewable energy. He completed the programme and obtained his Doctor of Philosophy degree in Materials Science in August 2009 (GPA 3.72 from 4.00).

JOURNALS PUBLICATION

- Preparation and characterization of activated carbon from the pyrolysis of physic nut (*Jatropha curcas* L.) waste (ENERGY & FUELS : Impact Factor = 1.519)
- Investigation of pyrolyzed chars from physic nut waste for the preparation of activated carbon (JSME INTERNATIONAL JOURNAL SERIES A-SOLID MECHANICS AND MATERIAL ENGINEERING : Impact Factor = 0.343)
- Physicochemical properties of carbons prepared from physic nut waste by phosphoric acid and potassium hydroxide activations (MATERIALS SCIENCE FORUM : Impact Factor = 0.399)
- Synthesis of Olivine (LiFePO_4) and Ni /Olivine (LiFePO_4) catalysts for upgrading syn-gas production (Ceramic Transactions Journal)